Regime occupation and transition information obtained from observable meteorological state variables in the stably stratified nocturnal boundary layer

Carsten Abraham

B. Sc. University of Hamburg, 2012
M. Sc. University of Hamburg, 2015

A Dissertation Submitted in Partial Fulfillment of the
Requirements for the Degree of

DOCTOR OF PHILOSOPHY

in the School of Earth and Ocean Sciences

Regime occupation and transition information obtained from observable meteorological state variables in the stably stratified nocturnal boundary layer

by

Carsten Abraham

B. Sc. University of Hamburg, 2012
M. Sc. University of Hamburg, 2015

Supervisory Committee

Dr. Adam H. Monahan, Supervisor
(School of Earth and Ocean Sciences)

Dr. Stan Dosso, Departmental Member
(School of Earth and Ocean Sciences)

Dr. Knut von Salzen, Departmental Member
(School of Earth and Ocean Sciences)

Dr. Ron McTaggert-Cowan, Additional Member
(School of Earth and Ocean Sciences)

Abstract

The stably stratified nocturnal boundary layer (SBL) can be classified into two distinct regimes: one with moderate to strong winds, weak stratification and mechanically sustained turbulence (wSBL) and the other one with moderate to weak wind conditions, strong stratification and collapsed turbulence (vSBL). With the help of a hidden Markov model (HMM) analysis of the three dimensional state variable space of stratification, mean wind speeds, and wind shear the SBL can be classified in these two regimes in both the Reynolds-averaged as well as turbulence state variables. The two-regime SBL is a generic structure at different tower sites around the world independent of the location specific conditions.

Besides clustering the data the HMM analysis calculates the most likely regime occupation sequence which allows for detailed analysis of the structure of the meteorological state variables in conditions of very persistent nights. Conditioning on these very persistent nights clear influences of external drivers (such as pressure gradient force and low level cloud cover) are found. As the HMM analysis captures regime transitions accurately changes of state variables and external drivers across transitions can easily be assessed. Different meteorological state variables behave in times of turbulence collapse (wSBL to vSBL transition) and turbulence recovery (vSBL to wSBL transitions) as expected physically. The results reveal further that clear precursors for transitions in the state variable profiles or external drivers are cannot be determined and that on observed timescales regime transitions are relatively sharp.

The absence of clear precursors suggests that parameterisations of SBL regime behaviour and turbulence in the two regimes in weather and climate models have to be stochastic. As regime statistics are relatively insensitive to changes in the stochastic properties of the HMM analysis observed regime statistics are compared to 'freely-running' Markov chains. The SBL regime statistics do not follow a simple Markov process and more complex parameterisations are necessary. A possible approach of parameterising SBL regime behaviour stochastically using climatological results from this analysis is presented.

Contents

List of Tables

List of Figures

Acknowledgements

I would like to thank Dr. Adam H. Monahan, my supervisor, who has made my research an incredible journey filled with fun, excitement, and pure joy due to his constant enthusiasm and availability, despite having a thousand and one other things to do. Furthermore, I want to thank him for the amount of time he spent on discussions that turned out to be helpful and most of all indispensable in order to create this study. Thank you very much Adam!

I also thank my committee members, Dr. Stan Dosso, Dr. Ron McTaggert-Cowan, and Dr. Knut von Salzen for their guidance along the way of conducting this study.

I would like to acknowledge special thanks to Allison Rose and Kalisa Valenzuela in the School of Earth and Ocean Sciences main office for all the help, support, organisation, and overwhelming kindness throughout all these years.

I would like to thank a number of individuals and institutes for their willingness to share their tower data which were indispensable in carrying out this extensive comparison of SBL structures at different location sites. My acknowledgements are presented in the order that the tower stations are presented in the dissertation but I am equally thankful to all. The NOAA Earth System Research Laboratory's (ESRL) Physical Sciences Division (PSD) operates the Boulder Atmospheric Observatory (BAO) tower and makes the data publicly available. Information how to obtain the data is given on `https://www.esrl.noaa.gov/psd/technology/bao/site/`. The Royal Dutch Meteorological Institute (KNMI) is thanked for providing tower data from the Cabauw Experimental Site for Atmospheric Research (CESAR) which can be downloaded at `http://www.cesar-database.nl`. Fred Bosveld from the KNMI is acknowledged in particular for providing one year of turbulence data from CESAR. Felix Ament and Ingo Lange provided an extensive amount of Reynolds-averaged and turbulence data from the Wettermast Hamburg of the Meteorological Institute of the University of Hamburg. Martin Kohler and the Institute for Meteorology and Climate Research of the Karlsruhe Institute of Technology (KIT) provided observations from the turbulence and meteorological mast in Karlsruhe. The French and Italian polar institutes (IPEV and PANRA,

respectively) which operate the DomeC observatory in Antarctica are acknowledged for providing data through IPEV (program CALVA 1013), INSU/LEFE (GABLS4 and DEPHY2), and OSUG (GLACIOCLIM). The data are available on the CALVA website `http://lgge.osug.fr/~genthon/calva/home.shtml`. The team of the Los Alamos National Laboratory (LANL) are thanked making data from the Environmental Monitoring Plan (EMP) freely available which can be downloaded from `http://environweb.lanl.gov/weathermachine/data_request_green_weather.asp`. The Bundesamt für Seeschifffahrt und Hydrographie (BSH), the Bundesministeriums für Wirtschaft und Energie (BMWi), the Projektträger Jülich (PTJ), and Olaf Outzen are thanked for granting access to the data from the offshore research platforms FINO-1, FINO-2, and FINO-3 in Germany.

Finally, I would like to thank Dr. Peter Baas, John R. Gyakum, Dr. Yanping He, Dr. Amber Holdsworth, Anton Hooft, Dr. Ivo G. S. van Hooijdonk, Jonathan Izett, Steven van der Linden, Dr. Norman McFarlane, Dr. Ron McTaggart-Cowan, Dr. Nikki Vercauteren, and Dr. Bas J. H. van de Wiel, for useful discussions and ideas along the way of conducting this research.

I am grateful to the National Science and Engineering Research Council and the University of Victoria for supporting me financially over the years of my study.

List of abbreviations

GHMM	hidden Markov model using parametric Gaussian mixture distributions
HMM	hidden Markov model
LLCC	low level cloud cover
LWR	long-wave radiation
MSHF	maximum sustainable heat flux
PBL	planetary atmospheric boundary layer
pdf	probability density function
TKE	turbulent kinetic energy
tSBL	transitional stably stratified nocturnal boundary layer
Ri	Richardson number
SBL	stably stratified nocturnal boundary layer
SWR	short-wave radiation
VP	Viterbi-Path
U_{geo}	geostrophic wind speed
$var(w)$	variance of vertical wind component
vSBL	very stable stably stratified nocturnal boundary layer
W	wind speed
WHMM	hidden Markov model using parametric Weibull distributions
wSBL	weakly stable stably stratified nocturnal boundary layer

1 Introduction

The planetary atmospheric boundary layer (PBL) is the lowest part of the atmosphere in which momentum, energy, and mass are exchanged between the atmosphere and the underlying surface. This layer is normally turbulent, with turbulence generated by wind shear or buoyant instabilities. Convectively-driven turbulence is normally produced by the absorption of incoming shortwave radiation from the sun at the surface or advection of colder air over warmer surface. These convective turbulence cells lead to extensive momentum and heat transport in the PBL. As a result during the day the PBL is characterised by large turbulence intensities leading to a well-mixed PBL. Over land and during the day the height of this convective PBL can vary substantially depending on the prevailing conditions but its extent is on the order of about a kilometre. During the evening transition and throughout the night the PBL over land is characterised by stable conditions due to the missing incoming shortwave radiation and the dominance of radiative cooling at the surface. The turbulence is exclusively shear driven and weaker than during the day leading to substantially shallower PBLs. Inspired by the prevailing stable conditions meteorologists refer to the nighttime PBL as the stably stratified nocturnal boundary layer (SBL). As with convective boundary layers the SBL can also be established by the advection of warm air over a colder surface, a process particularly important over water as radiative effects are generally much weaker at water surfaces. In the SBL the boundary layer flow displays strong vertical gradients as the PBL is less well-mixed than during the day. The stratification can become so strong that vertical motions are suppressed causing the atmospheric flow within the SBL to decouple from the surface. Under such conditions the turbulence intensities can become so weak that they come close to collapse.

A number of physical processes govern SBL dynamics, such as anisotropic turbulent mixing, radiative cooling, low-level jet formation, gravity waves, katabatic flows, and fog or dew formation. Although the SBL has been extensively studied, many individual processes and their interactions are incompletely understood as nonstationarities of the flow and inhomogeneities of the surface allow a diversity of ambiguous interpretations of observations [*Mahrt*, 2007], hindering development of model parameterisations and resulting in errors

of SBL representation in atmospheric models for weather and climate [*Dethloff et al.*, 2001; *Gerbig et al.*, 2008; *Bechtold et al.*, 2008; *Medeiros et al.*, 2011; *Kyselý and Plavcová*, 2012; *Tastula et al.*, 2012; *Sterk et al.*, 2013; *Bosveld et al.*, 2014; *Sterk et al.*, 2015]. Misrepresentation of the SBL includes unrealistic decoupling of the atmosphere from the surface resulting in runaway surface cooling [*Mahrt*, 1998a; *Walsh et al.*, 2008], underestimation of the wind turning with height within the PBL [*Svensson and Holtslag*, 2009], overestimation of the PBL height [*Bosveld et al.*, 2014], underestimation of low level jet speed [*Baas et al.*, 2009], and underestimation of near-surface wind speed and temperature gradients or their diurnal cycle [*Edwards et al.*, 2011]. Global and regional weather and climate models often use an artificially enhanced boundary layer drag under stable conditions in order to improve simulations of the large-scale flow [*Holtslag et al.*, 2013]. This approach has led to the introduction of long-tailed stability functions not justifiable by observations. In such models, turbulence is artificially sustained under very stable conditions.

Turbulence and its interactions with submesomotions (motions slightly larger than turbulence) are subgrid-scale phenomena for climate and weather modelling and will remain so for the foreseeable future. Therefore, gaining a better understanding of the mechanisms causing transitions within the SBL is important for improving simulations of nocturnal near-surface properties such as temperature structure which controls the formation of fog and frost [*Walters et al.*, 2007; *Holtslag et al.*, 2013]. This improvement accompanies a better representation of surface wind variability and wind extremes [*He et al.*, 2010; *Monahan et al.*, 2011; *He et al.*, 2012]. More accurate simulations of these properties are also important for simulations and assessments of pollutant dispersal, air quality [*Salmond and McKendry*, 2005; *Tomas et al.*, 2016], harvesting of wind energy [*Storm and Basu*, 2010; *Zhou and Chow*, 2012; *Dörenkämper et al.*, 2015], and agricultural forecasts [*Prabha et al.*, 2011; *Holtslag et al.*, 2013].

Classification of data into separate regimes of the underlying processes with different characteristics is a conceptual simplification which helps organize the understanding of the physical processes present in the SBL. Based on the Reynolds-averaged mean state and turbulence profiles, the most common classification distinguishes between the weakly stable boundary layer (wSBL) and the very stable boundary layer (vSBL) [*Mahrt*, 1998b; *Acevedo and Fitzjarrald*, 2003; *Mahrt*, 2014; *van Hooijdonk et al.*, 2015; *Monahan et al.*, 2015; *Vercauteren and Klein*, 2015; *Acevedo et al.*, 2016; *Vignon et al.*, 2017a]. The wSBL describes a regime of weakly stable stratification, often found under cloudy or overcast conditions or moderate to strong winds, with sustained turbulence due to mechanically driven shear instabilities. This regime conforms to the classical understanding of turbulence in the PBL with turbulent quantities decreasing with height and near-surface profiles which are well-

described by Monin-Obukhov similarity theory in horizontally homogeneous conditions [e.g. *Sorbjan*, 1986; *Mahrt*, 1998a; *Grachev et al.*, 2013]. The vSBL, on the other hand, describes strong statically stable stratification, often under clear-sky conditions or relatively weak winds, with turbulence profiles which can be decoupled from the surface [*Banta et al.*, 2007], turbulence intensities which can increase with height, or highly anisotropic turbulent motions [*Mauritsen and Svensson*, 2007]. Transitions between those regimes remain one of the least understood phenomenona in the PBL and challenge physical understanding as well as accurate simulation in weather and climate models [*Holtslag et al.*, 2013; *Mahrt*, 2014]. In this study the nature of these regimes and their transitions is analysed on the basis of observational tower data

During the nighttime transition over land, the net radiative energy flux at the surface changes sign and the atmospheric layers near the surface begin to cool. The result is a stable near-surface stratification. Under strong wind conditions, caused by strong pressure gradient forces, large shears produce sufficient turbulent kinetic energy (TKE) to sustain vertical turbulent mixing [*van de Wiel et al.*, 2012a]. Thus, vertical turbulent heat fluxes are present to compensate the energy loss at the surface and a very persistent wSBL is established. If winds are weak, TKE production and turbulent fluxes weaken to the point of collapse and the atmospheric layers decouple from each other. The decrease in vertical turbulent heat fluxes leads to strong cooling dominated by radiative fluxes such that a very stable temperature profile is produced and the vSBL is established. In addition to weak pressure gradient forces the vSBL is often accompanied by clear sky conditions which allow for effective radiative cooling [*Edwards*, 2009; *Monahan et al.*, 2015].

The existence of two distinct SBL regimes can be understood in terms of the conceptual framework of the maximum sustainable downward heat flux [MSHF; *van de Wiel et al.*, 2007, 2012a,b, 2017; *van Hooijdonk et al.*, 2015]. The MSHF is determined by two competing factors: the strength of the temperature gradient and the intensity of vertical mixing [*de Bruin*, 1994; *Malhi*, 1995; *van Hooijdonk et al.*, 2015; *van de Wiel et al.*, 2017]. In stably stratified conditions, turbulent fluxes are local and described by flux-gradient relationships. Neutral temperature profiles therefore result in a zero heat flux. Similarly, under very stable conditions turbulent fluxes are suppressed due to the strong density gradients and the turbulent sensible heat flux is weak. Between these two limiting cases, a flow-dependent maximum turbulent heat flux exists. If the MSHF is less than the turbulent heat flux needed to balance energy losses at the surface the turbulence collapses and the vSBL is established. Otherwise, a wSBL is established.

Recent research has introduced the concept of an altitude-dependent wind speed threshold

U_{min} separating the wSBL (for $U > U_{min}$) from the vSBL (for $U < U_{min}$). The existence of a threshold U_{min} was inspired by the MSHF concept [*van de Wiel et al.*, 2007, 2012a,b; *van Hooijdonk et al.*, 2015; *Holdsworth et al.*, 2016]. Evidence of two regimes that can be conceptually separated by U_{min} has been presented for the Cabauw observatory of the Royal Netherlands Meteorological Institute (KNMI) in the Netherlands [*van Hooijdonk et al.*, 2015; *van de Wiel et al.*, 2017] and DomeC in Antarctica [*Vignon et al.*, 2017a]. However, the existence of an unambiguous value of U_{min} is not clear as variations of this quantity with different PBL conditions are evident across the different sites. A similar threshold was also used to distinguish between strong turbulent and weak turbulent flow in the CASES-99 study [*Sun et al.*, 2012]. For wind speeds larger than the observed threshold, the TKE and the friction velocity (u_*) increase with wind speed almost linearly, while below they are almost independent of wind speed. A third wind speed threshold has beed defined as the wind speed at which vertical gradients of TKE and u_* reverse sign [*Acevedo et al.*, 2016]. Above the threshold, near-surface TKE decreases with height implying a fully-coupled boundary layer with turbulence that is mainly generated by shear near the surface. Below this threshold near-surface TKE initially increases with height away from the surface, characterising a decoupled system where turbulent fluxes generated at the surface are reduced by the stratification. Even though these particular definitions lead to different threshold values, they are based on a common physical concept of separating a regime with sustained mechanically driven shear turbulence from a regime with substantially weakened to collapsed turbulence activity.

In contrast to the two-regime SBL other classifications have suggested a third transitional regime (tSBL) separating the vSBL from the wSBL [*Mahrt*, 1998b, 2014]. In this classification scheme the vSBL is an extremely stable regime which is governed almost entirely by radiative fluxes such that turbulent fluxes are so weak that the ground heat flux comes nearly into balance with the energy loss at the surface [*van de Wiel et al.*, 2003]. Direct numerical simulations have also been interpreted in terms of a three-regime behaviour [*Ansorge and Mellado*, 2014]. In their simulations, the wSBL shows only slightly weakened TKE profiles relative to neutral stratification, the tSBL shows significant decreases of 50 % of integrated TKE, and the vSBL is characterised by an almost complete collapse of turbulence. A different set of three distinct regimes were also hypothesised by *Sun et al.* [2012], in which the third regime is defined by U_{min} and distinguished from the vSBL by the presence of intermittent top-down turbulent bursts. However, in contrast to a two-regime behaviour in which the boundary layer is characterised by a turbulent or non-turbulent flow, clear observational evidence of three distinct regimes is lacking.

A conceptual model by *van de Wiel et al.* [2017] provides further insight into the role

of energetic exchanges with the underlying surface SBL regime dynamics. Their model considers an equilibrium surface energy budget coupled to a bulk parameterisation of atmospheric turbulent transport with fixed near-surface wind speed, such that all feedbacks between the atmosphere and the surface (e.g. strength of atmosphere-surface coupling) are described by a single parameter related to thermal conductivity. This model produces a characteristic strong increase in equilibrium inversion strength for winds weaker than a predicted value U_{min}, strengthening the idea of a threshold wind speed separating the regimes. The model also predicts the existence of multiple equilibria and fold bifurcations near the threshold wind speed for weak atmosphere-surface coupling. Behaviour qualitatively similar to the predictions of this model is found in tower observations at Cabauw and DomeC. Even though the model is able to describe key aspects of the structural characteristics of the SBL regimes, it is highly idealised. In particular, it treats near surface wind as a fixed external parameter rather than as being determined by the dynamics of the PBL itself.

Although aspects of the SBL can be explained very well, no comprehensive theory explaining all aspects of the SBL behaviour exists as yet. In particular, mechanisms controlling transitions from the vSBL to wSBL are not well understood, and clear precursors of transitions between regimes have yet to be found. Transitions between these states result from different physical mechanisms. Over land and ice surfaces, the wSBL to vSBL transition (the collapse of turbulence) is normally caused by radiative cooling at the surface increasing the inversion strength and suppressing turbulent vertical fluxes of momentum and heat. This process is relatively well understood and can be explained by conceptual models [*van de Wiel et al.*, 2007, 2017; *Holdsworth et al.*, 2016] or in direct numerical simulations of stratified channel flows [*Donda et al.*, 2015; *van Hooijdonk et al.*, 2017a] or atmospheric boundary layers [e.g. *Flores and Riley*, 2011; *Ansorge and Mellado*, 2014]. Turbulence collapse can also occur when strongly stable stratification is produced by the advection of warm air over cold surface [*Dörenkämper et al.*, 2015]

The reverse transition, the recovery of turbulence (vSBL to wSBL transition), on the other hand, is less well-understood. One mechanism to recover turbulence includes the build-up of shear resulting in instabilities. Another potential class of processes initiating these transitions is associated with intermittent turbulent events [*Durst*, 1933; *Gifford*, 1952; *Kondo et al.*, 1978; *Nappo*, 1991; *van de Wiel et al.*, 2002a,b, 2003; *Acevedo and Fitzjarrald*, 2003; *Reina and Mahrt*, 2005; *Ohya et al.*, 2008; *White*, 2009; *Baklanov et al.*, 2011; *Medeiros and Fitzjarrald*, 2014; *Mahrt et al.*, 2012; *Mahrt*, 2014; *Vercauteren and Klein*, 2015] which have been found to dominate the turbulent transport in vSBL conditions [*Nappo*, 1991; *Coulter and Doran*, 2002; *Doran*, 2004; *Basu et al.*, 2006; *Acevedo et al.*, 2006;

Williams et al., 2013]. The turbulence intensities can be strong enough to break down the inversion, resulting in a transition to the wSBL. The recovered and vertically-transported turbulence also leads to a deeper planetary boundary layer.

Intermittent turbulence arises from a range of different phenomena such as breaking gravity waves or solitary waves [*Mauritsen and Svensson*, 2007; *Sun et al.*, 2012], density currents [*Sun et al.*, 2002], microfronts [*Mahrt*, 2010], Kelvin-Helmholtz instabilities interacting with the turbulent mixing [*Blumen et al.*, 2001; *Newsom and Banta*, 2003; *Sun et al.*, 2012], or shear instabilities induced from internal wave propagation [*Sun et al.*, 2004; *Zilitinkevich et al.*, 2008; *Sun et al.*, 2015]. It has even been suggested from direct numerical simulations that intermittency can arise as an intrinsic mode of the non-linear equations in the absence of external perturbations of the mean flow [*Ansorge and Mellado*, 2014].

Many of these intermittent turbulence events are subgrid-scale phenomena in weather and climate models. Furthermore, the structure and propagation of intermittent turbulence events has been found to be independent and decoupled from the mean states [e.g. *Rees and Mobbs*, 1988; *Lang et al.*, 2018]. It has simply been suggested that long-tailed stability functions account for the unresolved subgrid-scale variations in turbulence intensity due to surface heterogeneities or intermittent turbulent events [e.g. *McCabe and Brown*, 2007]. Even though *Medeiros and Fitzjarrald* [2014] showed in an observational surface station network spanning approximately a 1 by 1 degree geographical area that generally long-tailed stability functions are a good approximation to account for heterogeneity within a model grid-box, they found also in *Medeiros and Fitzjarrald* [2014, 2015] that intermittent turbulence events can occur simultaneously across the whole station network with very similar turbulence intensities at all stations, a phenomenon not included in the description by long-tailed stability functions. Thus, it has been proposed that parameterisations for these physical processes may be required to be explicitly stochastic [e.g. *He et al.*, 2012; *Mahrt*, 2014]. Stochastic subgrid-scale parameterisations to describe the physically different conditions in the SBL might help to capture the missing variability in the SBL and improve both climate mean states and forecast ensemble spread [e.g. *He et al.*, 2012; *Mahrt*, 2014; *Nappo et al.*, 2014; *Vercauteren and Klein*, 2015; *Berner et al.*, 2017]. Development of such parameterisations, however, requires information regarding temporal structures of regime dynamics, the relative occurrence of regimes and regime transitions, and possible dependencies of regime dynamics on meteorological patterns and local characteristics. Thus, a thorough characterisation of the SBL regimes and their climatology is indispensable.

As noted above, it is not clear that generic thresholds in the observed meteorological state

variables separating regimes exist as under similar combinations of wind at specific altitudes and stratification conditions large differences in the turbulent fluxes can be observed. External drivers such as pressure gradient force and cloud coverage have been found in several studies to have an important impact on local strengths of stratification and wind shear [*Nieuwstadt*, 1984; *Poulos et al.*, 2002; *van de Wiel et al.*, 2002a, 2012a; *Svensson et al.*, 2011; *Monahan et al.*, 2015]. The attribution of different regimes to the same mean state conditions complicates the systematic investigation of the dynamical processes, in particular those leading to transitions.

An empirical approach to distinguishing between SBL regimes that allows for different regime occupations under the same observable conditions was introduced in *Monahan et al.* [2015]. Using a statistical approach known as Hidden Markov Model (HMM) analysis, this study separated two distinct regimes in the state space spanned by Reynolds-averaged mean values of the mean wind speed, wind speed shear (between 200 and 10 m), and potential temperature difference (between 200 and 2 m) measured on the 213 m tower of the Royal Dutch Meteorological Institute observatory at Cabauw. Their analysis of the Reynolds-averaged mean states also showed a clear separation of turbulent fluxes in a one year sample into two distinct regimes: a wSBL with strong TKE and strong vertical turbulent transport in contrast to a vSBL with weak TKE and weak vertical turbulent transport [cf. *Monahan et al.*, 2015, Figures 7 and 8]. Vertical shear, dry static stratification, and mean wind are natural candidate variables to describe the physical system [e.g *van de Wiel et al.*, 2012a,b, 2017; *van Hooijdonk et al.*, 2015; *Monahan et al.*, 2015] because wind speeds at two observational levels contain information about the shear responsible for the production of TKE, and stable stratification for its consumption. A major limitation of the study of *Monahan et al.* [2015] was that they considered only data from the single location at Cabauw.

The research presented in this thesis aims to obtain a better understanding of SBL regime dynamics on the basis of observational data including a thorough analysis of SBL regime climatologies across different tower sites, extending the results found by *Monahan et al.* [2015]. Such climatologies allow quantification of the observed regime variability in the SBL for the first time which is useful for the validation of weather and climate models. Former studies usually relied on high frequency data sets (with observation of 20 Hz or higher) which have been obtained during relatively short research and field campaigns. Of particular interest is also the understanding of which mechanisms govern the different SBL regime transitions in a climatological sense and if possible systematic transition precursors can be extracted from the data allowing for deterministic relationships of regime dynamics to external influences. In case the obtained characteristics and statistics do not lead to de-

terministic relationships those can then inform a new class of stochastic parameterisations of turbulence under stable stratified conditions for weather and climate models.

The main results presented in this dissertation correspond to four submitted journal articles from which a continuous three part paper series systematically detects and classifies the SBL regime behaviour at different tower sites with varying surface conditions using the HMM analysis. The first part identifies in which state variables regime behaviour can be detected and what regime dynamics can be analysed based on the data that are available. The analysis further allows to investigate two basic differences in the SBL regime dynamics, the classification into nights without any transitions, defined in this work as very persistent nights, and nights with the occurrence of SBL regime transitions. The structure and temporal evolution of the meteorological state variables vary substantially in this coarse classification scheme of distinct nights and their occurrence can be related to relatively clear controls in external drivers. These structures and occurrence statistics have been contrasted in the second and third part of the suite of papers. The fourth paper aims to simulate the occurrence statistics in 'freely-running' Markov chains in order to work towards the development of a stochastic representation of the regime dynamics in the SBL. The four papers are:

1. Regimes of the stably stratified nocturnal boundary layer. Part I: Observable meteorological state variables containing information about regime occupation (*submitted with A. H. Monahan to Journal of Atmospheric Science*)

2. Regimes of the stably stratified nocturnal boundary layer. Part II: The boundary layer structure in times of very persistent weakly stable and very stable boundary layer conditions (*submitted with A. H. Monahan to Journal of Atmospheric Science*)

3. Regimes of the stably stratified nocturnal boundary layer. Part III: The structure of meteorological state variables and the role of external forces in times of regime transitions (*submitted with A. H. Monahan to Journal of Atmospheric Science*)

4. Characterising regime behaviour in the stably stratified nocturnal boundary layer on the basis of stationary Markov chains (*submitted with A. H. Monahan to Nonlinear Processes in Geophysics*)

Since all submitted journal papers make use of the same data sets and rely on the HMM analysis to detect the SBL regimes, sections of all papers introducing those information have been summarised in the first two chapters of this work leading to the following structure of the dissertation.

The data are described in chapter 2 and a short introduction to the HMM analysis is given in chapter 3. Using the HMM analysis we investigate first the common SBL regime behaviour and exhibit some location specific characteristics in chapter 4. We also assess the question how many physically-reasonable regimes can be determined by an HMM analysis. Additionally, a detailed analysis of which meteorological state variables contain information about the regime occupation with particular focus on regime transitions is presented. The classified data are then used in order to investigate the structures of meteorological state variables in observed atmospheric levels in very persistent vSBL and wSBL nights (which we will define as those in which the SBL remains in one regime for the entire duration of the night) across different tower sites (chapter 5). Furthermore, with the HMM analysis regime transitions can be effectively detected and changes of meteorological state variables during SBL transitions and possible precursors of transitions investigated (chapter 6). These analyses build the core of the climatological understanding of the importance of SBL regime dynamics and exhibits what SBL turbulence variability weather and climate models miss by suppressing the occurrence of the vSBL.

Having detected and exhibited the physical structures of the SBL regimes, the statistics of the HMM analysis are investigated in order to assess the possibility to use the information obtained in stochastic parameterisations. Therefore, in chapter 7 a sensitivity analysis of the regime statistics to changes in the stochastic properties of the HMM analysis is conducted demonstrating how robust the obtained statistics of the underlying Markov model are. The climatological regime statistics are then compared to statistics of a 'freely-running' Markov chain and results are discussed in the context of developing new stochastic parameterisations of SBL regime behaviour and turbulence in the different regimes.

Conclusions and directions of future research are presented in chapter 8.

2 Data

Observational data sets from nine different research towers measuring standard Reynolds-averaged meteorological state variables with a time resolution no coarser than 30 minutes are considered (Tables 2.1 and 2.2). Observations of TKE and vertical fluxes are also available at three of these sites (Cabauw, Hamburg, and Los Alamos; Table 2.3). The nine experimental sites differ substantially in terms of their surface conditions, surrounding topography, and meteorological setting. Tables 2.1, 2.2 and 2.3 present information regarding measurement heights, data record lengths, and time resolutions, alongside references describing the experimental sites in detail. The geographic locations are illustrated in Figure 4.1. Here, we give a short introduction and point out the most pertinent differences among the sites. In particular, we distinguish between land-based, ice-based, and ocean-based stations.

The land-based stations (Table 2.1) are characterized by quite different local conditions. Both the Cabauw and Hamburg towers lie in flat, moist, grassland areas, although the Hamburg tower is affected by the nearby large metropolitan area of Hamburg. Even though the Cabauw site is in a relatively horizontally homogeneous environment, under very stable stratification effects of surface heterogeneities are observable [*Optis et al.*, 2014]. The Karlsruhe tower is located in the Rhine valley, a rather hilly, forested area in the lee of the Karlsruhe urban area. The American sites are highly affected by the surrounding topography. The Boulder tower is located on a high plateau and is surrounded by a dry, agricultural, flat area in the lee of the Rocky Mountains. The Los Alamos TA-6 tower site is located in a valley surrounded by mountain ranges.

The DomeC observatory is located on a flat ice surface in the interior of Antarctica. This ice-based site is therefore influenced by completely different conditions than the other sites, including a higher albedo, a lower roughness length, and long-lasting polar nights. The sensor measurement heights are variable due to changing snow heights. The heights quoted in Table 2.2 represent averages over the 5 years considered.

The ocean-based stations (Table 2.2) considered are the offshore research platforms *Forschungsplattform in Nord- und Ostsee* (FINO) which are located in the German North-

Table 2.1: Information about the different meteorological weather tower sites and their measurement heights sorted alphabetically for the land-based sites. Detailed information about the sites is presented in the cited references. The data are available for Reynolds-averaged (avg.) mean values of wind speed (W), wind direction (θ), temperature (T), and pressure (P).

Institute	References	Geolocation	Time Period	Data	avg. [min]	Measurement Heights [m]
Land-based tower sites						
The Boulder Atmospheric Observatory (BAO), Boulder, USA	*Kaimal and Gaynor* [1983], *Blumen* [1984]	40.0500 N, 105.0038 W, 1584 m	2008-2015	P	10	SFC
				W	10	10, 100, 300
				θ	10	10, 100, 300
				T	10	10, 100, 300
The Royal Netherlands Meteorological Institute (KNMI), Cabauw, Netherlands	*Ulden and Wieringa* [1996]	51.9700 N, 4.9262 E, -0.7 m	2001-2015	P	10	SFC
				W	10	10, 20, 40, 80, 140, 200
				θ	10	10, 20, 40, 80, 140, 200
				T	10	2, 10, 20, 40, 80, 140, 200
Meteorologisches Institut der Universität Hamburg (MI), Hamburg, Germany	*Brümmer et al.* [2012], *Floors et al.* [2014], *Gryning et al.* [2016]	53.5192 N, 10.1051 E, 0.3 m	2005-2015	P	1	2
				W	1	10, 50, 110, 175, 250, 280
				θ	1	10, 50, 110, 175, 250, 280
				T	1	2, 10, 50, 110, 175, 250, 280
Karlsruher Institut für Technologie (KIT), Karlsruhe, Germany	*Kalthoff and Vogel* [1992], *Wenzel et al.* [1997], *Barthlott et al.* [2003], *Kohler et al.* [2017]	49.0925 N, 8.4258 E, 110.4 m	2003-2013	P	10	SFC
				W	10	2, 20, 30, 40, 50, 60, 80, 100, 130, 160, 200
				θ	10	40, 100, 200
				T	10	2, 10, 30, 60, 100, 130, 160, 200
Los Alamos National Laboratory (LANL), Los Alamos, USA	*Bowen et al.* [2000], *Rishel et al.* [2003]	35.8614 N, 106.3196 W, 2263 m	1995-2015	P	15	1.2
				W	15	11.5, 23, 46, 92
				θ	15	11.5, 23, 46, 92
				T	15	1.2, 11.5, 23, 46, 92

ern and Baltic Seas. Their meteorological measurements start at about 30 m above the lowest tidal level. As a result, actual heights of the measurements above the surface are variable due to tidal and wave height variations. The heat capacity of the water surface is considerably larger than that of the surfaces at all other sites considered in this study. At the FINO towers we exclude nights with statically unstable conditions as under these common conditions at ocean-based sites wind speed measurements have been found to be unreliable [*Westerhellweg and Neumann*, 2012]. Furthermore, at FINO-1 nights with primary wind directions between 280 and 340 degrees are excluded due to mast interference effects in the data. At the other stations such an exclusion is not necessary as three wind measurements at each level exist which are 120 degrees apart from each other.

Preliminary analyses showed that the first wSBL to vSBL transitions occur during the evening transition, i.e. during or before actual sunset. In order to capture these first transitions, allowing for a complete analysis of the transition statistics, we define the duration of the night on the basis of the surface energy budget. Net radiative loss at the surface leads to surface cooling and the inversion growth. Consequently, for those sites at which the sufficient suite of radiative flux measurements are made (Cabauw, Hamburg, and Los Alamos), we define the beginning of the night as the time the net radiative surface flux (Q_N; sum of upwelling and downwelling long-wave (LWR) and short-wave radiation (SWR)) becomes negative. The onset of the nights defined in this way is generally earlier than the actual sunset or the time that downwelling SWR becomes zero. For these three sites we find that our nighttime definition allows us to capture the timing of the first turbulence collapse. Importantly, the regime sequence during the time after sunset is unaffected by considering times before sunset in the HMM analysis. Usually Q_N changes sign between 2-3 hours before sunset, depending on season and the large-scale circulation. In order to capture the development for sites that do not measure all radiative components, we define nighttime at these locations as starting 2 hours before actual sunset given by the time and geographical location.

Data records at some towers contain missing measurements. While the HMM is able to accommodate records in discontinuous blocks (such as individual nights), it requires complete records within each block. If only a single data point is missing between two measurements, we choose to fill the gap by interpolating linearly in time. Nights with missing data sequences of more than one consecutive time step are excluded from the analysis.

At the Karlsruhe site some nights contain lower-level wind measurements of exactly 0 m s^{-1}. These nights are excluded from the analysis as wind speeds of exactly

Table 2.2: As Table 2.1, but for ice- and ocean-based tower sites

Institute	References	Geolocation	Time Period	Data	avg. [min]	Measurement Heights [m]
Ice-based tower sites						
Institut Polaire Français Paul-Émile Victor (IPEV), and Programma Nazionale Ricerche in Antartide (PNRA), DomeC, Antarctica	*Genthon et al.* [2010, 2013], *Vignon et al.* [2017b,a]	75.1000 S, 123.3000 E, 3233 m	2011-2016	P	30	0.7
				W	30	1.3, 2.3, 3.5, 9, 18.2, 25.6,32.9, 41.3
				θ	30	1.3, 2.3, 3.5, 9, 18.2, 25.6, 30 32.9, 41.3
				T	30	0.9, 1.9, 2.9, 10.3, 17.7, 25, 32.4, 41.6
Ocean-based tower sites						
Forschungs- und Entwicklungszentrum Fachhochschule Kiel GmbH, FINO-1, Germany	*Beeken et al.* [2008], *Fischer et al.* [2012]	54.0140 N, 6.5876 E, 0 m	2004-2015	P	10	20, 90
				W	10	33, 40, 50, 60, 70, 80, 90, 100
				θ	10	33, 40, 50, 60, 70, 80, 90
				T	10	30, 40, 50, 70, 100
Forschungs- und Entwicklungszentrum Fachhochschule Kiel GmbH, FINO-2, Germany	*Dörenkämper et al.* [2015]	55.0069 N, 13.1542 E, 0 m	2008-2015	P	10	30, 90
				W	10	32, 42, 52, 62, 72, 82, 92, 102
				θ	10	32, 42, 52, 62, 72, 82, 92
				T	10	30, 40, 50, 70, 99
Forschungs- und Entwicklungszentrum Fachhochschule Kiel GmbH, FINO-3, Germany	*Fischer et al.* [2012]	55.1950 N, 7.1583 E, 0 m	2010-2015	P	10	23, 95
				W	10	30, 40, 50, 60, 70, 80, 90, 100
				θ	10	29, 60, 100
				T	10	29, 55, 95

Table 2.3: Information about the turbulence variables measured at the weather tower sites and their measurement heights. The available data are variances in x-direction (σ_u), y-direction (σ_v), and z-direction (σ_w), as well as turbulent momentum fluxes $\overline{u'w'}$, $\overline{v'w'}$, and heat flux $\overline{w'T'}$.

Institute	Time Period	Data	avg. [min]	Measurement Heights [m]
The Royal Netherlands Meteorological Institute (KNMI), Cabauw, Netherlands	July 2007-June 2008	σ_u	10	5, 60, 100, 180
		σ_v	10	5, 60, 100, 180
		σ_w	10	5, 60, 100, 180
		$\overline{u'w'}$	10	5, 60, 100, 180
		$\overline{v'w'}$	10	5, 60, 100, 180
		$\overline{w'T'}$	10	5, 60, 100, 180
Meteorologisches Institut der Universität Hamburg (MI), Hamburg, Germany	2005-2015	σ_u	1	10, 50, 110, 175, 250, 280
		σ_v	1	10, 50, 110, 175, 250, 280
		σ_w	1	10, 50, 110, 175, 250, 280
		$\overline{u'w'}$	1	10, 50, 110, 175, 250, 280
		$\overline{v'w'}$	1	10, 50, 110, 175, 250, 280
		$\overline{w'T'}$	1	10, 50, 110, 175, 250, 280
Los Alamos National Laboratory (LANL), Los Alamos, USA	1995-2015	$\sqrt{\sigma_u^2 + \sigma_v^2}$	15	11.5, 23, 46, 92
		σ_w	15	11.5, 23, 46, 92

0 m s^{-1} are unphysical artefacts of cup anemometers for very low wind speeds. Furthermore, such discrete values are problematic for the HMM analysis we perform because its state variables are assumed to be continuous random variables.

At the Hamburg site we exclude turbulence data for north winds (335 to 25 degrees) because of clear evidence of mast effects under very stable conditions. For the same reasons, we exclude turbulence data for wind directions between 280 to 340 degrees at Cabauw.

In order to include information about directional wind shears in addition to scalar shears, wind components at height h across and along the wind at the highest observation height (h_{max}) are defined as

$$W_h \perp W_{h_{max}} = W_h \sin(\theta_{h_{max}} - \theta_h), \quad (2.1)$$

$$W_h \parallel W_{h_{max}} = W_h \cos(\theta_{h_{max}} - \theta_h), \quad (2.2)$$

where W and θ are respectively the wind speed and direction. Defining the components along and across the flow of the highest measured altitude results in a parsimonious measure

of directional shear independent of the wind direction, providing information about the coupling of the surface flow and higher levels. Note that *Monahan et al.* [2015] only considered speed differences between altitudes.

Static stabilities are calculated as the potential temperature (Θ) difference between two heights. Potential temperatures are calculated from observed temperature and surface pressure assuming hydrostatic equilibrium, an acceleration due to gravity of 9.81 m s^{-2}, a specific heat capacity of 1005 J kg^{-1} K^{-1}, and the specific gas constant of 287 J kg^{-1} K^{-1}.

We do not use humidity information in our analysis despite its general availability at the tower sites. A preliminary analysis indicated that water vapour has minor effects on the results of the HMM analysis, so we focus on dry static stability as the measurement for stratification. However, humidity might have an important effect in lower latitudes. A lack of observational towers in these regions prevented us from testing this hypothesis.

Information about the percentage of cloud cover is obtained from ceilometer measurements provided at Cabauw from 1 July 2007 to 31 December 2015. At this site, we have calculated estimates of geostrophic vector winds from hourly surface pressure measurements from 34 meteorological stations of the Royal Dutch Meteorological Institute (KNMI) within 80 km of Cabauw. A two dimensional spline fit of the pressure field is used to estimate the pressure gradient force.

3 The Hidden Markov Model

We now present a brief overview of the HMM analysis. An in-depth description can be found in *Rabiner* [1989] and an illustrative example is given in *Monahan et al.* [2015].

HMMs are statistical models to systematically detect and characterize regime behaviour by identifying an unobserved, or hidden, discrete Markov chain ($\mathbf{X} = \{x_1, x_2, \ldots, x_T\}$) from a time series of observable state variables ($\mathbf{Y} = \{\mathbf{y}_1, \mathbf{y}_2, \ldots, \mathbf{y}_T\}$) of arbitrary dimension. While the term "hidden state sequence" is often used in the HMM literature to refer to the Markov chain $\mathbf{X}$, we will use the term regime sequence to avoid confusion with input state variables. The hidden regime sequence is also called the Viterbi Path (VP). Here, we use the HMM as a classification scheme to allocate each time step of $\mathbf{Y}$ to different SBL regimes according to the VP. We also make use of information about regime dynamics by studying the stochastic transition matrix $\mathbf{Q}$ of the VP.

The HMM analysis estimates its parameters, $\mathbf{Q}$ and conditional distributions of $\mathbf{Y}$, simultaneously making use of the following assumptions.

1. Markov assumption: the value x_{t+1} depends exclusively on the current value of x_t, so:
$$P(x_{t+1} = i | x_t = j, x_{t-1} = k, \ldots, x_0 = n) = \mathbf{Q_{ij}} P(x_t = j) \qquad \forall t, \tag{3.1}$$
where the evolution of the system is governed by $\mathbf{Q}$ (a $K \times K$ matrix with K a predefined number of hidden regimes) such that $\sum_j \mathbf{Q_{ij}} = 1$.

2. Independence assumption: Conditioned on $\mathbf{X}$, values of $\mathbf{Y}$ are independent and identically distributed variables resulting in a probability of the observational data sequence of
$$P(\mathbf{Y}|\mathbf{X}, \lambda) = \pi_j p(\mathbf{y}_1 | x_1 = j, \lambda_j) \prod_{t=2}^{T} \mathbf{Q_{ij}} p(\mathbf{y}_t | x_t = i, \lambda_i) \qquad \text{with} \quad i, j = 1, \ldots, K, \tag{3.2}$$
where $\{\lambda_i\}_{i=1,\ldots,K}$ is the parameter set describing the probability distributions (p) of $\mathbf{y_t}$ conditioned on the regime i of x_t, and π_j is the probability that x_1 is in regime j.

Finally, the analysis assumes that $\mathbf{Q}$ and λ are time-independent.

The HMM analysis requires specification of the number K of hidden regimes and the form of the conditional distributions in each hidden regime described by the parameter set λ. We chose K to be 2 and 3 corresponding to two- and three-regime SBL classification schemes as discussed in chapter 1. Since continuous variables are evaluated, λ characterizes parametric pdfs. Usually, Gaussian distributions are chosen to describe the parametric pdfs: $\lambda_i = \{\mu_i, \sigma_i\}$, where μ_i, σ_i are the regime-dependent mean and covariance [*Monahan et al.*, 2015]. However, many variables observed in the PBL are highly non-Gaussian. In particular, the wind speed deviates substantially from Gaussianity [e.g. *Monahan*, 2007; *He et al.*, 2010, 2012, 2013; *Monahan et al.*, 2011; *Monahan*, 2018]. To account for non-Gaussianity, the regime-dependent pdfs can be extended to a Gaussian mixture model:

$$\mathrm{p}(\mathbf{y_t}|x_t = i) \sim \sum_{m=1}^{M} c_{i,m}\mathcal{N}(\mu_{i,m}, \sigma_{i,m}), \tag{3.3}$$

where $c_{i,m}$, $\mu_{i,m}$, and $\sigma_{i,m}$ are respectively the mixture coefficient, the mean, and the covariance of the m-th Gaussian mixture dependent on the hidden regime i. By construction, $\sum_m c_{i,m} = 1$. The use of a Gaussian mixture pdf requires the specification of the number of constituent Gaussians. Here, a mixture of five additive Gaussians is chosen as trade off between accurate representation of the real pdfs of the variables and computational time for the HMM expectation maximisation algorithm. Furthermore, for a finite dataset the quality of parameter estimates is expected to decrease as the number of parameters is increased. The results we obtain are not substantially different if we assume the conditional distributions within each regime to be Gaussian (cf. *Monahan et al.* [2015]).

We also consider an HMM model using only the one-dimensional wind observations, for which we take the conditional pdfs to be two-parameter Weibull:

$$\mathrm{p}(y_t|x_t = i) = \frac{b_i}{a_i}\left(\frac{y_t}{a_i}\right)^{b_i-1} \exp\left[-\left(\frac{y_t}{a_i}\right)^{b_i}\right], \tag{3.4}$$

where a_i and b_i are the scale and shape parameters. We found the Weibull estimates to be robust to the choice of estimator, so we use the simple moment-based estimator based on the conditional mean μ_i and standard deviation σ_i:

$$a_i = \frac{\mu_i}{\Gamma(1 + 1/b_i)}, \quad b_i = \left(\frac{\mu_i}{\sigma_i}\right)^{1.086}, \tag{3.5}$$

with Γ denoting the gamma function [*Monahan*, 2006].

The challenge of the HMM analysis is to estimate the full set of parameters $\Lambda = \{\mu_{i,m}, \sigma_{i,m}, c_{i,m}, \mathbf{Q}\}_{i=1,\ldots,K;m=1,\ldots,5}$ from $\mathbf{Y}$. Starting from the probability for the observational time series conditioned on the parameters $P(\mathbf{Y}|\Lambda)$ and applying Bayes theorem to obtain $P(\Lambda|\mathbf{Y})$, the problem reduces to a maximum-likelihood estimation which can be iteratively solved to find local maxima via the expectation maximisation algorithm [*Dempster et al.*, 1979]. Having estimated Λ, the most likely regime sequence (the VP) can be calculated.

The simplest HMM analysis algorithm requires a gap-free time series. As by definition the time series considered have gaps (from the end of one night to the beginning of the next), the algorithm for estimating Λ has to be modified. We assume that variables in successive nights are independent, which is a reasonable approximation for problems in the nocturnal PBL: during the morning transition the presence of the residual layer helps the inversion break down, and the increased entrainment buoyancy flux from the residual layer in the mixed layer causes a faster PBL depth growth resetting turbulent profiles of the PBL almost every day [*Blay-Carreras et al.*, 2014]. We assume that any dependence of subsequent nights due to slowly evolving large-scale forcing is negligible. Mathematically, the new concatenated observation sequence ($\mathbf{Y} = \{\mathbf{OS_1}, \mathbf{OS_2}, \ldots, \mathbf{OS_n}\}$, where n is the number of nights, and $\mathbf{OS_n}$ the observational vector in each night) then satisfies

$$P(\mathbf{Y}|\Lambda) = \prod_{n=1}^{N} P(\mathbf{OS_n}|\Lambda) = \prod_{n=1}^{N} P_n. \tag{3.6}$$

The estimation of the parameters in the expectation-maximisation scheme for such an analysis is described in detail in *Rabiner* [1989].

4 Observable meteorological state variables containing information about regime occupation

Chapter Abstract

The atmospheric SBL can be classified into two distinct regimes: the wSBL with sustained turbulence and the vSBL with collapsed turbulence. An HMM analysis of the three-dimensional state variable space of dry static stability, mean wind speed and wind speed shear classifies the SBL into these two regimes at nine different tower sites. Not only Reynolds-averaged data but also turbulence state variables are separated in a physically meaningful way. Fluctuations of the vertical wind component are identified to be much smaller in the vSBL than in the wSBL. Such generic structures cannot be robustly obtained if more than two SBL regimes are characterized. In order to locate which meteorological state variables carry the information about regime occupation, the HMM analyses are repeated using various different state variable subsets. Turbulence state variables at any observed altitude hold the same information as the original set, but do not add any additional information. In contrast, both stratification and shear depend on surface information to capture regime transitions accurately. Use of exclusively near-surface information (i.e. only information in the bottom 10 m of the boundary layer) is sufficient for HMM analyses to capture important information about regime occupations. It follows that the commonly-measured 10 m wind speed is a good indicator of regime occupation.

4.1 Introduction

With the help of a similar HMM analysis as described in chapter 3, *Monahan et al.* [2015] clustered the three dimensional state variable space of nocturnal mean wind speed, wind speed shear, and stratification at the 213 m tower in Cabauw, Netherlands, into physically-reasonable wSBL and vSBL regimes. In section 4.2 we first investigate to what extent the results found by *Monahan et al.* [2015] can be generalised to other locations using long records from towers in a range of geographical and meteorological settings (chapter 2). We also assess if a third robust and physically-reasonable regime can be determined by an HMM analysis (section 4.3). Additionally, we present a detailed analysis of which meteorological state variables contain information about the regime occupation with particular focus on regime transitions in sections 4.4 to 4.8. Conclusions follow in section 4.9. This chapter is based on *Abraham and Monahan* [2018a].

4.2 Generic structure of the two-regime SBL

Monahan et al. [2015] have characterized the wSBL and vSBL using an HMM analysis with the three-dimensional state variable input of wind speed shear and mean wind speed (both between 200 and 10 m), and dry static stability (between 200 and 2 m) at Cabauw. We assess the generality of these results by repeating the analysis at different tower sites. A difficulty with direct comparison is the fact that the different datasets do not share a common set of measurements or measuring altitudes. To obtain the most direct comparison of results at the nine different tower sites, data at the heights of observation levels closest to the surface (as 10 m state variables are not available for all towers) and to 100 m are used. The exception to this approach is DomeC, where the SBL is so shallow that measurements at 1 and 10 m are used.

Inspection of three-dimensional scatterplots shows two evidently distinct regimes in the SBL at all sites (Figure 4.1, cf. also Figure 2 in *Monahan et al.* [2015]), corresponding to one branch with very strong static stability and weak winds and to a second branch with strong winds and very weak static stability. We interpret these branches as corresponding respectively to the vSBL and the wSBL. The evident two-regime structure is found independent of the underlying surface type, meteorological setting, or the complexity of the surrounding area.

The bivariate pdf estimates in Figure 4.1 show that Cabauw, Hamburg, Karlsruhe, Los Alamos, and DomeC exhibit hints of a threshold in vertical-mean wind speed separat-

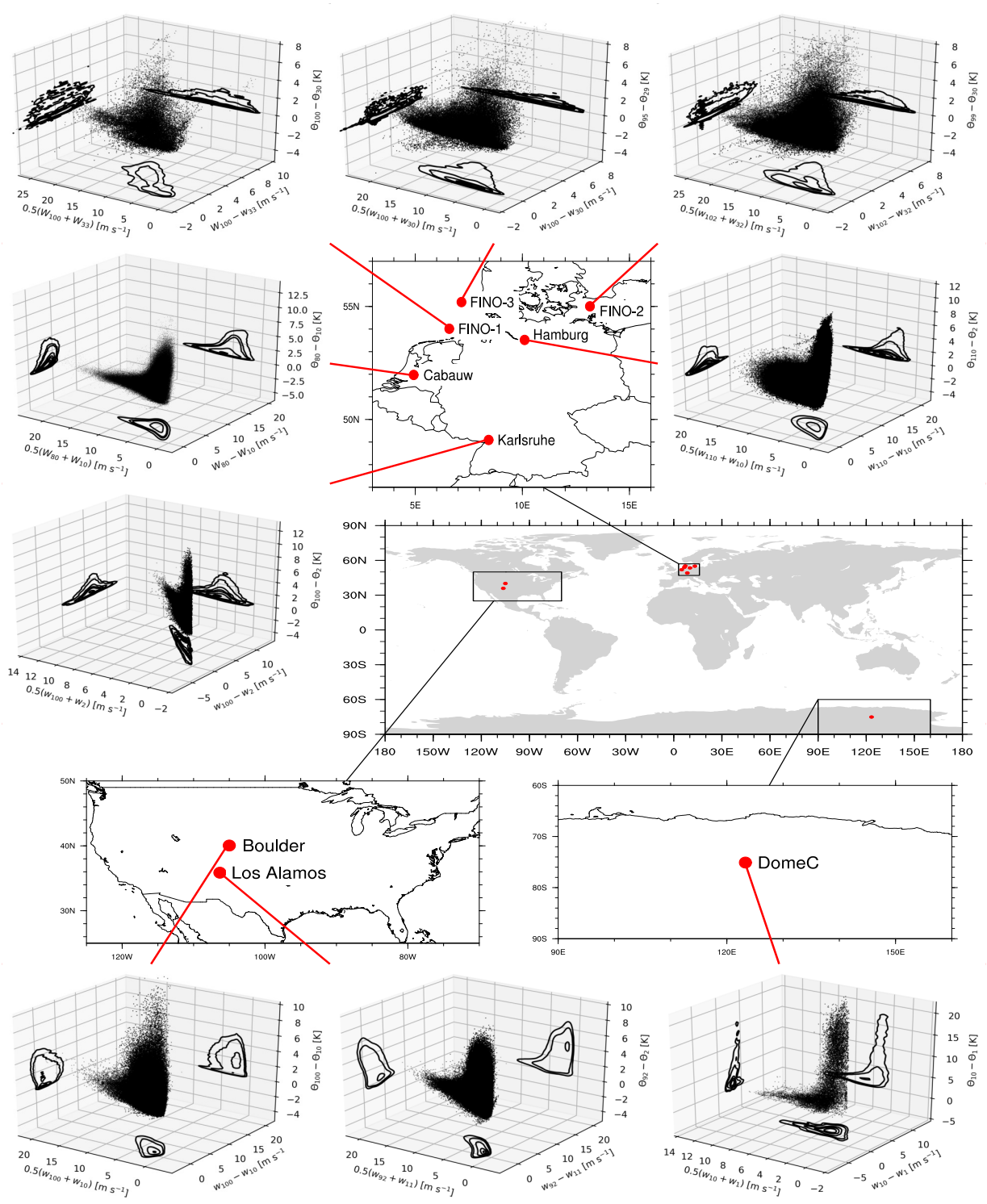

Figure 4.1: Scatterplot of nighttime three dimensional state variable space of mean wind speed ($0.5(W_h + W_{sfc})$, with h being closest to 100 m), scalar wind shear (ΔW), and static stability ($\Delta\Theta$) between observation levels closest to the surface and h for the nine different tower sites as depicted by the maps. The bivariate joint probability distributions (calculated with the multivariate kernel density estimation of *O'Brien et al.* [2014, 2016]) are shown for all data (black).

ing the wSBL and vSBL populations. Such a clear regime contrast with respect to the vertical-mean wind speed corresponds well with the concept of a U_{min} below which mechanically driven turbulent mixing becomes sufficiently weak that a strong inversion can form. The other sites show a much broader domain where strong stratification can be found for moderate wind speeds. The European midlatitude land-based stations agree both in scatterplot structure and inversion strength values. The similarity is likely due to comparable surface properties as these towers are built in cropped grasslands. As shown in the conceptual model of *van de Wiel et al.* [2017] the energetic coupling between the surface and the lower boundary layer strongly influences the inversion strength.

Interestingly, even though the Boulder and Los Alamos sites experience different meteorological processes from the European land-based sites (e.g mountain and valley breezes, katabatic winds, density currents etc.) which can substantially affect the local stability, the two-regime structure is evident. At Boulder the structures of the two regimes overlap considerably with a high density of data points in the region of low static stability and low wind speeds. The inversion strengths at both sites are similar to those at European sites.

At DomeC the coupling with the underlying ice surface leads to very strong inversion strengths. The thermal conductivity of the ice-snow surface is very low leading to strong radiative cooling at the surface enhanced by low water vapour amount in the atmosphere which results in efficient LWR energy loss to space. The values of the largest potential temperature differences the across first 10 m are more than twice what is measured at the midlatitude land-based stations across the bottom 100 m.

Evidently, the inversion strengths at ocean-based FINO sites are only about half as strong as over land. Over oceans surface cooling is ineffective due to the large surface heat capacity of the water which does not allow for inversions to build up. Instead, at these stations the vSBL is established exclusively by the advection of warm-air aloft (cf. chapters 5 and 6). The sites show broadly similar structures, in particular FINO-1 and FINO-3 which are both located in the North Sea. FINO-2 is surrounded by land masses in all compass directions and so is influenced particularly by advection of air aloft from the mainland [*Dörenkämper et al.*, 2015] which causes slightly stronger inversions than occur at FINO-1 and FINO-3. A direct comparison of the structures at these ocean-based stations to those of the land-based sites is further complicated by the fact that the observations start 30 m above the sea surface at low tide. Thus, the heights are variable above the surface due to tidal and surface wave variations. These variations contribute a kind of variability not seen at other stations and likely blur the two-regime structure.

The HMM analyses at all locations considered separate the vSBL branch with a strong

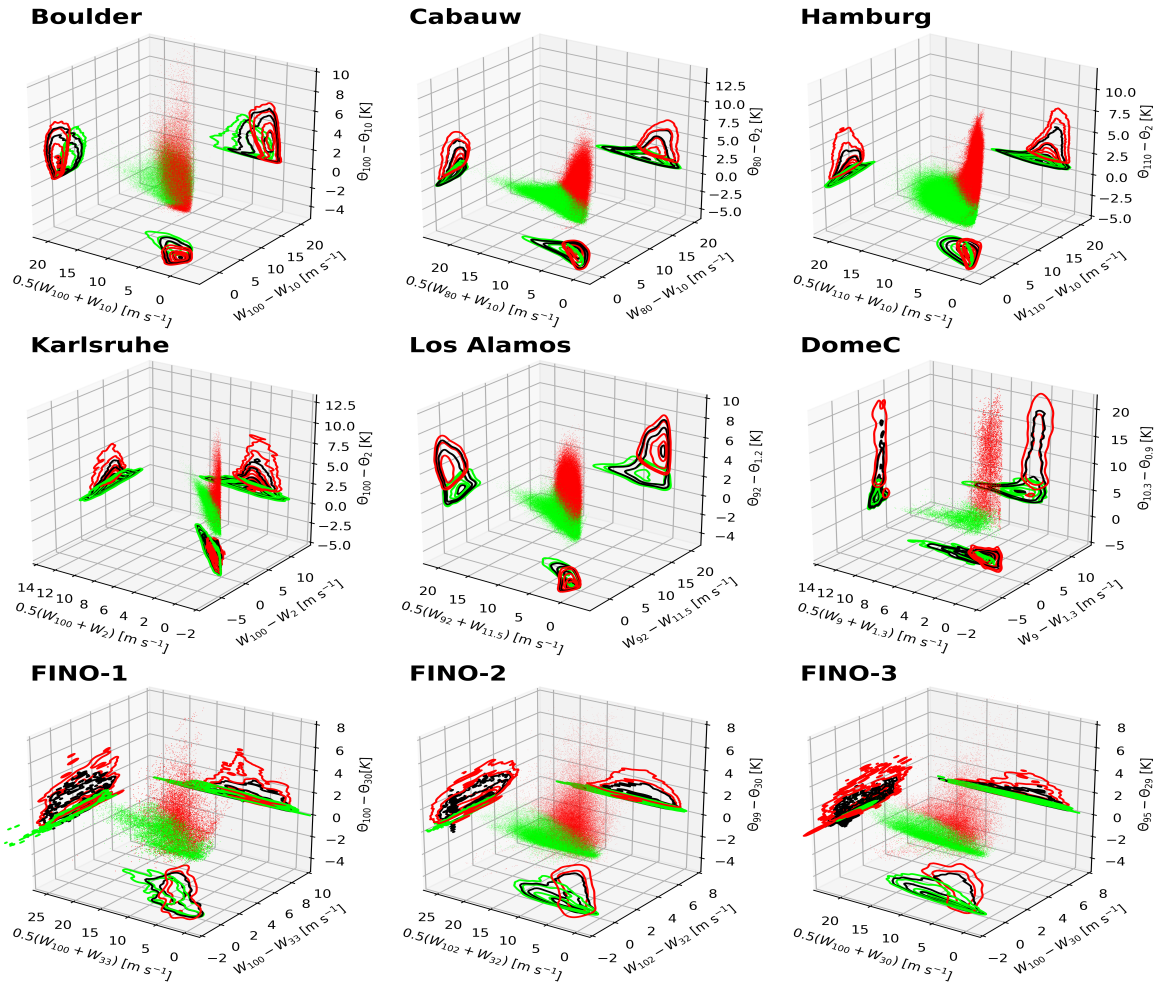

Figure 4.2: As in Figure 4.1 with the scatter conditioned on HMM regimes (wSBL in green and vSBL in red) for the nine different tower sites.

inversion and weak wind speeds from the wSBL branch (Figure 4.2). In this Figure, points in the scatter associated with the different regimes are represented by different colours. The HMM classification is particularly useful for distinguishing the SBL regimes in regions of the state space with low wind speeds and weak inversion strength where the regimes overlap (although this overlap may partially be an effect of the low-dimensional projection). The conditional joint pdfs of mean wind speed and inversion strength show no clear wind speed threshold separating the regimes. Similarly, a common stratification threshold is absent. Whilst at Cabauw, Hamburg, Los Alamos, and DomeC conditions of very weak dry static stability (smaller than 1 K) are never classified as being part of the vSBL, such a hard stratification threshold is not apparent at the other sites. The possibility exists that the populations would be clearly separated in a higher dimensional state variable space. However, we were unable to find such a space given the state variables provided.

In order to compare transition matrices between sites, we bring these matrices to a common time resolution of 10 minutes by the transformation $\mathbf{Q}^{10/T}$ with $T = 1$, 15, 30, for Hamburg (1 min resolution), Los Alamos (15 min resolution), and DomeC (30 min resolution), respectively. The two-regime $\mathbf{Q}$ values (Table 4.1) are similar for the different tower sites. We analyse the sensitivity of the VPs to $\mathbf{Q}$ in chapter 7.

The turbulence state variables are separated in a physically meaningful way by the HMM sequence of the Reynolds-averaged mean data (Figure 4.3). Large values of TKE are found in the wSBL while very low TKE values are found in the vSBL. Again, no clear wind speed threshold separates these states as for intermediate wind speeds the conditional joint pdfs of TKE and wind speed at 10 m (W_{10}) overlap. Across all tower sites, consideration of measurement altitudes other than illustrated in Figure 4.3 show qualitatively the same results in joint and conditional joint pdfs of wind speeds and TKE values.

Under very stable conditions vertical turbulent motions are suppressed causing the fluctuations in the vertical to be smaller than those in the horizontal. We measure this anisotropy by the ratio $3var(w)/(var(u)+var(v)+var(w))$, where u, v, and w are respectively zonal, meridional, and vertical wind components. This measure should take a value of 1 for isotropic turbulence. The isotropy measurements have smaller values near the surface than around 100 m (Figure 4.3, cf. columns 2 and 4). At Cabauw the pdfs of isotropy at the measuring altitudes at 5 and 100 m show a maximum and a shoulder naturally separated by conditioning on the two HMM regimes. This separation is more evident at higher altitudes. While hints of this behaviour are noticeable at the other stations, at Hamburg the conditional pdfs of the isotropy are not separated near the surface and only very weakly-separated at 110 m. At Los Alamos times of absent vertical fluctuations are

Table 4.1: Transition probability matrices for two ($\mathbf{Q}(K=2)$), and three ($\mathbf{Q}(K=3)$) hidden regimes in the HMM, using mean wind speeds, scalar wind shears, and static stabilities between the surface and observational levels nearest to 100 m (10 m at DomeC) for different tower sites. Stars denote the regime the transition is coming from. Transition probabilities at Hamburg, Los Alamos, and DomeC are transformed to a 10 minute time resolution, as described in the text.

Tower site	Observations	$\mathbf{Q}(K=2)$			$\mathbf{Q}(K=3)$			
Land-based tower sites								
Boulder	$\mathbf{Y}_{\text{Boulder}} = (W_{100}-W_{10}, 0.5(W_{100}+W_{10}), \Theta_{100}-\Theta_{10})$		*wSBL*	*vSBL*		*wSBL*	*tSBL*	*vSBL*
		wSBL*	0.9570	0.0430	*wSBL**	0.9687	0.0278	0.0035
		vSBL*	0.0268	0.9732	*tSBL**	0.0308	0.9324	0.0368
					vSBL*	0.0069	0.0387	0.9544
Cabauw	$\mathbf{Y}_{\text{Cabauw}} = (W_{80}-W_{10}, 0.5(W_{80}+W_{10}), \Theta_{80}-\Theta_{2})$		*wSBL*	*vSBL*		*wSBL*	*tSBL*	*vSBL*
		wSBL*	0.9834	0.0166	*wSBL**	0.9791	0.0209	0.0000
		vSBL*	0.0190	0.9810	*tSBL**	0.0148	0.9620	0.0232
					vSBL*	0.0025	0.0248	0.9727
Hamburg	$\mathbf{Y}_{\text{Hamburg}} = (W_{110}-W_{10}, 0.5(W_{110}+W_{10}), \Theta_{110}-\Theta_{2})$		*wSBL*	*vSBL*		*wSBL*	*tSBL*	*vSBL*
		wSBL*	0.9786	0.0214	*wSBL**	0.9559	0.0435	0.0006
		vSBL*	0.0389	0.9611	*tSBL**	0.0464	0.9234	0.0302
					vSBL*	0.0075	0.0361	0.9564
Karlsruhe	$\mathbf{Y}_{\text{Karlsruhe}} = (W_{100}-W_{2}, 0.5(W_{100}+W_{2}), \Theta_{100}-\Theta_{2})$		*wSBL*	*vSBL*		*wSBL*	*tSBL*	*vSBL*
		wSBL*	0.9782	0.0218	*wSBL**	0.9708	0.0290	0.0002
		vSBL*	0.0457	0.9543	*tSBL**	0.0197	0.9483	0.0320
					vSBL*	0.0069	0.0578	0.9353
Los Alamos	$\mathbf{Y}_{\text{LosAlamos}} = (W_{92}-W_{11.5}, 0.5(W_{92}+W_{11.5}), \Theta_{92}-\Theta_{1.2})$		*wSBL*	*vSBL*		*wSBL*	*tSBL*	*vSBL*
		wSBL*	0.9662	0.0338	*wSBL**	0.9770	0.0091	0.0139
		vSBL*	0.0231	0.9769	*tSBL**	0.0153	0.9534	0.0313
					vSBL*	0.0044	0.0127	0.9829
Ice-based tower sites								
DomeC	$\mathbf{Y}_{\text{DomeC}} = (W_{9}-W_{1.3}, 0.5(W_{9}+W_{1.3}), \Theta_{10.3}-\Theta_{0.9})$		*wSBL*	*vSBL*		*wSBL*	*tSBL*	*vSBL*
		wSBL*	0.9916	0.0084	*wSBL**	0.9897	0.0094	0.0009
		vSBL*	0.0076	0.9924	*tSBL**	0.0109	0.9770	0.0121
					vSBL*	0.0017	0.0120	0.9863
Ocean-based tower sites								
FINO-1	$\mathbf{Y}_{\text{FINO}-1} = (W_{100}-W_{33}, 0.5(W_{100}+W_{33}), \Theta_{100}-\Theta_{30})$		*wSBL*	*vSBL*		*wSBL*	*tSBL*	*vSBL*
		wSBL*	0.9833	0.0167	*wSBL**	0.9777	0.0104	0.0119
		vSBL*	0.0232	0.9768	*tSBL**	0.0111	0.9743	0.0146
					vSBL*	0.0097	0.0198	0.9705
FINO-2	$\mathbf{Y}_{\text{FINO}-2} = (W_{102}-W_{32}, 0.5(W_{102}+W_{33}), \Theta_{99}-\Theta_{30})$		*wSBL*	*vSBL*		*wSBL*	*tSBL*	*vSBL*
		wSBL*	0.9908	0.0092	*wSBL**	0.9674	0.0163	0.0162
		vSBL*	0.0138	0.9862	*tSBL**	0.0101	0.9874	0.0025
					vSBL*	0.0184	0.0023	0.9793
FINO-3	$\mathbf{Y}_{\text{FINO}-3} = (W_{100}-W_{30}, 0.5(W_{100}+W_{30}), \Theta_{95}-\Theta_{29})$		*wSBL*	*vSBL*		*wSBL*	*tSBL*	*vSBL*
		wSBL*	0.9918	0.0082	*wSBL**	0.9734	0.0183	0.0083
		vSBL*	0.0157	0.9843	*tSBL**	0.0152	0.9832	0.0016
					vSBL*	0.0163	0.0029	0.9808

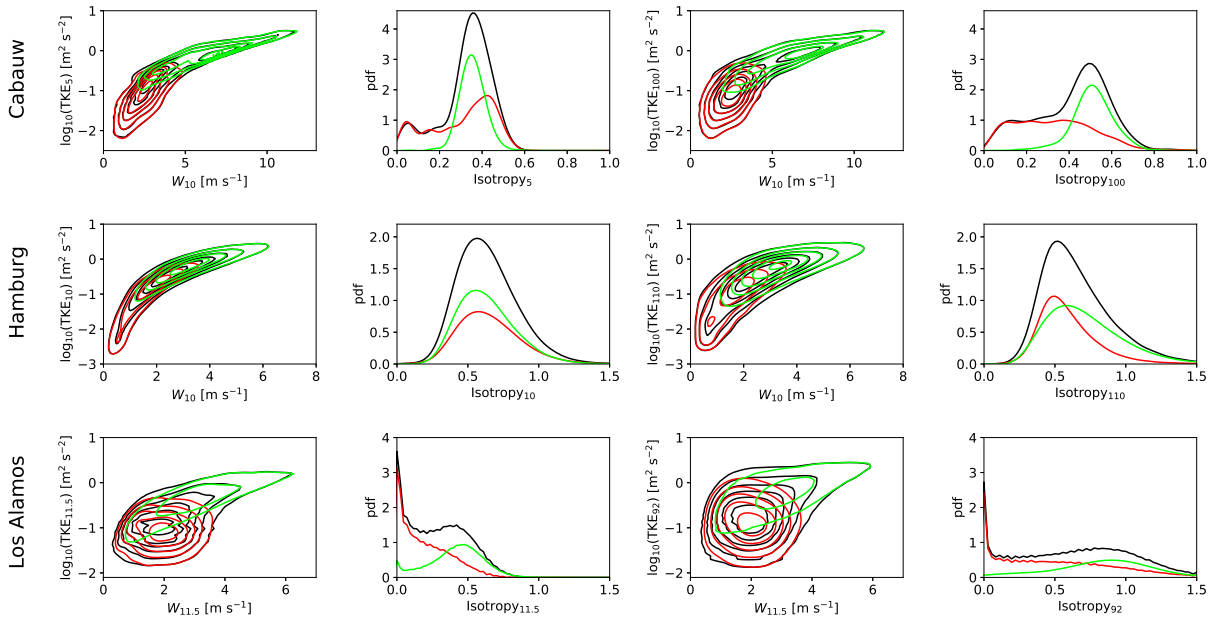

Figure 4.3: Joint probability density functions of 10 m wind speeds and $\log_{10}(\text{TKE})$ values near the surface (first column) and near 100 m (third column) and probability density function of the isotropy $(3var(w)/(var(u) + var(v) + var(w)))$ of turbulence near the surface (second column) and 100 m (fourth column) at Cabauw, Hamburg, and Los Alamos. Distributions using all data are shown in black, while distributions conditioned on wSBL and vSBL are respectively shown in green and red. All pdfs are calculated with the multivariate kernel density estimation by *O'Brien et al.* [2014, 2016].

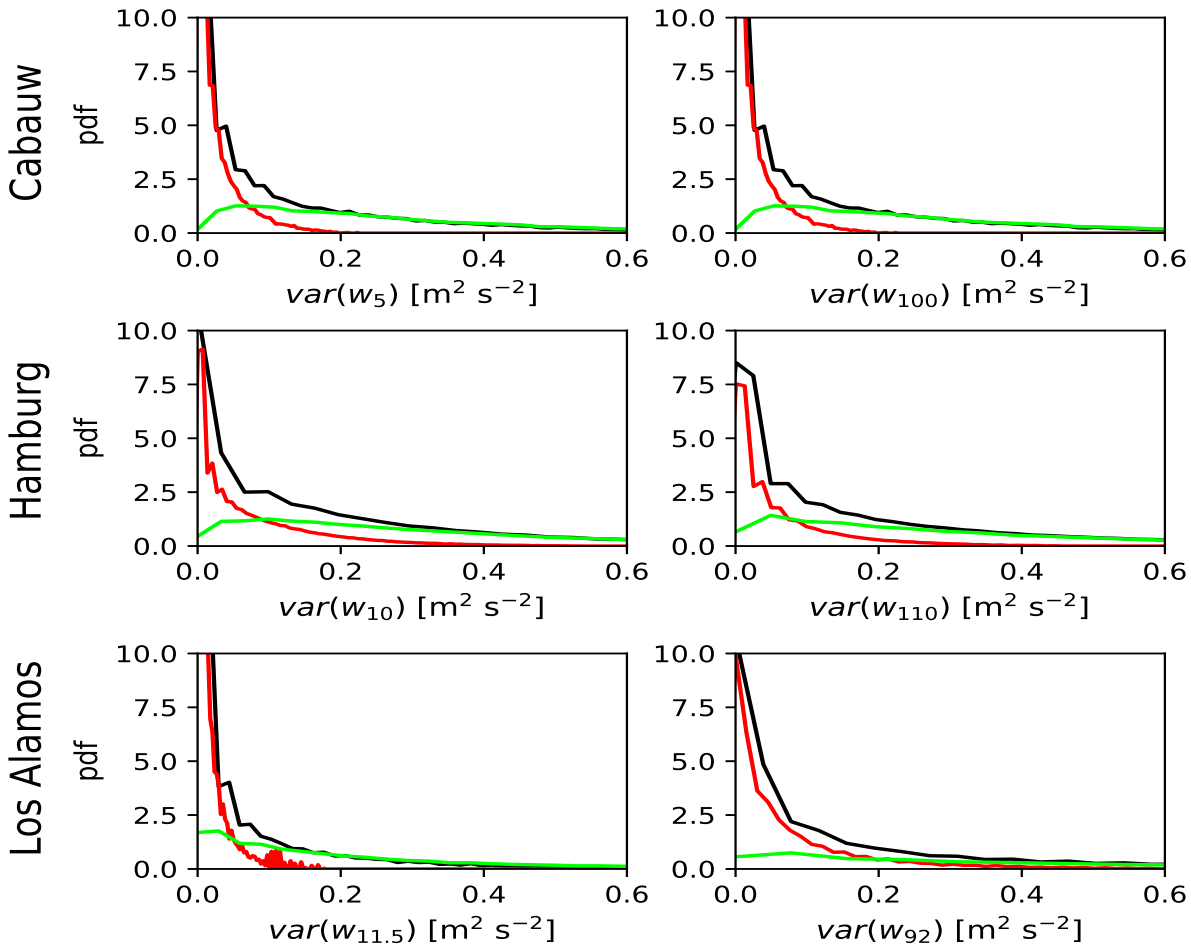

Figure 4.4: Probability density functions of the variance of the vertical wind component w near the surface (first column) and near 100 m (second column) for all data (black), wSBL (green), and vSBL (red) at Cabauw, Hamburg, and Los Alamos. All pdfs are calculated with the multivariate kernel density estimation by *O'Brien et al.* [2014, 2016].

exclusively affiliated with the vSBL, although the conditional pdfs overlap substantially.

Although this measure of turbulent anisotropy is not clearly separated between regimes, the fluctuations in the w-component are evidently-separated into the vSBL and wSBL across all stations and all measurement heights (Figure 4.4). In the vSBL vertical fluctuations are very weak with probability concentrated near zero. Vertical wind fluctuations classified to be in the wSBL, on the other hand, populate solely the long tails of the distributions.

4.3 The three-regime SBL

Whilst at least two-regimes of SBL behaviour are evident from the two clear branches in scatterplots of the three-dimensional state variable space of mean wind speed, wind speed shear, and stratification, no obvious third regime is apparent (Figure 4.5, column one). The turbulence data also lack clear evidence of more than two regimes (Figure 4.3). In particular, there is no observational evidence of a distinct population corresponding to strong turbulent bursts under weak wind conditions as hypothesised by *Sun et al.* [2012].

To further investigate if there is robust evidence of a third regime in the data, the HMM analysis is repeated using three hidden regimes. We find that the structure of the three regimes in the three-dimensional state variable space of wind speed shear, mean wind speed, and dry static stability is less evidently meaningful than regime structures in the two-regime SBL. First, in contrast to the two-regime SBL, no robust structure identifying a third regime appears across the tower sites considered (Figure 4.5, column 4). At Cabauw and Hamburg, for instance, the third regime sits at the hinge of the vSBL and wSBL and consists of points from both the two regimes of the two-regime classification. For Boulder, Los Alamos, and DomeC the two-regime vSBL is cut in half with the third regime populating the weaker stratification values. At Karlsruhe, the wSBL as classified by the two-regime SBL is divided into two regimes by a third regime. The ocean-based stations show a completely different three-regime SBL structure. While the third regime at the land- and ice-based stations populates the space of weak stratification combined with weak winds, at ocean-based sites it corresponds to very weak to neutral stratification across a broad range of wind speeds. No consistent three-regime structure is evident across sites. The joint pdfs of TKE and surface winds exhibit no robust structure in a three-regime SBL. The three regimes overlap for intermediate values of TKE and wind speed, without a clear separation (not shown).

If we interpret the third regime as the tSBL regime separating the wSBL from the vSBL

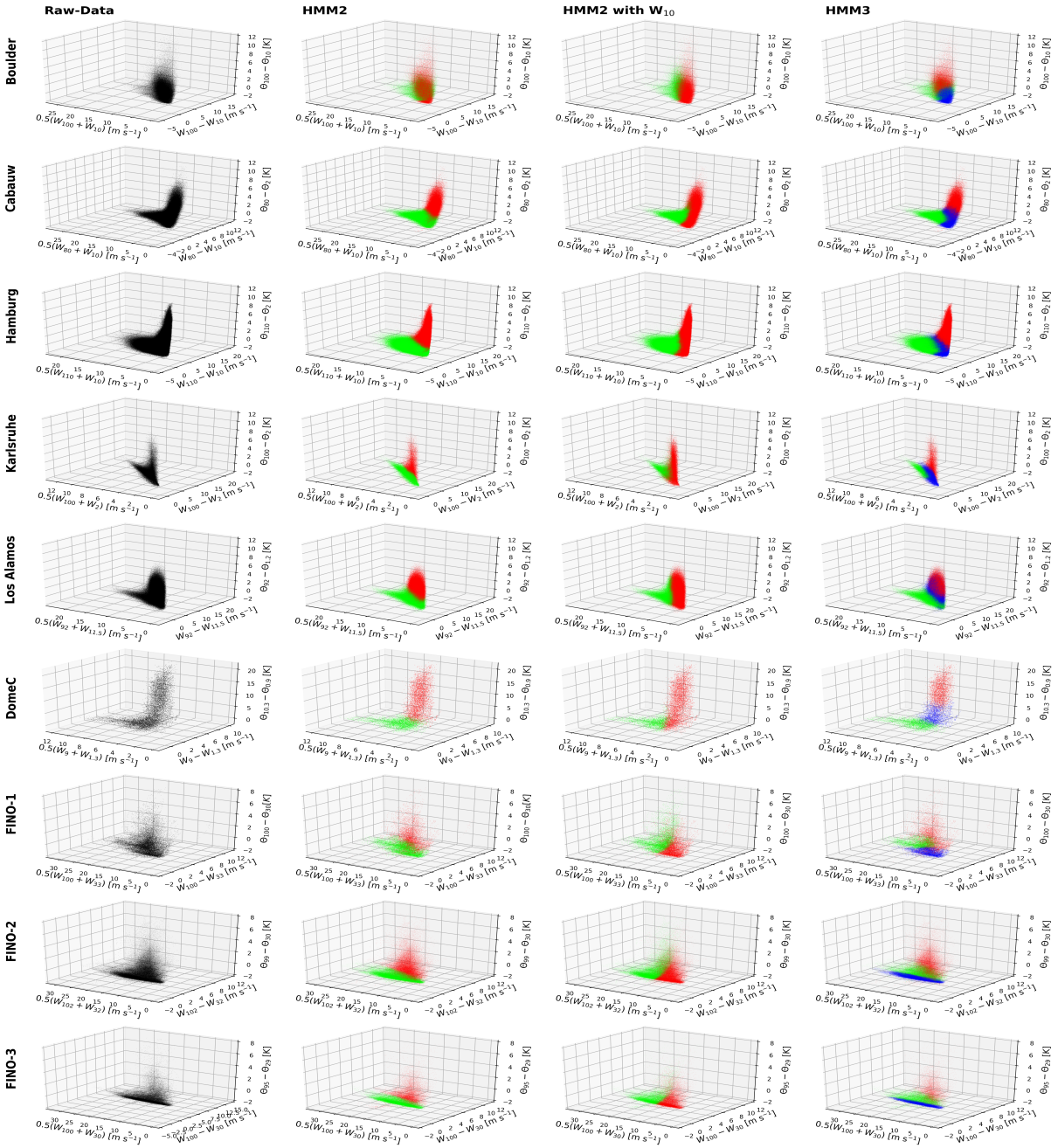

Figure 4.5: Scatterplots of the nighttime three dimensional state variable space of mean wind speed ($0.5(W_h + W_{sfc})$, with h being closest to 100 m), scalar wind shear (ΔW), and static stability ($\Delta\Theta$) between observation levels closest to the surface and to h for the nine different tower sites ordered from top to bottom by land-based, ice-based, ocean-based stations. First column: the unclassified nighttime data (black). Second column: the data as clustered into the wSBL (green) and vSBL (red) by the HMM analysis with two hidden regimes for the three-dimensional state variable space. Third column: the data as clustered into the wSBL (green) and vSBL (red) by the HMM analysis with two hidden regimes for the one-dimensional state variable space of the observation level closest to 10 m using the WHMM. Fourth column: data as clustered into the wSBL (green), tSBL (blue), and vSBL (red) by the HMM analysis with three hidden regimes for the three-dimensional state variable space.

[*Mahrt*, 1998b, 2014; *Ansorge and Mellado*, 2014], it is natural to expect that the system must pass through the tSBL in the transition from the wSBL into the vSBL. Rather than an abrupt change, this transition is expected to be a gradually evolving process in which the gradual strengthening of the inversion suppresses vertical fluxes which in turn further increases the inversion strength further [*van Hooijdonk et al.*, 2017b]. In such a framework the probability of a regime transition from the wSBL to the vSBL ($P(\text{wSBL} \rightarrow \text{vSBL})$) would be expected to be zero and the regime persistence (transition probability to remain in the same regime) of the tSBL ($P(\text{tSBL} \rightarrow \text{tSBL})$) should be lower than those of $P(\text{wSBL} \rightarrow \text{wSBL})$ or $P(\text{vSBL} \rightarrow \text{vSBL})$. On the other hand, nonzero values of $P(\text{vSBL} \rightarrow \text{wSBL})$, interpreted as the sudden recovery of sustained turbulence (due to strong intermittent events or changes in external forcing), are consistent with this picture. The stochastic matrix at Cabauw shows such a structure (Table 4.1, column 4). At all other tower sites, however, $P(\text{wSBL} \rightarrow \text{vSBL})$ values are larger than zero. Even at the original time resolution of 1 minute, which should be short enough to capture all transitions, $P(\text{wSBL} \rightarrow \text{vSBL})$ is larger than zero at Hamburg (corresponding to approximately two events per year). Moreover, at Karlsruhe and the ocean-based sites, $P(\text{tSBL} \rightarrow \text{tSBL})$ is larger than $P(\text{vSBL} \rightarrow \text{vSBL})$. A simple exchange of these two regimes (as the HMM analysis identifies the regimes but the interpretation is ours) does not compensate this result because under such conditions the tSBL would be populated by larger inversion strengths than the vSBL. At ocean-based stations the tSBL is the most persistent regime of all. For those reasons the third regime as classified by the HMM is not in general naturally interpreted as a tSBL in the sense of *Mahrt* [1998b, 2014] or *Ansorge and Mellado* [2014].

Furthermore, and in marked contrast to the two-regime HMM results, composites of state variables across times of transitions (discussed in detail in chapter 6) do not show systematic behaviour distinguishing the tSBL from the vSBL (at Cabauw, Hamburg, and Los Alamos, those sites with turbulence records). While the two-regime SBL shows a systematic and substantial reduction in TKE at times of collapse, no such structure is evident for the three-regime SBL.

Finally, the structure of the three-regime SBL is not very robust if other observational levels are used to define the three-dimensional state space for the HMM analysis. While structures of the two-regime analyses at the different tower sites do not change qualitatively using different observational levels (as discussed in the next section), substantial changes in the regime structure result when a three-regime model is used (not shown). We conclude that for three hidden regimes no generic or meaningful structure across the sites considered can be found using the HMM analysis. A similar result was found when increasing the number of hidden states beyond three. As a result, the rest of our analysis will focus on

the two-regime model.

4.4 Reference state variable set for the HMM analysis

The HMM analysis presented above shows that the three state variables of stratification, mean wind speed, and wind speed shear produce a two-regime classification of the SBL that is robust across tower sites. We will now investigate which single variable or combinations of variables carry the majority of SBL regime occupation information. To do this, we must first establish a reference state variable set against which HMM analyses using other input can be compared. It is expected that HMM analyses using different sets of state variables will lead to different VPs, and we do not have an external reference for the 'true' sequence of regime occupation. Hence, our reference state variables from the observational data available must be defined empirically, guided by physical reasoning.

As discussed above, the shear, stratification, and mean wind are natural variables to describe the turbulence energy budget and therefore the state of the boundary layer [e.g *van de Wiel et al.*, 2012a,b, 2017; *van Hooijdonk et al.*, 2015; *Monahan et al.*, 2015]. However, the possibility exists that essential information regarding the VP might exist in a lower-dimensional subspace of the original variables, or in other variables. Increasing the dimensionality of the input vector, on the other hand, might include more information about the SBL structure relevant to regime affiliation, and a more accurate VP estimate. For an arbitrarily long time series, the more relevant information the HMM is provided, the more accurate the VP should be. However, consideration of more complex models for time series of fixed duration also results in an increasing influence of sampling variability on the estimation of the HMM parameters. In the following we analyse the dependence of HMM regime structure on input data using the Cabauw dataset because its long and gap-free character at all measurement heights allows for a thorough analysis of various combinations of meteorological state variables. We find qualitatively similar results at the other tower sites. The reference variable set at Cabauw is found to be $\mathbf{Y_{ref}} = (W_{200} - W_{10}, 0.5(W_{200} + W_{10}), \Theta_{200} - \Theta_2)$, the same set as was used in *Monahan et al.* [2015]. Reference models for the other tower sites are determined following the same approach described below and are listed in Table 4.4.

As our first criterion for determining the reference model we consider VP robustness, defined as how well the HMM analysis of random daily subsamples of the time series reproduce the VP of the full dataset. Secondly, we assess the robustness of $\mathbf{Q}$ obtained from subsamples. Finally, we assess the robustness of the timing of transitions between the

wSBL and vSBL as well as how well nights remaining in one regime throughout the whole night are modelled. At Cabauw, for instance, we search for the simultaneity of transitions in a $\pm$ 30 minute time window. This time window is selected based on the maximum time lag between the lower and upper parts of the observed PBL to experience the impacts of a transition.

We found that increasing the state variable space to include variables such as wind speed and stratification data at all available levels, shear values of the along and across wind components, or surface pressures lead to essentially the same results as $\mathbf{Y_{ref}}$. Reducing the number of state variables, on the other hand, can result in to substantial changes in $\mathbf{Q}$ and the VP.

To justify the focus on shear and stratification as proxies for the TKE budget, we investigate the HMM structure obtained from the turbulence data available at Cabauw, Hamburg, and Los Alamos. We find that at each location an HMM analysis with $var(w)$ (as an estimate for the TKE which is not contaminated by non-turbulent horizontal motions) using values at two measurement heights estimates almost exactly the same VP and $\mathbf{Q}$ as the reference HMM. The fact that essentially the same information can be retrieved using the Reynolds-averaged mean values which are more widely available than turbulence state variables further justifies the choice of $\mathbf{Y_{ref}}$. We note in passing that the fact that the TKE and mean state data carry the same information suggests that vertical turbulent fluxes and the mean flow state are usually close to equilibrium on the timescales of the data considered.

4.5 Regime occupation information at different altitudes of the three-dimensional state variables

Having defined the reference models, we now investigate the Cabauw regime paths relative to those of the reference state variable spaces using data at varying measurement heights in order to assess where regime information resides. Preliminary analyses indicated the importance of always including surface values in these calculations. Therefore, we choose the HMM inputs to be $\mathbf{Y_{obs}} = (W_{h_W} - W_{10}, 0.5(W_{h_W} + W_{10}), \Theta_{h_\Theta} - \Theta_2)$, where h_W and h_Θ are the upper altitudes of wind speed shear and stratification calculations.

Changing the values of h_Θ, h_W can result in substantially different VPs from that of the reference (Figure 4.6). We find that h_Θ must be above 80 m in order to produce VP

Table 4.2: Information about the reference state variable sets and the reference transition probability ($\mathbf{Q_{ref}}$) of HMM analyses at land- and ice-based tower sites as shown in Tables 2.1 and 2.2. Starting regimes for the transition probabilities are denoted with a star. HMM analyses of the surface winds with Gaussian mixture parametric pdfs (G) or Weibull parametric pdfs (W) are compared to the reference stating the agreement of Viterbi paths as compared to the reference (cons. [%]) as well as the accuracy of the wSBL to vSBL (coll. acc. [%]) and vSBL to wSBL (recov. acc. [%]), consistency of nights remaining exclusively in the wSBL (wSBL cons. [%]) and vSBL (vSBL cons. [%]), and the transition probability anomalies compared to $\mathbf{Q_{ref}}$. Transition probabilities at Hamburg, Los Alamos, and DomeC are transformed to a 10 minute time resolution.

Tower site	Reference state variables	$\mathbf{Q_{ref}}$(K=2)		
Land-based tower sites				
Boulder	$\mathbf{Y_{ref}} = (W_{100} - W_{10}, 0.5(W_{100} + W_{10}), \Theta_{100} - \Theta_{10})$		$wSBL$	$vSBL$
		$wSBL^\star$	0.9570	0.0430
		$vSBL^\star$	0.0268	0.9732
Cabauw	$\mathbf{Y_{ref}} = (W_{200} - W_{10}, 0.5(W_{200} + W_{10}), \Theta_{200} - \Theta_{2})$		$wSBL$	$vSBL$
		$wSBL^\star$	0.9850	0.0150
		$vSBL^\star$	0.0175	0.9825
Hamburg	$\mathbf{Y_{ref}} = (W_{250} - W_{10}, 0.5(W_{250} + W_{10}), \Theta_{250} - \Theta_{2})$		$wSBL$	$vSBL$
		$wSBL^\star$	0.9776	0.0224
		$vSBL^\star$	0.0312	0.9688
Karlsruhe	$\mathbf{Y_{ref}} = (W_{200} - W_{2}, 0.5(W_{200} + W_{2}), \Theta_{200} - \Theta_{2})$		$wSBL$	$vSBL$
		$wSBL^\star$	0.9809	0.0191
		$vSBL^\star$	0.0339	0.9661
Los Alamos	$\mathbf{Y_{ref}} = (W_{92} - W_{11.5}, 0.5(W_{92} + W_{11.5}), \Theta_{92} - \Theta_{1.2})$		$wSBL$	$vSBL$
		$wSBL^\star$	0.9662	0.0338
		$vSBL^\star$	0.0231	0.9769
Ice-based tower sites				
DomeC	$\mathbf{Y_{ref}} = (W_{9} - W_{1.3}, 0.5(W_{9} + W_{1.3}), \Theta_{10.3} - \Theta_{0.9})$		$wSBL$	$vSBL$
		$wSBL^\star$	0.9916	0.0084
		$vSBL^\star$	0.0076	0.9924
Ocean-based tower sites				
FINO-1	$\mathbf{Y_{ref}} = (W_{100} - W_{33}, 0.5(W_{100} + W_{33}), \Theta_{100} - \Theta_{30})$		$wSBL$	$vSBL$
		$wSBL^\star$	0.9833	0.0167
		$vSBL^\star$	0.0232	0.9768
FINO-2	$\mathbf{Y_{ref}} = (W_{102} - W_{32}, 0.5(W_{102} + W_{33}), \Theta_{99} - \Theta_{30})$		$wSBL$	$vSBL$
		$wSBL^\star$	0.9908	0.0092
		$vSBL^\star$	0.0138	0.9862
FINO-3	$\mathbf{Y_{ref}} = (W_{100} - W_{30}, 0.5(W_{100} + W_{30}), \Theta_{95} - \Theta_{29})$		$wSBL$	$vSBL$
		$wSBL^\star$	0.9918	0.0082
		$vSBL^\star$	0.0157	0.9843

consistencies of more than 90 % and to capture more than 70 % of the turbulence collapse and recovery events. If only stratification information below 80 m is used, VP and transition consistencies are smaller irrespective of the wind information provided. Nights remaining in the wSBL throughout the whole night are well-captured by all combinations of h_θ and h_W information, demonstrating how prevalent the signal is in all parts of the observed PBL in these usually strong wind conditions (cf. chapter 5). Nights classified as being exclusively in the vSBL, however, are not well-captured using only information below 140 m. With lower altitudes of h_Θ, h_W the HMM estimates transitions towards the vSBL at later times than the reference model. A possible explanation could be that under low wind conditions combined with warm-air advection aloft, conditions known to appear at Cabauw [*Optis and Monahan*, 2017], the regime transition diagnosed using near-surface information does not account for the advective enhancement of stratification and the transition to the vSBL is delayed.

In general, larger values of h_Θ, h_W result in a larger contrast in stratification and shear between the two regimes and a more accurate estimate of the VP. In particular, for h_W above 40 m improvements of the accuracy of the timing of the transitions are evident. This improvement might be related to the fact that in the two regimes the lower and upper levels show opposite wind speed tendencies in times of a transition as the flow changes between coupled and uncoupled flow. This mechanism is consistent with the existence of a level with minimal wind speed variability, a so called crossing point height. At Cabauw this height has been suggested to be in the range of 20 to 50 m [*van de Wiel et al.*, 2012a], consistent with the improvement in our results when h_W is above 40 m.

The importance of using h_Θ above 80 m can also be seen in the difference between stochastic matrices $\mathbf{Q_{obs}}$ and $\mathbf{Q_{ref}}$ for $P(\text{wSBL} \rightarrow \text{wSBL})$ (Figure 4.6, bottom panels). These differences are substantially smaller if h_Θ is larger than 80 m. This result is presumably due to the larger potential temperature contrast over larger differences in altitude. Even though near-surface temperature gradients in the established wSBL or vSBL differ substantially, at the times of transitions a strong difference in the near-surface temperature profile is not evident (cf. chapter 6).

In general, the differences $\mathbf{Q_{obs}} - \mathbf{Q_{ref}}$ reveal that use of wind and potential temperature information below 200 m results in a less persistent vSBL and a generally more persistent wSBL, consistent with the differences in the accuracy of the classification of nights without transitions. Absolute values of differences in $P(\text{wSBL} \rightarrow \text{vSBL})$ between $\mathbf{Q_{obs}}$ and $\mathbf{Q_{ref}}$ are mostly smaller than those of $P(\text{vBSL} \rightarrow \text{wSBL})$, so transitions leading to turbulence collapse are better captured using lower-altitude data (relative to the reference model)

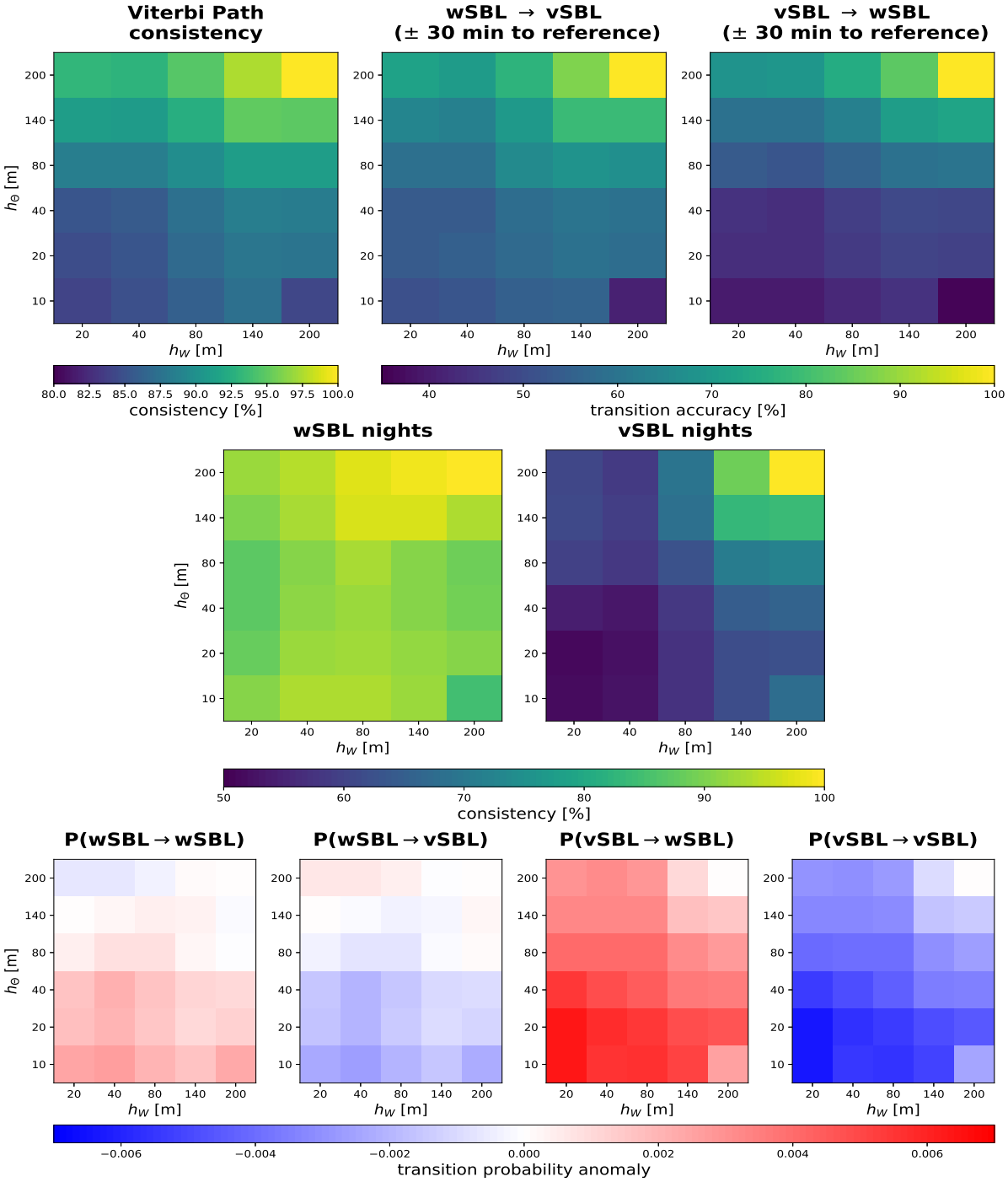

Figure 4.6: Comparison of HMM regime sequence paths of the three dimensional state variable space of mean wind speed, scalar wind shear between different heights (h_W), and static stability between different heights (h_Θ) and the surface with the regime sequence path from the HMM analysis of $\mathbf{Y_{ref}} = (0.5(W_{200}+W_{10}), W_{200}-W_{10}, \Theta_{200}-\Theta_2)$ at Cabauw. First row from left to right: Consistency of the Viterbi paths, accuracy of the wSBL to vSBL transitions (turbulence collapse), and accuracy of the vSBL to wSBL transitions (turbulence recovery). Second row: Consistency of nights remaining exclusively in the wSBL (left) and vSBL (right). Third row from left to right: Transition probability anomalies compared to the reference.

than are turbulence recovery transitions.

4.6 Regime occupation information in reference state variable subspaces

We now investigate lower-dimensional state variable sets in order to understand how much information is contained in the wind and potential temperature information separately. We conduct HMM analyses defining wind shear ($\mathbf{Y_{obs}} = W_{h(x)} - W_{h(y)}$; results below the diagonal in Figure 4.7) and stratification ($\mathbf{Y_{obs}} = \Theta_{h(y)} - \Theta_{h(x)}$; results above the diagonal in Figure 4.7) as well as analyses using one-dimensional state variables spaces of wind speed ($\mathbf{Y_{obs}} = W_{h(x)}$; triangles with $h(x) = h(y)$ below the diagonal in Figure 4.7) and potential temperature ($\mathbf{Y_{obs}} = \Theta_{h(x)}$; triangles with $h(x) = h(y)$ above the diagonal in Figure 4.7).

The best agreement with the reference VP using only one of stratification or flow information is obtained using stratification for altitude ranges spanning the 40 m level or shear information below 40 m (Figure 4.7, upper row). Agreement in VP of these subdimensional state variable spaces ranges between 80-95 %. The stratification information is sufficient to capture 60-70 % of the turbulence collapse or recovery events. Flow measures best capture the timing of transitions when the lower level considered is 10 m. Evidently, the performance using shear information alone is not as good as using stratification information alone.

Stratification information is sufficient to identify nights that are exclusively in the wSBL, whereas near-surface flow information models the vSBL nights without transitions with almost a 100 % accuracy, demonstrating that nights remaining exclusively in the vSBL show prevalent low wind conditions which do not lead to substantial shear production of TKE (cf. section 4.5 and chapter 5). These results again show that clear thresholds between regimes in one state variable are absent: nights staying exclusively in the wSBL can display a broad range of wind speed values and a small range of stratifications. Contrary, wind speeds are low and steady in nights staying exclusively in the vSBL while stratification can vary over a broad range of values (cf. chapter 5).

Using single-level wind speeds in the HMM analysis with Gaussian mixture parametric pdfs, best agreement with the reference is found for wind speeds at 10 m. Interestingly, including flow information at additional levels other than 10 m does not substantially improve the accuracy of the transitions (not shown). We interpret this result as being a

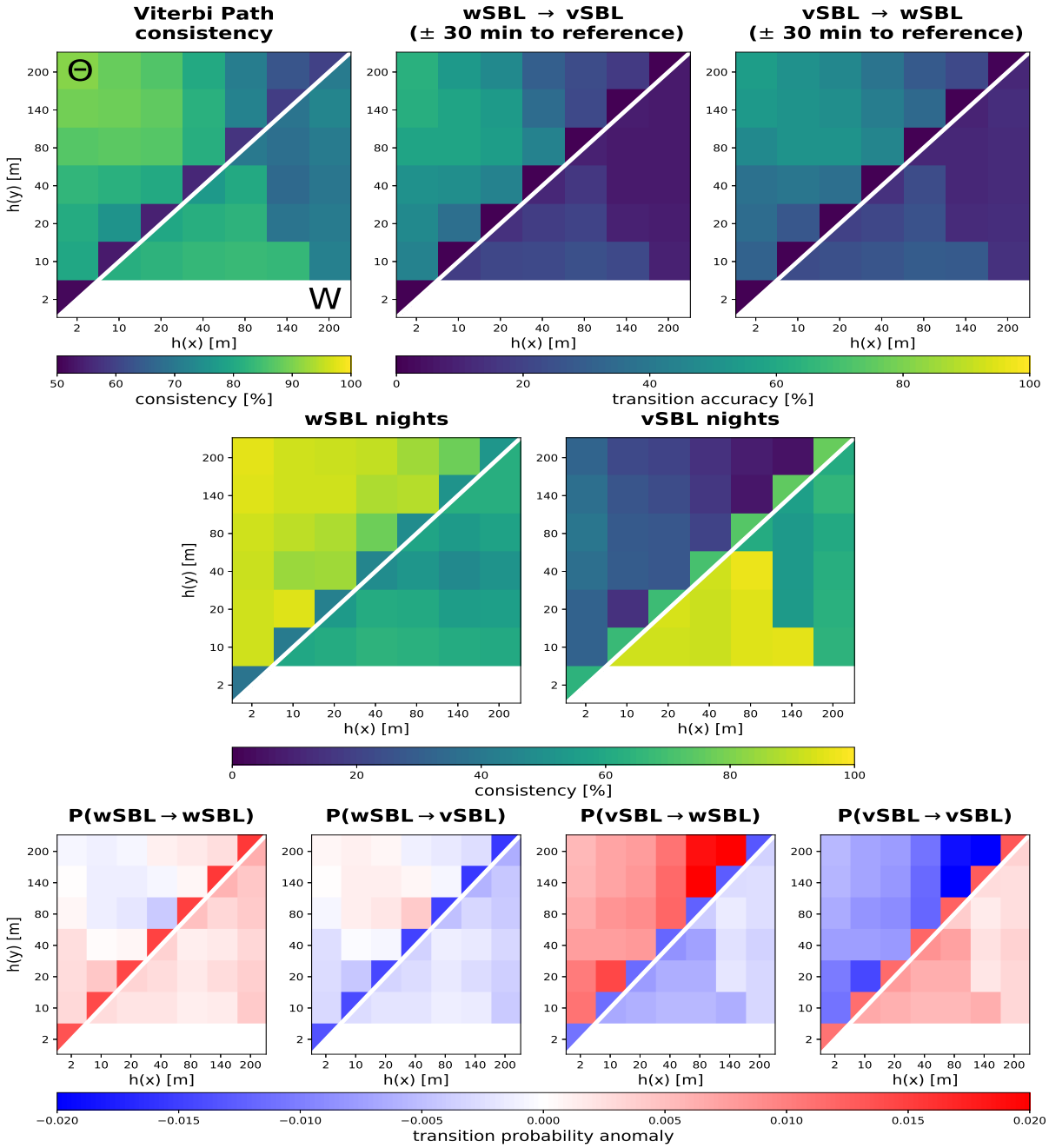

Figure 4.7: Comparison of the HMM regime sequence paths of lower dimensional state variable spaces with HMM regime sequence paths of $\mathbf{Y_{ref}} = (0.5(W_{200} + W_{10}), W_{200} - W_{10}, \Theta_{200} - \Theta_2)$ at Cabauw. Above the diagonal line: stratification calculated as $\Theta_{h(y)} - \Theta_{h(x)}$; below the diagonal line: shear calculated a $W_{h(x)} - W_{h(y)}$; triangles above the diagonal line: one-dimensional temperature; triangles below the diagonal line: one-dimensional wind speed. First row from left to right: Consistency of the Viterbi paths, accuracy of the wSBL to vSBL transitions (turbulence collapse), and accuracy of the vSBL to wSBL transitions (turbulence recovery). Second row: Consistency of nights remaining exclusively in the wSBL (left) and vSBL (right). Third row from left to right: Transition probability anomalies compared to the reference.

consequence of the fact that the largest changes in wind speed during regime transitions occur near the surface.

Unsurprisingly, HMM analyses of potential temperatures at single altitudes carry essentially no regime information and the agreement of the VP is just slightly above the value of 50 % expected for a completely random VP. Correspondingly, the accuracy of the transitions is about 0 % and probabilities of transitions are much smaller than the reference model.

The diagonal elements of $\mathbf{Q_{obs}}$ (characterising the persistence of the wSBL and vSBL) are overestimated using flow information alone (Figure 4.7, bottom row). Consistent with the discussion above, $P(\text{wSBL} \rightarrow \text{wSBL})$ values are underestimated when only stratification information spanning the 40 m level are used and overestimated for stratification quantified entirely using altitudes below 40 m. $P(\text{vSBL} \rightarrow \text{vBSL})$ is always underestimated when only stratification information is used.

4.7 Regime occupation information in near-surface state variables

The relatively high skill of regime identification by near-surface (bottom 10 m) data is a result of particular practical utility because surface observations are much more widely available than are tower data. Therefore, we investigate HMM analyses of surface data available at Cabauw (Table 4.3). As described above, reasonably good estimates of the VP are given by the 1-dimensional observation state variables of the surface wind (W_{10}) and stratification ($\Theta_{10} - \Theta_2$). The results presented in Table 4.3 show that the combination of W_{10} with $\Theta_{10} - \Theta_2$ is found to be the best Reynolds-averaged mean surface state variable set for the HMM analysis: the VP has almost 85 % agreement with the reference state variables and captures almost 50 % of turbulence collapses, 40 % of the recoveries, and 94 % (57 %) of nights remaining in the wSBL (vSBL). This set of surface state variables alone provides much, but not all, of the information needed to obtain the reference HMM results.

The accuracy of the VP using a low-dimensional input space is also high (85 % agreement) using the pair of the along and across wind components of W_{10} ($\mathbf{Y_{obs}} = (W_{10} \parallel W_{200}, W_{10} \perp W_{200})$). The along-wind component on its own performs similarly to W_{10} whereas the across-wind component on its own performs poorly. A VP agreement of almost 90 % and transition accuracies of around 50 % are achieved when the along and across wind components are combined with the near surface stratification ($\mathbf{Y_{obs}} = (W_{10} \parallel W_{200}, W_{10} \perp$

Table 4.3: HMM analyses of different surface-based state variable sets ($\mathbf{Y}$) at Cabauw compared to the reference ($\mathbf{Y_{ref}} = (0.5(W_{200} + W_{10}), W_{200} - W_{10}, \Theta_{200} - \Theta_2)$) showing the agreement of Viterbi paths compared to the reference model for Cabauw (cons. [%]) as well as the accuracy of the wSBL to vSBL (coll. acc. [%]) and vSBL to wSBL (recov. acc. [%]), consistency of nights remaining exclusively in the wSBL (wSBL cons. [%]) and vSBL (vSBL cons. [%]), and the transition probability anomalies compared to $\mathbf{Q_{ref}}$. Starting regimes for the transition probabilities are denoted with a star.

$\mathbf{Y}$	Viterbi path accuracy					$\mathbf{Q}$ anomaly to $\mathbf{Q_{ref}}$		
	cons. [%]	coll. acc. [%]	recov. acc. [%]	wSBL cons. [%]	vSBL cons. [%]			
W_{10}	81.33	18.67	23.03	59.76	92.24		$wSBL$	$vSBL$
						$wSBL^\star$	0.0027	-0.0027
						$vSBL^\star$	-0.0067	0.0067
$\Theta_{10} - \Theta_2$	79.71	44.62	31.87	92.39	31.09		$wSBL$	$vSBL$
						$wSBL^\star$	0.0029	-0.0029
						$vSBL^\star$	0.0108	-0.0108
W_{10}, $\Theta_{10} - \Theta_2$	84.80	49.41	39.09	93.33	57.09		$wSBL$	$vSBL$
						$wSBL^\star$	0.0034	-0.0034
						$vSBL^\star$	0.0046	-0.0046
$W_{10} \parallel W_{200}$, $W_{10} \perp W_{200}$	85.31	29.39	32.05	64.16	95.72		$wSBL$	$vSBL$
						$wSBL^\star$	0.0008	-0.0008
						$vSBL^\star$	-0.0055	-0.0055
$W_{10} \parallel W_{200}$	83.85	24.21	26.94	63.76	95.27		$wSBL$	$vSBL$
						$wSBL^\star$	0.0025	-0.0025
						$vSBL^\star$	-0.0064	0.0064
$W_{10} \perp W_{200}$	42.63	3.80	9.14	4.55	26.07		$wSBL$	$vSBL$
						$wSBL^\star$	-0.0150	0.0150
						$vSBL^\star$	0.0103	-0.0103
$W_{10} \parallel W_{200}$, $W_{10} \perp W_{200}$, $\Theta_{10} - \Theta_2$	88.41	61.77	50.45	93.49	55.91		$wSBL$	$vSBL$
						$wSBL^\star$	0.0006	-0.0006
						$vSBL^\star$	0.0056	-0.0056
TKE_5	89.28	86.83	78.82	78.57	99.26		$wSBL$	$vSBL$
						$wSBL^\star$	-0.0096	0.0096
						$vSBL^\star$	0.0064	-0.0064
W_{10}, TKE_5	87.55	68.29	67.06	67.86	99.75		$wSBL$	$vSBL$
						$wSBL^\star$	-0.0057	0.0057
						$vSBL^\star$	-0.0002	0.0002
$\Theta_{10} - \Theta_2$, TKE_5	89.64	86.83	82.36	89.29	98.96		$wSBL$	$vSBL$
						$wSBL^\star$	-0.0065	0.0065
						$vSBL^\star$	0.0092	-0.0092
W_{10}, $\Theta_{10} - \Theta_2$, TKE_5	90.21	86.83	79.41	80.36	99.28		$wSBL$	$vSBL$
						$wSBL^\star$	-0.0109	0.0109
						$vSBL^\star$	0.0077	-0.0077
$var(w_5)$	91.38	89.56	88.73	93.42	99.60		$wSBL$	$vSBL$
						$wSBL^\star$	-0.0043	0.0043
						$vSBL^\star$	0.0023	-0.0023

Table 4.3

$\mathbf{Y}$	Viterbi path accuracy					$\mathbf{Q}$ anomaly to $\mathbf{Q_{ref}}$		
	cons.	coll.	recov.	wSBL	vSBL			
W_{10}, $var(w_5)$	86.88	60.00	60.00	66.07	99.91		*wSBL*	*vSBL*
						wSBL*	-0.0026	0.0026
						vSBL*	-0.0024	0.0024
$\Theta_{10}-\Theta_2$, $var(w_5)$	90.86	89.27	85.29	91.07	99.18		*wSBL*	*vSBL*
						wSBL*	-0.0046	0.0046
						vSBL*	0.0064	-0.0064
W_{10}, $\Theta_{10}-\Theta_2$, $var(w_5)$	91.14	87.80	79.41	83.93	99.53		*wSBL*	*vSBL*
						wSBL*	-0.0046	0.0046
						vSBL*	0.0064	-0.0064
U_*	91.14	87.80	79.41	83.93	99.53		*wSBL*	*vSBL*
						wSBL*	-0.0046	0.0046
						vSBL*	0.0064	-0.0064
W_{10}, U_*	82.63	0.67	0.60	0.94	95.20		*wSBL*	*vSBL*
						wSBL*	0.0005	-0.0005
						vSBL*	-0.0047	0.0047

$W_{200}, \Theta_{10}-\Theta_2$)). However, this result is of more theoretical than practical interest and cannot be used for a regime analysis based exclusively on surface data, as these wind components are defined in terms of the direction of flow aloft.

Using only TKE_5, an agreement of almost 90 % in the VP is found and 80 % (75 %) of all turbulence collapses (recoveries) are captured as well as 80 % (100 %) accuracy of nights remaining exclusively in the wSBL (vSBL). This result underlines again that nights remaining exclusively in the vSBL are dominated by low-wind speed conditions with very low turbulence activity. As mentioned in the determination of the reference model, including TKE at another level additional to TKE_5 is able to reproduce the reference VP with almost 100 % accuracy, so the good performance of TKE_5 is unsurprising. Including W_{10} in the analysis (such that $\mathbf{Y_{obs}} = (W_{10}, \mathrm{TKE}_5)$) does not improve the agreement to the reference substantially. A small improvement in the accuracy is achieved when near-surface stratification is included ($\mathbf{Y_{obs}} = (\Theta_{10}-\Theta_2, \mathrm{TKE}_5)$); no other single state variable (such as $\mathbf{Y_{obs}} = (W_{10}, \Theta_{10}-\Theta_2, \mathrm{TKE}_5)$) further improves the results. However, TKE_5 is a state variable much less commonly observed than W_{10} or air temperature.

The single near-surface state variable that best captures the reference is $var(w_5)$. All comparison criteria we used before are very close or well above 90 %. Adding any other near-surface information does not improve the accuracy of the VP estimation. While TKE_5

and $var(w_5)$ are quite similar, $var(w_5)$ outperforms TKE_5 as vertical fluctuations are not contaminated by non-turbulent horizontal fluctuations.

Analysing exclusively the friction velocity U_* shows that the information is slightly better than TKE_5 but worse than $var(w)$. Interestingly, combing near-surface stratification or W_{10} with U_* removes all information about SBL transitions and nights that stay exclusively in the wSBL.

4.8 Information in the surface wind alone

Wind speed at 10 m is a standard meteorological observation commonly measured at operational meteorological stations. As demonstrated in the previous subsection, W_{10} carries much of the regime information in the SBL. Therefore, it is worth examining HMM analyses of W_{10} alone in more detail. If similar accuracy of HMM analyses using W_{10} alone is found at the other tower sites considered, we can imagine a systematic global analyses of the SBL behaviour across a variety of climate regions, surface types etc. This discussion will focus on the land- and ice-based stations, as W_{10} is not available at the ocean-based towers considered.

Considering all land- and ice-based tower sites, HMM analyses using W_{10} alone generally have 75-85 % agreement with reference VPs (Table 4.4). In contrast to the reference models at each site, HMM analyses based on W_{10} alone show less overlap between states (Figure 4.5 columns 2 and 3). Classification of times of low static stability and moderate winds as vSBL rather than wSBL (as in the reference models) causes the majority of the differences in the VPs and transition times.

HMM analyses using a single wind speed variable can easily be formulated using the two-parameter Weibull distribution often used to model wind speeds [e.g. *Monahan*, 2007; *Monahan et al.*, 2011; *He et al.*, 2010, 2012, 2013]. Using a Weibull parametric pdf in the HMM analysis (which we denote WHMM) instead of Gaussian mixture parametric pdfs (which we denote GHMM) reduces the number of parameters to be estimated resulting in faster computations and potentially less sensitivity to sample size.

For all tower heights at Cabauw, the VP is not substantially changed using a GHMM or WHMM to analyze wind speeds (Figure 4.8). However, the accuracy of the transitions increases substantially in the WHMM compared to the GHMM across all levels (Figure 4.8, upper-middle panel) showing that the improvement is a robust result not particular

Table 4.4: Information about the reference state variable sets and the reference transition probability ($\mathbf{Q_{ref}}$) of HMM analyses at land- and ice-based tower sites as shown in Tables 2.1 and 2.2. Starting regimes for the transition probabilities are denoted with a star. HMM analyses of the surface winds with Gaussian mixture parametric pdfs (G) or Weibull parametric pdfs (W) are compared to the reference stating the agreement of Viterbi paths as compared to the reference (cons. [%]) as well as the accuracy of the wSBL to vSBL (coll. acc. [%]) and vSBL to wSBL (recov. acc. [%]), consistency of nights remaining exclusively in the wSBL (wSBL cons. [%]) and vSBL (vSBL cons. [%]), and the transition probability anomalies compared to $\mathbf{Q_{ref}}$. Transition probabilities at Hamburg, Los Alamos, and DomeC are transformed to a 10 minute time resolution.

Reference		HMM analysis of W_{10}							
Tower site		Viterbi Path accuracy					$\mathbf{Q}$ anomaly to $\mathbf{Q_{ref}}$		
		cons. [%]	coll. acc. [%]	recov. acc. [%]	wSBL cons. [%]	vSBL cons. [%]			
Land-based tower sites									
Boulder	G	75.67	31.78	30.60	93.90	91.80		*wSBL*	*vSBL*
							$wSBL^\star$	-0.0080	0.0080
							$vSBL^\star$	-0.0042	0.0042
	W	72.64	48.26	47.85	93.43	82.88		*wSBL*	*vSBL*
							$wSBL^\star$	-0.0269	0.0269
							$vSBL^\star$	0.0228	-0.0228
Cabauw	G	81.33	18.67	23.03	59.76	92.25		*wSBL*	*vSBL*
							$wSBL^\star$	0.0027	-0.0027
							$vSBL^\star$	-0.0067	0.0067
	W	80.67	32.02	30.85	65.41	72.08		*wSBL*	*vSBL*
							$wSBL^\star$	-0.0041	0.0041
							$vSBL^\star$	0.0034	-0.0034
Hamburg	G	77.61	32.19	38.83	80.51	93.86		*wSBL*	*vSBL*
							$wSBL^\star$	-0.0300	0.0300
							$vSBL^\star$	0.0212	-0.0212
	W	77.78	49.55	52.66	80.65	91.98		*wSBL*	*vSBL*
							$wSBL^\star$	-0.0050	0.0050
						$vSBL^\star$	0.0688	-0.0688	
Karlsruhe	G	74.09	50.88	45.77	85.71	94.95		*wSBL*	*vSBL*
							$wSBL^\star$	-0.0185	0.0185
							$vSBL^\star$	-0.0030	0.0030
	W	72.42	53.03	47.89	84.65	95.26		*wSBL*	*vSBL*
							$wSBL^\star$	-0.0249	0.0249
							$vSBL^\star$	-0.0019	0.0019
Los Alamos	G	75.27	27.14	38.26	50.29	87.53		*wSBL*	*vSBL*
							$wSBL^\star$	-0.0096	0.0096
							$vSBL^\star$	-0.0095	0.0095
	W	70.36	41.35	46.07	52.49	49.70		*wSBL*	*vSBL*
							$wSBL^\star$	-0.0196	0.0196
							$vSBL^\star$	0.0144	-0.0144
Ice-based tower sites									
DomeC	G	83.70	13.64	21.43	–	–		*wSBL*	*vSBL*
							$wSBL^\star$	-0.0005	0.0005
							$vSBL^\star$	-0.0031	0.0031
	W	86.39	33.33	21.43	–	–		*wSBL*	*vSBL*
							$wSBL^\star$	-0.0015	0.0015
							$vSBL^\star$	0.0000	0.0000

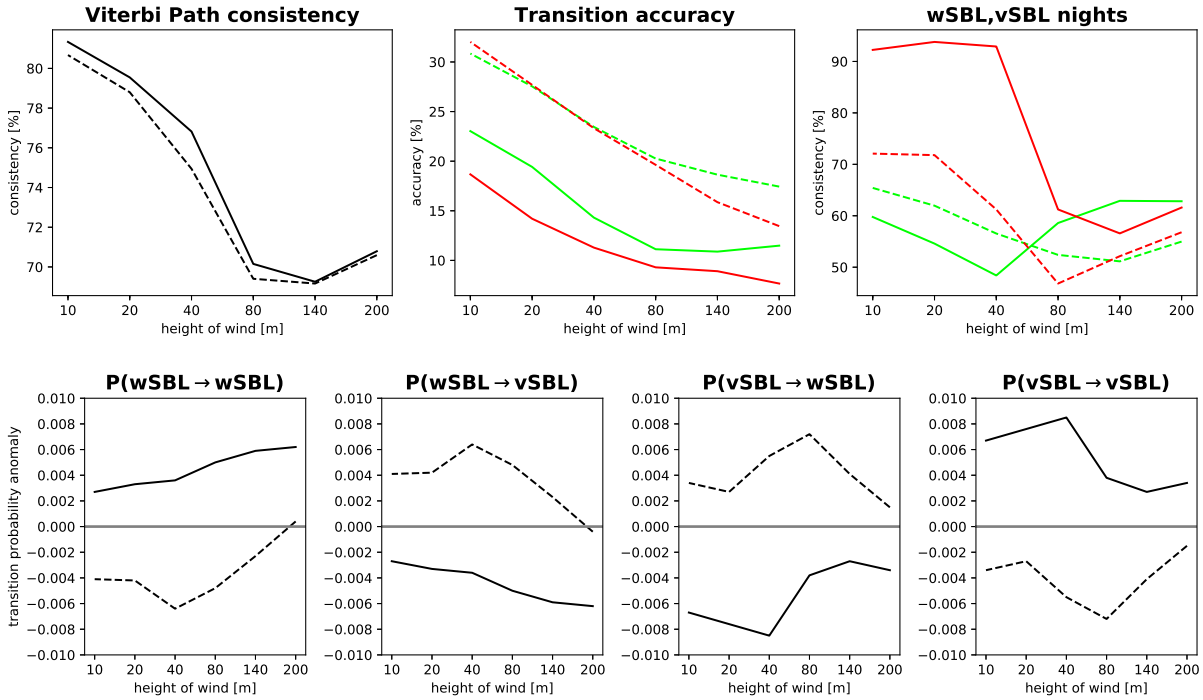

Figure 4.8: HMM regime sequence paths of one dimensional wind speeds with Gaussian mixture parametric pdfs (solid lines) or Weibull parametric pdfs (dashed lines) compared to the HMM regime sequence paths of $\mathbf{Y_{ref}} = (0.5(W_{200}+W_{10}), W_{200}-W_{10}, \Theta_{200}-\Theta_2)$ at Cabauw. Top panels from left to reight: the consistency of Viterbi paths (black, left panel), accuracy of wSBL to vSBL transitions (red, middle panel), accuracy of vSBL to wSBL transitions (green, middle panel), and the accuracy of nights remaining completely in the wSBL (green, right panel) and vSBL (red, right panel). Bottom row from left to tight: Transition probability anomalies compared to the reference.

---

to surface winds. The better agreement of the transitions is associated with the fact that the persistence probabilities are reduced while transitions become more likely (Figure 4.8, bottom panels). Consistent with the previous results, W_{10} contains more information about the regime transitions than wind speeds aloft. However, this improvement in transition accuracy in the WHMM is accompanied by decreases in the accuracy of nights being classified as very persistent nights (no transition occurrence). In contrast, the GHMM analyses identify nights remaining in the vSBL particularly well (Figure 4.8, upper-right panel).

HMM analyses using surface wind speed information without stratification information misclassify some wSBL times as vSBL over land- and ice-based tower sites (Figure 4.9, first column). This misclassification rate is lower for the WHMM than for the GHMM. Pdfs of W_{10} are more clearly divided into two almost completely separated populations

(relative to the reference model). Winds aloft are classified similarly by the GHMM or WHMM and agree at some stations remarkably well with their reference HMMs.

4.9 Conclusions

Nine tower sites at locations around the world with different surface types (sea water, grassland and ice) and surrounding terrains of different complexity (flat surfaces, mountain ridges, and metropolitan regions) all show a clear structure of two distinct regimes in the SBL. At all tower sites, the three dimensional state spaces of mean wind speed, wind shear, and stratification exhibit one regime with weak static stability and moderate to strong winds, referred to as the wSBL, and a second regime with strong static stability and moderate to weak winds, referred to as the vSBL.

The HMM analyses at the different tower sites are able to separate the data into two physically-reasonable regimes. The classification finds that no clear wind speed or stratification threshold separating regimes: under similar conditions of weak wind speed and weak stratification the HMM can assign different regimes based on the history of the regime occupation sequence. HMM analyses of this three-dimensional state variable set classify both the Reynolds-averaged means as well as the turbulence state variables into distinct states. In the wSBL, large TKE and vertical velocity variance values are found whereas the vSBL shows very weak or collapsed turbulence. Observations of vertical fluctuations as classified by the HMM to be in the vSBL are almost completely suppressed whilst the wSBL is governed by vertical turbulent transports.

HMM analyses using three hidden regimes do not produce robust results either in the regime sequence or in the transition probabilities across the tower sites. A third regime blurs overlapping regions in Reynolds-averaged mean and eddy state variables joint probability distributions, resulting in less clear physical interpretations.

HMM analyses of the two-regime SBL using higher-dimensional input spaces of Reynolds-averaged mean variables or turbulence state variables yield the same results as the three-dimensional analysis, indicating that these results have in some sense 'converged'. This result indicates that the shear and stratification information in these data which describe the TKE production and consumption are sufficient for regime identification. That the turbulence state variables do not add significant information suggests that the turbulence and the mean flow in the SBL are generally close to being in equilibrium.

Considering the representation of SBL regime occupation in lower-dimensional data sets, we find that best results are obtained using stratification and wind shear measured from the lowest-most observational altitude. Stratification and shear individually estimate the regime state sequence reasonably well but show weaknesses in capturing the time of the transitions. Stratification information accurately captures nights that are exclusively in the wSBL while near-surface shear information capture those remaining exclusively in the vSBL.

Of particular practical importance is the potential use of surface observational data for the classification of regimes. For land-based stations, a quite accurate representation of regime occupation in the SBL is given by near-surface turbulence intensity or a combination of near-surface stratification and near-surface wind speed.

The near-surface wind itself (which is a measure of the shear between the measurement height of typically 10 m and the surface) is also a reasonably good state variable for regime classification. We analyzed the near-surface wind speed with Gaussian mixture (GHMM) and Weibull parametric (WHMM) distributions in the HMM analysis and find that, relative to the reference, the WHMM estimates the occurrence of regime transitions slightly better than the GHMM.

As surface winds are extensively measured around the world, an interesting direction of future research will be a surface wind based SBL regime analysis, potentially allowing a more detailed characterization of influences of different surface types and climatological regions as the tower sites are mostly located in the Northern hemisphere midlatitudes. Furthermore, the transition probabilities obtained and the information they contain can be used in order to inform stochastic parameterisations of the SBL in models for weather and climate [*He et al.*, 2012]. Information that can be obtained from the transition probability matrices and how this information could inform such a parameterisation is discussed chapter 7, together with the sensitivity analysis of the HMM regime occupation sequence to the transition probabilities.

In chapter 5 the state variable structures in nights without transitions between SBL regimes according to the HMM regime occupation sequence is examined. The regime occupation sequence also allows an investigation of how Reynolds-averaged mean and turbulence state variables change across transitions. Furthermore, potential transition precursors in external forcing or in internal state variables can be examined. These analyses are presented in chapter refchap:part3.

One limitation of this study is that even though the generic structure of two SBL regimes is

found at different tower sites, all of them are located in the mid- to high-latitudes. We found no evidence that moist processes (other than the radiative effect of clouds; cf. chapters 5 and 6) have a strong effect on the formation of the SBL or transitions between SBL regimes. However, moist processes might be of importance in tropical regions. A lack of access to data from observational towers in these regions prevented us from analysing such effects. Data from the 325 m Amazonian Tall Tower Observatory [ATTO, *Andreae et al.*, 2015] would permit such an analysis; this is an interesting question for future research.

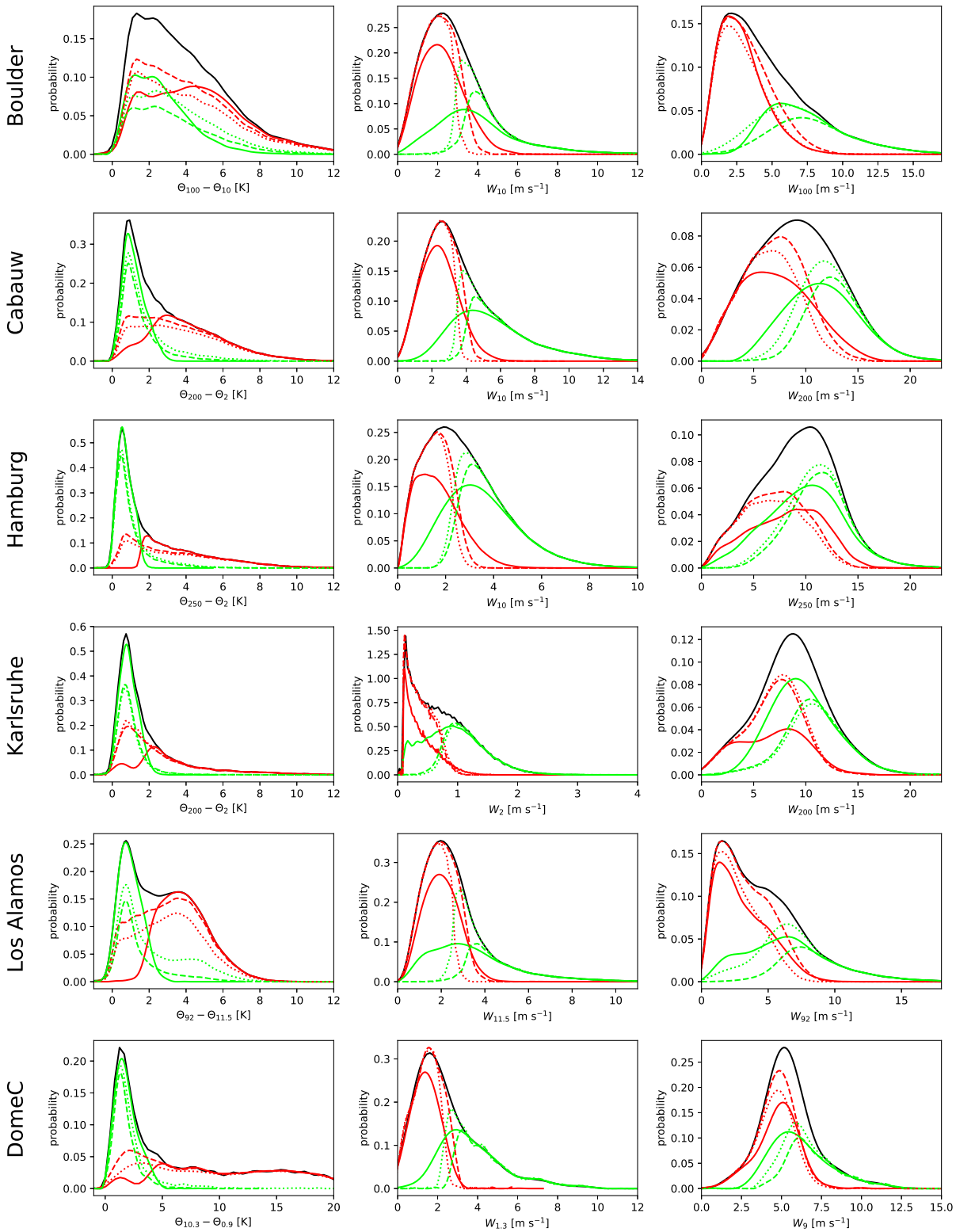

Figure 4.9: Probability density functions of the three dimensional reference state variables of dry static stability, near surface wind, and wind aloft (as used in the HMM analyses) for the land- and ice-based tower sites. Pdfs of the reference HMM analysis (solid) are compared to HMM analyses of the surface winds with Gaussian mixture parametric pdfs (dashed) or Weibull parametric pdfs (dotted) for all data (black), wSBL (green), and vSBL (red). All pdfs (calculated with the multivariate kernel density estimation by *O'Brien et al.* [2014, 2016]) of wSBL and vSBL classified data are scaled by the probability of regime occupation so that their sum is equal to pdfs pf the full dataset.

5 The boundary layer structure in times of very persistent weakly stable and very stable boundary layer conditions

Chapter Abstract

The HMM analyses have been conducted to classify the SBL into wSBL and vSBL conditions at different tower sites. With the HMM regime sequence we identify very persistent wSBL and vSBL nights. The occurrence of those nights is more likely in homogeneous surroundings than in regions with complex terrain. At land-based stations persistent wSBL nights are always accompanied by strong turbulence fluxes with strong winds sustaining the weakly stable temperature profile. The vSBL has weak turbulence intensities and weak wind conditions leading to strong inversions. At ocean-based stations wind speeds do not differ substantially between the regimes and the vSBL is established by advection of warm air aloft. Across land-based stations wind conditions stay relatively steady in each persistent regime whereas temperature structures develop respectively up to sunset for for the very persistent wSBL or 2 for the very persistent vSBL. At Cabauw in the Netherlands, persistent wSBL and vSBL nights are usually accompanied by completely overcast or clear-sky conditions, respectively. Geostrophic wind speeds (U_{geo}) differ between the persistent wSBL and vSBL nights. Under overcast conditions only very low U_{geo} are associated with very persistent vSBL nights whereas stronger U_{geo} can be observed under clear-sky conditions, indicating the importance of radiative effect of clouds on the regime persistence. Similarly, under clear sky conditions only strong U_{geo} lead to very persistent wSBL nights.

5.1 Introduction

In chapter 4 we used the HMM analysis to obtain regime occupation sequences classifying nighttime data into the wSBL and vSBL at the different tower sites. The analysis turned out to be reliable across different tower sites. With the regime occupation sequence two basic types of nights can be classified: nights with the occurrence of transitions and very persistent nights without transitions. As will be discussed in this chapter and the next, both types of nights are relatively frequent across the tower sites. Therefore, understanding the mechanisms that lead to either class of night is of importance. In this chapter, we investigate the structures of the meteorological state variables in the cases of very persistent vSBL and wSBL nights, with particular focus on how location-specific properties and external drivers control these. The atmospheric structures of meteorological state variables in the very persistent wSBL and vSBL nights as well as their evolution over the course of the night are described in sections 5.2 and 5.3. We assess the relationship between the occurrence of very persistent nights and external drivers such as the U_{geo} and the low level cloud coverage (LLCC) in section 5.4. Finally, the occurrence probabilities of nights without any regime transitions are investigated (section 5.5) followed by conclusions in section 5.6. This chapter is based on *Abraham and Monahan* [2018b].

5.2 Contrasts in the PBL structure between persistent wSBL and vSBL nights

Across the land-based stations, nights without transitions between SBL regimes show clear differences in the distributions of the wind and stratification profiles (Figure 5.1; note that the vertical axes differ between towers). In Figure 5.1, the stratification is calculated as the potential temperature difference between each height and the measurement nearest the surface. The very persistent wSBL is characterized by strong winds at all altitudes, while wind speeds are substantially smaller in the vSBL. Near-surface shears are stronger in the wSBL than in the vSBL. At Boulder, Cabauw, and Los Alamos the interquartile ranges of wind profiles are well separated. At Hamburg and Karlsruhe the separation of the wind profile distributions is weaker.

The weaker separation of wind profiles at Hamburg and Karlsruhe may be related to the fact that both tower sites are close to urban regions which can decelerate the wind speeds in the wSBL substantially due to their larger surface roughness. Additionally, Karlsruhe is also located in the Rhine valley and therefore in the wind shadow of the surrounding hills.

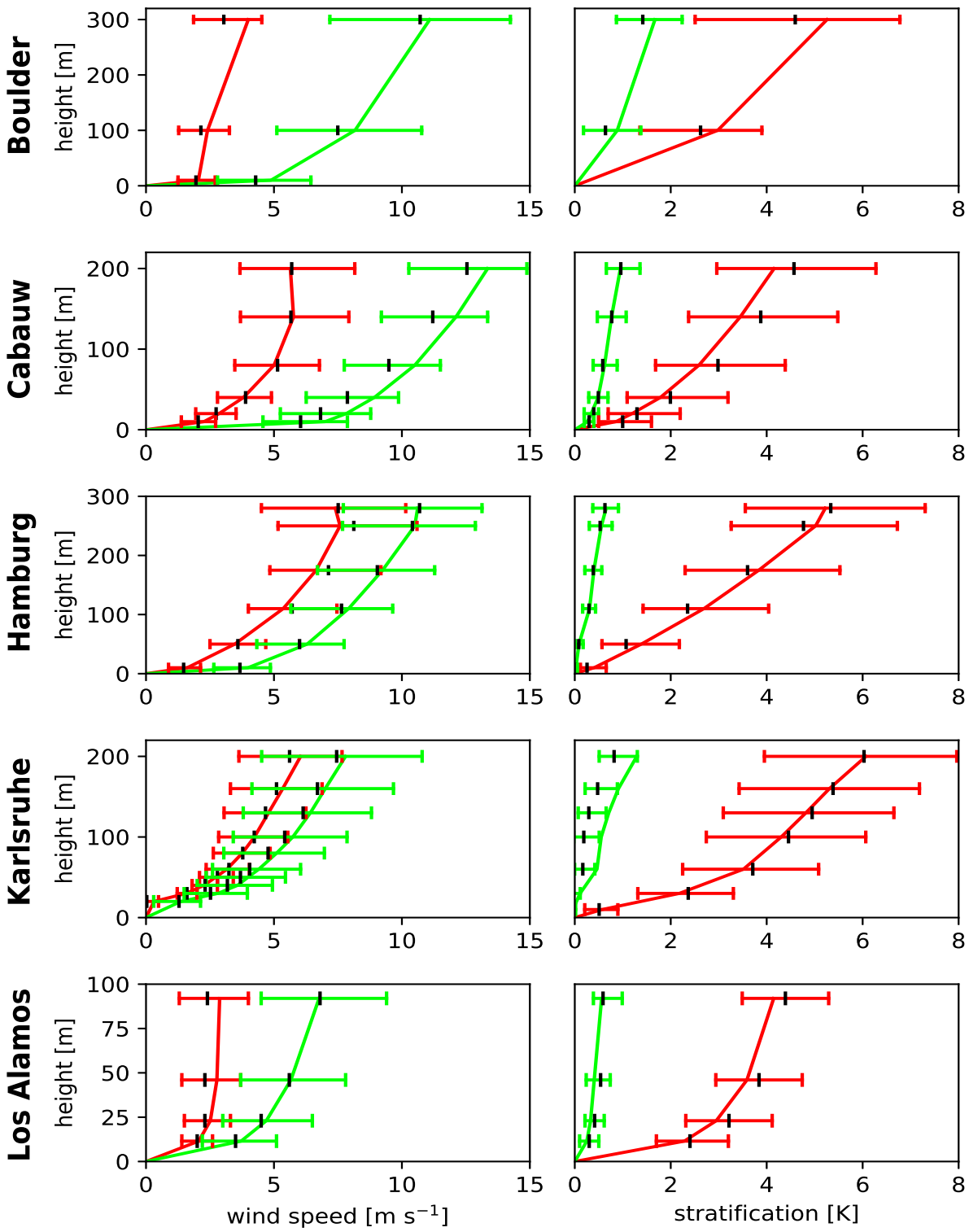

Figure 5.1: Wind and stratification mean profiles of nights remaining exclusively in the wSBL (green) and vSBL (red) as classified by the reference HMMs for the land-based stations. Lines denote the mean, while horizontal bars indicate the 25th to 75th quartiles. The median is marked in black.

While Los Alamos is also located in a valley, the different surface properties (grassland at Karlsruhe vs. sandy dry surface at Los Alamos) can affect the strength of the inversion induced by radiative cooling and therefore the turbulence and the near-surface shear which may be responsible for clearer separations of the wind profiles.

The stratification profiles are well separated across all land-based stations, showing how strong the signal of very persistent nights is in the potential temperature field. The persistent wSBL nights have an almost neutral temperature profile whereas in the vSBL the potential temperature gradients are large (particularly near the surface). Across the towers, the potential temperature difference between the lowest measured altitude and about 100 m is between 2 to 6 K. Los Alamos shows a particularly large near-surface stratification which is matched in intensity only at Karlsruhe. Quantitative differences in our measure of stratification between sites are likely partially due to differences in the height of the lowest observational level, as vSBL near-surface temperature gradients are particularly strong (cf. differences in stratification at Cabauw illustrated in Figure 1 of *van de Wiel et al.* [2017] and Figure 5.1 in this study).

At all ocean-based FINO towers, in contrast, the clear separation between nights that stay persistently in either regime is only evident in the stratification profiles (Figure 5.2). Relatively small differences in wind speed profiles are evident in the overlap of the interquartile ranges. At FINO-1 and FINO-3 the mean profiles have larger wind speeds at all altitudes in the wSBL and smaller wind speeds in the vSBL. Such a systematic difference is not present at FINO-2 where mean wind profiles are very similar in both types of persistent regimes. Interestingly, FINO-2 shows stronger shears above the lowest observational level in the vSBL than in the wSBL suggesting that at this site vertical turbulent fluxes are suppressed and less momentum transport between atmospheric layer occurs. Consistent with the other sites the near-surface shears are also larger in the very persistent wSBL in comparison to very persistent vSBL nights.

As the underlying ocean at these stations has a high heat capacity and the surface shows smaller variations in temperature than surfaces at the land-based stations, the build-up of strong stratification by surface radiative cooling is reduced. The evolution of composite potential temperature profiles from just before the sunset to eight hours afterwards shows that the strong stratification in the vSBL is primarily due the presence of warm air aloft rather than surface cooling (Figure 5.3, right column). A natural interpretation of very persistent vSBL nights at ocean-based stations is that these arise due to the horizontal advection of warm air aloft, consistent with the findings at FINO-2 in *Dörenkämper et al.* [2015]. The persistent wSBL nights, on the other hand, show a slow cooling of the air with

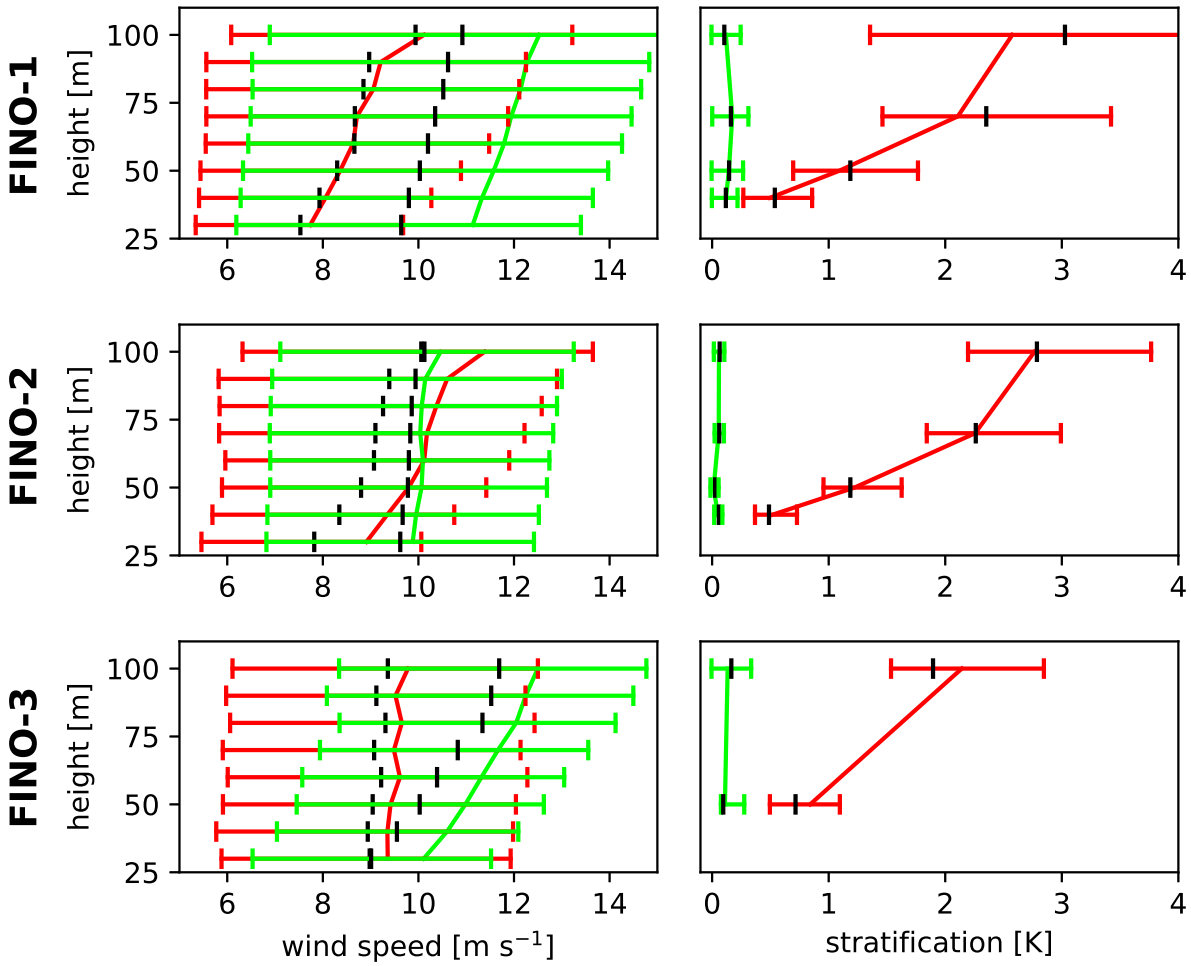

Figure 5.2: As in Figure 5.1 but for the ocean-based stations.

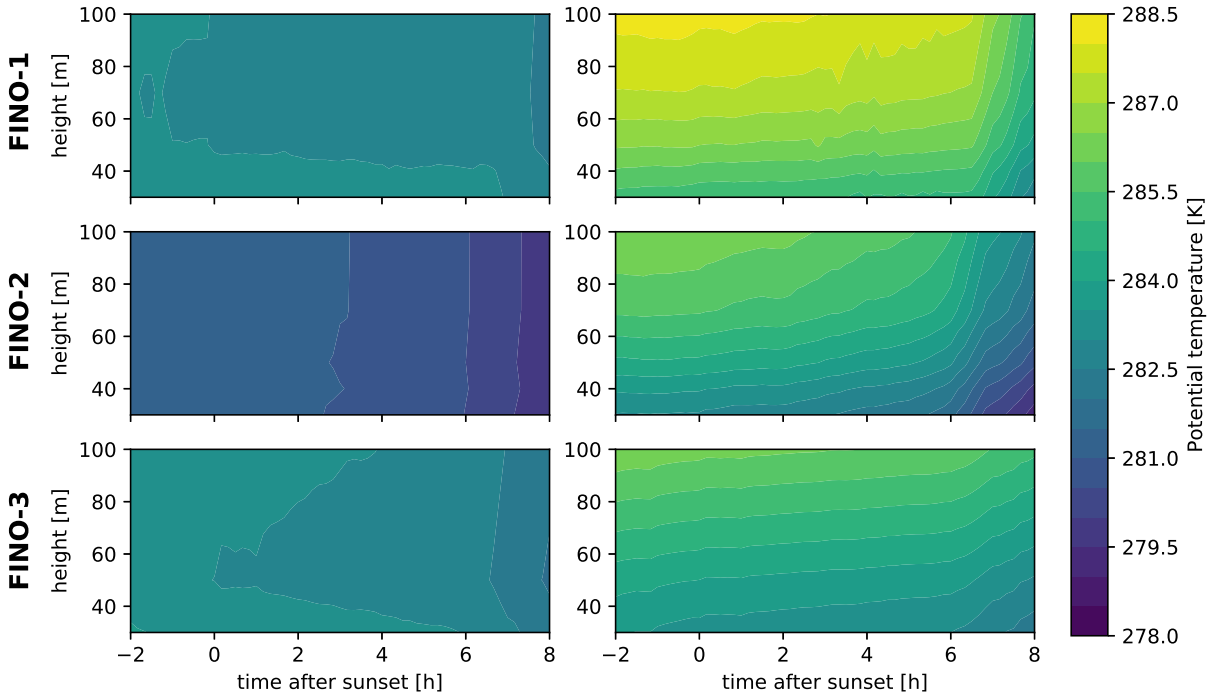

Figure 5.3: Evolution of the mean potential temperature profiles of nights remaining exclusively in the wSBL (left) and vSBL (right) as classified by the reference HMMs for the ocean-based stations.

---

a near-neutral stratification demonstrating how well-mixed (due to sustained turbulence) the boundary layer at observed atmospheric layers is.

We expect that reductions of turbulent momentum fluxes in the vSBL decouple the atmospheric layers resulting in larger vertical directional shears. To investigate this effect, we analyse the along- and across-wind components relative to the highest observational altitude. The along-wind component profiles at the different land-based stations show the same general features of differences between regimes as the wind speed profiles in Figure 5.1 (cf. Figure 5.4, first column). The across-wind component profiles, however, differ between the tower sites (Figure 5.4, second column). At Cabuw, Hamburg, and Karlsruhe the across-wind component is positive as expected for veering winds in the Northern hemisphere. At these sites a clear separation of the across-wind component mean profiles between regimes exists. In the wSBL less directional shear in the PBL is observed as the flow is vertically coupled by relatively strong turbulent momentum fluxes. However, at Boulder, the across-wind component is similar in both regimes and takes both signs at all observational levels with very similar pdfs (not shown). Similar results are found for Los Alamos, except that the across-wind component exhibits much more variability in

the vSBL. A clear separation between regimes is observed at Los Alamos when composites of the absolute values of the across-wind component are considered (Figure 5.4, third column).

The behaviour of the directional shear is also evident in the hodographs of the wind in the boundary layer in the different persistent regimes (Figure 5.5). Consistent with the observations of the mean across-wind components, at all land-based locations except Boulder the wind veering with height is weaker in the very persistent wSBL than in the very persistent vSBL. The increase in the across-wind component in the vSBL leads to more pronounced Ekman spirals. In contrast to Cabauw and Hamburg, other stations show both veering and backing of the wind in the vSBL. One possible explanation for these differences in the across-wind components could be the complex terrain at the American sites and Karlsruhe. The proximity to the mountain ridges can induce for example density currents which affect the near surface wind directions. Another influence could be the presence of thermal wind shear due to differential warming in the complex topography. Evident Ekman-like spirals are evident at Karlsruhe and Los Alamos in hodographs using the absolute value of the across-wind component (Figure 5.5, columns two and four).

Over the ocean the across-wind component exhibits a clear separation in the distributions of the different persistent regimes (Figure 5.6). The along-wind component profiles are very similar in both regimes consistent with the wind speed measurements (Figure 5.2). Hodographs show a very typical increase in the Ekman spiral of the wind across all ocean-based stations (not shown).

As with the stratification, TKE is separated well between the very persistent SBL regimes (Figure 5.7). The same is true of $var(w)$. Across all locations with turbulence measurements the vSBL median in $var(w)$ is very close to zero showing how effectively vertical fluctuations are suppressed. Interestingly, values of TKE and $var(w)$ systematically increase with height at Los Alamos. Though largest TKE values are expected where shears are strongest (near the surface; Figure 5.1) this result provides further evidence of a lack of horizontal homogeneity of the turbulence at this location.

Across the tower stations for which turbulence measurements are provided the variability of TKE and $var(w)$ within the vSBL nights is generally small, and the fact that the mean values of these quantities generally exceed the 75th percentiles indicate highly-skewed distributions. Under very stable conditions bursts of turbulence are observed [e.g *van de Wiel et al.*, 2003; *Mahrt*, 2014]. These intermittent events are evidently not strong enough to break down the stratification and do not result in a transition to the wSBL, as by

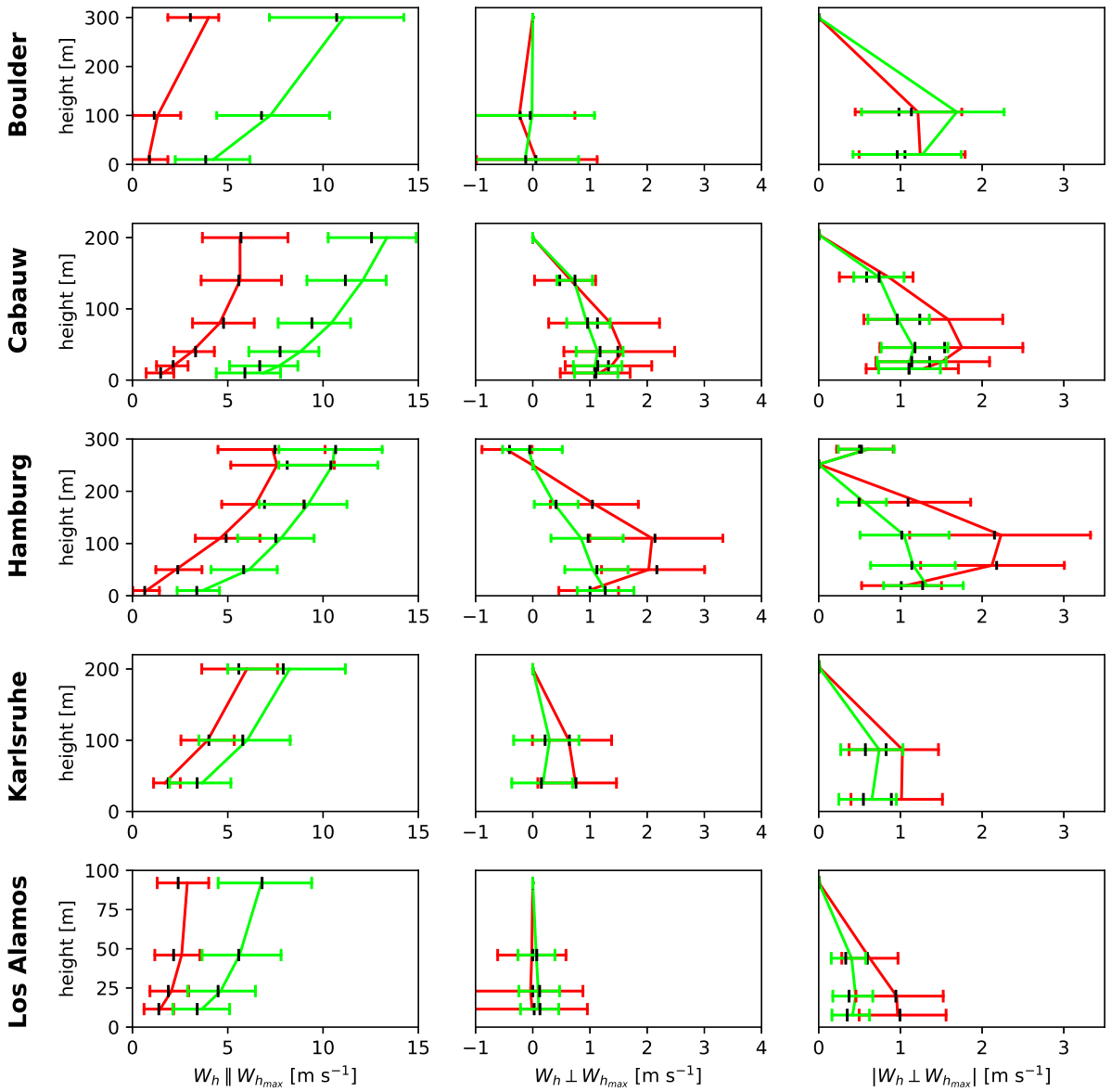

Figure 5.4: As in Figure 5.1 but for the wind component along (first column) and across (second column) the flow direction of the highest observational level at land-based sites. The third column shows the distributions of the absolute value of the across-wind component.

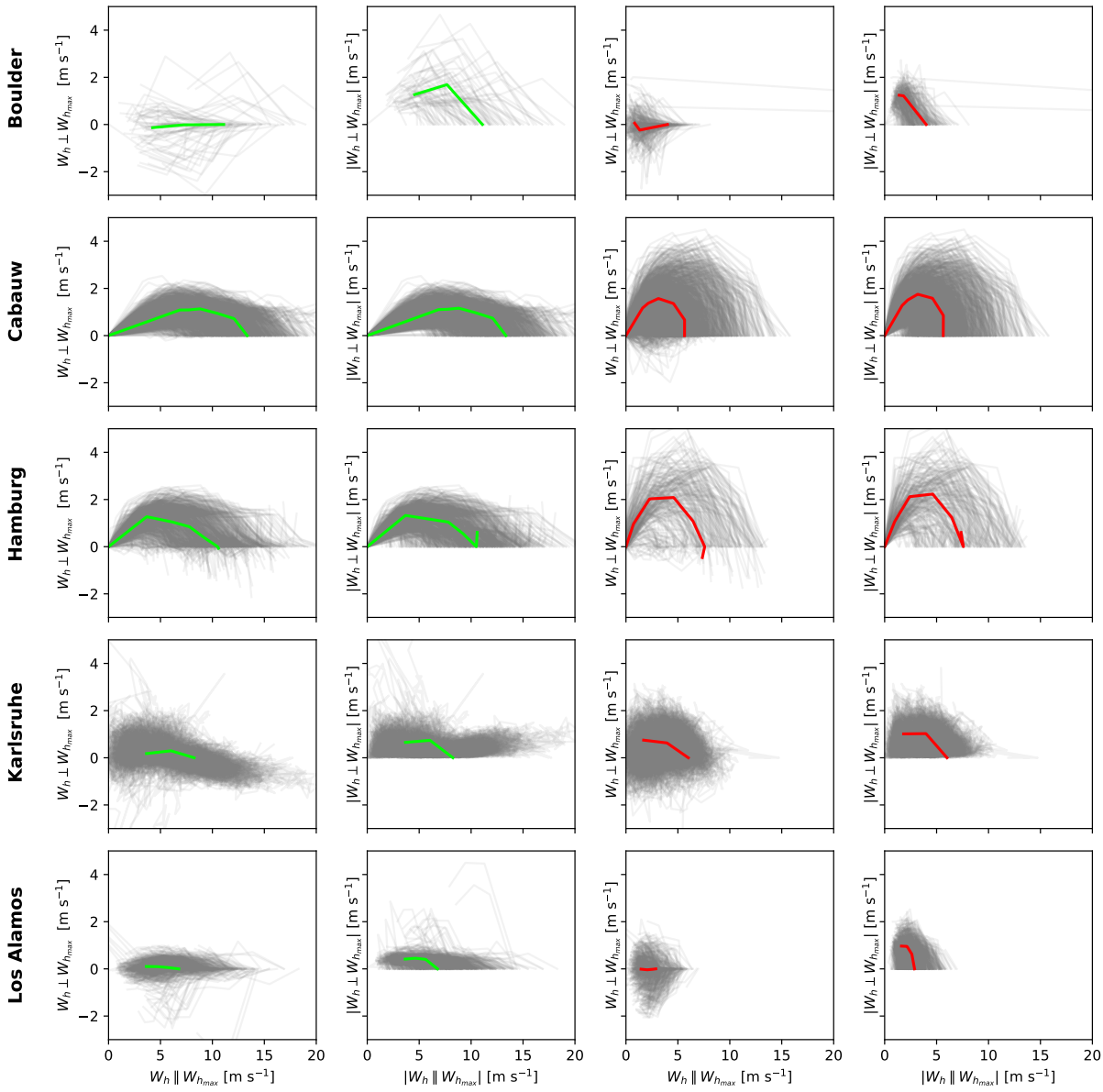

Figure 5.5: Hodographs vertical wind profiles of nighttime means for land-based stations in very persistent wSBL (first column) and very persistent vSBL (third panel) nights. Hodographs with absolute values of the components are depicted in columns two and four. Means over all nights are depicted in green (wSBL) and red (vSBL).

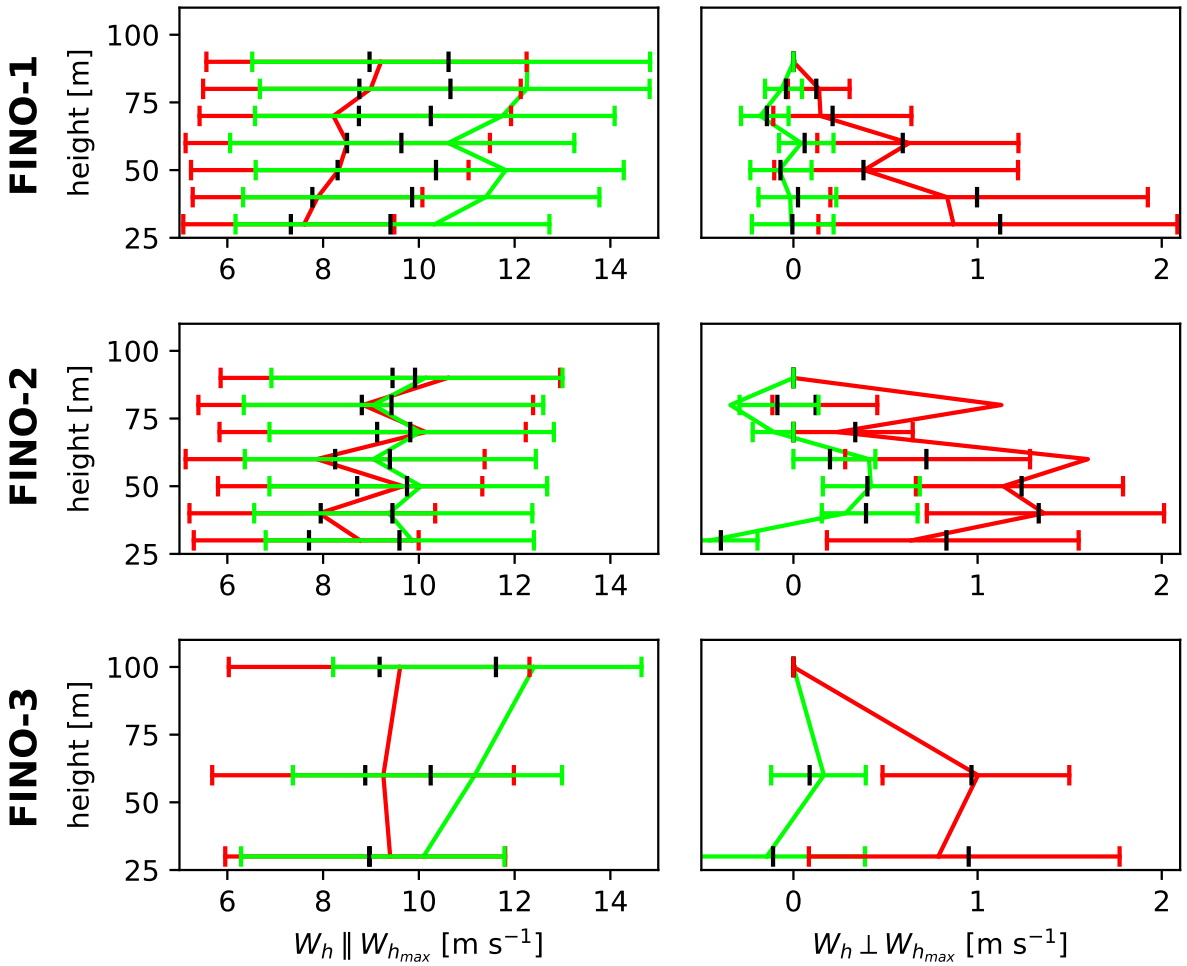

Figure 5.6: As in Figure 5.1 but for the wind components along (first column) and across (second column) the flow direction of the highest observational level for ocean-based stations.

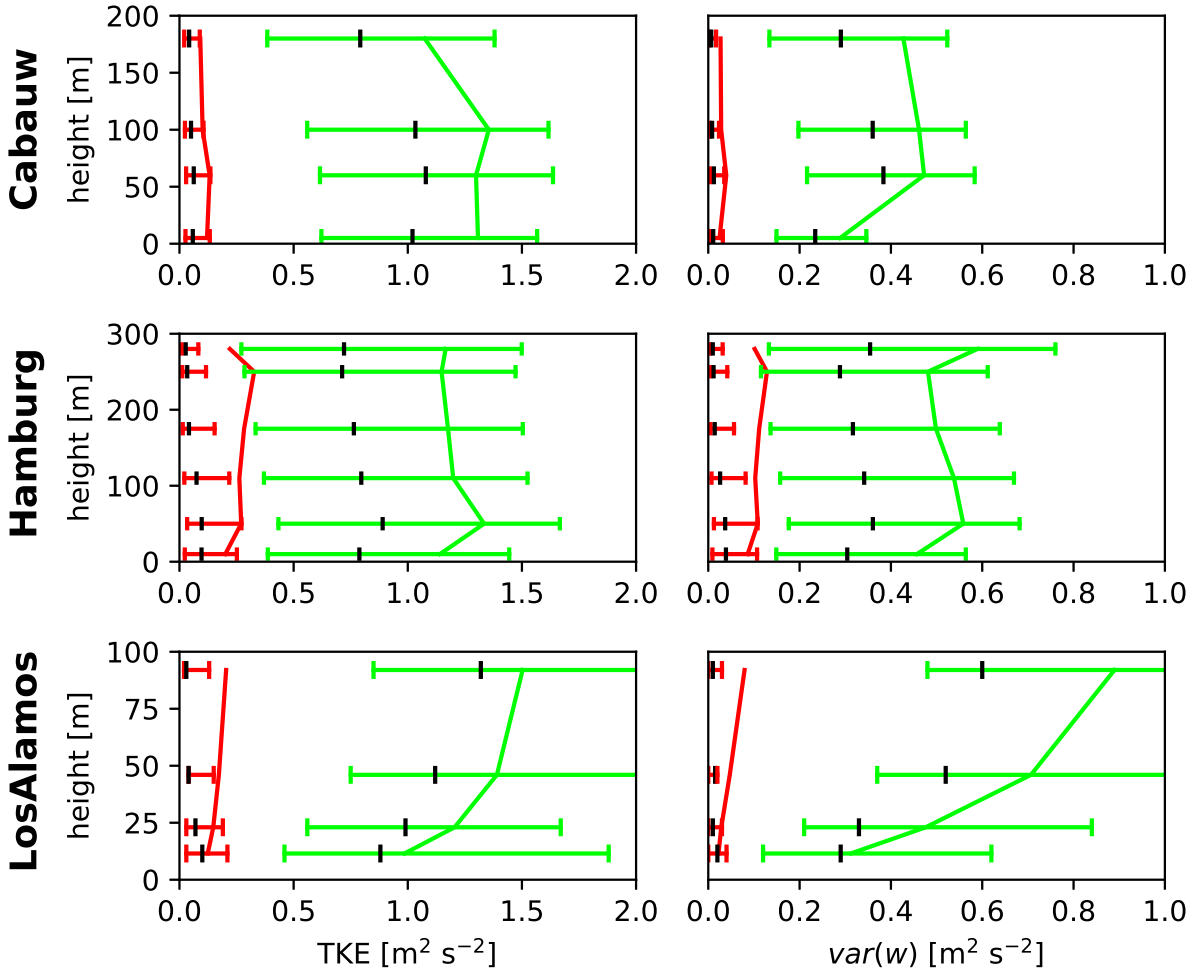

Figure 5.7: As in Figure 5.1 but for profiles of TKE and the variance of the vertical wind component ($var(w)$). These data are only available for Cabauw, Hamburg, and Los Alamos.

construction only persistent vSBL nights are considered. The distributions of TKE and $var(w)$ are clearly skewed in the wSBL, but much less so than in the vSBL.

The magnitude of the turbulent stress (here expressed as $U_*(z) = [\overline{u'w'}^2(z) + \overline{v'w'}^2(z)]^{1/4}$) is also clearly separated between large values in the wSBL and small values in the vSBL (Figure 5.8, left column). Again, the distributions are positively skewed with larger skewness in the very persistent vSBL nights. Differences in turbulent heat fluxes ($\overline{w'T'}(z)$) between the regimes are small (in Cabauw) or absent (in Hamburg), consistent with the MSHF perspective (Figure 5.8, right panels). The stronger wSBL turbulent heat fluxes at Cabauw might be related to the fact that the stratification is slightly stronger than at Hamburg (Figure 5.1) while the $var(w)$ values (indicative of the vertical turbulent transports) are very similar at both sites (Figure 5.7). Interestingly, at Hamburg considerable amounts of time in very persistent wSBL nights are associated with positive (upward) heat fluxes though all stratification measurements are positive. The reason for these countergradient heat fluxes is unclear. Another possibility for the positive heat fluxes could be that between the discrete observational levels unstable near-surface layers exist that lead to the upward heat fluxes. In fact, the layers below 100 m at Hamburg or Karlsruhe suggest nearly neutral to possibly unstable conditions (Figure 5.1). A more thorough analysis of local vertical stabilities at all heights rather than the bulk measurements used here can clarify this.

5.3 The evolution of the persistent wSBL and vSBL over the course of the night

The time evolution of the stratification and near-surface shear (as represented by the near-surface wind speed) is now investigated in order to understand the temporal behaviour of the competing mechanisms of TKE consumption and production (Figure 5.9). We consider here only the first 8 night hours, the length of the the shortest nights in a year at around 45 N. Analyses of the individual seasons analyses produce very similar results (not shown).

Relatively strong wind speeds are found in the wSBL over the whole night (Figure 5.9), consistent with sustained relatively large shear generation of turbulence. Across all land-based stations the stratification develops in broadly similar ways. Before sunset, stratification increases slightly from near-neutral to weakly stable conditions. The pdfs of tendencies of the stratification before and after sunset reveal that the very persistent wSBL is completely established at the time of sunset (not shown).

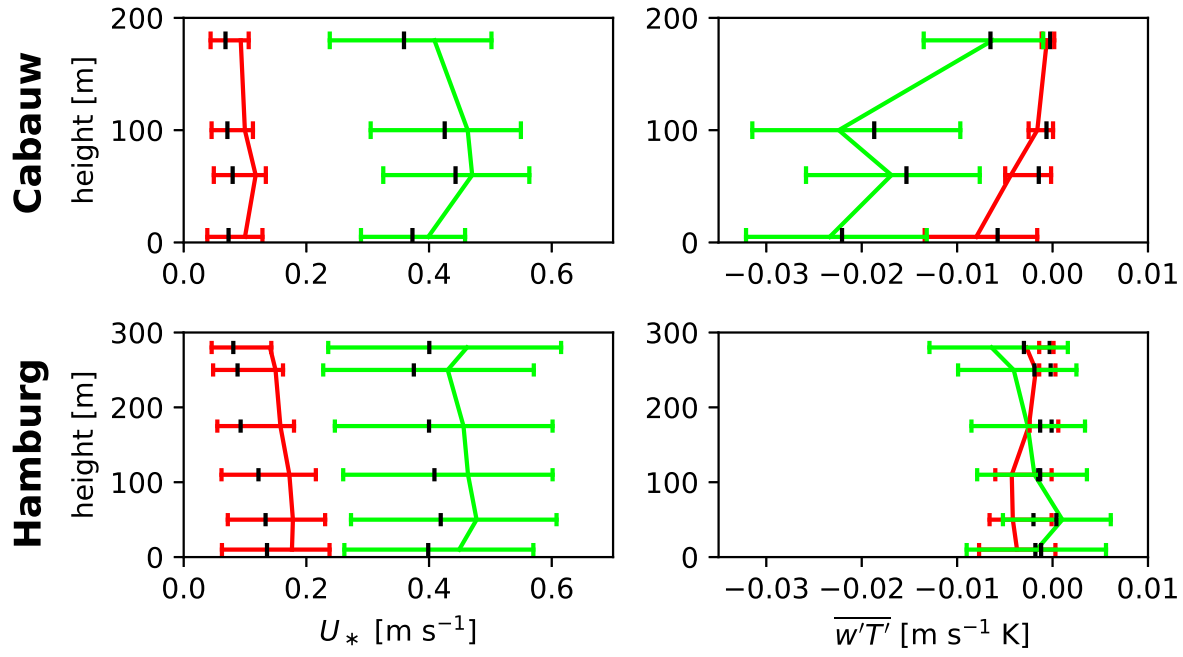

Figure 5.8: As Figure 5.7 but for of the turbulent stress (U_*) and turbulent heat flux ($\overline{w'T'}$). These data are only available for Cabauw and Hamburg.

The strongest stratification in persistent wSBL nights occur in Boulder and Los Alamos, the stations where strong radiative cooling can occur due to climatological low cloud coverage. The midlatitude European sites show all very similar mean stratification values which are systematically smaller than at the American sites. The positive skewness of stratification at Karlsruhe evident in the fact that the mean generally exceeds the 75th percentile is not observed at other stations, and may result from measurement errors (the median stratification value is close to zero). While the very persistent near-surface wind speeds are similar across most sites, relatively low wind speeds are observed at Karlsruhe. The reasons for this different behaviour at Karlsruhe are not clear.

Very persistent vSBL nights already show stratification values of 1-2 K in the bottom 100 m two hours before sunset and rapidly increase to about 4-5 K (Figure 5.9, left column). With the exception of Boulder where the stratification continues to gradually increase, these strong stratifications are completely developed within 1-2 hours after sunset. A possible reason for this different behaviour at Boulder is the greater height of the near-surface temperature measurement (10 m as opposed to 2 m at most other stations), such that the temperature at this altitude exhibits a delayed response to surface cooling. In contrast to other sites at which the stratification is relatively constant or increasing throughout the night, at Karlsruhe the stratification takes a maximum shortly after sunset and decreases again. The developed vSBL corresponds to low wind speeds of about 2 m s^{-1} at all tower stations except Karlsruhe (Figure 5.9, right column), where about 50 % of the measurements show a near-zero wind speed near the surface. Interestingly, at Boulder and Los Alamos wind speeds decrease after an initial increase near sunset. While the very persistent wSBL is completely established at sunset, pdfs of the very persistent vSBL stratification tendencies show distributions centred around positive values to about 1-2 hours after sunset, after which the tendencies are distributed narrowly around zero (not shown).

The separation of wind speed distributions between very persistent wSBL and vSBL nights is broadly consistent with the MSHF framework: turbulence can be sustained and turbulent heat fluxes can balance the energy loss due to radiative cooling under strong wind conditions while turbulence collapses under weak wind conditions [*van de Wiel et al.*, 2017]. The absence of clear wind speed thresholds for transitions between regimes (cf. chapter 6) complicates this perspective, however.

For ocean-based stations the role of warm-air advection was discussed above (Figure 5.3). The evolution of the wind speeds over the course of the night has a considerable variability and no clear separation between persistent wSBL and vSBL nights is evident (not shown).

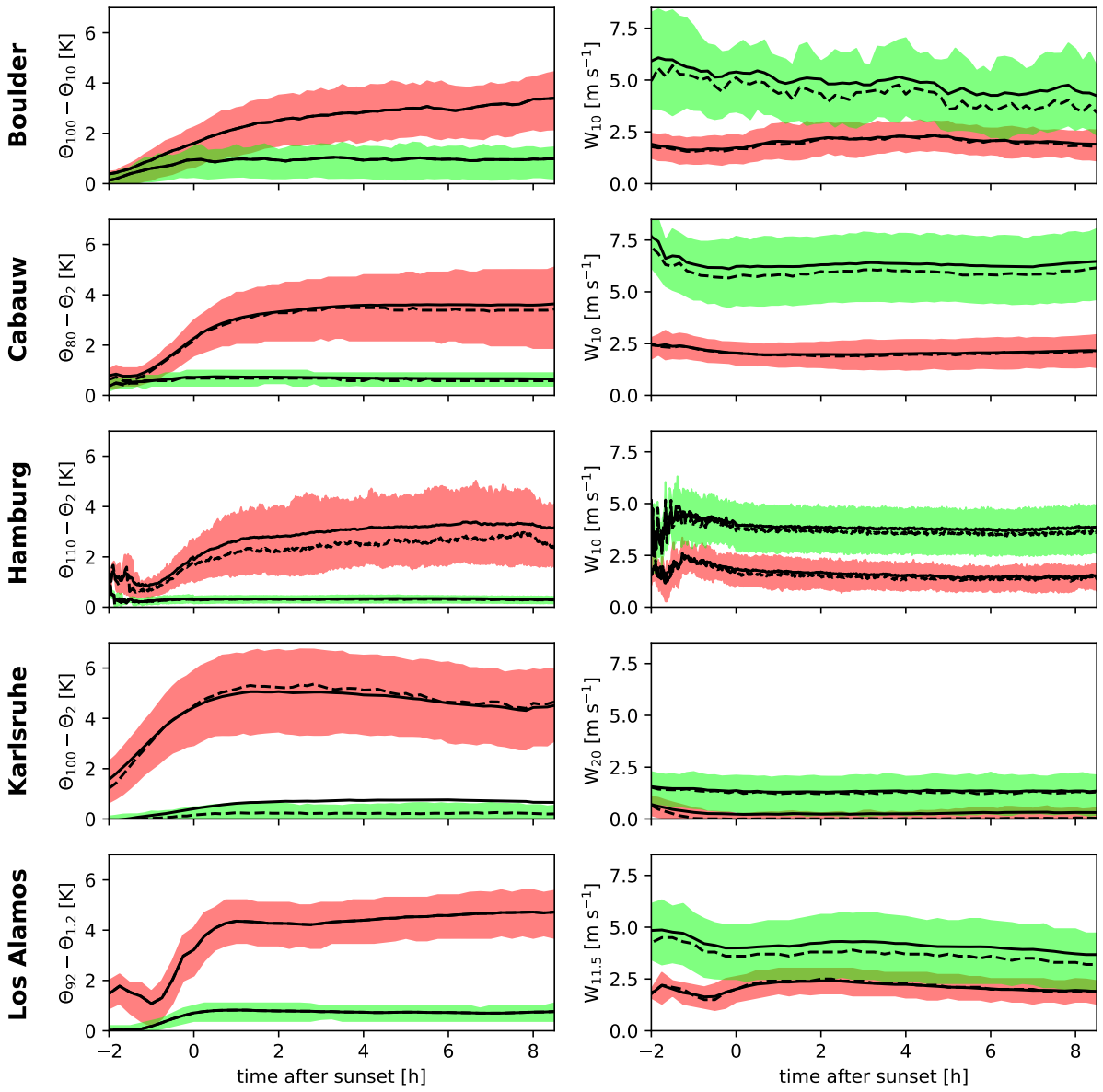

Figure 5.9: Evolution of the stratification (left column) and near-surface wind speed (right column) in nights remaining exclusively in the wSBL (green) and in the vSBL (red) as classified by the reference HMMs for the land-based stations. The means are depicted by the black solid lines, the medians by the black dashed lines, and the 25th to 75th percentile by the respectively green and red contours.

5.4 The influence of external influences on persistent wSBL and vSBL nights

Due to the clear separation of wind speed distributions of persistent wSBL and vSBL nights over land, it is expected that the regimes will be associated with different meteorological conditions. Here, we investigate the relationship between external drivers and very persistent nights at land-based sites: the external pressure gradient force, as measured by the geostrophic wind U_{geo}, and LLCC. Overcast conditions increase the downwelling longwave radiation flux reducing radiative cooling at the surface and weakening the strength of the inversion. Conversely, clear sky conditions enhance the radiative cooling and favour strong inversions. As we have information about these external influences only at Cabauw, the following analysis concentrates on that site.

We find that very persistent wSBL is accompanied 63 % of the time with overcast conditions (LLCC $>$ 95 %) and about 16 % of the time with clear sky conditions (LLCC $<$ 5 %). Conversely, 55 % of the persistent vSBL nights are accompanied by clear-sky conditions and only 22 % by overcast conditions.

Similarly to the evolution of the near surface winds, the tendencies of U_{geo} over the course of the night are very small and have narrow pdfs around zero (not shown). The pdfs of the geostrophic wind U_{geo} in persistent wSBL and vSBL nights show distributions with clearly separated maxima at about 4-5 m s^{-1} (vSBL) and 17 m s^{-1} (wSBL) and overlapping for speeds between 5 to 15 m s^{-1} (Figure 5.10, dashed lines). Interestingly, this is exactly the region where pdfs of U_{geo} in the 6 hours around wSBL to vSBL and reverse transitions show their maxima (Figure 5.10, solid lines). Thus, for intermediate U_{geo} values the boundary layer does not tend to remain persistently in one regime. The value of U_{geo} cannot be used as a clear predictor of very persistent nights as pdfs of nights with transitions and persistent nights overlap considerably.

The joint distribution of U_{geo} and LLCC in the wSBL shows that in overcast conditions the largest probabilities of U_{geo} are found between 10 and 20 m s^{-1} (Figure 5.11, left panel). In contrast, for very persistent vSBL nights the most probable combination is low U_{geo} (between 3 to 8 m s^{-1}) with clear sky conditions (Figure 5.11, right panel). Overcast conditions are associated with the vSBL only for very low U_{geo} values. These results show that for overcast (LLCC $>$ 95 %) or clear-sky (LLCC $<$ 5 %) conditions different U_{geo} ranges separate the very persistent vSBL from the very persistent wSBL. For clear-sky conditions the value U_{geo} of 12 m s^{-1} approximately separates the two regimes. Due to the influence LLCC has on the longwave radiative fluxes this threshold value decreases

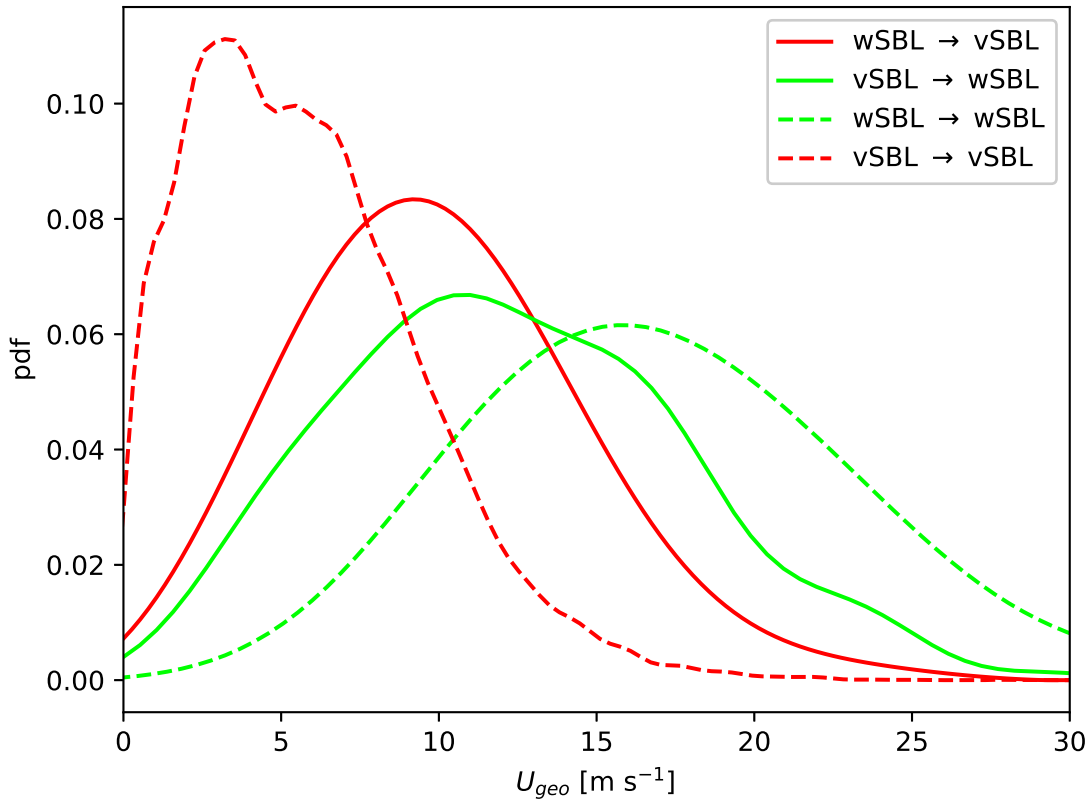

Figure 5.10: Probability density functions of the geostrophic winds in nights remaining exclusively in the wSBL (green dashed line) and the vSBL (red dashed line), and in the 3 hours before and after transitions from the wSBL to the vSBL (red solid line), and in the 3 hours before and after transitions from the vSBL to wSBL (green solid line) at Cabauw. All pdfs are calculated with the multivariate kernel density estimation by *O'Brien et al.* [2014, 2016].

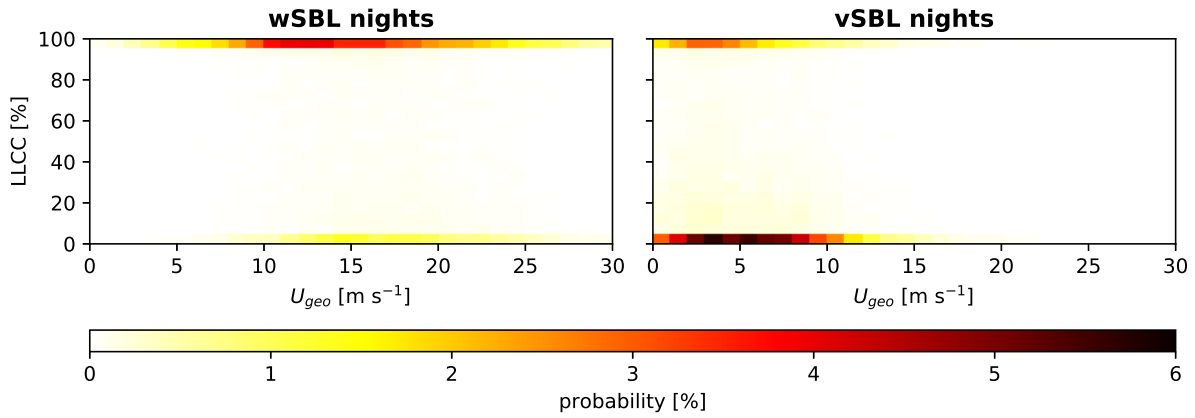

Figure 5.11: Joint of U_{geo} and LLCC for very persistent wSBL (left panel) and vSBL nights (right panel) at Cabauw.

---

to about 7 m s^{-1} under overcast conditions. These results are broadly consistent with findings of *Monahan et al.* [2015], in which regime occurrence was conditioned on values of external forcing (in contrast to the conditioning of external forcing on regime occupation considered here).

5.5 Frequency of occurrence of very persistent wSBL and vSBL nights

Across the land-based stations nights without transitions are least likely at the North American sites, Boulder and Los Alamos (Table 5.1, colums 2-3). At Boulder about 20 % of the nights considered are found to persist in one of the two regimes. Of these very persistent nights only about one fourth are in the wSBL. At Los Alamos nights remaining completely in the wSBL or vSBL are approximately equally likely and in total occur combined in about 25 % of the time. At Cabauw and Karlsruhe persistent vSBL nights are slightly more probable than persistent wSBL nights, with a combined frequency of occurrence of about 50 %. Finally, while a persistent wSBL is quite probable at Hamburg (occurring about 30 % of all nights), a very persistent vSBL occurs only about 10 % of the time.

Differences among these frequencies reflect different characteristics of the local environment at the different tower sites. The much higher probability of persistent vSBL nights at Boulder than wSBL nights can be related to the fact that in the lee of the Rocky mountains,

Table 5.1: Percentages of persistent wSBL and vSBL nights as classified by the regime sequences estimated from HMM on the state variables set indicated in Tables 2.1 and 2.2 at each tower site compared to probabilities calculated stationary Markov chains.

Tower site	wSBL nights [%]	vSBL nights [%]	π_{wSBL} [%]	π_{vSBL} [%]
Land-based tower sites				
Boulder	4.28	15.44	55.31	44.69
Cabauw	22.17	27.86	61.37	38.63
Hamburg	29.64	8.30	84.99	15.01
Karlsruhe	22.18	25.47	65.25	34.75
Los Alamos	12.51	11.81	77.75	22.25
Ocean-based tower sites				
FINO-1	55.45	15.89	67.76	32.24
FINO-2	38.26	31.22	51.84	48.16
FINO-3	52.06	23.28	66.56	33.44

times of large-scale subsidence and relatively low cloud coverage are relatively common. Even though Los Alamos is also located in a region of climatologically low cloud coverage, the complexity of the surrounding terrain may be responsible for strong TKE production and a higher frequency of persistent wSBL nights. Other processes such as persistent strong density currents may result in the higher frequency of persistent wSBL nights than at Boulder.

Even though Cabauw, Hamburg, and Karlsruhe are located in the European midlatitudes (with similar synoptic conditions) substantial differences between Hamburg and the other sites exist. The approximately equal probability of very persistent wSBL and vSBL nights at Cabauw and Karlsruhe is consistent with the fact that the sites are relatively close and share similar meteorological conditions. Though Hamburg is located in the same climatological region, the elevated probability of persistent wSBL than vSBL nights might be related to the influence of the nearby city. The tower is more often downwind of the city than upwind, and we find that all persistent vSBL nights are observed for times when the tower is upwind of the city.

At the ocean-based FINO-2 tower (located in the Baltic sea) the frequencies of occurrence differ considerably from the other sites in the Northern Sea. At FINO-1 and FINO-3 about half of the nights experience very persistent wSBL nights whereas at FINO-2 this frequency is only about 30 %. Very persistent vSBL nights, on the other hand, are more probable at FINO-2 (approximately 30 %) than at the other sites (approximately 20 %). The higher likelihood of very persistent SBL conditions at these ocean sites is consistent

with the controlling influence of the presence or absence of warm air advection aloft. This advection is expected to be often associated with synoptic-scale processes, and therefore relatively slowly evolving with time. More frequent very persistent vSBL nights at FINO-2 may result from the fact that FINO-2 is most influenced by the advection of warm air from the nearby land, by which it is surrounded in almost all directions [*Dörenkämper et al.*, 2015].

The occurrence of very persistent nights is found to depend strongly on the duration of the night, which evolves over the year (Figure 5.12). In the midlatitudes the shortest nights are about 8 hours (summer) and longest about 15 hours (winter). With the exception of Boulder the probabilities of the occurrence of very persistent wSBL nights increase with longer durations of nights (Figure 5.12, upper panel). Such an increase in very persistent wSBL nights in winter is consistent with the fact that in the Northern midlatitudes meteorological conditions favour stronger winds than in summer months due to stronger geostrophic forcing. Consistent with this picture, the occurrence of very persistent vSBL nights decreases with lengths of nights across all stations except for Boulder, where the occurrence frequency increases (Figure 5.12, lower panel).

The results suggests that at most sites the occurrence of very persistent nights is influenced by the nonstationary seasonal development of large-scale meteorological conditions.

5.6 Conclusions

The regime sequences from HMM analyses of the nighttime mean wind, wind speed shear, and stratification data at eight different land- and ocean-based tower sites have been used in order to focus on persistent wSBL and vSBL conditions, defined as nights without any regime transitions. We find systematic changes in frequency of such nights with variations in surface conditions: such nights are relatively rare in arid regions (Boulder and Los Alamos), more common in cloudier regions (Cabauw, Hamburg, and Karlsruhe), and most common at ocean-based tower sites (FINO-1, FINO-2, and FINO-3).

For the land-based stations only Boulder and Hamburg experience a large difference in the occurrence of persistent wSBL and vSBL nights. At other sites the occurrence is approximately equally likely. Near Hamburg persistent wSBL nights are substantially more frequent than persistent vSBL nights. In contrast, at Boulder persistent wSBL nights are considerably less frequent than vSBL nights.

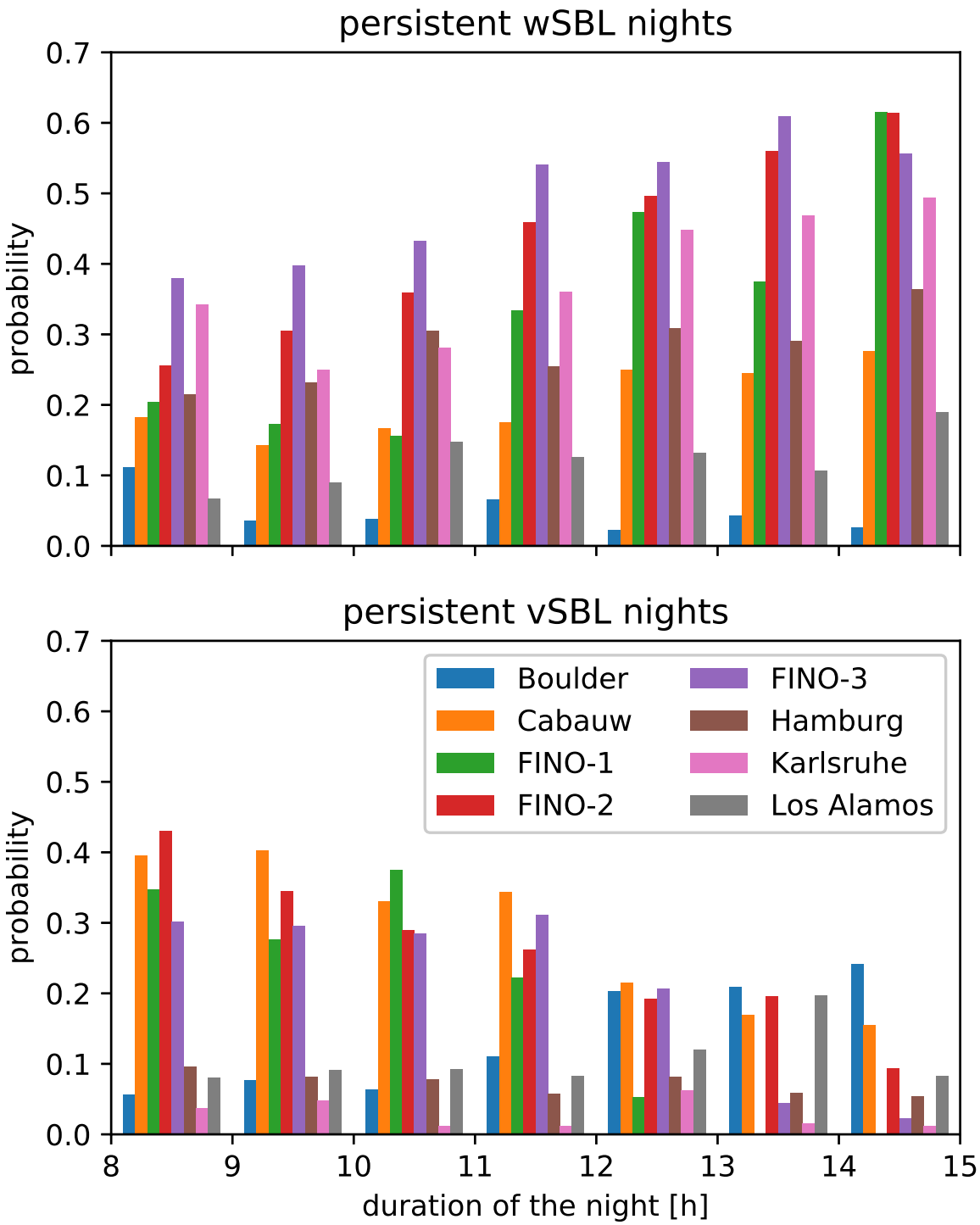

Figure 5.12: Probabilities of the occurrence of persistent wSBL (upper panel) and vSBL (bottom panel) nights in bins of 1 hour at the different tower sites as determined by the HMM analyses using the reference state variable sets.

Across all sites the occurrence of very persistent nights depends strongly on the season. Very persistent wSBL are more frequent in wintertime than in summer whereas very persistent vSBL nights are more frequent in summer nights (with the exception of Boulder).

Stratification and wind profiles show a clear separation between the two regimes across the land-based stations. The wSBL is governed by strong wind conditions and near neutral to weakly stable stratification profiles. Strong winds, in particular near the surface and therefore indicating strong shears, lead to relatively large TKE production, vertical velocity variations, and turbulent momentum transports. Because of the relatively large vertical turbulent fluxes, the near-surface atmospheric layers are coupled and directional shears are relatively small.

The vSBL is governed by strong stratifications and low wind conditions which lead to low TKE values and weak vertical turbulent momentum flux. The atmospheric levels are uncoupled from each other and at most sites directional shears increase. While at some tower sites where terrain-induced baroclinicity may affect the vertical wind profiles, the magnitude of across-wind components relative to highest observational altitudes is larger in the vSBL in than the wSBL (with the exception of Boulder).

In both the very persistent wSBL and vSBL nights, wind conditions are relatively steady throughout the entire nights. Wind speeds are relatively strong in the wSBL and weak in the vSBL, and the distributions are well-separated. The stratification profiles in very persistent wSBL nights are established at the time of sunset, whereas in very persistent vSBL nights the temperature profiles adjust up to 2 hours after sunset and stay steady afterwards.

At the ocean-based stations the wind profiles are not separated between very persistent vSBL and wSBL nights. At these locations, the very persistent vSBL is induced by the advection of warm air aloft rather than by surface cooling. The across-wind components are well-separated between regimes at these stations, reflecting the difference between relatively strong turbulence coupled states and weak turbulence uncoupled states.

Consistent with the fact that the wind speed distributions are separated in persistent wSBL and vSBL nights over land, we find a separation of the pressure gradient force (as measured by U_{geo}). However, U_{geo} is not an effective predictor of very persistent regime nights as nights with transitions are associated with a broad range of values overlapping those associated with persistent nights. Another external driver on the SBL dynamics is the LLCC. Very persistent wSBL nights are 4 times more likely to be accompanied by overcast than clear-sky conditions. Conversely, very persistent vSBL are about 3 times

more likely to be found with clear-sky than overcast conditions. Very persistent wSBL nights are most likely to occur under overcast conditions with strong U_{geo} while persistent vSBL nights are most likely under clear-sky conditions with weak U_{geo}. Under clear-sky conditions we find an approximate threshold of U_{geo} equal 12 m s^{-1} separating persistent vSBL from wSBL nights. Under overcast conditions very persistent wSBL nights tend to occur at lower U_{geo} and very persistent vSBL nights only occur with very low U_{geo} of approximately below 6 m s^{-1}. While U_{geo} separates persistent wSBL from vSBL nights, regime transitions are most likely in the intermediate U_{geo} range (centred at about 10 m s^{-1}).

Persistent wSBL and vSBL nights at land sites are associated with relatively steady wind speed and stratification profiles. The absence of transitions and the steadiness of the flow are consistent with relatively steady large-scale forcing (geostrophic wind and cloud cover).

We find many features of persistent nights are broadly the same across the different towers. Nevertheless, there are differences between towers (both qualitative and quantitative). A more detailed analysis of the reasons for these differences is an interesting direction of future study.

In this study we have focused on very persistent nights and described the clear differences in the characteristics of the boundary layer structures. In general, for nights remaining persistently in one regime the distributions of state variables overlap only weakly providing a clear picture of the structures that can be related to the two regimes. In chapter 6, we will focus on the transitions between regimes, investigating how atmospheric conditions evolve during regime transitions and which processes lead to transitions.

6 The structure of meteorological state variables and the role of external influences in times of regime transitions

Chapter Abstract

The evolution of profiles of meteorological state variables during transitions in the SBL between wSBL and vSBL regimes, as classified by the HMM, is examined at nine different tower sites. During wSBL to vSBL transitions, corresponding to the collapse of turbulence, inversion strengths increase, near-surface winds decelerate, and atmospheric layers vertically decouple. The TKE steadily decreases before wSBL to vSBL transitions and the variance of the vertical velocity collapses. Across land-based sites the frequency of occurrence of these transitions is enhanced close to sunset when the surface radiative energy budget becomes negative. Across ocean-based stations the transition is initiated by advection of warm air aloft and only weak maxima in the timing of transitions are evident. The reverse transition, the recovery of turbulence from the collapsed regime, is characterised by fast break-downs of the inversion strength, acceleration of wind profiles, and a restored vertical coupling of the atmospheric flow. TKE recovers first in atmospheric levels between 50 to 100 m on timescales of minutes. The occurrence of recovery events is approximately independent of the time of night. At the one station where cloud cover and geostrophic wind data are available (Cabauw in the Netherlands), many transitions are associated with LLCC changes: decreasing LLCC with wSBL to vSBL transitions, and increasing LLCC with turbulence recovery events. The pressure gradient force, on the other hand, shows no systematic tendencies during times of transitions.

6.1 Introduction

The hidden state occupation sequence of the HMM analysis (the classification of each observational time step into one of the vSBL or wSBL) obtained in chapter 4 allows for a systematic examination of the structure and timing of transitions. First we present composites of the evolution of Reynolds-averaged mean and turbulence state variables across transitions in sections 6.2 and 6.3. We then examine the relationship between transitions and changes in external drivers such as LLCC and the pressure gradient force (section 6.4). Finally, we analyse the distribution of transition occurrences as well as the distribution of event durations in section 6.5 followed by conclusions in section 6.6. This chapter is based on *Abraham and Monahan* [2018c].

6.2 The structure of Reynolds-averaged mean state variables across times of transitions

In order to systematically analyse the change in the structure of meteorological state variables at times of transitions we investigate composites of the evolution of these quantities. Such composites provide information about the average behaviour during transitions across the different tower locations. The composites are centred on the times of transitions and extend 90 minutes before and after. For Reynolds-averaged mean state variables, composites computed from median values are much the same as those based on the means and so are not shown.

Although the transition probabilities themselves depend on the time of the night (particularly the wSBL to vSBL transition as demonstrated in section 6.5), the transition composites are not qualitatively sensitive to transition time (not shown). Furthermore, specification of composites based on only first or subsequent transitions in a night does not qualitatively change the results.

6.2.1 Land-based tower sites

Composite wind and stratification profiles (which include all state variables used in the HMM analyses) across times of transitions are qualitatively similar for all land-based tower sites (Figure 6.1; note that the scale of the vertical axes differ between the different sites). A statistical testing analysis of the similarities between towers can confirm the agreement,

however, qualitative similarities and differences as represented in the composites are more important for the discussion at hand than quantitative ones. Even though a formal assessment of the probability that the observed differences result from sampling could be done it would also require a number of approximations due to different measurement altitudes and sampling frequencies across the different tower sites.

With the exception of Hamburg and Karlsruhe, the near-surface wind decreases by about 2 to 3 m s^{-1} during the wSBL to vSBL transition (Figure 6.1, first column). Whilst the wind speed at Boulder and Los Alamos decreases substantially at all observed altitudes, at Cabauw, Hamburg, and Karlsruhe the wind aloft decreases moderately at the moment of the transition. After an initial deceleration of the whole wind profile, wind speeds aloft start to accelerate steadily about 20-30 minutes after the wSBL to vSBL transition, likely due to the development of a low level jet. Only at Karlsruhe is no low level jet development evident.

As expected, the static stability increases during wSBL to vSBL transitions (Figure 6.1, second column). At these land-based sites the SBL starts with a nearly-neutral to weakly-stable stratification (at Boulder only in the bottom 100 m). The stratification then begins to strengthen about 60-30 minutes before the moment of the wSBL to vSBL transition, and continues to increase gradually after the transition. At Los Alamos the stratification in the lowest 50 m becomes particularly strong. In the established vSBL the European sites have quite similar stratification strengths, somewhat weaker than at the North American sites.

The vSBL to wSBL transition shows a clear increase of wind speeds at all measurement levels (Figure 6.1, third column). In particular, at Boulder and Los Alamos an increase of about 2-3 m s^{-1} is observed. At the European sites the increase is about 1-2 m s^{-1}. The change in wind speed has the same sign at all measurement altitudes, suggesting that it results from the entrainment of high-momentum fluid from above the highest observational levels. Another possibility is that in a vertically-coupled boundary layer the surface momentum flux is balanced across a deeper layer (making the vertical mean turbulent momentum flux convergence smaller) allowing the flow to accelerate [*Samelson et al.*, 2006].

In contrast to the rather slow build-up of inversion strength at times of the wSBL to vSBL transition, the reverse transition happens rather abruptly, with the first evidence of changes occuring about 20-30 minutes before the transition (Figure 6.1, fourth column). Across the land-based stations, the inversion strength is substantially decreased in the lower 100 m. Shortly after the transition the stratification remains relatively steady, except at

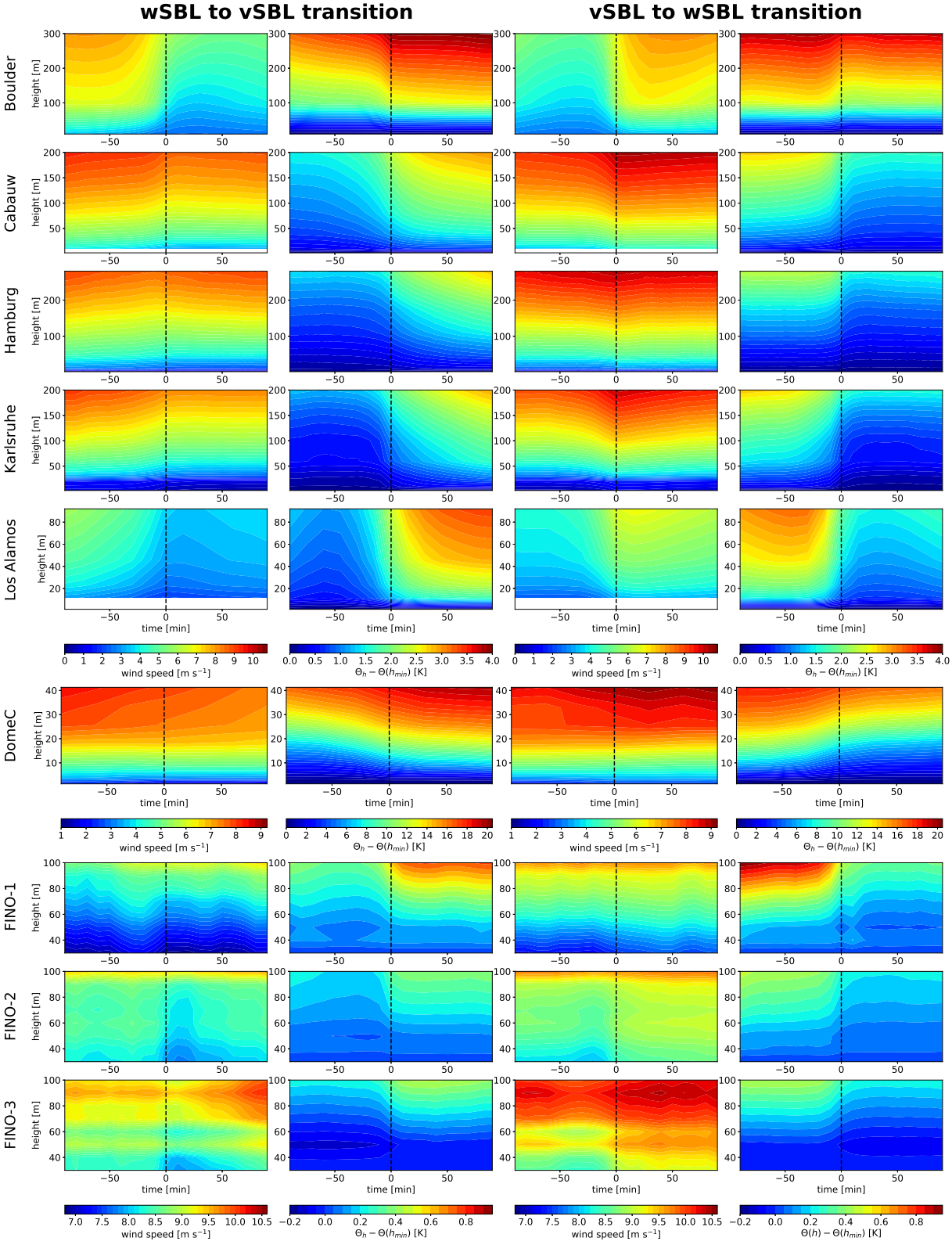

Figure 6.1: Time evolution of the composite means of the stratification (first and third column) and wind speed profiles (second and fourth columns) at the different tower sites in times of turbulence collapse (wSBL to vSBL transition; first and second columns) and turbulence recovery (vSBL to wSBL transition; third and fourth columns) as determined by the HMM analyses. The composites show the 90 minutes before and after the transitions at time equals zero (dashed reference line).

Los Alamos where the inversion recovers relatively quickly. This difference may result from the fact that the site is characterised by a low thermal conductivity and little cloud cover, encouraging radiative cooling at the surface. Interestingly, at Boulder reduction in inversion strength is most prominent between about 50 to 150 m.

Across all land-based sites stratification evolves gradually in wSBL to vSBL transitions due to the continuous surface cooling (caused by increasing near-surface radiative flux divergence) which continuously strengthens the inversion. In fact, potential temperature profiles reveal the formation of cold-air pools near the surface preceding the occurrence of wSBL to vSBL transitions (Figure 6.2, first column). Deviations from the 180-minute time mean show that the cooling at higher levels is substantially smaller than that at the surface (Figure 6.2, second column). In the reverse transition, from the vSBL to the wSBL, the strongest changes in temperature appear aloft while surface temperatures change little or increase only slightly (Figure 6.2, third and fourth columns). The temperature changes show the same overall cooling as the wSBL to vSBL transitions due to the continuous radiative cooling over the course of the night. However, the recovery of turbulence and the related increased mixing of fluid with higher potential temperature from aloft towards surface layers (and of cooler air from the surface to higher levels) leads to reduced cooling near the surface (or even an initial warming) and a more pronounced cooling aloft. Evidence of this mixing is the positive temperature anomaly in the band extending from about 50 m and 10 minutes before the transition occurrence to the surface and about 30-40 minutes after the transition. The strongest signal is near the surface in the moment of the transition.

With an increased inversion strength, vertical momentum transports are expected to be reduced causing coupling of atmospheric layers to weaken. Conversely, vertical momentum transports should increase during turbulence recovery transitions and recouple atmospheric layers. Changes in the along- and across-wind component during transitions provide information about changes in directional shear caused changes in the strength of coupling (cf. chapter 5). Because the across-wind component is generally smaller than the along-wind component, behaviour of the along-wind component during transitions broadly reflects that of the wind speed profiles (Figure 6.3, first and third columns).

For these land-based stations we analyse composites of the absolute values of the across-wind component as the across-wind components take both positive and negative signs at stations located in mountain regions (cf. Figure 6 of cf. chapter 5). The absolute across-wind component increases rapidly during wSBL to vSBL transitions, in particular below 100 m (Figure 6.3, second column). The increase in the value of the across-wind component

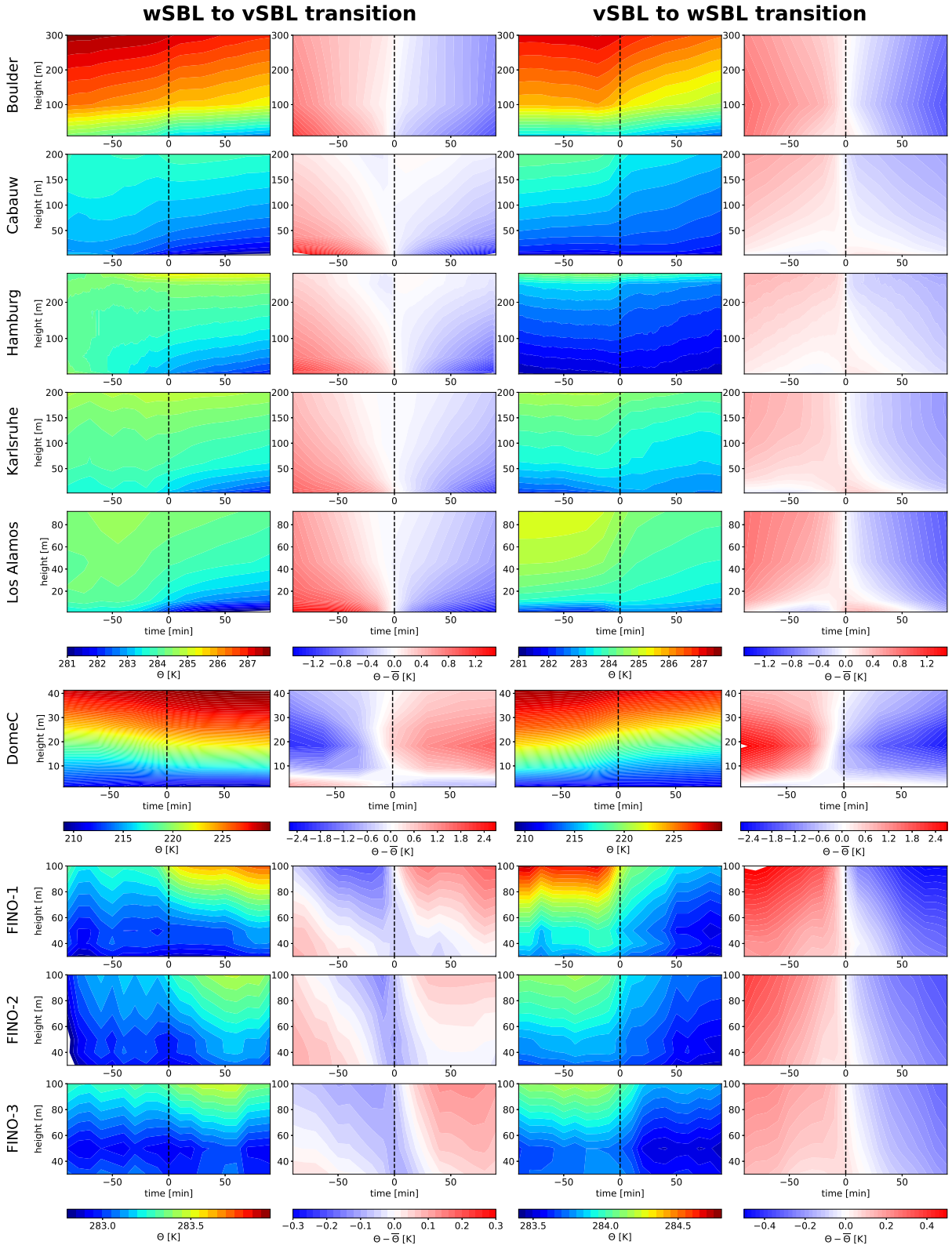

Figure 6.2: As in Figure 6.1, but for potential temperature profiles (first and third columns) and their mean of deviations of the 180 minute time mean during each transition (second and fourth columns).

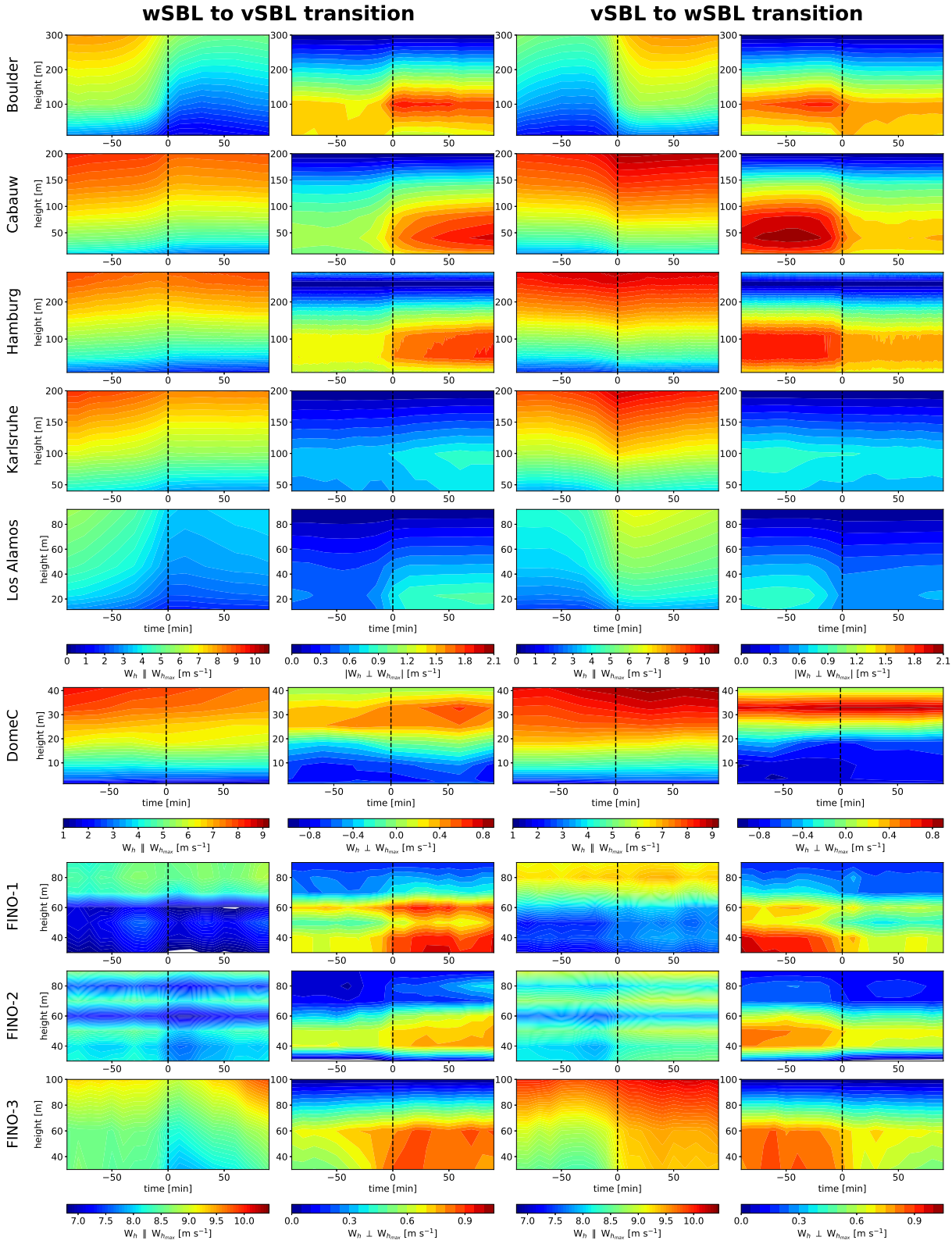

Figure 6.3: As in Figure 6.1, but for along wind (first and third columns) and across wind components (second and fourth column, absolute values at land-based stations) profiles.

during the transition is largest at Boulder, Cabauw, and Hamburg. The relatively small magnitude of the change at Los Alamos is a consequence of the fact that the highest observational level is around 100 m (in contrast to 200-300 m at the other sites) and the across-wind components are calculated relative to this reference. Taking 100 m as the reference height at other sites results in across-wind magnitudes below 50 m similar to that observed at Los Alamos (not shown). Transitions from the vSBL to the wSBL are associated with a rapid decrease of the absolute across-wind component around the time of transition (Figure 6.3, fourth column).

Previous studies [e.g. *Mahrt*, 2007, 2008; *Lang et al.*, 2018] have argued that abrupt changes in wind directional shears are associated with the propagation of submeso motions such as microfronts, density currents etc. Our results show that rapid changes in shear can also be associated with transitions between SBL regimes.

6.2.2 Ice-based stations

The extreme conditions at DomeC result in vertical scales of SBL transition structures being much smaller than at the land-based stations. Wind speed changes across transitions with magnitudes of about 2-3 m s^{-1} between 3-40 m at DomeC are similar to the values observed at land-based stations (Figure 6.1, first and third colum). In contrast to the land-based stations there is no evidence of a subsequent development of a low level jet at DomeC within the time range considered. The stratification shows a clear increase during wSBL to vSBL transitions, and a decrease during reverse transitions (Figure 6.1, second and fourth columns). The mean stratification between 1 m and 10 m increases from 1 K to 6 K during times of turbulence collapse. Interestingly, the gradual increase in stratification following wSBL to vSBL transitions observed at land-based stations is not present at DomeC. Instead a steady vSBL is rapidly established.

Evidence that radiative cooling at the surface is one mechanism leading to the formation of the inversion is provided by the fact that the 180-minute anomaly of the potential temperatures in the lowest 10 m shows the same structure as the anomalies in the bottom few hundred metres at land-based sites (Figure 6.2). Interestingly, the temperature above 10 m increases across wSBL to vSBL transitions. Such a development is indicative of the advection of warm air. It is possible that the composites contain both events in which transitions are driven by warm-air advection aloft (above 10 m) or radiative cooling (below 10 m).

An increase in the directional shear across times of wSBL to vSBL transitions is also evident in such a way that the upper and lower levels separated by the 10 m height increase in opposite directions (Figure 6.3). Here, we do not consider the absolute value, in order to depict the complex behaviour of the across wind component at this site. Relative to the land-based stations the across wind-component gradients at DomeC are much stronger, consistent with much stronger stratifications which can sustain larger shears. In times of turbulence recovery a decrease in the directional shear below 20 m is evident but not at higher altitudes. The signs of the across-wind component are consistent with the structure of an Ekman-like spiral in the Southern hemisphere.

6.2.3 Ocean-based stations

At the FINO towers the atmospheric structures observed during transitions at land- and ice-based stations are similar but the signals are smaller. Transitions from the wSBL to vSBL are evidently driven by advection of warm air aloft, as these changes are associated with a temperature increase aloft rather than a cooling at the surface (Figure 6.1, Figure 6.2). The fact that ocean-based stations experience wSBL to vSBL transitions exclusively due to advection of warm-air is physically reasonable, as radiatively-driven surface cooling over an ocean surface with high heat capacity is very weak (cf. chapter 4). Consistent with the wSBL and vSBL contrasts in very persistent nights (cf. chapter 5), wind speed changes across times of transitions between the two SBL regimes are not as pronounced as over land and ice-based stations. However, wind speed decreases and increases can be associated with the respectively wSBL to vSBL and reverse transitions. Both SBL transitions show relatively fast changes in the flow and stratification and stay relatively steady after the moment of the transition in contrast to the slow build up of stratification which is observed over land.

The across-wind components at the ocean-based stations exhibit the same structures as demonstrated for the land- and ice-based stations, with relatively strong increases and decreases during SBL regime transitions due to changes in the vertical momentum transports (Figure 6.3). The advection of warm air aloft at these locations leads to a pronounced vertical decoupling of atmospheric layers below about 60 m from those above.

6.3 The structure of turbulence state variables across times of transitions

Consistent with the evolution of Reynolds-averaged shear and stratification (which control TKE production and consumption), TKE values across times of transitions reflect the conceptual picture of transitions between strong and weak turbulence regimes. In constructing composites, we consider both means and medians because of the highly-skewed TKE distribution. Turbulence data are available only at the land-based stations at Cabauw, Hamburg, and Los Alamos.

The steadily increasing inversion strength preceding wSBL to vSBL transitions coincides with steadily decreasing TKE values (Figure 6.4, first and second column). These transitions are marked by a clear turbulence collapse, such that mean TKE values decrease by 1-2 orders of magnitude. In contrast to Cabauw and Los Alamos, at Hamburg a shallow layer of weak turbulence persists in the vSBL. This feature appears to result from horizontal advection of TKE generated by flow over nearby rough urban elements. Conditioning the evolution of TKE profiles on wind directions from the East to Southeast (for which the tower is upwind of the city) this residual TKE is almost absent (not shown). Strong contrasts between the SBL regimes are also evident in $var(w)$, a measure of the turbulence intensity which is not influenced by non-turbulent two-dimensional motions. Composites of $var(w)$ show that vertical motions are almost completely suppressed after wSBL to vSBL transitions. The collapse of $var(w)$ is particularly evident in the median composite.

As a result of the suppression of vertical motion in strongly stably stratified conditions, we expect that the turbulence should be less isotropic in the vSBL than in the wSBL. We measure the turbulence anisotropy by the ratio $3var(w)/(var(u)+var(v)+var(w))$, where u, v, and w are respectively zonal, meridional, and vertical wind components. This measure takes a value of 1 for isotropic turbulence. As expected, the turbulence becomes more anisotropic across the wSBL to vSBL transition (Figure 6.4, first and second columns). In particular, at Los Alamos the turbulence aloft changes from almost perfectly isotropic to clearly anisotropic. While such strong changes in the turbulent isotropy are not evident at Cabauw and Hamburg, the qualitative features of the changes agree. One difficulty in the direct comparison of isotropy characterized at the sites is that the averaging times differ (from 1 minute at Hamburg to 15 minutes at Los Alamos) which likely affects the relative influence of non-turbulent quasi-2-dimensional motions on the TKE.

As found with the Reynolds-averaged mean variables, the recovery of turbulence occurs on timescales of a few minutes. TKE recovers throughout the range of observed altitudes

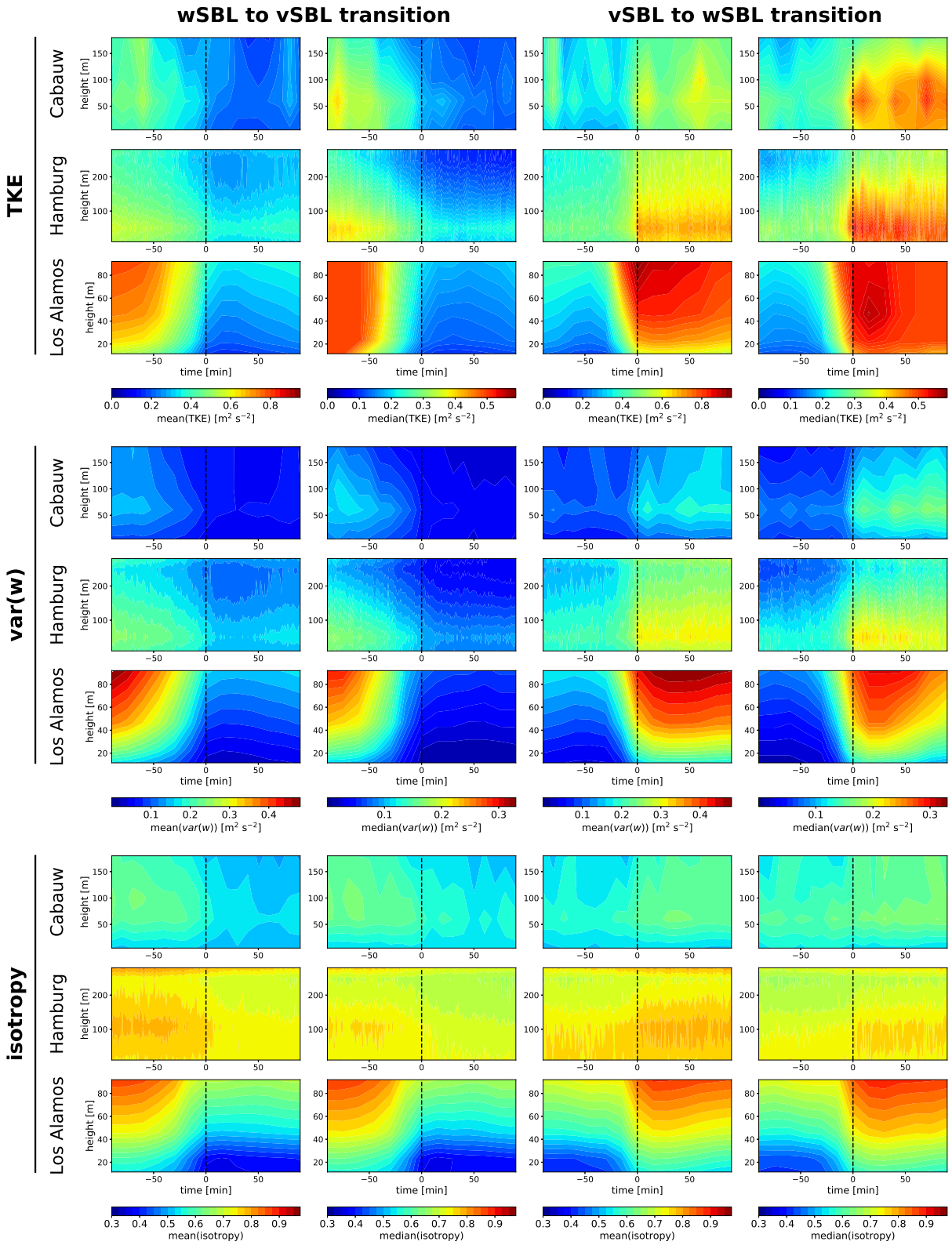

Figure 6.4: Time evolution of the composite means (first and third columns) and composite medians (second and fourth columns) of TKE profiles (upper panel block), the variance in the vertical wind component w ($var(w)$, middle panel block), and the isotropy ($3var(w)/(var(u)+var(v)+var(w))$) of turbulence profiles (lower panel block) at the different tower sites where turbulence data is available in times of turbulence collapse (wSBL to vSBL transition; first and second columns) and turbulence recovery (vSBL to wSBL transition; third and fourth columns) as determined by the HMM analyses. The composites show the 90 minutes before and after the transitions at time equals 0 (dashed reference line).

in less than 10 minutes for all of the tower sites considered (Figure 6.4, third and fourth columns). TKE values after the transition increase by factors of two (Cabauw and Hamburg) to four (Los Alamos). Interestingly, at Cabauw and Hamburg the onset of turbulence appears to be located in the atmospheric layers between 50 to 100 m. At Los Alamos the turbulence originates at altitudes above the observational levels. These results are broadly consistent with the picture of top-down turbulent bursts breaking down the inversion [e.g. *Acevedo et al.*, 2006; *Basu et al.*, 2006], possibly due to intermittent events such as breaking gravity waves. The fact that the medians of $var(w)$ before a turbulence recovery event are much weaker than afterwards indicates that there are many cases in which the onset of turbulence is abrupt. Consistent with an increase in $var(w)$ and reduced stratification the isotropy of turbulence increases and structures become more three-dimensional than before.

The average TKE before turbulence recovery is larger than that immediately after a turbulence collapse. At Hamburg, vertical fluctuations show larger values before a recovery than after collapse. One possible explanation consistent with slightly larger TKE values before a recovery event than after a collapse event could be a slow build-up of shear, resulting to the local production of TKE to the point that the inversion breaks down.

Other turbulent state variables such as the magnitudes of the turbulent stresses show similar results (not shown). Whilst turbulent heat fluxes towards the surface decrease during times of turbulence collapse and increase during recovery, they do not show such large changes as the momentum turbulent fluxes. This result is consistent with the fact that same heat fluxes can result from strong stratification with weak turbulence or weak stratification with relatively strong turbulence [e.g. *van de Wiel et al.*, 2012a,b, 2017].

6.4 External drivers of transitions

External influences on the SBL state are advection of warm-air aloft, cloud cover, and pressure gradient force. The results shown above and in chapter 5 demonstrate that warm air advection is important for driving transitions to the vSBL at ocean-based sites, and likely at DomeC. Such a clear signal could not be found for the land-based stations, where radiative cooling evidently dominates. At land-based stations external influences expected to most influence transitions in the SBL state are cloud cover and pressure gradient force [*Monahan et al.*, 2015]. Increasing LLCC increases the downwelling longwave radiation and reduces the radiative cooling at the surface. On the other hand, decreasing LLCC enhances

surface radiative energy loss. Variations in the pressure gradient force can change near-surface shears and shear production of TKE. As LLCC and U_{geo}, used as a measure of the pressure gradient force) are only available at Cabauw the following analysis focuses on that site.

The instantaneous geostrophic wind shows no evident differences at transition times: the probability distributions of U_{geo} magnitudes at times of transitions are almost the same for both kinds of transitions, with nearly equal maxima at around 10 m s^{-1} (cf. chapter 5). These results agree well with the finding of *van der Linden et al.* [2017] that there is no clear U_{geo} threshold between the vSBL or wSBL. Therefore, we analyse the tendency of the geostrophic wind in the 90 minutes before and after the transitions (approximated by linear regression) in order to evaluate if changes in large-scale pressure gradient force can initiate a transition. No strong relationship is evident between geostrophic wind tendency and regime transitions (Figure 6.5). We find that turbulence collapse events are associated with both increasing and decreasing U_{geo}, with roughly equal probability (Figure 6.5, top panel). Similar results are found for recovery events, of which roughly 60 % are associated with an increase and 40 % with a decrease in pressure gradient force (Figure 6.5, bottom panel). Tendencies of U_{geo} show approximately the same range of values during either kind of transition (Figure 6.6, top panel). The maxima of the U_{geo} tendency pdfs in the different transitions show the expected signs: decreasing U_{geo} for the turbulence collapse and increasing for recovery. However, the values of these most likely values are very small relative to the breadths of the distributions and therefore this result does not imply any useful predictive skill.

Changes in LLCC have a stronger effect on transitions than those of U_{geo}. We measure the change of the LLCC by subtracting 30-minute averages following and preceding transitions (Figure 6.5, vertical axis). The LLCC tendencies can then broadly be examined in three different classes: increasing, decreasing, and steady (no change). The wSBL to vSBL transition is associated about 35 % of the time with decreasing LLCC and about 20 % of the time with increasing LLCC (Figure 6.5, top panel). No LLCC change is found for the rest of the transitions. The pdf of LLCC tendency in times of wSBL to vSBL transitions has a peak around zero, as these transitions are most probable in the absence of cloud cover tendencies (Figure 6.6, bottom panel). Nevertheless, the negative skewness of this distribution shows that decreasing LLCC is more probable than increasing in times of turbulence collapse.

A closer relationship is found between turbulence recovery events and cloud cover tendency. An increasing LLCC is found in about 50 % of recovery events, no LLCC change in about

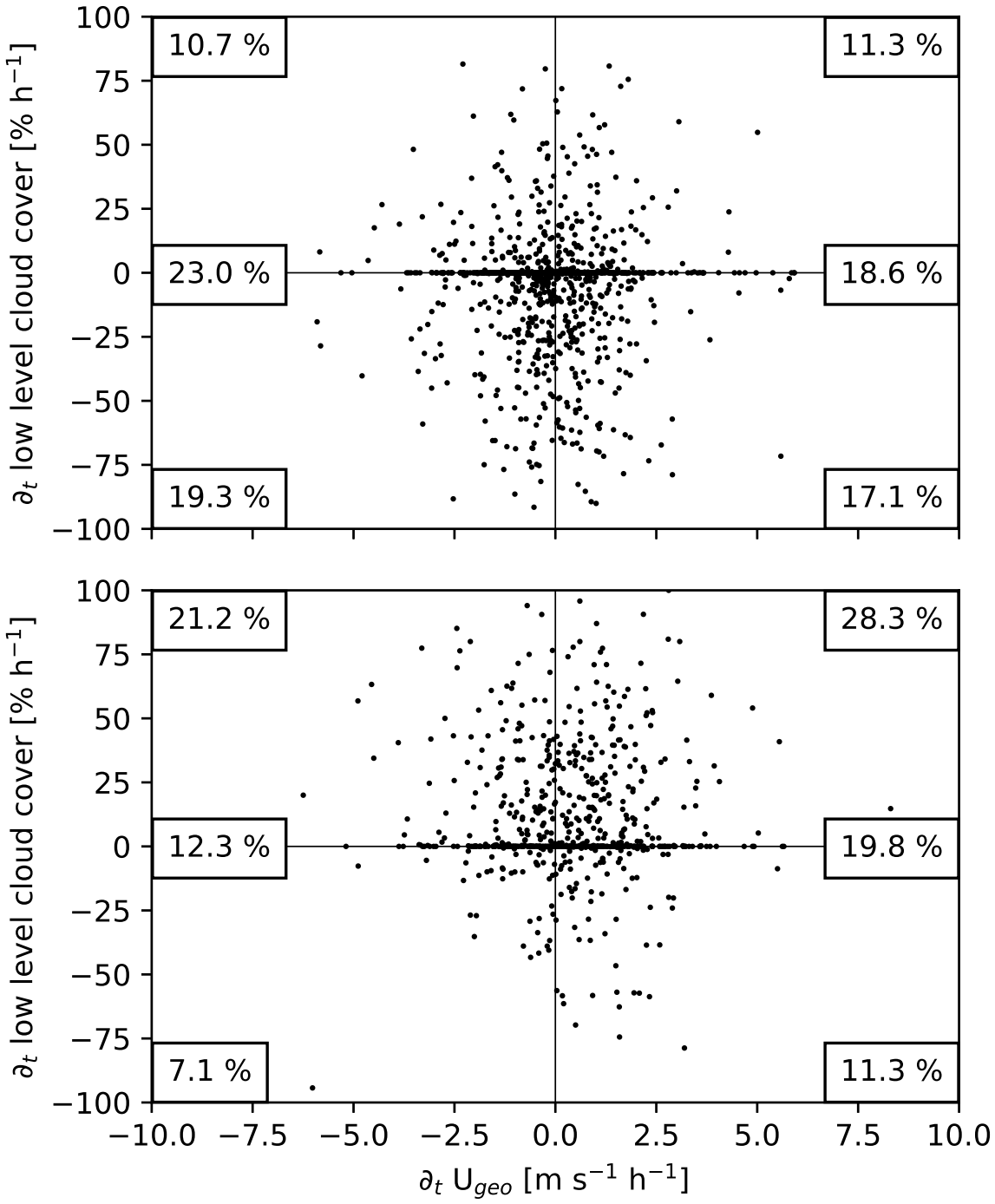

Figure 6.5: Scatterplot of the tendency (as determined by linear regression) of the geostrophic wind in the 90 minutes before and after transitions and the low level cloud cover change of the 30 minute means before and after transitions for wSBL to vSBL transitions (upper panel) and reverse transitions (lower panel) at Cabauw. Relative occupation times of the quadrants are indicated as well as the relative occupation times of increasing and decreasing geostrophic winds conditioned on no low level cloud cover changes.

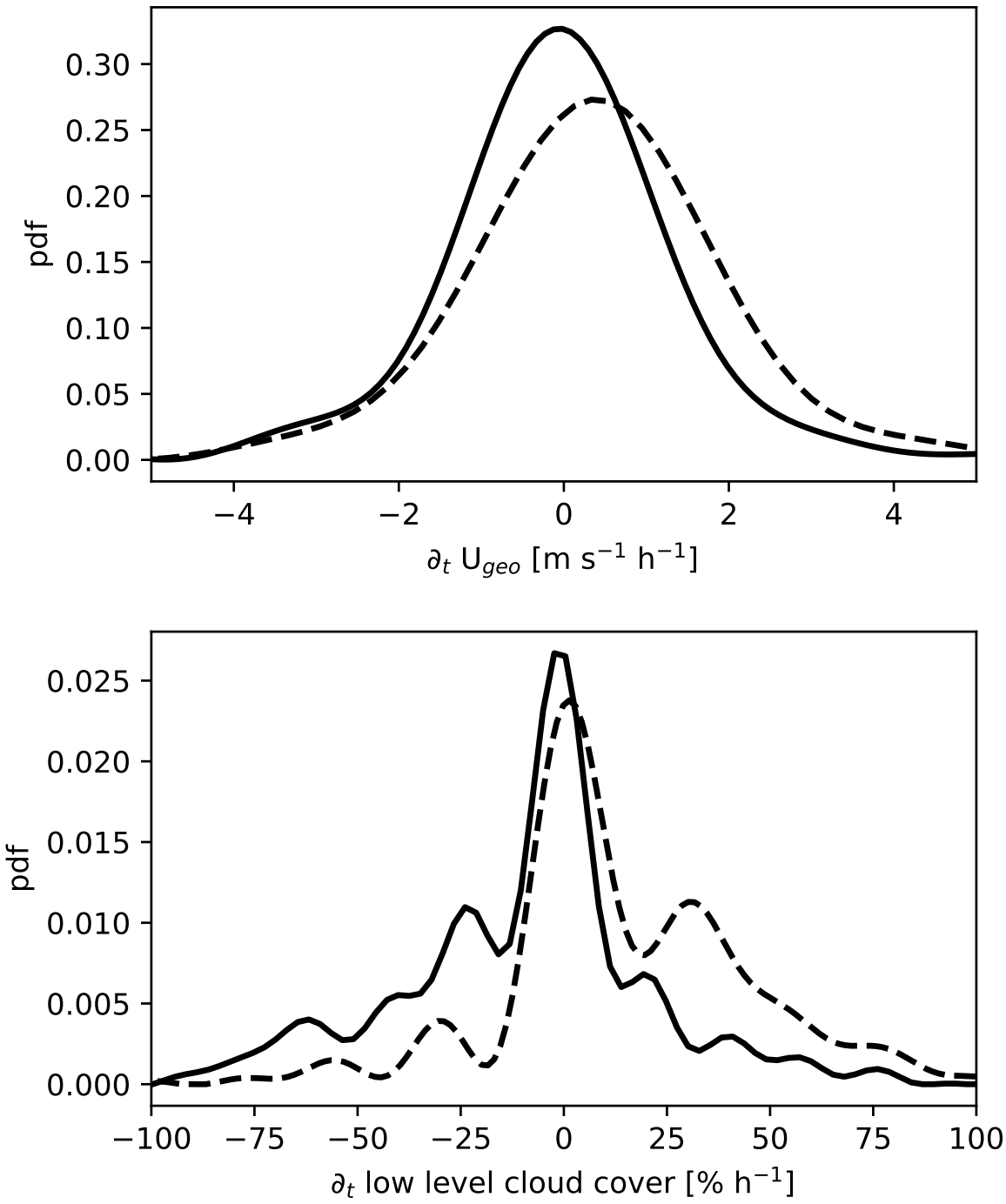

Figure 6.6: Pdfs of the tendency (as determined by linear regression) of the geostrophic wind in the 90 minutes before and after wSBL to vSBL (solid) and reverse (dashed) transitions at Cabauw (upper panel). Conditional pdfs of the change of the 30 minute means of low-level cloud cover before and after wSBL to vSBL (red) and reverse (green) transitions at Cabauw (lower panel). All pdfs are calculated with the multivariate kernel density estimation by *O'Brien et al.* [2014, 2016].

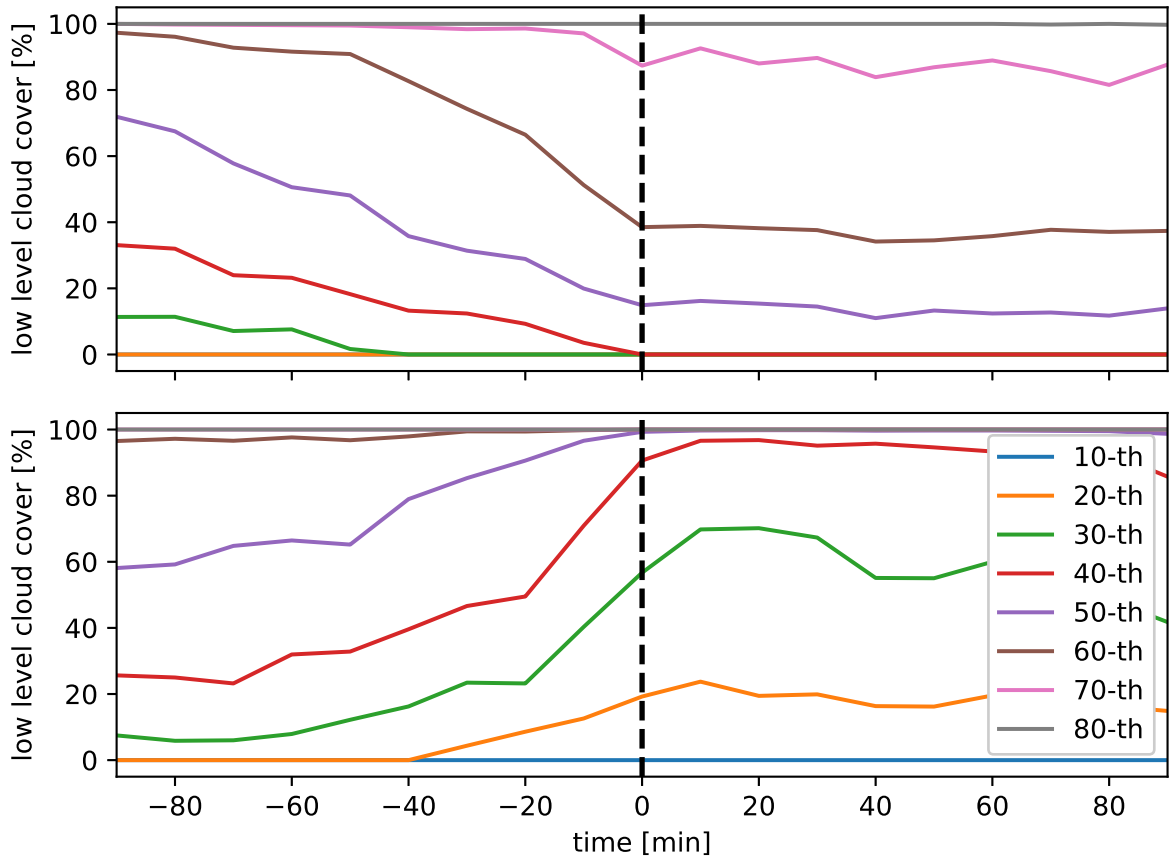

Figure 6.7: Time evolution of low-level cloud cover percentiles from 90 minutes before to 90 minutes after transitions at Cabauw of wSBL to vSBL transitions (upper panel) and vSBL to wSBL transitions (lower panel).

---

30 % of events, and only 20 % of events are associated with a LLCC decrease (Figure 6.5, bottom panel). While the most probable LLCC changes are around zero during vSBL to wSBL transitions, the pdf is prominently positively skewed (Figure 6.6).

We further analyse the relationship between LLCC changes and transitions by evaluating the evolution of LLCC quantiles across times of transitions. We find that LLCC changes associated with turbulence collapse or recovery events occur before the transitions take place (Figure 6.7). After the transitions the LLCC percentiles are relatively steady, further suggesting a causal relationship between LLCC changes and transitions. Higher clouds (above approximately 2000 m) have no impact on transitions (not shown).

Even though no clear general dependence of tendencies in U_{geo} on transitions can be found,

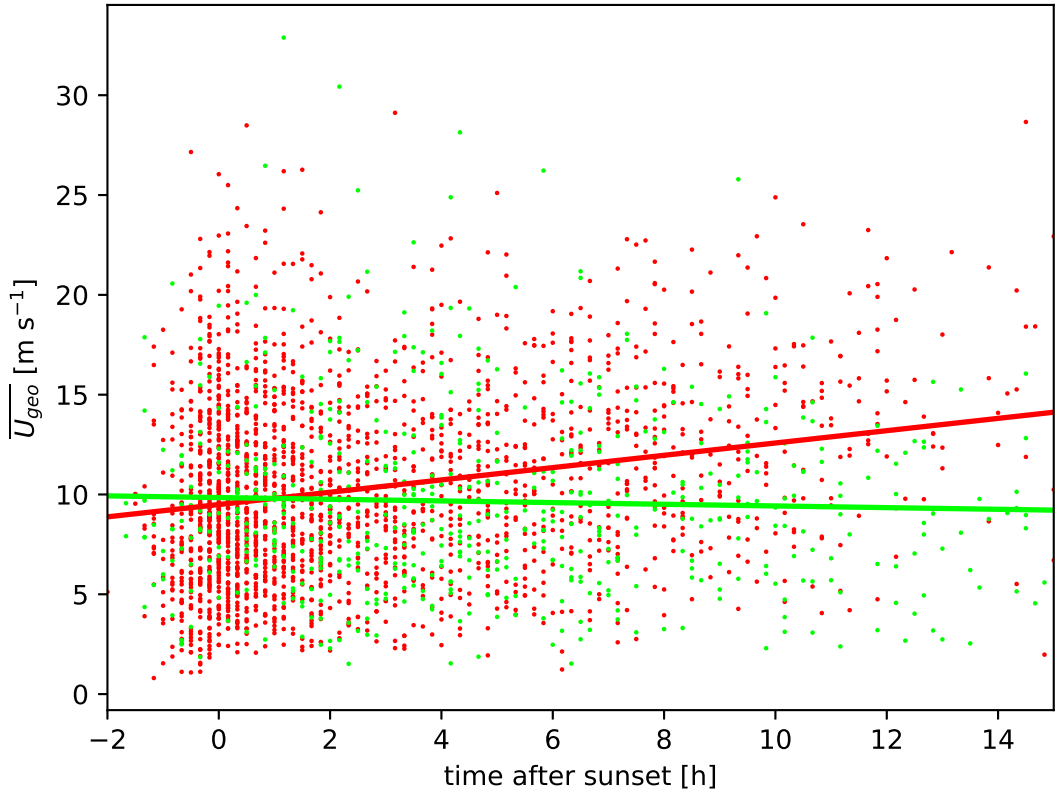

Figure 6.8: Scatterplot of the timing of first turbulence collapse (red) and first event of turbulence recovery (green) in a night depending on the mean geostrophic wind of each night. Regression lines of geostrophic wind on collapse time are also illustrated.

---

the timing of the first transitions occurring in a night depends weakly on the night-time mean geostrophic wind, denoted $\overline{U_{geo}}$ (Figure 6.8). Larger values of $\overline{U_{geo}}$ are associated with later times of first turbulence collapses, indicating that larger shears sustain the turbulence longer before radiative cooling at the surface results in the transition. This dependence is weak, and the most probable time of turbulence collapse is observed to occur within the first two hours after sunset for $\overline{U_{geo}}$ values between 1 and 30 m s^{-1}. This weak dependence is found independent of the LLCC.

In contrast, timing of events of turbulence recovery is unaffected by the value of the $\overline{U_{geo}}$ during nights. This result is consistent with the picture of the vSBL to wSBL transition resulting due to LLCC changes or due to intermittent events which are unpredictable by the large-scale meteorological state [*Rees and Mobbs*, 1988; *Lang et al.*, 2018].

Table 6.1: Percentages of nights experiencing turbulence collapse (wSBL to vSBL transition) and recovery events (vSBL to wSBL transition) as classified by the HMM regime sequences and the climatological initial probabilities to start a night in the wSBL (π_{wSBL}) or vSBL (π_{vSBL}).

Tower site	wSBL to vSBL [%]	vSBL to wSBL [%]	π_{wSBL} [%]	π_{vSBL} [%]
Land-based tower sites				
Boulder	75.14	55.42	55.31	44.69
Cabauw	42.03	24.47	61.37	38.63
Hamburg	58.49	30.14	84.99	15.01
Karlsruhe	41.34	25.38	65.25	34.75
Los Alamos	71.32	35.91	77.75	22.25
Ocean-based tower sites				
FINO-1	16.36	21.50	67.76	32.24
FINO-2	15.89	25.64	51.84	48.16
FINO-3	16.03	17.40	66.56	33.44

6.5 Probability distribution of transition times

Turbulence collapse and recovery events are common occurrences. At land-based stations turbulence collapses occur in 40-75 % of all nights, and in about 16 % of nights over the oceans (Table 6.1). The occurrence of wSBL to vSBL transitions (Table 6.1, column 2) is much higher at Boulder and Los Alamos (about 75 % of all nights) than at other land-based stations (about 50 % of nights). Boulder and Los Alamos experience less cloud cover in the climatological mean leading to a more effective radiative cooling. Furthermore, drier surfaces at these sites have lower heat capacities and lower thermal conductivities which encourage the formation of strong inversions and turbulence collapse [*van de Wiel et al.*, 2017]. The other land-based sites are located in humid environments with more frequent low-level cloud cover. The ocean-based stations likely show fewer turbulence collapses than any of the land-based stations as transitions are exclusively caused by advection of warm air aloft, which requires that the flow be aligned against the temperature gradient. The DomeC data are not considered in this analysis as because of their long duration the long lasting polar-nights are not directly comparable to those at the other locations considered.

Probabilities of the occurrence of turbulence recovery events within a night have about the same probability (20-30 %) at stations other than Boulder and Los Alamos, where the occurrence is much more frequent. This difference might simply be caused by the higher frequency of turbulence collapse episodes at these locations allowing for the possibility of more vSBL to wSBL transitions.

Seasonal variability in the occurrence of transitions is relatively weak, particularly, the occurrence of turbulence recovery events (Figure 6.9). The occurrence of turbulence collapse events tend to decrease slightly at the American sites from summer (about 80 %) to winter (about 70 %). In contrast, the frequency of such events increases slightly at Cabauw and the sites in the Northern Sea over the course of the year. One possible reason for small changes in the occurrence of turbulence collapse transitions is that the longest nights occur in winter, which is associated at midlatitude stations with more synoptic scale variability. Decreasing occurrence of wSBL to vSBL transitions in winter months may be related to stronger pressure gradient forces which mechanically sustain turbulence and encourage persistent wSBL states (cf. chapter 5). As mentioned above, the trend in the occurrence is very weak, consistent with the weak relationship between transition occurrences and external influences (as discussed in the previous section).

The wSBL to vSBL transition is caused by suppression of vertical turbulent fluxes, over land normally due to the radiative cooling at the surface. As a result, the collapse of turbulence at these stations occurs most often around sunset, when the surface radiative energy budget changes sign (Figure 6.10, upper panel). The ocean-based stations demonstrate smaller near-sunset probability maxima of wSBL to vSBL transitions. At ocean-based stations transitions are initiated by warm-air advection; such advection events will not happen at fixed times of the day at most locations. A notable exception is FINO-2, which is surrounded by land masses in most directions. Turbulence collapse due to the advection of warm air from land to over water coincidentally has the largest frequency of occurrence near to the evening transition [*Dörenkämper et al.*, 2015]. Broader and less pronounced maxima of turbulence collapse occurrences about 2-3 hours after sunset are found at FINO-1 and FINO-3. Beyond about four hours after sunset, the probability of turbulence collapse is approximately the same at all stations.

The pdfs of turbulence recovery events show only very weak maxima about 4-6 hours after sunset (Figure 6.10, lower panel). At Los Alamos a more pronounced maximum of the vSBL to wSBL transitions about 2 hours after sunset is apparent (Figure 6.10, lower panel). The minimum at the beginning of the night at this location can be explained by the fact that the probability of starting the night in the vSBL is much smaller than at most other locations (Table 6.1). While the smallest such probability is actually observed at Hamburg, the local surface roughness there is much larger than at Los Alamos due to the adjacent city, possibly leading to a faster recovery of turbulence. Other stations experience more common early-evening turbulence recoveries as the probabilities of starting a night in the vSBL are higher.

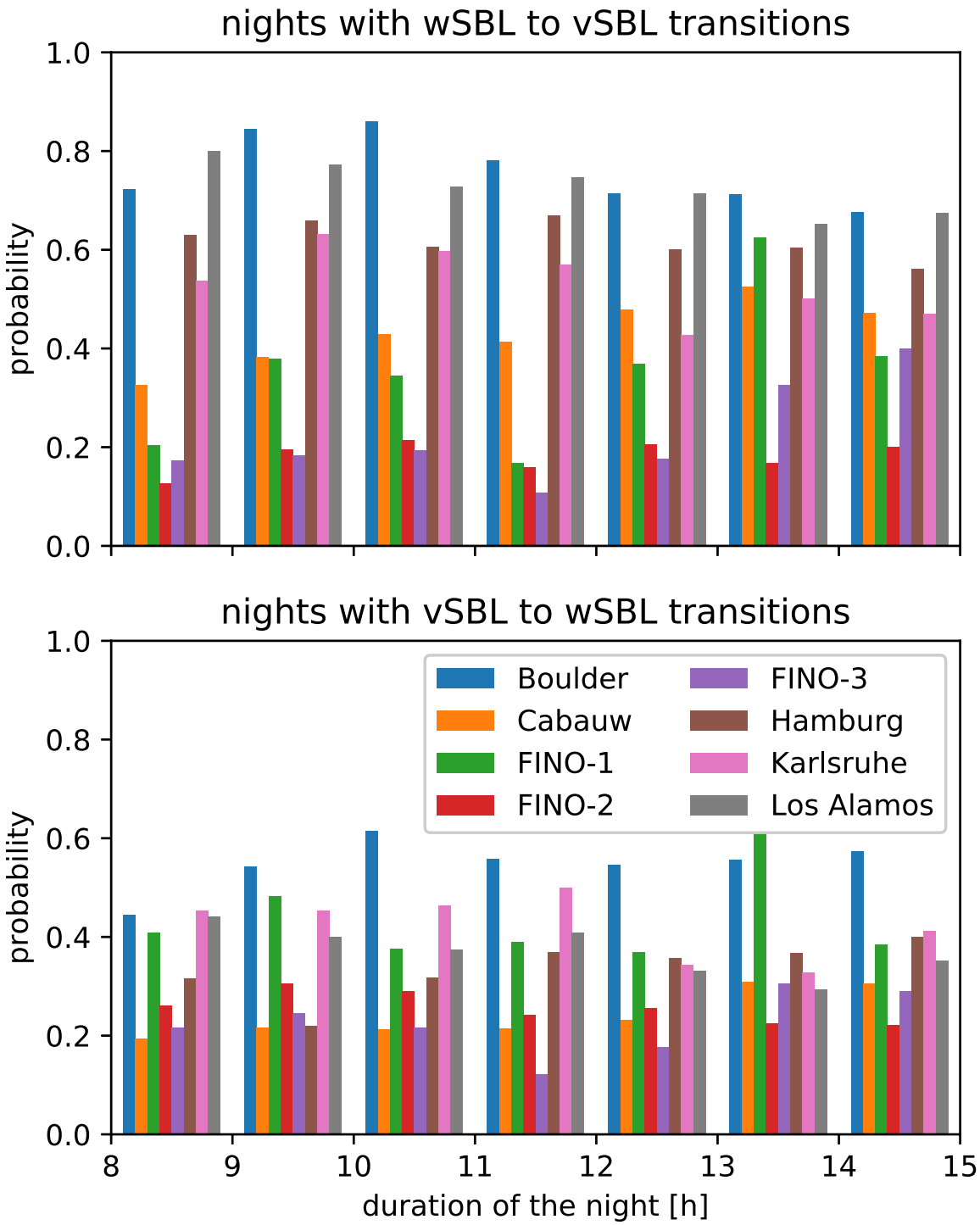

Figure 6.9: Probabilities of the occurrence of wSBL to vSBL (upper panel) and vSBL and wSBL (lower panel) transitions in bins of 1 hour at the different tower sites as determined by the HMM analyses.

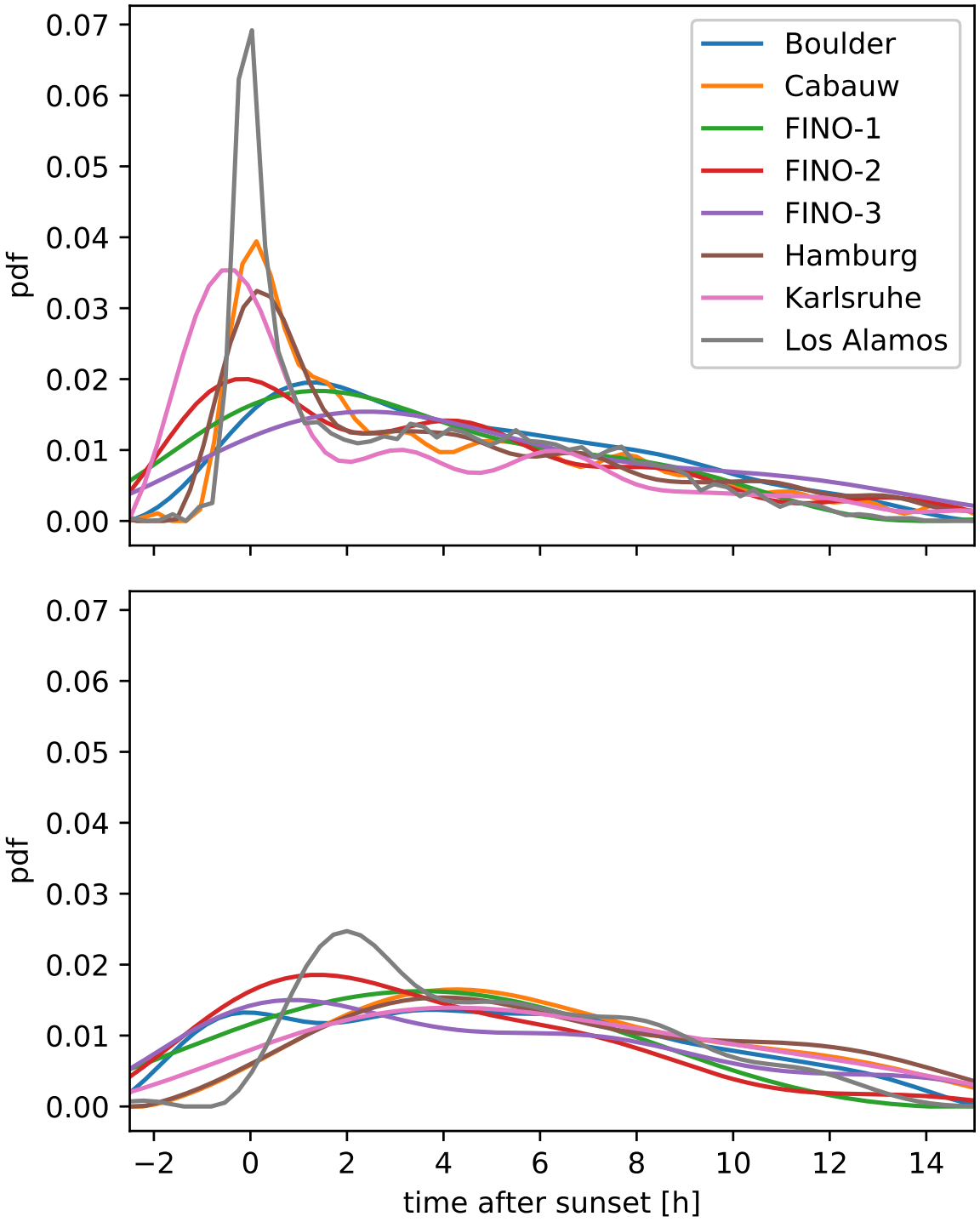

Figure 6.10: Probability density distribution of the frequency of HMM regime transition times (for nights in which transitions occur) at the different tower sites. The wSBL to vSBL transitions are shown in the upper panel, while vSBL to wSBL transitions are shown in the lower panel. All pdfs of the observations are calculated with the multivariate kernel density estimation by *O'Brien et al.* [2014, 2016].

Across all tower sites, the frequencies of turbulence collapse and recovery events are in approximate statistical equilibrium from about 4 hours after sunset to sunrise. The steady decrease of transition frequencies with increasing durations of the night is related to fact that those particular times of the night are less common (only in winter months) than earlier times in the night (all seasons). Otherwise, transition statistics depend only weakly on the season. For example, the frequencies of the timing of transitions in different seasons at Cabauw are similar to each other, each showing pronounced maxima in wSBL to vSBL transitions around sunset and statistical equilibrium between turbulence collapses and recoveries afterwards (Figure 6.11). Though the probabilities also decrease with increasing durations of the nights, the tails of the seasonal distributions are flatter than those of the whole-year distributions. The winter season shows a less pronounced maximum in wSBL to vSBL transitions. Qualitatively similar results are obtained across all the other tower stations. Although the enhanced frequency of wSBL to vSBL regime transitions found by the HMM near sunset is physically reasonable, this behaviour indicates the presence of nonstationarities in the SBL dynamics exist linked to the diel cycle which are not accounted for in the HMM model.

The fact that after about 4 hours after sunset all land-based stations exhibit the same vSBL to wSBL transition frequencies is consistent with the fact that the occurrence probabilities of subsequent turbulence recovery are approximately the same across these stations (30-50 %, Table 6.2). FINO-2 shows a relatively high frequency of subsequent recovery events (about 60 %) which is likely related to the fact that the advection of warm-air aloft weakens over the course of the night [*Dörenkämper et al.*, 2015, chapter 5]. Evidently, the probability of the occurrence of subsequent recovery events increases with the durations of nights (Figure 6.12, upper panel). This increase of the probability of a transition is consistent with the longer time available for such a transition to occur. Furthermore, longer nights occur in winter when pressure gradient forces are typically larger.

The occurrence of subsequent turbulence collapse events after a recovery event are with the exception of FINO-3 more probable over land-based stations than over ocean-based stations (Table 6.2), likely due to the continuing radiative cooling at the surface. Boulder and Los Alamos show the highest frequencies of such subsequent collapse events. Similar to the general occurrence of wSBL to vSBL transitions, the probabilities of subsequent collapse events are relatively similar (or slightly declining) with increasing length of night (Figure 6.12, lower panel).

The mean time between turbulence collapse and subsequent recovery events is about 3 to 4 hours in the observations across all sites (Table 6.2, column 4). The mean duration

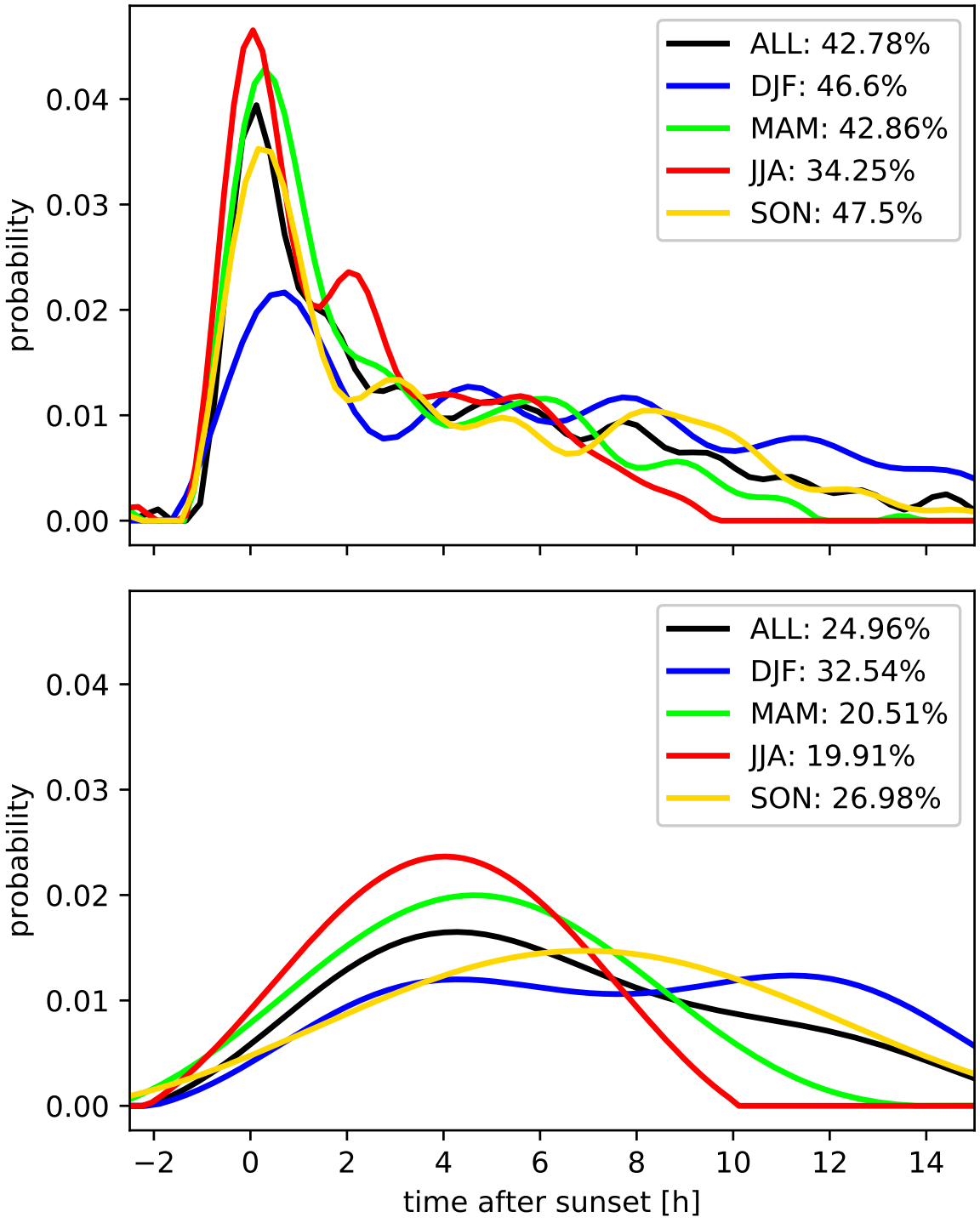

Figure 6.11: Probability density distribution of the frequency of HMM regime seasonal (all seasons: black; winter: blue; spring: green; summer: red; fall: orange) transition times (for nights in which transitions occur) at Cabauw. The wSBL to vSBL transitions are shown in the upper panel, while vSBL to wSBL transitions are shown in the lower panel. The percentages are the relative probabilities of the occurrence of respectively wSBL to vSBL and reverse transitions in a night. All pdfs are calculated with the multivariate kernel density estimation by *O'Brien et al.* [2014, 2016].

Table 6.2: Percentages of nights in which turbulence recovery events occur after a previous turbulence collapse (column 2, upper panel) and probability of subsequent recovery events (column 3) as classified by the HMM regime sequences. The mean and median time between the collapse and subsequent recovery of turbulence events are stated in columns 4 to 5. Percentages of nights in which turbulence collapse events occur after a previous turbulence recovery (column 2, lower panel) and probability of subsequent collapse events (column 3) as classified by the HMM regime sequences. The mean and median time between the recovery and subsequent collapse of turbulence events are stated in columns 4 to 5.

	Subsequent recovery events			
Tower site	nights with occurrence [%]	subsequent recovery [%]	mean time [h]	median time [h]
Land-based tower sites				
Boulder	37.22	49.53	3.1	2.5
Cabauw	15.90	37.84	3.9	3.0
Hamburg	29.05	49.66	3.4	2.5
Karlsruhe	16.97	41.06	4.1	3.0
Los Alamos	25.66	35.98	3.5	2.7
Ocean-based tower sites				
FINO-1	8.57	52.38	3.4	2.7
FINO-2	9.96	62.71	2.9	2.2
FINO-3	4.99	31.11	3.8	2.8
	Subsequent collapse events			
Tower	nights with occurrence [%]	subsequent collapse [%]	mean time [h]	median time [h]
Boulder	39.56	71.38	2.7	2.2
Cabauw	9.17	37.46	3.2	2.5
Hamburg	16.16	53.63	2.3	1.7
Karlsruhe	7.66	30.20	3.2	2.3
Los Alamos	21.57	60.08	2.9	2.3
Ocean-based tower sites				
FINO-1	7.41	34.50	2.7	2.4
FINO-2	7.77	30.31	2.6	2.0
FINO-3	10.02	57.59	3.1	2.3

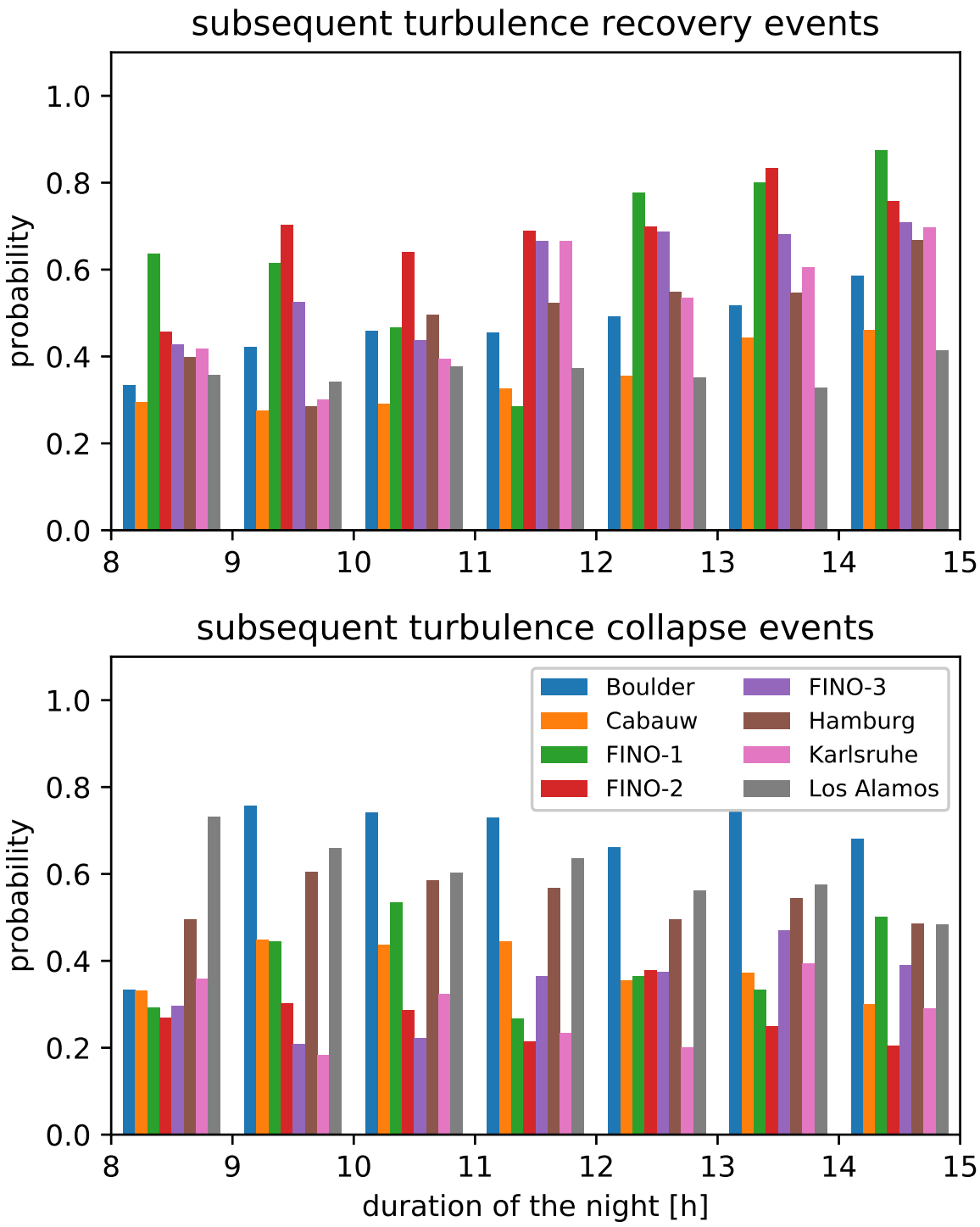

Figure 6.12: As in Figure 6.9, but showing the probabilities of the occurrence of subsequent turbulence recovery events after preceding turbulence collapse (upper panel) and subsequent turbulence collapse events after preceding turbulence recovery events (lower panel).

between a turbulence recovery event and the subsequent turbulence collapse of 2.5 to 3 hours is somewhat shorter (Table 6.2, columns 8). The enhanced mechanical driving in winter apparently counteracts the increased transition probability following from having a longer time in which to occur (Figure 6.13).

The pdfs of the time between successive transitions show approximately the same structures across all tower sites (Figure 6.14). These event duration pdfs show clear maxima about 1-3 hours after the collapse, demonstrating that subsequent transitions occur only after a recovery period of about an hour or two. Over land, factors contributing to the existence of such recovery period are the time needed to build up enough shear to break down the inversion after a turbulence collapse (vSBL to wSBL transition) or to cool down the near-surface layers to rebuild a stably stratified temperature profile (wSBL to vSBL transition). It is not clear why the vSBL event durations should be so similar, or why distributions of either type of event over land should resemble those over water.

It is a striking fact that the pdfs between SBL transitions are largely insensitive to the surface type, the latitude, or the surrounding conditions suggesting a physical mechanism which has yet to be uncovered. Furthermore, the similarity of vSBL and wSBL event duration pdfs is striking as it is not obvious why such similarities should occur as different physical mechanisms lead to the different regime transitions. The most likely timescale of 1-3 hours between transitions is not explainable with the data available for this study but is an important direction of future research. A through analysis of the raw data around the transitions and the understanding of interactions between the different turbulence scales might reveal more insight to this apparently universal timescale of SBL regime transitions incorporating also the spatial structure. Thus, the

6.6 Conclusions and Discussion

Regime sequences obtained from an HMM allow for systematic characterisation of transitions between regimes of the SBL at nine different tower sites. Across land-based stations, surface radiative cooling starts around sunset and leads to a maximum in the transition frequency from wSBL to vSBL conditions in this time period. Across ocean-based stations only very weak maxima in the timing of transitions are present as transitions are caused by advection of warm-air aloft which is not generally closely tied to the diel cycle. The frequency of occurrence of turbulence recovery, on the other hand, shows a weaker dependence on the time after sunset. After about four hours after sunset frequencies of the two transitions are in approximate statistical equilibrium suggesting that transitions

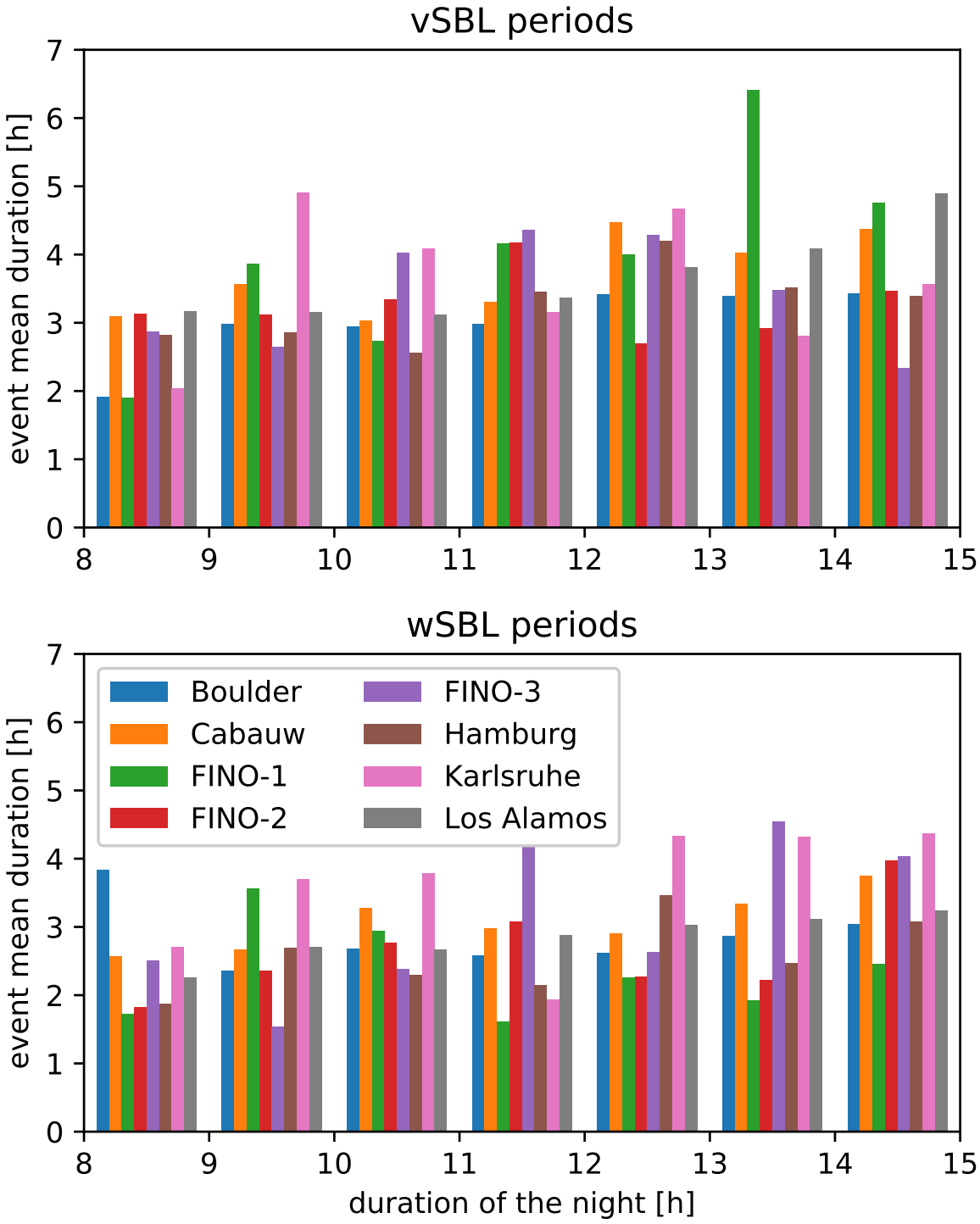

Figure 6.13: As in Figure 6.9, but showing the event mean duration between subsequent turbulence recovery events after preceding turbulence collapse (upper panel) and subsequent turbulence collapse events after preceding turbulence recovery events (lower panel).

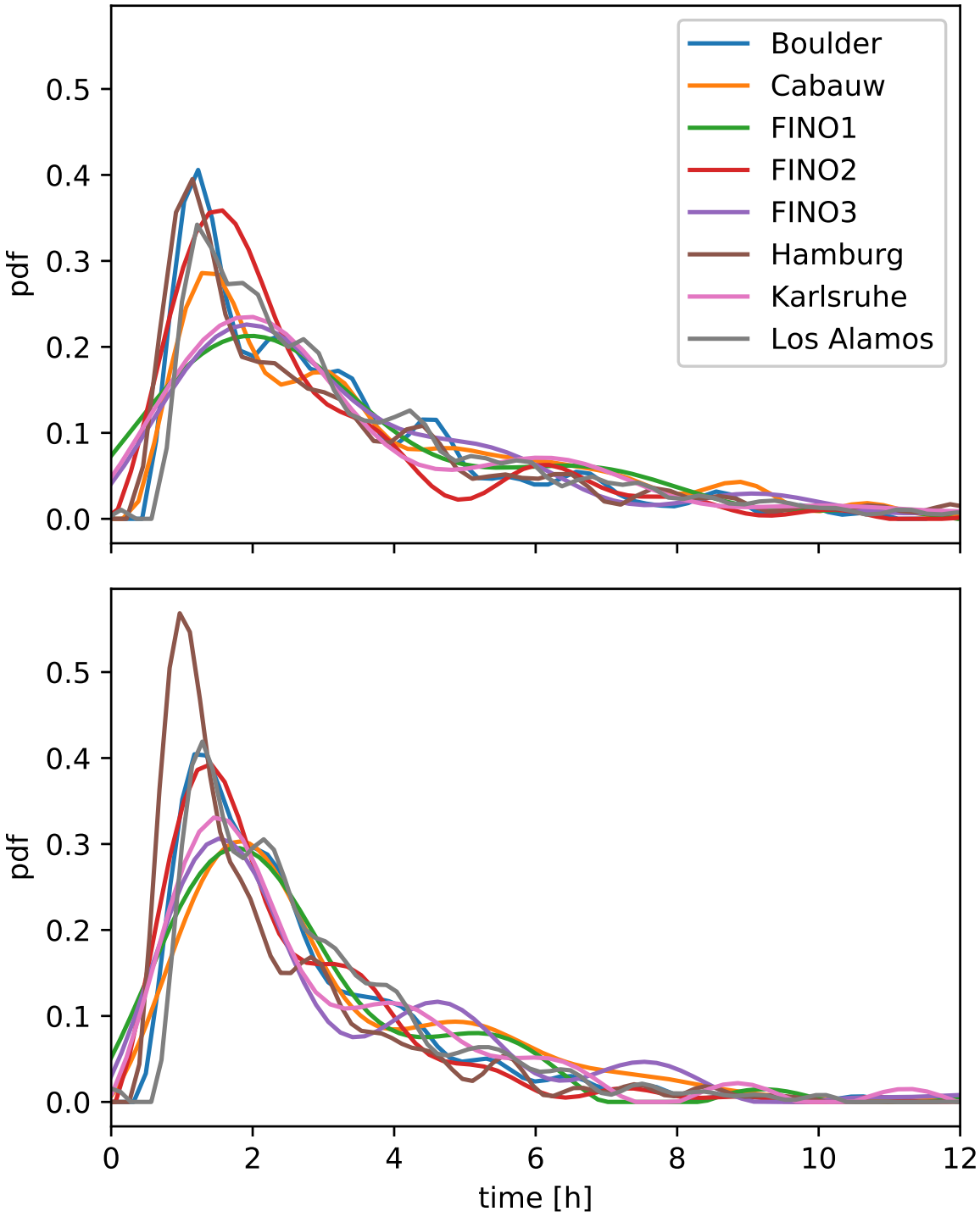

Figure 6.14: Probability density function of the time between a turbulence collapse and subsequent turbulence recovery event (upper panel) and between a turbulence recovery event and a subsequent turbulence collapse (lower panel) at the different tower sites as determined by the HMM analyses. All pdfs are calculated with the multivariate kernel density estimation by *O'Brien et al.* [2014, 2016].

during this period depend on internal or external influences that are not tied to the diel cycle. These statistics depend only weakly on the season. Statistics such as the probability of any transition event or multiple events occurring in a night show some evidence of seasonal modulation, reflecting the difference in large-scale meteorological conditions for these midlatitude locations.

Interestingly, the pdfs of the time between one transition and the next shows the same structure wSBL and vSBL episodes. Both distributions are characterized by an initial recovery time of approximately one hour exists before a subsequent transition occurs. The physical reasons for these distributions, which are not consistent with the Markov assumption underlying the HMM analysis, are unclear and represent an interesting direction of future research.

Composites of the Reynolds-averaged mean and turbulence state variables, considering the 90 minutes before and after each transition, show generic structures across land-based tower sites. Across these stations, radiative cooling at the surface causes a continual decrease in the temperatures near the surface building up the inversion strength which results in the wSBL to vSBL transition. The enhanced inversion strength decreases resulting in vertical decoupling of the dynamics, most evident in the increase of the wind components perpendicular to the direction of the flow at the highest observational level. The TKE values show a strong decrease to complete collapse in wSBL to vSBL transitions and while the anisotropy of the turbulence increases. Vertical fluctuations are almost completely suppressed after a wSBL to vSBL transition.

Recovery of turbulence happens on timescales of a few minutes. The turbulence recovers throughout all observational levels starting at atmospheric levels between 50 to 100 m. In times of these transitions, the turbulence structures become more isotropic. The recovery of turbulence leads to the weakening of the inversion and the coupling of the atmospheric levels. The across-wind component decreases abruptly and the along-wind component accelerates in all atmospheric levels.

Similar results are found at the ice-based station of DomeC, although there is evidence here to indicate that advection of warm-air aloft is also a mechanism leading to turbulence collapse. A more detailed analysis of differences between transitions caused by advection of warm-air aloft or radiative cooling at the surface is an interesting direction for future research.

At ocean-based sites regime shifts are clearly related to the advection of warm air aloft. Therefore, during transitions changes are more pronounced in the stratification than in

the flow. Consistent with the fact that stratifications are generally weaker than over land and ice, decoupling of the atmospheric layers in the vSBL is weaker. Nevertheless, winds decrease and increase with respect to wSBL to vSBL and reverse transitions, and the across-wind component shows clear evidence of vertical decoupling and coupling.

Regime transitions are found to be insensitive to changes in pressure gradient forces within 180 minutes of the transitions. Pdfs of tendencies in U_{geo} show very broad distributions suggesting that neither wSBL to vSBL nor vSBL to wSBL transitions generally result from changes in the large-scale meteorological state. Only the timing of the first turbulence collapse is weakly dependent on the nighttime average $\overline{U_{geo}}$ values as larger $\overline{U_{geo}}$ lead to later turbulence collapse.

In contrast to U_{geo}, changes in LLCC have a larger effect on transitions in the SBL. During wSBL to vSBL transitions LLCC is more likely to decrease or to stay the same than to increase. Half of vSBL to wSBL transitions are accompanied by LLCC increase. As LLCC changes are found to occur before the transition and LLCC values stay steady after it they are likely to initiate SBL transitions.

The absence of clear SBL regime transition precursors in internal or external state variables indicate that parameterisations of the effects of these transitions in weather and climate models may be required to be explicitly stochastic [e.g. *He et al.*, 2012; *Mahrt*, 2014]. In particular, phenomena such as intermittent turbulence events will likely rely on stochastic parameterisations as their structure and propagation are found to be independent of the mean states [e.g. *Rees and Mobbs*, 1988; *Lang et al.*, 2018]. Stochastic subgrid-scale parameterisations to describe the physically different conditions in the SBL have been proposed to help capturing the missing variability in the SBL and improve both climate mean states and forecast ensemble spread [e.g. *He et al.*, 2012; *Mahrt*, 2014; *Nappo et al.*, 2014; *Vercauteren and Klein*, 2015; *Berner et al.*, 2017]. In order to understand if such parameterisations for the turbulence under SBL conditions can be based on Markov chains we we will analyse the sensitivity of the transition matrices in the HMM analyses as well as in theoretical calculations in a stationary Markovian system (as assumed in the HMM analyses) in detail in chapter 7. Further development of such parameterizations requires also information regarding horizontal length scales and temporal structures of regime dynamics. As demonstrated in chapters 4, 5 and the present the HMM analyses based on Reynolds-averaged mean states can be used as a tool to diagnose and analyse the SBL regimes and address questions concerning the spatial and temporal organisation of regimes, with the ultimate goal of improving parameterisations of these processes in operational models. The existence of non-Markov behaviour such as the existence of the

recovery time between transitions (indicating that dynamics beyond a simple two-state Markov chain are required to physically model transitions between regimes) and nonstationarities such as near-sunset maximum in wSBL to vSBL transition probability imply that simple formulations of such stochastic effects may not be adequate.

7 Characterising regime behaviour in the stably stratified nocturnal boundary layer on the basis of stationary Markov chains

Chapter Abstract

The HMM analysis is an effective tool to classify regimes of the SBL at different tower sites. Here we analyse if SBL regime statistics (the occurrence of regime transitions, subsequent transitions after the first, and very persistent nights) in observations match theoretical calculations obtained from a stationary Markov chain with the goal of developing the foundations of novel Markov-chain-based boundary layer schemes which capture the effects of SBL regime dynamics. The regime statistics of a stationary Markov chain using the best estimate transition probabilities from the HMM analyses generally overestimate occurrence probabilities of regime transitions, resulting in an underestimation of persistent nights. Across the locations considered, sensitivity analyses of transition probability matrices in the HMM and the stationary Markov chain reveal that regimes are generally required to be more persistent in the stationary Markov chain in order to simulate observations accurately. A range of transition probability matrices allowing for a relatively accurate description of the occurrence of at least one transition within a night, multiple transitions, and the mean event durations is identified. The occurrence of very persistent nights (nights without regime transitions) is found to depend highly on the season. Therefore, for better representations of very persistent nights a nonstationary Markov chain linked to external drivers is likely appropriate. The observed transition probability maximum between one and two hours after a previous transition cannot be accounted for by two-state Markov processes (stationary or not).

7.1 Introduction

In the previous chapters we have demonstrated that the HMM analysis of Reynolds-averaged mean states can be used as a tool to systematically detect, diagnose, and analyse the SBL regimes and transitions between them at tower sites in a range of different settings. Furthermore, the regime sequences allow for an assessment of the climatology of the SBL regime statistics. Global and regional weather and climate models do not account for the SBL regime statistics and often use an artificially enhanced surface flux formulation under stable conditions in order to improve simulations of the large-scale flow [*Holtslag et al.*, 2013]. This approach has led to the introduction of long-tailed stability functions not justifiable by observations. In such models, turbulence is artificially sustained under very stable conditions and the two-regime characteristic of the SBL is suppressed, biasing near surface winds and temperature profiles. Without this parameterisation the nocturnal boundary layers can experience a single turbulence collapse which persists for the entire night. Although the long-tailed stability functions in relatively coarse-resolution models mimic to some extent the grid box mean effect of the two-regime structure (as it is unlikely that a whole grid box experiences a simultaneous turbulence collapse or recovery), with increasing horizontal and vertical resolution, in particular in weather forecast models, more accurate process-based parameterisations are necessary.Even though it is unlikely that an entire gridbox in a climate model (current resolution typically 1 to 2.5 degrees) experiences SBL regime transitions, *Medeiros and Fitzjarrald* [2014, 2015] showed in an observational surface station network spanning approximately a 1 by 1 degree geographical area that intermittent turbulence events can occur simultaneously across the whole station network with very similar turbulence intensities at all stations. However, there is a lack of an observational data set allowing for a characterisation of long-term spatial regime dependences on the scale of a degree. Therefore, this analysis should be understood as a local analysis which is directly relevant to high-resolution simulations in which spatial structure is less important but which can potentially also lay the foundation towards a general parameterisation incorporating spatial structure.

The vSBL to wSBL transition does not demonstrate clear precursors in internal or external state variables (chapter 6), indicating that parameterisations of the effects of these kinds of transitions in weather and climate models may be required to be explicitly stochastic [e.g. *He et al.*, 2012; *Mahrt*, 2014]. In particular, phenomena such as intermittent turbulence events will likely rely on stochastic parameterisations as their structure and propagation are found to be only weakly-dependent on the mean states [e.g. *Rees and Mobbs*, 1988; *Lang et al.*, 2018]. Stochastic subgrid-scale parameterisations to describe the physically

different conditions in the SBL have been proposed to help capturing the missing variability in the SBL and improve both climate mean states and forecast ensemble spread [e.g. *He et al.*, 2012; *Mahrt*, 2014; *Nappo et al.*, 2014; *Vercauteren and Klein*, 2015]. One possible approach to developing a stochastic parameterisation of turbulence with the ability to simulate regime transitions is to use the transition probability matrices estimated by the HMM (chapter 4). Such an approach would require the introduction of a regime sequence variable in existing parameterisations which tracks the regime (the wSBL or vSBL) and stochastically forces the system out of the turbulence collapsed state according to defined transition probability matrices. The HMM analyses presented in chapter 4 assumes stationary regime dynamics estimating transition probabilities which are relatively universal across the stations. A stationary universal transition probability which could work in all parameterisations would be a desirable result which can simplify the form of a stochastic parameterisation substantially. In chapters 5 and 6 clear evidence of nonstationarities were found, such as an elevated probability of turbulence collapse during sunset linked to the diel cycle and seasonally-varying probabilities of very persistent nights. Nonetheless, we chose to consider stationary analyses in this study in order to investigate the simplest possible approach to a stochastic parameterisation of the turbulence under SBL conditions. With this approach we can assess the potential of such relatively simple parameterisation and identify where extra complexity is warranted.

As a first approach to establishing a foundation of a stochastic parameterisation of turbulence in the SBL, we analyse in the following how well a stationary Markov chain (using the best-fit transition matrix $\mathbf{Q}_{\mathrm{ref}}$ from the HMM analysis in chapter 4, Table 4.2) can model SBL regime statistics (event durations and the probabilities of very persistent nights, of any transition occurrences within a night, of multiple transition occurrences within a night) as found in chapters 5 and 6 (section 7.2). Repeating the HMM analysis using a specified $\mathbf{Q}$ held fixed at values other than $\mathbf{Q}_{\mathrm{ref}}$, we then investigate the sensitivity of the estimated regime statistics of these perturbed VPs relative to the reference VP from $\mathbf{Q}_{\mathrm{ref}}$ ($\mathrm{VP}_{\mathrm{ref}}$) in section 7.3. Finally, we vary $\mathbf{Q}$ to assess if persistence probabilities exist that match SBL statistics in both theoretical calculations using a stationary Markov chain and in observations (section 7.4). In order to base new parameterisations of turbulence in the SBL on stationary Markov chains such as are produced by the HMM, it is important that these model the observed regime statistics accurately. The mathematical expressions used to compute the statistics of interest with given transition matrices are presented in the Appendix. A discussion of how a parameterisation can be informed by the results of this study and conclusions follow in section 7.5. This chapter is based on *Abraham and Monahan* [2018d].

7.2 Comparison of observations and stationary Markov chain calculations

As described in chapter 5, the occurrence of very persistent nights varies with the duration of the night in a manner consistent with the influence of seasonal changes in large-scale meteorological conditions (respectively higher and lower probabilities of the wSBL and vSBL in wintertime; Figure 7.1). Using $\mathbf{Q}_{\text{ref}}$ (based on data from all seasons), we can compute theoretical probabilities of the occurrence of persistent SBL nights in a stationary Markov chain (c.f. eq. A.1 and A.2) against which we can compare the observed relative frequencies for different lengths of nights. As the tower sites are located in the midlatitudes seasonal changes lead to nighttime duration changes between 8 to 15 hours (at 45 N) between summer and

For a stationary Markov chain, the frequency of the occurrence of persistent wSBL nights decreases monotonically with the length of the night. The probabilities of very persistent wSBL nights in summer (of duration 8 to 10 hours) agree relatively well with the theoretical calculations (Figure 7.1). However, for the longer duration nights the stationary Markov chain underestimates the occurrence of persistent wSBL nights as the observed probabilities increase rather than decrease. The increase of wSBL probability with length of night is consistent with larger synoptic-scale variability (with stronger mechanical generation of turbulence) in the winter, but not consistent with a stationary Markov chain. The observed probability of very persistent vSBL nights decreases with increasing length of the night, consistent with the increase in mean pressure gradient force. While the stationary Markov chain also shows this behaviour, it systematically underestimates the observed occurrence of very persistent vSBL nights. Furthermore, the non-stationary change in synoptic driving is not embedded in the stationary Markov chain.

In chapter 6 we have shown that the probability of at least one wSBL to vSBL transition (including nights in which the first wSBL to vSBL transition follows an initial one from the vSBL to the wSBL) occurring within a night shows no systematic dependence of the length of the night across the tower sites (Figure 7.2). At most land-based stations the probability of occurrence slightly decreases, with the exception of Cabauw where the probability slightly increases. At ocean-based stations the probability of the occurrence of wSBL to vSBL transitions is not systematically sensitive to the length of the night. The probability of the occurrence turbulence recovery events is also insensitive to the season. In contrast, the occurrence probability of at least one transition obtained from the stationary Markov chain (Eqns. A.3 and A.4) increases with the length of the night, and is larger

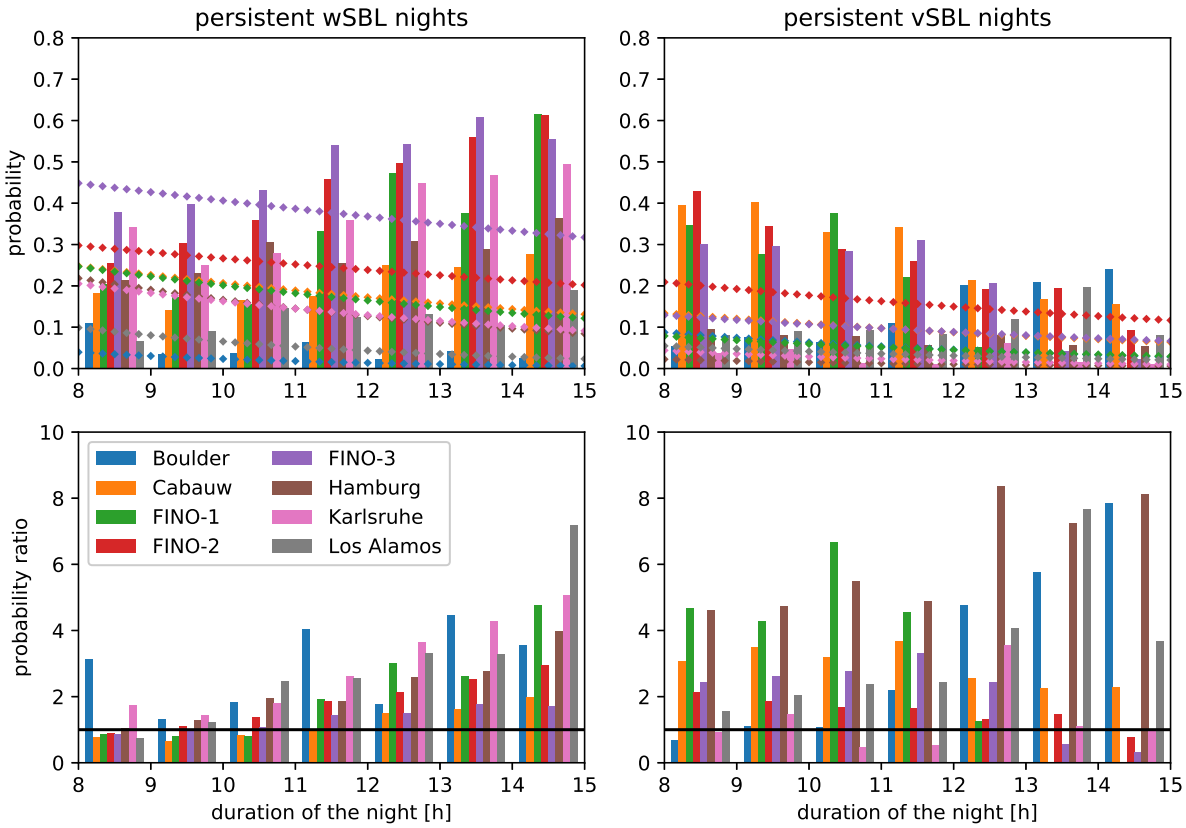

Figure 7.1: Occurrence probabilities of very persistent wSBL (upper left panel, bars) and vSBL (upper right panel, bars) from the for nights of different lengths (in one hour increments) at the different tower sites compared to the occurrence probabilities of very persistent nights computed from the stationary Markov chain (diamonds). Lower panels show the ratio the probabilities in the upper panels (observed values divided by those from the stationary Markov chain).

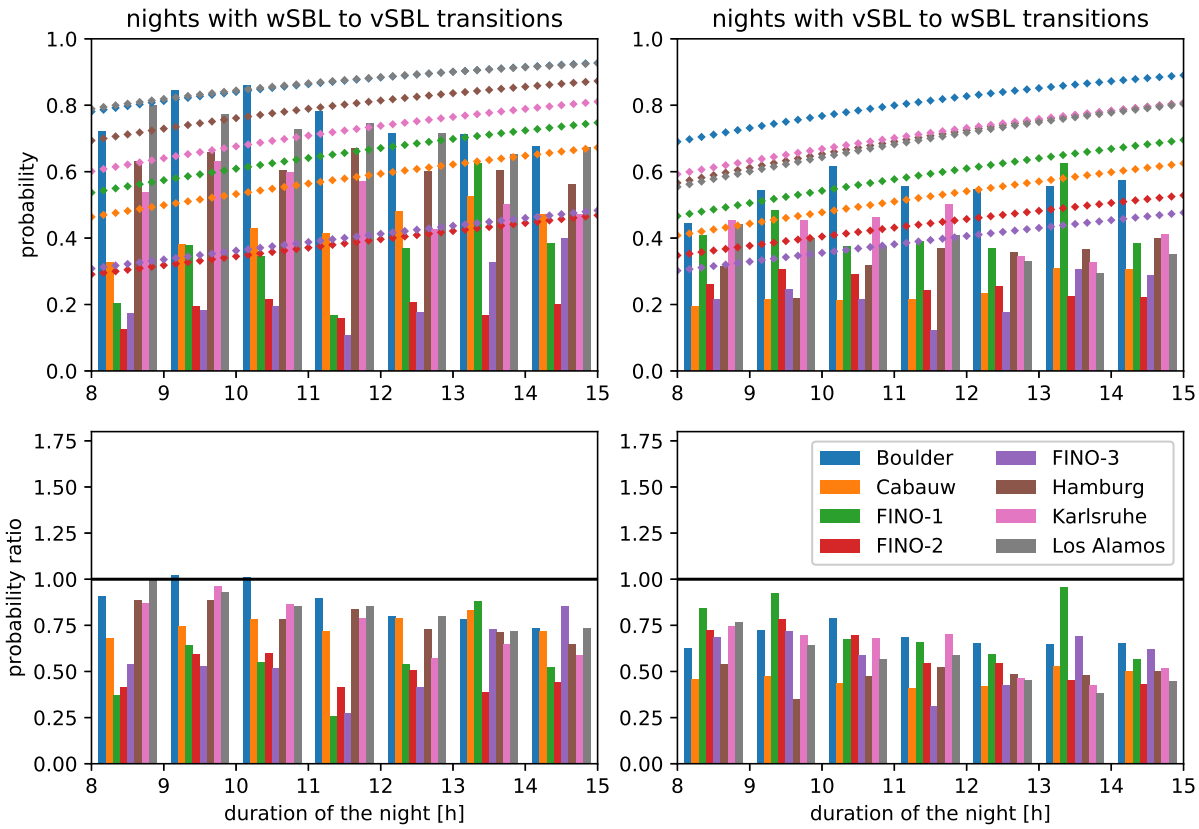

Figure 7.2: As in Figure 7.1 but for the occurrence probabilities of wSBL to vSBL (upper left panel) and vSBL and wSBL (upper right panel) transitions.

---

than those of observations at all sites (Figure 7.2, lower panels). The overestimation of turbulence recovery events by the stationary Markov chain is slightly larger than that of turbulence collapse events at land-based stations, while the opposite is true at ocean-based stations.

The occurrence of a recovery event subsequent to a turbulence collapse is better estimated by a stationary Markov chain (Eqns. A.6 and A.8, Figure 7.3) than the overall occurrence of a at least one wSBL to vSBL transition (Figure 7.2, left panels). Both observed and modelled probabilities increase with the length of the night, at about the same rate. Interestingly, at land-based stations fewer subsequent turbulence recovery events are observed than expected, and over oceans more are observed. The distributions of turbulence collapse events subsequent to a recovery event theoretical calculations of the Markov chain are generally close to the observations in summer and worsen slightly for winter conditions (Figure 7.3, right panels).

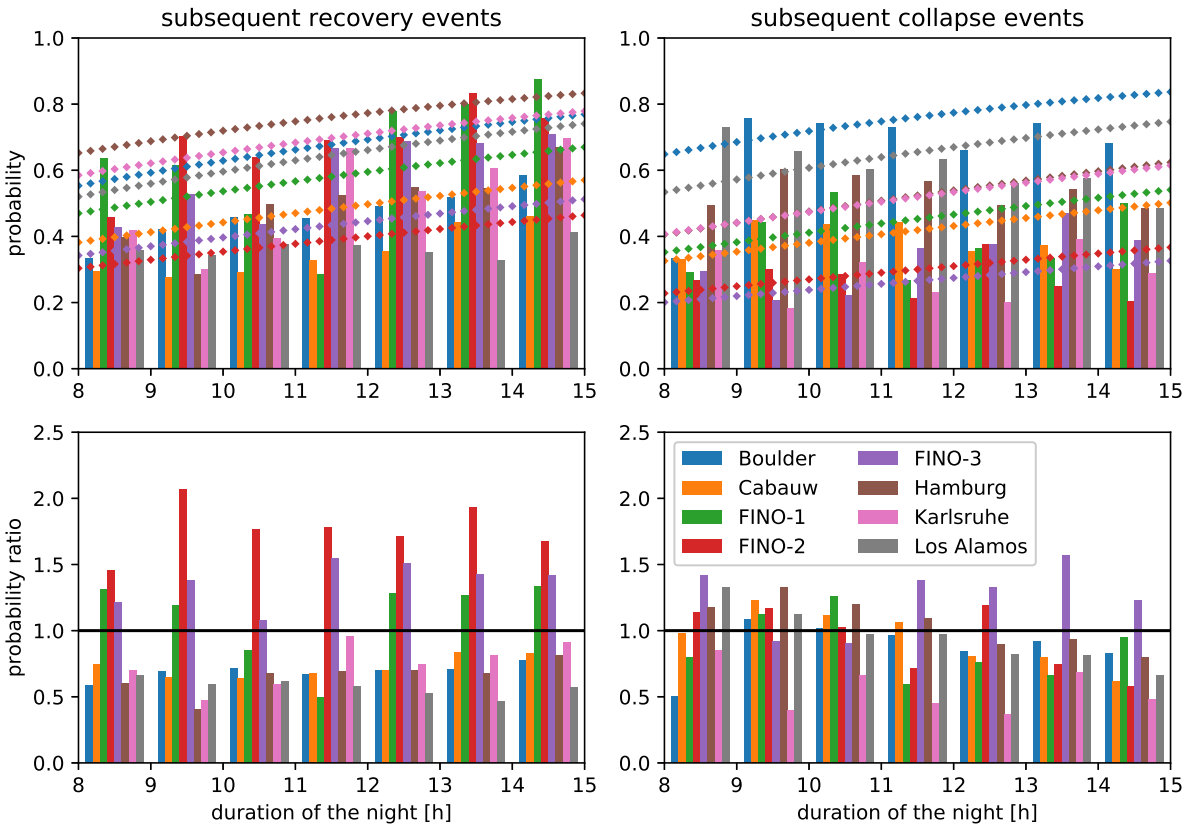

Figure 7.3: As in Figure 7.1, but for the probabilities of the occurrence of turbulence recovery events subsequent to turbulence collapse (upper left panel) and turbulence collapse events subsequent to turbulence recovery (upper right panel).

The occurrence of subsequent transition events can be also associated with event durations in the vSBL (subsequent recovery event) and wSBL (subsequent collapse event). The observed mean event vSBL durations are generally close to the theoretical values obtained from the stationary Markov chain for nights of all durations between 8 and 15 hours (Figure 7.4). While agreement is reasonably good for wSBL events, the stationary Markov chain generally underestimates the mean duration. In chapter 6 we demonstrated that the pdfs of the time between successive transitions show very similar structures for wSBL and vSBL event durations (Figure 7.5). Interestingly, these pdfs display clear maxima between one and two hours after the preceding transition, demonstrating that the occurrence of subsequent transitions most often requires some relaxation time. These recovery periods following the transitions cannot be accounted for by the stationary two-regime Markov chain we consider. The theoretical duration pdfs of events for nights lasting from 8 to 15 hours (equations A.5 and A.7) decay monotonically. The probabilities of subsequent transition occurrence after about 2 hours are similar in the theoretical stationary Markov chain and the observations.

The results above demonstrate the existence of at least two aspects of the regime statistics which cannot be accounted for by a two-regime stationary Markov chain. First, the occurrence of very persistent regimes and (to lesser extent) the occurrence of transitions are subject to non-stationary seasonal changes. Accounting for these nonstationarities would require seasonally-varying persistence probabilities or (more naturally) persistence probabilities that depend on seasonally-varying external parameters. Such behaviour could potentially be represented by a non-homogeneous HMM [e.g *Hughes et al.*, 1999; *Fu et al.*, 2013]. Note that these results do not invalidate the use of the HMM for classification purposes, as the VP is only weakly sensitive to $\mathbf{Q}$ (as will be shown in the next section). Second, the maximum in event duration pdfs one to two hours after the preceding transition is inconsistent with the statistics of a two-regime Markov chain. Nonetheless, results indicate that even though the occurrence probability of the first transition in the night by the stationary Markov chain is biased, once the first transition has occurred a stationary Markov chain is able to predict the general occurrence of subsequent transitions and their mean regime duration. Due to the fact the values on the diagonal of $\mathbf{Q}_{\text{ref}}$ are close to one (Table 4.2), theoretical regime statistics calculated from the from the stationary Markov chain are sensitive to these values (cf. Eqns. A.1-A.8). In contrast, the estimated VP has a weak sensitivity to the those elements of $\mathbf{Q}$. We now turn to these sensitivity analyses.

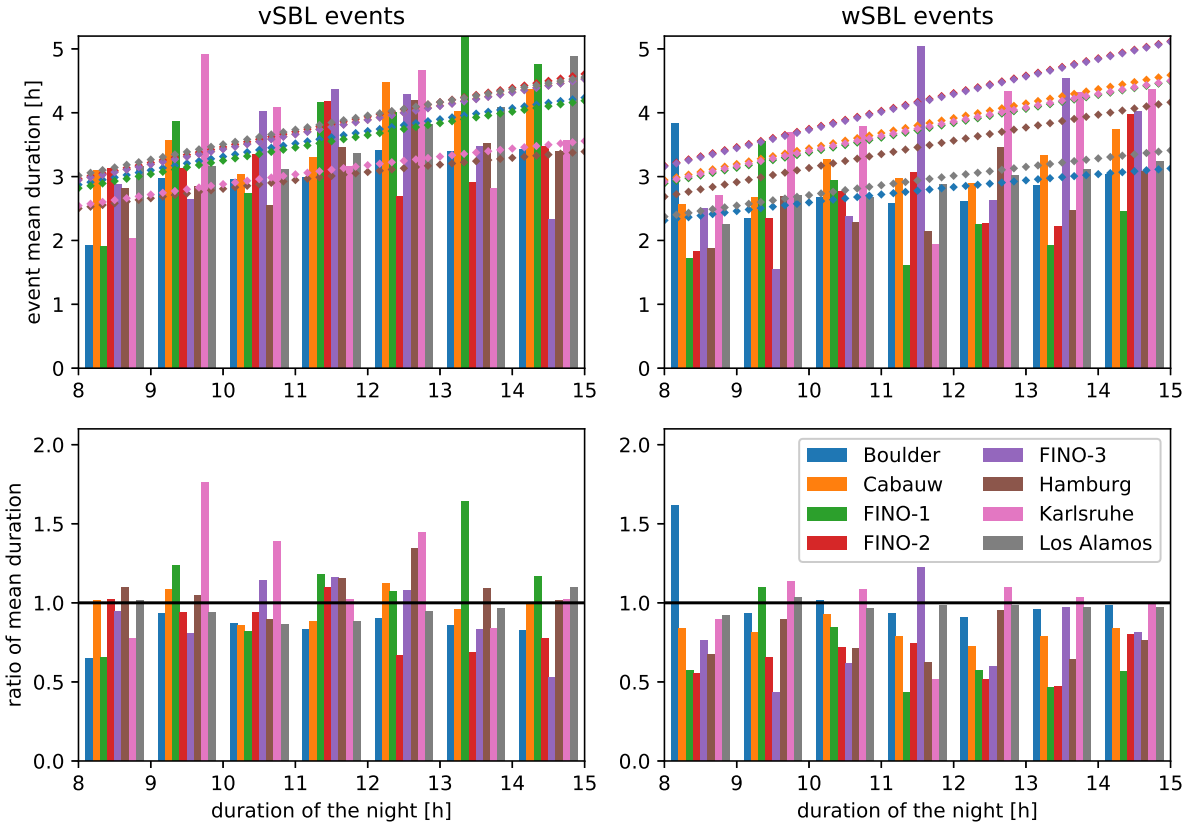

Figure 7.4: As in Figure 7.1, but for the mean event duration in the vSBL (upper left panel, bars) in the wSBL (upper right panel, bars).

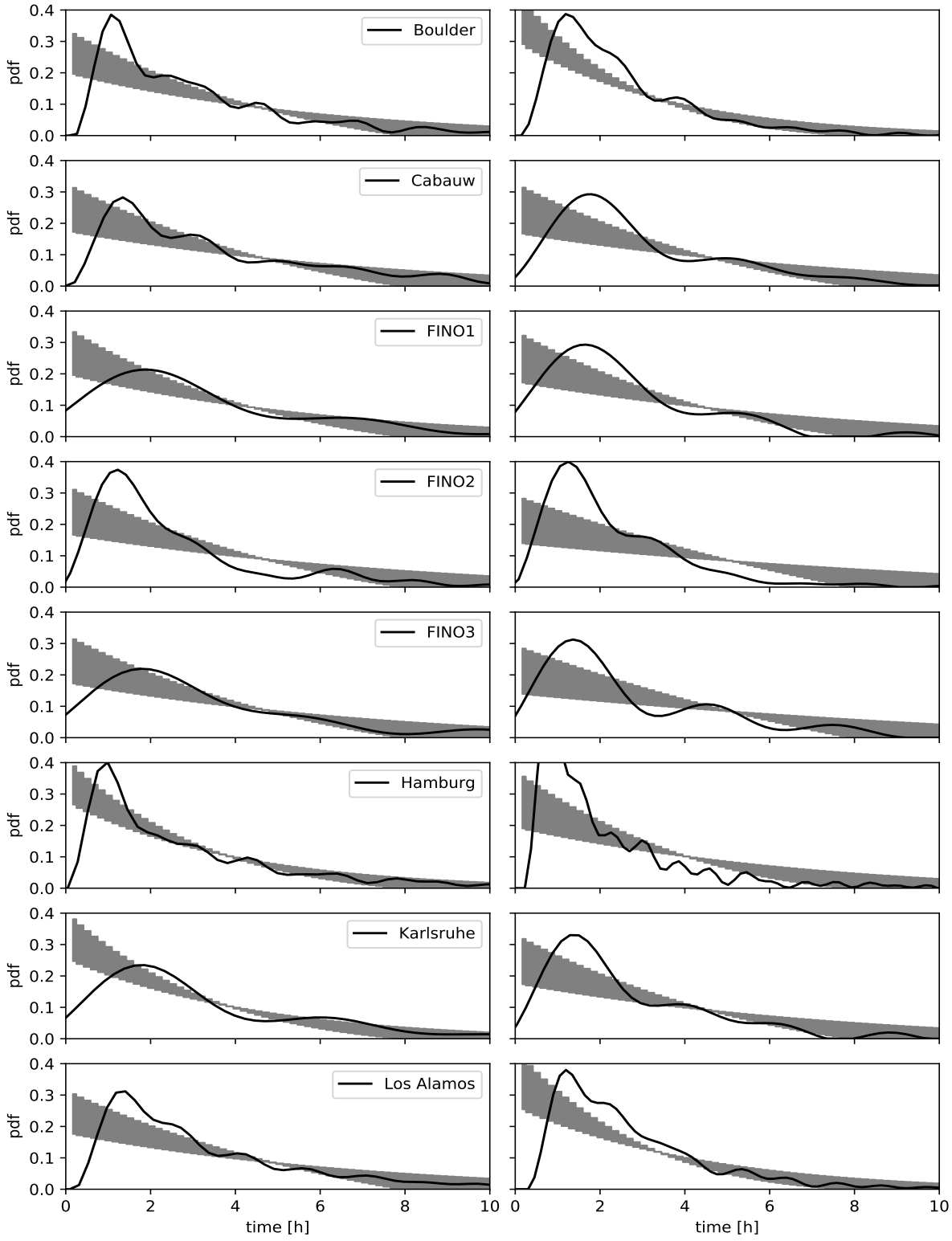

Figure 7.5: Probability density function of the vSBL events (left panels) and wSBL events (right panels) at the different tower sites. Black lines represent the observed event durations as determined by the HMM analyses and the grey bands denote the pdfs estimated from the stationary Markov chain for nights lasting 8 to 16 hours. All pdfs are calculated with the multivariate kernel density estimation by *O'Brien et al.* [2014, 2016].

7.3 Sensitivity of the VP to perturbed persistence probabilities

We consider the sensitivity of the VPs to changes of the persistence probabilities in $\mathbf{Q}$ by holding this matrix fixed and repeating the HMM analysis. We will show that there is a relatively large range of persistence probabilities in which the perturbed VPs are in high agreement with $\mathrm{VP}_{\mathrm{ref}}$. These ranges of persistence probabilities could then be appropriate to inform a two-regime stochastic parameterisation of SBL turbulence. In order to assess if the perturbed VPs are consistent with $\mathrm{VP}_{\mathrm{ref}}$ we consider first the overall consistency between the two (fraction in which both VPs are in the same regime). Similar as in chapter 4, we then assess the consistency of the timing of transitions (simultaneity of transitions in the reference and perturbed VPs) as well as the representation of very persistent nights to obtain the total VP consistency. For this part of the analysis, we focus on the Cabauw tower data as we have analysed these data extensively in chapter 4. The same qualitative results are found using all tower station data we have considered (not shown).

The VP of the HMM model is robust to quite substantial changes in $\mathbf{Q}$, with an overall accuracy of more than 90 % obtained for ranges of wSBL and vSBL persistence probabilities between 0.5 and about 0.9999 (Figure 7.6, upper left panel). Agreement at the 99 % level is found for persistence probabilities between approximately 0.9 and 0.9999. Accurate representation of the timing of transitions is found for a broad range of low persistence probabilities and a small range of persistence probabilities spanning approximately from 0.96 to 0.99. Evidently, if both persistence probabilities are below 0.5 (regime transitions in a single step are more probable than remaining in the regime) the accuracy of the transitions is above 99 %. However, this result is a consequence of the high frequency of modelled transitions improving the ability to capture individual observed transitions (at the expense of modelling far too many transition events). Because regime transitions are relatively rare, the physically meaningful range of persistence probabilities corresponds to relatively large values of both. The accuracy of the occurrence of persistent wSBL nights in the perturbed VP is best for high $P(\mathrm{wSBL} \rightarrow \mathrm{wSBL})$ and is weakly sensitive to $P(\mathrm{vSBL} \rightarrow \mathrm{vSBL})$. This result is not surprising as the high wSBL persistence probability ensures that the majority of very persistent wSBL nights are captured. This measure is unaffected by any underestimate of the occurrence of persistent vSBL nights. Complimentary results are found for the occurrence of persistent vSBL nights.

Each of the five consistency measures illustrated in Figure 7.6 capture distinct aspects of agreement between the reference and perturbed VPs. We define a good total consistency

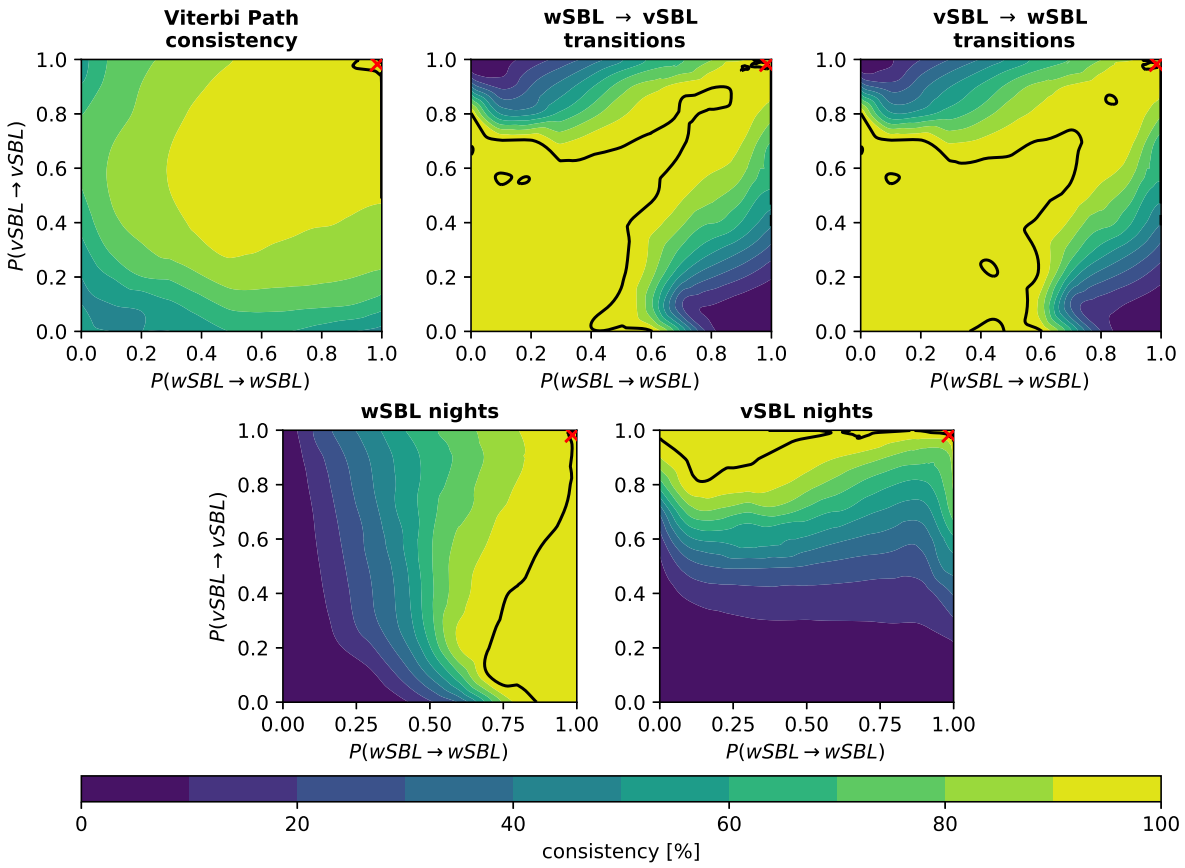

Figure 7.6: Consistency of reference and perturbed regime occupation statistics as functions of Markov chain persistence probabilities. Displayed are: the overall consistency of the VP (upper left), the consistency of wSBL to vSBL (upper middle) and vSBL to wSBL (upper right) transitions in the VP, the consistency of the occurrence of persistent wSBL (lower left) and vSBL (lower right) nights. In each panel the reference value at Cabauw is shown by a red cross. The 99 % consistency values in each VP characteristic is delineated by a black line.

relative to VP_{ref} as each of the five described VP consistencies exceeding 99 %. At Cabauw, a 99 % total consistency can be achieved for $P(\text{wSBL} \rightarrow \text{wSBL})$ between approximately 0.97 and 0.99 and $P(\text{vSBL} \rightarrow \text{vSBL})$ between 0.98 and 0.99 (Figure 7.7). Figure 7.7 also depicts the ranges of persistence probabilities for which all five criteria exceed 95 %. If only a 95 % total VP consistency is required, $P(\text{wSBL} \rightarrow \text{wSBL})$ and $P(\text{vSBL} \rightarrow \text{vSBL})$ can range approximately between 0.95 and almost 1.

In chapter 4 a set of different transition matrices $\mathbf{Q}$ were estimated from HMM analyses of different state variable inputs: surface data such as friction velocity, surface pressure tendencies, and surface radiative fluxes; stratification; shear; turbulence variables such as TKE and vertical turbulent fluxes; and all combinations of these at different measurement altitudes. Most of these $\mathbf{Q}$ estimates fall within the 95 % total VP consistency levels (Figure 7.7). That the best agreement with the reference HMM is found for HMM analyses with state variable inputs including turbulence information (at any measurement height, and with or without combinations of shear and stratification information) is not surprising as the two regimes distinguish the turbulent wSBL from the (essentially) non-turbulent vSBL. Outliers in the $\mathbf{Q}$ estimates using turbulence data come from state variable input vectors combining surface data such as the surface pressure with the near surface TKE. Highly consistent estimates of $\mathbf{Q}$ are obtained from combinations of shear and stratification, as these state variables describe the competing mechanisms of turbulence production and consumption and are used in the reference HMM. Interestingly, with respect to $\mathbf{Q}_{ref}$ the HMM analyses of shear information alone tend to estimate larger persistence probabilities of regimes than those using stratification information alone. Less agreement is found for $\mathbf{Q}$ estimated from either stratification or shear information aloft without near-surface information (yellow and green dots outside of the 95 % total VP consistency level in Figure 7.7, cf. chapter 4). These results demonstrate that the regime information is carried in a broad range of state variables.

The sensitivity analysis of the estimated regime occupation sequence to changes in $\mathbf{Q}$ values reveals that reasonably accurate regime statistics can be obtained over a relatively large range of persistence probabilities. We will now repeat the sensitivity analysis for the theoretical regime statistics of the stationary Markov chain to assess if a range of persistence probabilities exists where observed and modelled statistics are consistent. Such an analysis shows how well the SBL regime statistics can be approximated by a stationary two-regime Markov chain.

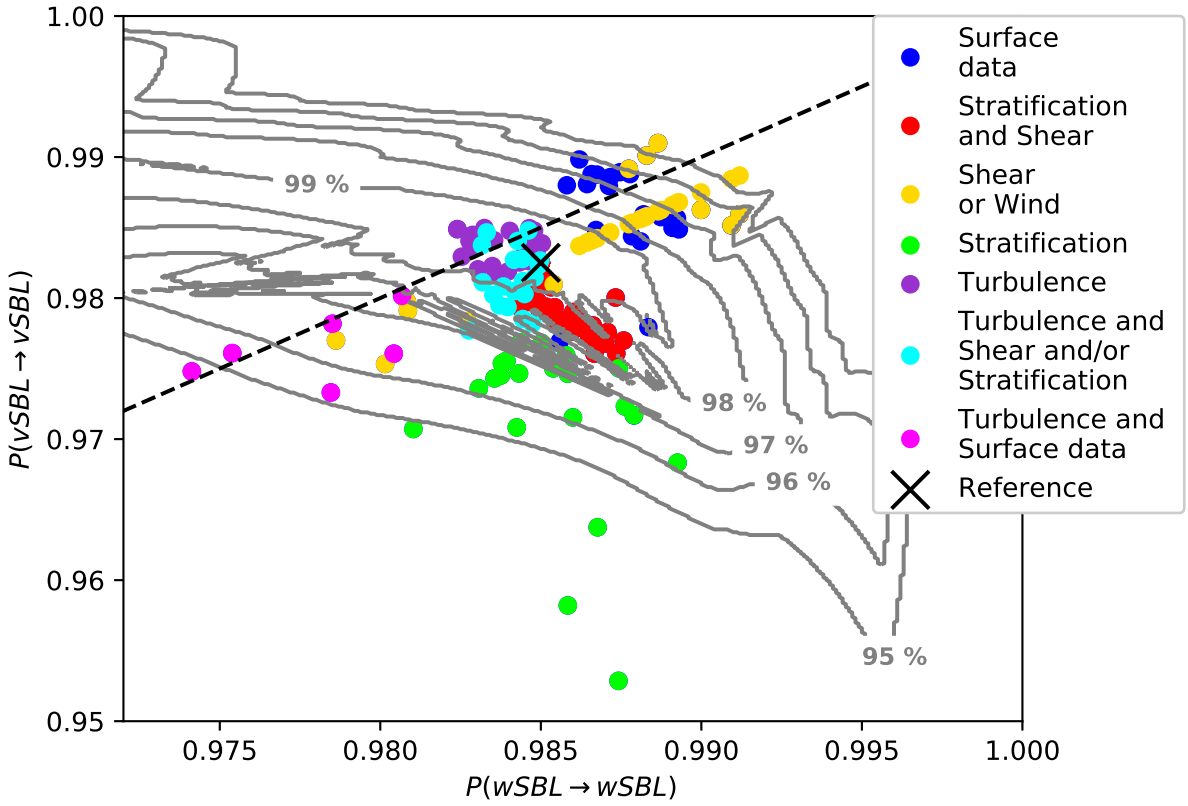

Figure 7.7: Grey contours: isolines of the total consistency of the perturbed and reference VP (ranges of persistence probabilities where the general VP, transition accuracies, and the accuracy in the occurrence of persistent wSBL and vSBL nights have the same or higher consistencies with the reference VP) at Cabauw. Persistence probabilities estimated from other state variable sets at different observational heights than used in $\mathbf{Y}_{\mathrm{ref}}$ are depicted by coloured dots.

Table 7.1: Nighttime durations (d) for the different seasons and corresponding average durations for Markov chain calculations.

Season	Observational duration [h]	Markov chain [h]
winter	$13 \leq d$	14
spring / autumn	$11 \leq d \leq 13$	12
summer	$d \leq 11$	10

7.4 Sensitivity of SBL regime statistics to changing persistence probabilities in a stationary Markov chain

Calculation of the theoretical values of SBL regime statistics from a stationary Markov chain requires specifying the duration of the night (cf. Figures 7.1 to 7.4). For simplicity, we compare theoretical and observed regime statistics for three durations representative of individual seasons (Tables 7.1 and 7.2). The statistics considered include the individual probabilities of starting the night in the wSBL or vSBL (respectively π_{wSBL} and π_{vSBL}). While these probabilities of initial regimes do not affect the HMM analyses (not shown) they can have a substantial impact on the theoretical calculations in a stationary Markov chain. This dependence is illustrated in Figure 7.8, which shows the sets of persistence probabilities for which the probability of at least on wSBL to vSBL transition (upper row) or reverse transition (middle row) from the stationary Markov chain matches the observed values, for a range of different values of π_{wSBL} and π_{vSBL}. Also shown are the isolines of total consistency of perturbed VP and $\mathrm{VP_{ref}}$ from Figure 7.7 (grey lines). Depending on the values of π_{wSBL} and π_{vSBL}, large parts of the persistence probability curves fall within the range of persistence probabilities in which perturbed VPs are in good agreement with $\mathrm{VP_{ref}}$. Furthermore, for a range of π_{wSBL} and π_{vSBL} values, the lines corresponding to at least one of each transition intersect in a region of high total agreement of the perturbed and reference VP. For other ranges of π_{wSBL} and π_{vSBL}, no such intersections occur. However, the persistence probabilities needed in a stationary Markov chain to match occurrence probabilities of very persistent nights span a range of persistence probabilities well outside the contours for the 95 % total VP consistency of the perturbed VP (Figure 7.8, lower row). Persistence probabilities which ensure the right observational occurrence probability of persistent nights and are closest to the range of perturbed VP consistency with $\mathrm{VP_{ref}}$ are given for π_{wSBL} between 40 % to 60 %. These results are relatively insensitive to the season

As demonstrated in the previous section the persistence probabilities ensuring good total

VP consistency are relatively broad. We will now evaluate the range of persistence probabilities in a stationary Markov chain which is consistent with the observed persistence probabilities across all tower sites discussed in section 7.2. In order to account sampling variability in the observed regime statistics and the effects of changes in π_{wSBL} we consider occurrence probabilities in an arbitrary 10 % error range (± 5 %) around the values from $\mathrm{VP}_{\mathrm{ref}}$. In the following Figures the solid, dashed, and dotted lines respectively correspond to the reference, 5% decreased, and 5 % increased observational occurrence probabilities of at least one transition in a night (wSBL to vSBL in red; vSBL to wSBL in black). The range of persistence probabilities for which the stationary Markov chain models the observed occurrence probabilities of very persistent nights with 10 % uncertainties is displayed by a shaded rectangle with $\mathbf{Q}$ with a mark for the exact observation. As in previous Figures isolines of total consistency of perturbed VP to $\mathrm{VP}_{\mathrm{ref}}$ are depicted in grey lines.

Similar to what was found at Cabauw, across all land-based stations the perturbed VP is not very sensitive to the values of $\mathbf{Q}$ and a relatively broad range of persistence probabilities allows for a 95 % total VP consistency in the HMM analyses (Figure 7.9). The persistence probabilities corresponding to the most likely VPs are reasonably similar across the different stations, with regime persistence probabilities between 0.95 and 0.99.

At almost all stations, the persistence probability values for which the stationary Markov chain regime transition statistics match the observed values fall outside the region of high total VP consistency between the reference and perturbed VPs (Figure 7.9). This fact is true for all seasons. Only at Cabauw do these ranges of persistence probabilities coincide fairly well. With the exception of Boulder and summertime in Los Alamos, the persistence probabilities in the stationary Markov chain needed to capture the observed regime transition statistics exceed those of the VP. This fact is consistent with the underestimation of occurrence probabilities of transitions by stationary Markov chains using $\mathbf{Q}_{\mathrm{ref}}$ shown in Figure 7.2.

As discussed in section 7.2 and chapter 5, the probability of very persistent nights varies more with season than the occurrence of transitions (cf. Table 7.2 and Figure 7.1). This result is reflected in the fact that the range of persistence probabilities capturing the right regime transition statistics in a stationary Markov chain changes less dramatically between seasons than the optimal value to capture the occurrence probabilities of persistent nights (Figure 7.9). Only at Cabauw in wintertime and Hamburg in spring or autumn we can identify a range of persistence probabilities for the stationary Markov chain which is able to model all SBL regime statistics accurately within our imposed uncertainty range. At all other times and stations such a common range of persistence probabilities is generally

Table 7.2: Probabilities of the occurrence of a wSBL to vSBL (turbulence collapse) or reverse transition (turbulence recovery) in a night, of the occurrence of very persistent wSBL or vSBL nights, and of the climatological initial distributions of starting a night in the wSBL or vSBL (respectively π_{wSBL} and π_{vSBL}) at the different tower sites for different seasons.

Tower station	season	Observations					
		Turbulence		Persistent nights		clim.	
		collapse [%]	recovery [%]	wSBL [%]	vSBL [%]	π_{wSBL}[%]	π_{vSBL} [%]
Land-based stations							
Boulder	winter	68.95	56.5	3.22	22.94	45.59	54.41
	spring & autumn	74.84	55.18	4.44	15.43	56.24	43.76
	summer	82.07	54.41	5.32	7.29	65.2	34.8
Cabauw	winter	48.03	31.69	29.22	14.87	73.44	26.56
	spring & autumn	44.75	22.37	21.36	27.68	63.16	36.84
	summer	35.99	19.1	16.49	38.92	50.50	49.50
Hamburg	winter	54.58	38.78	37.25	5.01	87.36	12.64
	spring & autumn	63.16	36.26	28.36	7.02	89.77	10.23
	summer	59.94	22.86	24.89	10.81	82.22	17.78
Karlsruhe	winter	38.41	31.49	58.13	0.69	95.85	4.15
	spring & autumn	49.45	41.76	40.66	3.85	89.56	10.44
	summer	40.96	22.5	13.85	32.18	57.23	42.77
Los Alamos	winter	65.16	30.95	13.24	16.88	74.41	25.59
	spring & autumn	72.99	36.92	12.86	10.13	79.46	20.54
	summer	74.32	38.57	11.73	9.58	78.75	21.25
Land-based stations							
FINO-1	winter	37.84	37.84	62.16	0.00	91.89	8.11
	spring & autumn	23.64	38.18	38.18	16.36	52.73	47.27
	summer	13.64	18.73	56.73	16.91	67.64	32.36
FINO-2	winter	18.93	23.33	58.89	12.81	75.72	24.28
	spring & autumn	18.12	24.83	47.65	22.82	64.77	35.23
	summer	15.1	26.72	28.2	40.19	39.75	60.25
FINO-3	winter	31.56	29.51	57.38	6.97	86.48	13.52
	spring & autumn	14.08	14.79	54.23	26.06	66.2	33.80
	summer	12.23	14.61	50.32	27.16	61.36	38.64

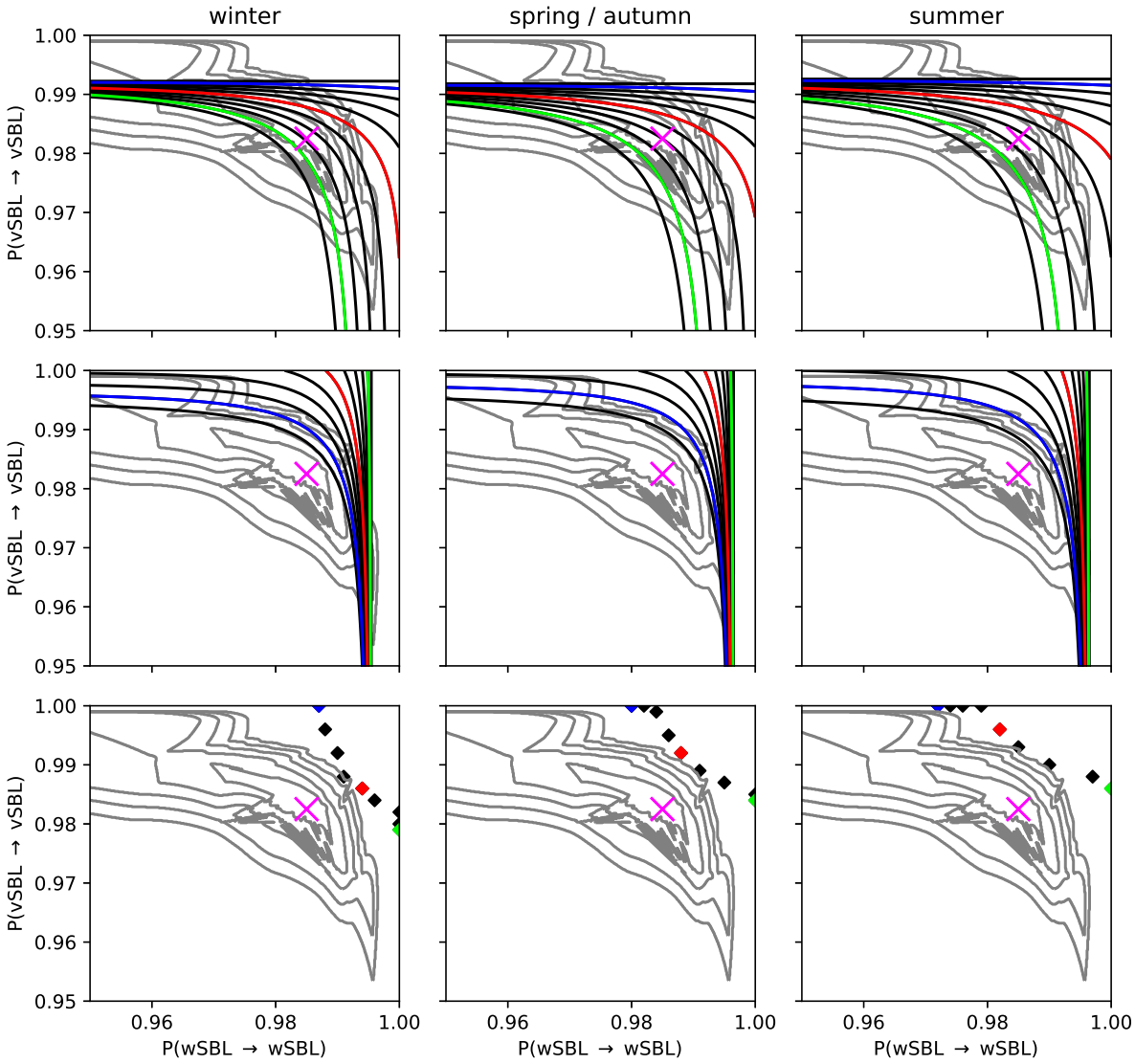

Figure 7.8: Curves of persistence probabilities yielding stationary Markov chain occurrence probabilities of a at least one wSBL to vSBL (turbulence collapse, top row) and reverse transitions (turbulence recovery, middle row) equal to the observed values, for a range of initial state probabilities π_{wSBL} in 10 % intervals ranging from 0 % to 100 % (10 % in green, 50 % in red, and 90 % in blue) at Cabauw. The bottom row illustrates in the same colour coding the persistence probabilities producing the observational occurrence probability of very persistent wSBL and vSBL nights in a stationary Markov chain. The persistence probability values denoting 95 to 99 % total consistency levels of the perturbed VP with $\mathrm{VP}_{\mathrm{ref}}$ are depicted in grey contours. The persistence probabilities corresponding to $\mathbf{Q}_{\mathrm{ref}}$ value are marked by a pink cross.

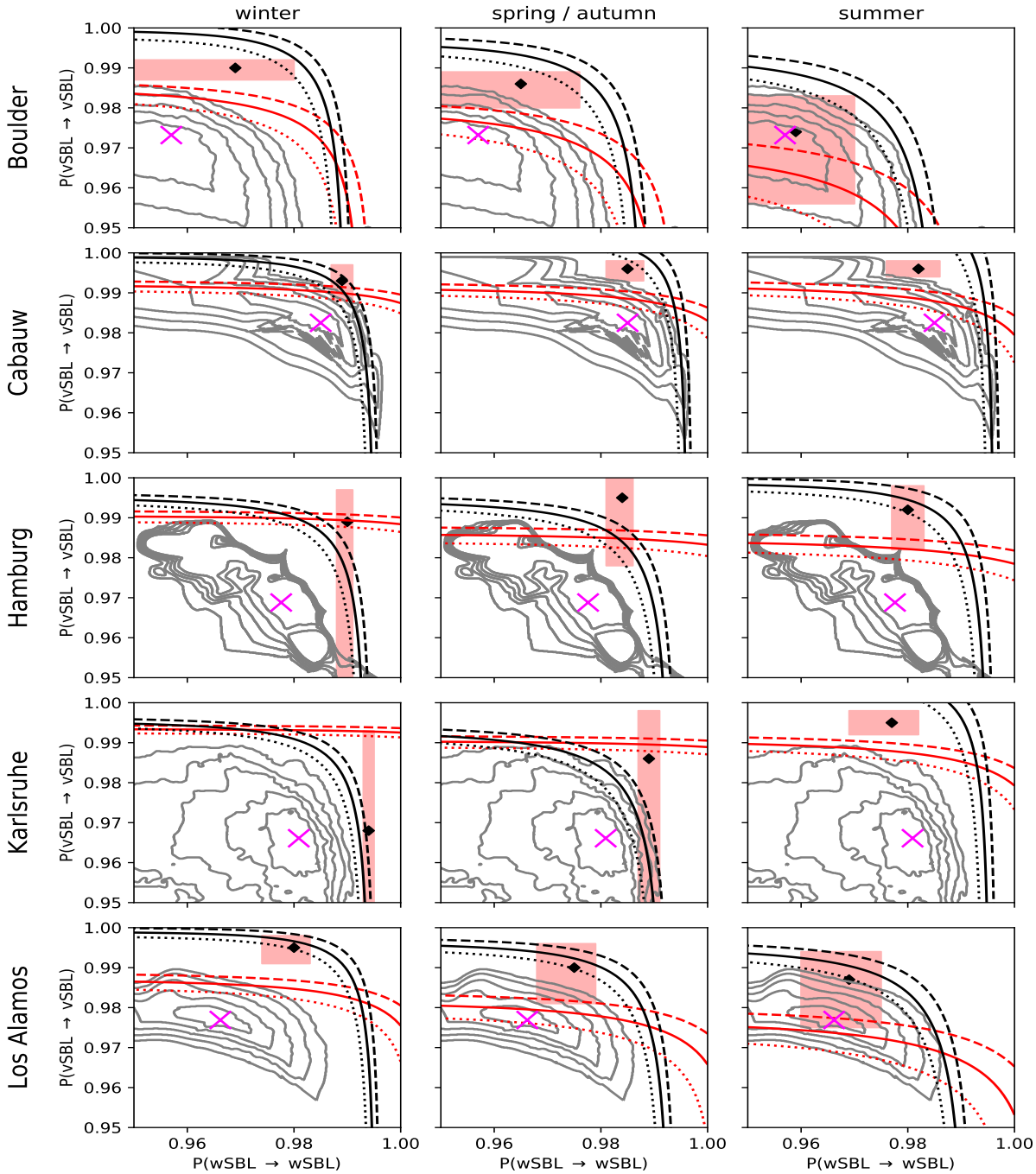

Figure 7.9: Values of persistence probabilities for which the occurrence probability of at least one wSBL to vBSL transition (turbulence collapse) in a night (red lines) or one vSBL to wSBL (turbulence recovery) in a night (black lines) as computed from a stationary Markov chain equal the observed values. Solid, dashed, and dotted lines correspond respectively the observed values, a probability 5 % below the observed values and a probability 5 % above the observed values. The ranges of persistence probabilities where the occurrence probability of very persistent nights in a stationary Markov chain agrees with observations in a $\pm$ 5 % uncertainty band is depicted by the red rectangle with a diamond displaying the values for the exact observational probability occurrence of persistent nights. The persistence probabilities values corresponding to 95 to 99 % total consistency of the perturbed VP with $\mathrm{VP}_{\mathrm{ref}}$ in the HMM analysis are depicted in grey contours. The persistence probabilities corresponding to $\mathbf{Q}_{\mathrm{ref}}$ value are marked by a pink cross.

absent. Similar to the occurrence probability of regime transitions, the exact occurrence probability of very persistent nights can only be modelled in a stationary Markov chain with higher persistence probabilities than the $\mathbf{Q}$ directly estimated from observations (with the exception of summertime at Cabauw and Karlsruhe where $P(\text{wSBL} \rightarrow \text{wSBL})$ has to be slightly smaller than $\mathbf{Q}_{\text{ref}}$). Again this result is consistent with the general underestimation of occurrence probabilities of very persistent nights in a stationary Markov chain illustrated in Figure 7.1.

In almost all cases, the range of persistence probabilities accounting for uncertainties in the occurrence of very persistent nights includes the occurrence probability of one type of regime transitions. The statistics of turbulence recovery events and very persistent nights most often correspond to the same ranges of persistence probabilities than statistics of turbulence collapses with very persistent nights. Very rarely do these overlapping ranges of persistence probabilities also fall in the range persistence probabilities ensuring a good agreement between VP_{ref} and perturbed VPs.

At ocean-based stations the range of persistence probabilities that ensures good agreement between the VP_{ref} and the perturbed VPs is substantially larger than for land-based stations (Figures 7.10 and 7.10). The total VP consistency exceeds 95 % for regime persistence probabilities ranging from approximately 0.92 to 0.99. Similar to land based stations, the range of persistence probabilities for which both kinds of transitions agree well with the stationary Markov chain lies generally at larger persistence probabilities than values assuring good agreement between the reference and perturbed VPs. Only in winter do the persistence probabilities for which the stationary Markov chain captures the observed persistence probabilities fall below $\mathbf{Q}_{\text{ref}}$ for $P(\text{wSBL} \rightarrow \text{wSBL})$ and above $\mathbf{Q}_{\text{ref}}$ for $P(\text{vSBL} \rightarrow \text{vSBL})$. These results do not have a simple relationship to the underestimation of occurrence of transitions illustrated in Figure 7.2 as both persistence probabilities are important to calculate the occurrence probability of at least one transition (cf. A.3 and A.4). The agreement between observed and modelled occurrence probabilities of at least one transition is better at FINO-2 and FINO-3. For each season at these two sites, the region of persistence probabilities needed to capture the occurrence of at least one transition in a night in a stationary Markov chain is much closer to $\mathbf{Q}_{\text{ref}}$ than is the case for land-based stations. This result might be related to the fact that while our analysis has accounted to some degree for seasonal nonstationarities it has not allowed for diel nonstationarities. Over the oceans diel nonstationarities are substantially weaker than over land (cf. chapter 6), where there is a pronounced maximum in the probability of wSBL to vSBL transitions occurring during sunset.

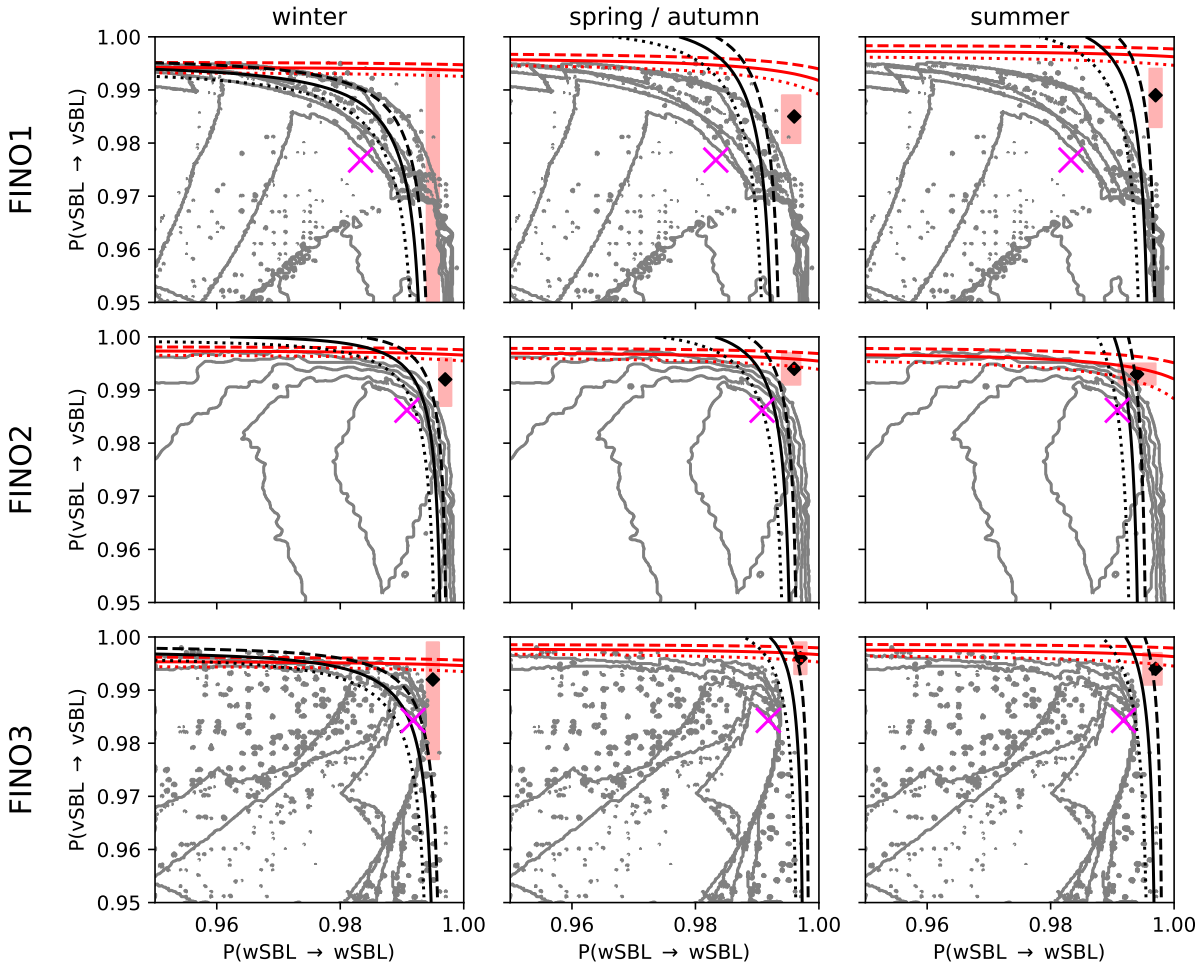

Figure 7.10: As Figure 7.9 only for ocean-based stations.

With the exception of FINO-1 the ocean-based stations show that a range of persistence probabilities can be identified in a stationary Markov chain for which all considered regime statistics match observations. These values tend to be in ranges of persistence probabilities exceeding 0.99. These values are considerably different from those found at land-based stations. This fact agrees well with the findings in chapters 5 and 6 that transitions are radiatively-driven over land but advectively-driven over oceans. A result of these different mechanisms is a much lower occurrence of transitions and therefore higher frequency of persistent nights over oceans. Nonetheless, the appropriate range of persistence probabilities capturing the regime statistics in a stationary Markov chain lie outside of the isolines where good agreement between reference and perturbed VPs

As discussed in section 7.2, the occurrence of subsequent transitions and the event durations can be explained relatively well by a stationary Markov chain using $\mathbf{Q}_{\mathrm{ref}}$. In fact, we find that the statistics of subsequent transitions are simulated well over the whole range of persistence probabilities corresponding to a 95 % total VP accuracy in perturbed VPs (not shown). This result reinforces the fact that once the first transition is captured or simulated many aspects of SBL regime statistics are modelled well by a stationary Markov process.

7.5 Discussion and Conclusions

In the previous chapters we have demonstrated that HMM analysis is an effective tool to classify the SBL into wSBL and vvSBL conditions [also cf. *Monahan et al.*, 2015]. Due to the fact that weather and climate models are unable to accurately simulate SBL regime dynamics, the goal of this study is to investigate how this stationary two-regime Markov chain could be used as the foundation of new stochastic parameterisations for turbulence in the SBL for local processes, in other words, for models with a high horizontal resolution but also as a foundation for more general parameterisations once information of spatial regime dependencies are available. We have assessed the performance of the stationary Markov chain relative to the observed probabilities event durations and of the occurrences of very persistent nights (nights without SBL regime transitions), of any regime transitions, and of multiple subsequent transitions.

The observed occurrence of very persistent wSBL (vSBL) nights increases (decreases) from summer to winter, likely due to changes in the mean large-scale forcing between these seasons in the midlatitudes which are not accounted for by the stationary Markov chain. Using the HMM persistence probabilities the occurrence of regime transitions is overestimated by the stationary Markov chain. However, the modelled occurrence of transitions subsequent to a preceding one and the mean event durations in each regime are relatively close to observations across all sites and seasons. The event duration pdfs, on the other hand, display a maximum an hour or two after sunset. Such a recovery time between regime transitions (cf. chapter 6) is not explainable by any stationary two-regime Markov chain. However, after these two hours event duration pdfs can be very well approximated by a stationary Markov chain.

By fixing the persistence probability matrix and producing new perturbed HMM regime sequences we have quantified the range of persistence probabilities that are consistent with the most likely HMM regime sequence. Across all land-based sites similar ranges of

persistence probabilities are appropriate to describe the regime statistics of the SBL. The persistence probabilities estimated by HMM analyses using other observed state variables generally also fall into this range. This result reinforces the findings in chapter 4 that the regime statistics are evident in many near-surface state variables. Across ocean-based sites the range of persistence probabilities that allows for accurate perturbed regime sequences is larger than at land-based sites.

The result that broadly the same range of persistence probability values describes the SBL regime statistics across tower sites indicates that a stochastic parameterisation based on the two-state Markov chain does not require parameters tuned to the fine details of local conditions. Systematic differences do exist between land- and ocean-based stations due to the different mechanisms of transitions (cf. chapters 5 and 6).

An analysis of the ranges of persistence probabilities for which a 'freely-running' stationary Markov chain is consistent with the observed regime transition statistics indicated that these generally exceed the values obtained from the HMM analysis. At ocean-based stations we find a better agreement between ranges of appropriate persistence probabilities in a stationary Markov chain and in observations. This result may be related to the fact that diel nonstationarities are weaker over oceans than over land (cf. chapter 6). As with the regime statistics for the occurrence of transitions, the occurrence probabilities of persistent nights can only be simulated in a stationary Markov chain with larger persistence probabilities than estimated from observations. In general, no range of persistence probabilities can be identified that is consistent with both the occurrence probabilities of both transitions and very persistent nights. The results indicate that the occurrence of very persistent nights cannot be accurately simulated by the same stationary Markov chain which is appropriate to capture the statistics of regime transitions because the different classes of nights (with and without transitions) depends on the large-scale synoptic conditions.

Our results have direct relevance to the representation of SBL regimes in weather and climate models. The regime statistics show clear evidence of nonstationarity and non-Markov behaviour. These facts, and the fact that aspects of regime transitions such as radiatively-driven turbulence collapse can be simulated by models, indicate the need for state-dependent transition probabilities in any explicitly stochastic representation of SBL regime transitions.

We now discuss the form that such an explicitly stochastic parameterisation for local processes which directly can be related to the tower observations might take. State-of-the-art boundary layer turbulence parameterisations in weather and climate models are generally able to produce turbulence collapses during the nocturnal transition. However, the models

do not correctly simulate turbulence recovery events as for instance intermittent turbulence events are not explicitly resolved. To overcome the resulting grid-box mean errors long-tailed stability function under stable conditions have been used causing turbulence never to collapse [e.g. *Holtslag et al.*, 2013]. A process-based stochastic parameterisation, on the other hand, could simulate turbulence recovery events by driving the SBL episodically into a turbulence active regime [e.g *He et al.*, 2012]. Such turbulence impulses can be interpreted as being related to intermittent turbulence events. As in *He et al.* [2012], this stochastic forcing can be implemented as an extra source term in the TKE budget.

The stochastic parameterisation would use a new local variable tracking the SBL regime (wSBL or vSBL). At each time step, the occurrence of a transition would be determined randomly using instantaneous state-dependent transition probabilities. For instance, $P(\text{wSBL} \rightarrow \text{vSBL})$ could depend on the Richardson-number (Ri) in such a way that the probability of turbulence collapse is very small for small Ri, but increases to virtual certainty for sufficiently large Ri. The presence of such a transition range in which either regime could be occupied is consistent with the observed overlap of the wSBL and vSBL in the distributions of shear, stratification, and turbulence (cf. chapter 4). In the vSBL state, random 'kicks' of TKE can be added as representation of the effects of intermittent turbulent events which erode the stratification and reduce Ri. With a Ri dependent $P(\text{vSBL} \rightarrow \text{wSBL})$, after a sufficiently large input of energy, the system will have a high probability of transitioning back into the wSBL. We propose a compound Poisson process representation of the random 'kicks' as intermittent turbulence events are associated with many different phenomena (such as breaking gravity waves, density currents etc.) which are independent from each other and can produce very different turbulence intensities. Such a parameterisation can account for the observed non-Markov recovery time between transitions as after entering the wSBL state a certain time is required to build up the stratification so that a transition to the vSBL occurs, and in the vSBL time is required for intermittent turbulence kicks to sufficiently erode the stratification and result in the reverse transition. Furthermore, this picture is consistent with the observed enhancement of TKE values before a vSBL to wSBL transition and with the relatively gradual decay of turbulence across the wSBL to vSBL transition (cf. chapter 6). The fact that event duration distributions are very similar between the tower sites suggests that the compound Poisson process can be parameterised independent of the local complexity of the surface conditions (such as surface type, topography etc.). As the proposed parameterisation uses the fact that the wSBL to vSBL transition is a relatively well-resolved process, with a strong dependence of the transitions probability on Ri the wSBL to vSBL transition stays in such an approach effectively deterministic in contrast to the stochastic vSBL to wSBL

transition.

The observational information on climatological regime statistics, and event duration distributions (cf. chapters 5, 6, and the present) can then be used to tune the parameterisation to generate the appropriate SBL regime variability. The results obtained for stationary Markov chain average persistence probabilities in this study can be used to constrain the average behaviour of the state-dependent persistence probabilities. The fact that no set of persistence probabilities allows the stationary Markov chain to produce both the observed very persistent night statistics and transition statistics suggests that some compromise between these two might be necessary (although the extra freedom provided by the state-dependent transition probabilities may result in better simulations of both sets of regime statistics than was possible by the stationary Markov chain).

Finally, the development of such a parameterisation requires further information regarding horizontal dependence of regime statistics, as it is not reasonable to expect an entire large-scale weather or climate model grid box to always be in one or the other state. This horizontal dependence will be the subject of a future study. Assessment of the dependence length scales relative to the grid box size will allow the determination of to what extent the subgrid-scale variability can be represented by a deterministic average, or if its parameterisation must be explicitly stochastic.

8 Conclusion

The goal of this study has been to systematically analyse the long-term climatology of the occurrence and structure of regimes and regime transitions in the SBL, denoted wSBL and very vSBL conditions. In order to increase confidence in the generality of the results we have analysed nocturnal data from nine tower sites at locations around the world with different surface types (sea water, grassland, sand, and ice) and surrounding terrains of different complexity (flat surfaces, mountain ridges, and metropolitan regions). All these stations show a clear structure of two distinct regimes in the SBL in the three dimensional state variable space of mean wind speed, wind shear, and stratification exhibiting one regime with weak static stability and moderate to strong winds (wSBL), and a second regime with strong static stability and moderate to weak winds (vSBL).

HMM analyses using observed Reynolds-averaged data are able to separate the data into two physically-reasonable regimes robustly across the different tower sites. HMM analyses of the above mentioned three-dimensional state variable set classify both the Reynolds-averaged means as well as the turbulence state variables into the two distinct states. In the wSBL, large TKE and vertical velocity variance values are found whereas the vSBL shows very weak or collapsed turbulence. Sensitivity analyses of the input information for the HMM analyses indicates that turbulence, Reynolds-averaged data of wind shears and stratification, or combined vectors of these state variables result in almost the same regime affiliation of the data demonstrating how robust the signal in the observed quantities is.

The regime sequence obtained from the HMM analyses allows for the assessment of the climatology of two basic types of nights: nights with regime transition occurrences and nights without (referred to as very persistent nights). We find systematic changes in the occurrence probabilities of very persistent nights with variations in surface conditions: such nights are relatively rare in arid regions, more common in cloudier regions, and most common at ocean-based tower sites. Furthermore, the occurrence of very persistent nights depends strongly on the season across all sites. Very persistent wSBL are more frequent in wintertime than in summer whereas very persistent vSBL nights are more frequent in summer nights. Statistics such as the probability of at least one transition event or of

multiple events occurring in a night, on the other hand, show only a weak dependence on seasonal modulation. At land-based stations, surface radiative cooling starts around sunset leading to a maximum in the transition frequency from wSBL to vSBL conditions in this time period. Across ocean-based stations such pronounced maxima in the timing of transitions are absent as transitions are caused by advection of warm-air aloft which is not generally closely tied to the diel cycle. The frequency of occurrence of turbulence recovery events, on the other hand, shows a weaker dependence on the time after sunset. The probability density functions (pdf) of event duration in the wSBL or vSBL are very similar and both distributions are characterised by an initial recovery time of approximately one hour before a subsequent transition occurs.

With respect to the atmospheric structure in times of very persistent nights we find that the stratification and wind profiles show a clear separation between the two regimes across the land-based stations. The very persistent wSBL is governed by strong wind conditions and near-neutral to weakly-stable stratification profiles. Strong winds, and the resulting strong near-surface shears, lead to relatively large TKE production, vertical velocity variations, and turbulent momentum transports. Because of the relatively large vertical turbulent fluxes, the near-surface atmospheric layers are coupled and directional shears are relatively small. The very persistent vSBL is governed by strong stratification and low wind conditions which lead to low TKE values and weak vertical turbulent momentum flux. The atmospheric levels are uncoupled from each other and at most sites directional shears are larger than in the wSBL. In order to sustain these very persistent night we find that wind conditions are relatively steady in strong or weak wind conditions for the respectively very persistent wSBL and vSBL throughout the entire nights. At the ocean-based stations the very persistent vSBL is induced by the advection of warm air aloft rather than by surface cooling. At these locations, the difference in very persistent nights between coupled states with relatively strong turbulence and uncoupled states with relatively weak turbulence is also found.

In times of regime transitions we identify very robust evolutions of the structures of the Reynolds-averaged mean and turbulence state variables. Across land-based stations, radiative cooling at the surface causes a continual decrease in the temperatures near the surface building up the inversion strength which results in the wSBL to vSBL transition. The enhanced inversion strength decreases resulting in vertical decoupling of the dynamics. Accordingly, TKE values show a strong decrease to complete collapse with almost complete suppression of vertical fluctuations in wSBL to vSBL transitions. Recovery of turbulence happens more quickly, on timescales of a few minutes. The turbulence initially recovers aloft and then spreads throughout all observational levels. The recovery of

turbulence leads to the weakening of the inversion and the coupling of the atmospheric levels. Similar results are found at the ice-based stations, although there is evidence indicating that advection of warm-air aloft is also a mechanism leading to turbulence collapse. At ocean-based sites regime shifts are clearly related to the advection of warm air aloft. Consistent with the fact that stratifications are generally weaker than over land and ice, decoupling of the atmospheric layers in the vSBL is weaker. Nevertheless, winds decrease and increase combined with respectively vertical decoupling and coupling during wSBL to vSBL and reverse transitions.

Consistent with the fact that the wind speed distributions are separated in very persistent wSBL and vSBL nights over land, we find a separation of the pressure gradient force (as measured by U_{geo}). However, U_{geo} is not an effective predictor of very persistent regime nights as nights with transitions are associated with a broad range of values overlapping those associated with very persistent nights. Another external driver on the SBL dynamics is the LLCC. Very persistent wSBL nights are most likely to be accompanied by overcast conditions with strong U_{geo} while very persistent vSBL nights are most likely accompanied by clear-sky conditions with weak U_{geo}. While U_{geo} and LLCC separate very persistent wSBL from vSBL nights to some extent, regime transitions occur for intermediate U_{geo} ranges and under all LLCC conditions. Furthermore, regime transitions are found to be completely insensitive to changes in pressure gradient forces. In contrast to U_{geo}, changes in LLCC have a larger effect on transitions in the SBL. However, no clear precursor for transitions can be determined.

The absence of clear precursors suggests that parameterisations in weather and climate models of SBL regime behaviour and turbulence in the two regimes should be stochastic. Therefore, we assessed to what extent such a stochastic parameterisation of local SBL regimes could be based on stationary Markov chains. In order to base a parameterisation on a stationary Markov chain it is important that such a model is able to reproduce the observed statistics of the regime sequence. Our results demonstrate that a stationary Markov chain using the best-fit parameters from the HMM analysis is not able to reproduce the correct SBL regime statistics at any tower location. The occurrence of very persistent nights is systematically underestimated whilst regime transitions are systematically overestimated. Furthermore, recovery times between transitions as found in the observations display non-Markov behaviour.

By fixing the transition probability matrix and producing new perturbed HMM regime sequences we have quantified the range of persistence probabilities that are consistent with the most likely HMM regime sequence and could be used in a 'freely-running' stationary

Markov chain. Across sites similar ranges of transition matrices are appropriate to describe the SBL regime statistics. However, an analysis of the ranges of persistence probabilities for which a 'freely-running' stationary Markov chain is consistent with the observed regime transition statistics indicate that these generally exceed the values obtained from the HMM analysis. Furthermore, no general range of transition probability matrices can be identified that is consistent with all SBL regime statistics at any site. Our results confirm that a simple stochastic parameterisation on the basis of 'freely-running' Markov chains is not sufficient. A possible stochastic parameterisation with state-dependent transition probabilities was presented and discussed.

8.1 Future research and challenges

This research is the first of its kind to quantify systematically the climatology of SBL regime occupation and transitions statistics for a broad range of different locations. However, although data from several tower sites have been analysed, all are located in the mid- to high-latitudes. SBL regime dynamics in several areas on the globe such as in low-latitudes might exhibit different SBL statistics. In particular, in low-latitude regions moist effects might play a more important role than in the mid- to high-latitudes. Consideration of data from the 325 m Amazonian Tall Tower Observatory [ATTO, *Andreae et al.*, 2015] which would permit such an analysis is an important direction of future research. However, our analysis demonstrates that tall towers may not be necessary for classification purposes. Thus, a global analysis of smaller towers with many years of observation, which are much more common around the world, is possible and can complete the picture of the global distribution of SBL regime statistics. Furthermore, recently ESA's Earth Explorer Aeolus satellite has been launched into orbit with the new technology to measure winds around the globe particularly in the proximity of the surface. More satellites are about to join the project in the next years in order to ensure a continuous mapping of winds. These data products may allow us to do a thorough global SBL regime analysis and assess the generality of the results presented in this thesis.

This work has only quantified and explained the SBL statistics in an average sense. Quantifying the triggering mechanism for the recovery of turbulence still remains a challenge. In general, intermittent turbulence events are believed to be caused by instabilities or fluctuations in the stably stratified flow. However, our analysis clearly demonstrates that external influences can also play a role in reactivation of turbulence (cf. chapter 6). Other influences of atmospheric disturbances outside the boundary layer causing the generation

of intermittent turbulence have also been identified [*Sun et al.*, 2004]. Therefore, a better climatology of the actual origins of intermittent events is necessary to improve the understanding of the SBL statistics as well as revealing the physics leading to the dominant 1-3 hour timescale between SBL transitions. Such a research also includes a better understanding of the coherent spatial structure of these intermittent turbulence events and how they propagate in the SBL. However, observations consist typically of weather tower observations and high resolution data in both space and time has not been available at this point. A promising initial experiment which can be used to address that question is the pilot field campaign in Perdigão, Portugal, which was conducted in 2017. The data consist of measurements from more than 50 different towers over an area of about four square kilometres. Fortunately, the data have also a large time resolution which allows for a determination if interactions of different turbulence scales or mechanisms in the intrinsic modes of the geophysical flow cause the dominant 1-3 hour timescales between SBL transitions. Some data have been made available recently and could be used in a future study. Unfortunately, this project is just a field campaign and not sufficient to derive climatologies. Nonetheless, it can help to evaluate the initialisation of vSBL to wSBL transitions, their structure in space and time, and the propagation of turbulence patches. As the current analysis is only based on local one dimensional tower sites it is not possible to quantify at what spatial scale the 'stochastic' intermittent events can be approximated by deterministic averages. The Perdigão measurement field might already be already be large enough in order to address that question.

The most important research question that emerges from this study is to how its results can be translated into stochastic parameterisations of the effect of SBL regimes on resolved variables in weather and climate models. In chapter 7 we have discussed a framework for how such a parameterisation might be realised for a model with high horizontal resolution, informed by the regime statistics we have obtained. The framework of the stochastic parameterisation can be implemented in a conceptual model, such as the well-studied Couette flow [Holdsworth et al., 2016], to test its potential. If the representation of SBL processes turns out to be improved by the suggested parameterisation, subsequent tests in a comprehensive single-column model such as the single column version of the Canadian Centre for Climate Modelling and Analysis fourth-generation atmospheric general circulation model (CanAM4) can be conducted. In other words, this work lays the foundation of developing such stochastic parameterisations in order to ultimately improve weather and climate models. In order to obtain parameterisations for models with low horizontal resolution (for example climate models) based on the proposed concepts for a stochastic parameterisation the determination of the spatial dependence of regime behaviour on spatial scales of about

one geographical degree is indispensable. Such an analysis has to quantify at what scale the regime dynamics are accounted for in a deterministic relationship and at what scale explicit stochastic approaches are necessary. *Medeiros and Fitzjarrald* [2014, 2015] showed in an observational surface station network spanning approximately a 1 by 1 degree geographical area that simultaneous intermittent turbulence events can occur across such a domain, however, without the spatial climatology the likelihood of such an event cannot be determined at this point.

As the development of new parameterisation for large-scale circulation models can take several years in order to derive an actual improved representation of a process due to the fact that all parameterisations are heavily-tuned in order to simulate an appropriate mean model state. This study can therefore be used in order to tune subgrid-scale turbulent flux parameterisations for the wSBL and vSBL without considering transitions between them. Our analysis of very persistent nights can describe the turbulent flux limits in the two stably stratified regimes which should be represented in weather and climate model.

Not only weather prediction models would benefit from a more accurate representation of the SBL regimes, but climate models would also benefit. With better representations of the SBL variability an assessment of the response of SBL regime statistics to climate change is possible. State-of-the-art climate models usually still use relatively simplified boundary layer schemes which leads in particular to substantial errors in the SBL [*Davy and Esau*, 2016]. The result is that the models predict trends in the minimum nighttime temperatures (which are among the key climate extreme indices) to be much more pronounced than for the day-time maximum temperatures [*Vose et al.*, 2005; *McNider et al.*, 2012]. Our proposed approach can potentially improve climate models and therefore future projections and assess these results carefully. Furthermore, an analysis of quantifying the long-term trend in SBL regime statistics and the response to climate change from observations as well as comparing those to models is an interesting direction of future research.

Another interesting direction of future research could be the determination if in established regimes (in a state where state variables do not change substantially anymore) and in very persistent nights state variable profiles generally agree with Monin-Obukhov similarity theory. If Monin-Obukhov similarity theory is substantially violated even in relatively steady conditions without transitions, scientific challenges arise which are not just associated with the SBL regime transitions, but also with our fundamental understanding of how the large-scale flow is affected by turbulent mixing.

A Markov chain probability calculations

Here, we demonstrate how quantities of theoretical occurrence probabilities based on stationary Markov chains are calculated.

A.1 Calculation of very persistent regimes

The occurrence probability of very persistent SBL nights in a stationary Markov chain is calculated using the transition probabilities of the Markov chain to remain in the same regime (i.e. $P(\text{wSBL} \rightarrow \text{wSBL})$ and $P(\text{vSBL} \rightarrow \text{vSBL})$) as follows

$$Pr(\text{wSBL}|n) = \pi_{\text{wSBL}} P(\text{wSBL} \rightarrow \text{wSBL})^n, \tag{A.1}$$

$$Pr(\text{vSBL}|n) = \pi_{\text{vSBL}} P(\text{vSBL} \rightarrow \text{vSBL})^n. \tag{A.2}$$

where π_{wSBL} and π_{vSBL} are respectively the initial climatological distributions of being in the wSBL or vSBL and n equals the length of the night in hours multiplied by six (corresponding to a data resolution of 10 min)

A.2 Calculation of at least one particular SBL transition occurrence

The probability of the occurrence of a particular SBL transition in a night of duration n can be expressed in terms of the probability of the absence of any transitions and the probability of single transitions of the complementary transition. In the case of the wSBL to vSBL transition the single complementary transitions start in the vSBL is only allowed a transition to the wSBL. Naturally, the reverse is true for vSBL to wSBL transitions. That way we account for all possibilities that definitely do not have a transition of the considered type.

The probability of the occurrence of turbulence collapse is:

$$\begin{aligned} Pr((\text{wSBL} \rightarrow \text{vSBL}|n) > 0) = 1 - & \underbrace{\pi_{\text{wSBL}} P(\text{wSBL} \rightarrow \text{wSBL})^n}_{\text{prob. of remaining in the wSBL}} \\ & - \underbrace{\pi_{\text{vSBL}} P(\text{vSBL} \rightarrow \text{vSBL})^n}_{\text{prob. of remaining in the vSBL}} \\ - & \underbrace{\sum_{t=0}^{n-1} \pi_{\text{vSBL}} P(\text{vSBL} \rightarrow \text{vSBL})^t P(\text{vSBL} \rightarrow \text{wSBL}) P(\text{wSBL} \rightarrow \text{wSBL})^{n-t-1}}_{\text{prob. of only vSBL to wSBL transitions, remaining in the wSBL afterwards}} , \end{aligned} \tag{A.3}$$

Equivalently, the probability of a turbulence recovery (vSBL to wSBL transition) is given by

$$\begin{aligned} Pr((\text{vSBL} \rightarrow \text{wSBL}|n) > 0) = 1 - & \underbrace{\pi_{\text{wSBL}} P(\text{wSBL} \rightarrow \text{wSBL})^n}_{\text{prob. of remaining in the wSBL}} \\ & - \underbrace{\pi_{\text{vSBL}} P(\text{vSBL} \rightarrow \text{vSBL})^n}_{\text{prob. of remaining in the vSBL}} \\ - & \underbrace{\sum_{t=0}^{n-1} \pi_{\text{wSBL}} P(\text{wSBL} \rightarrow \text{wSBL})^t P(\text{wSBL} \rightarrow \text{vSBL}) P(\text{vSBL} \rightarrow \text{vSBL})^{n-t-1}}_{\text{prob. of only wSBL to vSBL transitions, remaining in the vSBL afterwards}} . \end{aligned} \tag{A.4}$$

A.3 Calculation of the probability of subsequent turbulence recovery or collapse event occurrences

The probability that a turbulence recovery event occurs after a turbulence collapse in a night of duration n is equal to the sum of the probabilities of all events that include the occurrence of SBL patterns starting at time t_1 in the wSBL, and afterwards showing the sequence wSBL $\rightarrow \overbrace{\text{vSBL} \rightarrow \ldots \rightarrow \text{vSBL}}^{t\times} \rightarrow$ wSBL with no further subsequent recovery events, i.e. the SBL remains in the wSBL or have a maximum of one more collapse. The last part of this calculation assures that no double counting of sequences with length t occur as the probability calculation of being in the wSBL at time t_1 does not include information of the preceding path. The probability of a certain subsequent recovery pattern of length

t can then be calculated as

$$Pr((\text{wSBL} \rightarrow \overbrace{\text{vSBL} \rightarrow \ldots \rightarrow \text{vSBL}}^{t\times} \rightarrow \text{wSBL}|n) > 0) = \sum_{t_1=0}^{n-t-2} (\pi^T \mathbf{Q}^{t_1})_{\text{wSBL}}$$
$$P(\text{wSBL} \rightarrow \text{vSBL}) P(\text{vSBL} \rightarrow \text{vSBL})^t P(\text{vSBL} \rightarrow \text{wSBL}) \Bigg[P(\text{wSBL} \rightarrow \text{wSBL})^{n-t-t_1-2}$$
$$+ \sum_{t_2=0}^{n-t-t_1-3} P(\text{wSBL} \rightarrow \text{wSBL})^{t_2} P(\text{wSBL} \rightarrow \text{vSBL}) P(\text{vSBL} \rightarrow \text{vSBL})^{n-t-t_1-t_2-3} \Bigg], \tag{A.5}$$

where π is the vector of climatological initial probabilities.

To calculate the overall probability that such a subsequent event occurs is then the summation over all possible t:

$$\sum_t Pr((\text{wSBL} \rightarrow \overbrace{\text{vSBL} \rightarrow \ldots \rightarrow \text{vSBL}}^{t\times} \rightarrow \text{wSBL}|n) > 0) = \sum_{t=0}^{n-2} \sum_{t_1=0}^{n-t-2} (\pi^T \mathbf{Q}^{t_1})_{\text{wSBL}}$$
$$P(\text{wSBL} \rightarrow \text{vSBL}) P(\text{vSBL} \rightarrow \text{vSBL})^t P(\text{vSBL} \rightarrow \text{wSBL}) \Bigg[P(\text{wSBL} \rightarrow \text{wSBL})^{n-t-t_1-2}$$
$$+ \sum_{t_2=0}^{n-t-t_1-3} P(\text{wSBL} \rightarrow \text{wSBL})^{t_2} P(\text{wSBL} \rightarrow \text{vSBL}) P(\text{vSBL} \rightarrow \text{vSBL})^{n-t-t_1-t_2-3} \Bigg] \tag{A.6}$$

Equivalently, the probabilities of subsequent turbulence collapses after recovery events are

$$Pr((\text{vSBL} \rightarrow \overbrace{\text{wSBL} \rightarrow \ldots \rightarrow \text{wSBL}}^{t\times} \rightarrow \text{vSBL}|n) > 0) = \sum_{t_1=0}^{n-t-2} (\pi^T \mathbf{Q}^{t_1})_{\text{vSBL}}$$
$$P(\text{vSBL} \rightarrow \text{wSBL}) P(\text{wSBL} \rightarrow \text{wSBL})^t P(\text{wSBL} \rightarrow \text{vSBL}) \Bigg[P(\text{vSBL} \rightarrow \text{vSBL})^{n-t-t_1-2}$$
$$+ \sum_{t_2=0}^{n-t-t_1-3} P(\text{vSBL} \rightarrow \text{vSBL})^{t_2} P(\text{vSBL} \rightarrow \text{wSBL}) P(\text{wSBL} \rightarrow \text{wSBL})^{n-t-t_1-t_2-3} \Bigg] \tag{A.7}$$

To calculate the overall probability that such a subsequent event occurs is then the sum-

mation over all possible t:

$$\sum_t Pr((\text{vSBL} \rightarrow \overbrace{\text{wSBL} \rightarrow \ldots \rightarrow \text{wSBL}}^{t\times} \rightarrow \text{vSBL}|n) > 0) = \sum_{t=0}^{n-2} \sum_{t_1=0}^{n-t-2} (\pi^T \mathbf{Q}^{t_1})_{\text{vSBL}}$$
$$P(\text{vSBL} \rightarrow \text{wSBL}) P(\text{wSBL} \rightarrow \text{wSBL})^t P(\text{wSBL} \rightarrow \text{vSBL}) \Bigg[P(\text{vSBL} \rightarrow \text{vSBL})^{n-t-t_1-2}$$
$$+ \sum_{t_2=0}^{n-t-t_1-3} P(\text{vSBL} \rightarrow \text{vSBL})^{t_2} P(\text{vSBL} \rightarrow \text{wSBL}) P(\text{wSBL} \rightarrow \text{wSBL})^{n-t-t_1-t_2-3} \Bigg] \tag{A.8}$$

Bibliography

Abraham, C., and A. H. Monahan (2018a), Regimes of the stably stratified nocturnal boundary layer. Part I: Observable meteorological state variables containing information about regime occupation, *submitted to J. Atmos. Sci.*

Abraham, C., and A. H. Monahan (2018b), Regimes of the stably stratified nocturnal boundary layer. Part II: The boundary layer structure in times of very persistent weakly stable and very stable boundary layer conditions, *submitted to J. Atmos. Sci.*

Abraham, C., and A. H. Monahan (2018c), Regimes of the stably stratified nocturnal boundary layer. Part III: The structure of meteorological state variables and the role of external forces in times of regime transitions, *submitted to J. Atmos. Sci.*

Abraham, C., and A. H. Monahan (2018d), Characterising regime behaviour in the stably stratified nocturnal boundary layer on the basis of stationary Markov chains, *submitted to Nonlinear Process. Geophys.*

Acevedo, O. C., and D. R. Fitzjarrald (2003), In the Core of the Night-Effects of Intermittent Mixing on a Horizontally Heterogeneous Surface, *Bound. Lay. Meteorol.*, *106*(1), 1–33, doi:10.1023/A:1020824109575.

Acevedo, O. C., O. L. L. Moraes, G. A. Degrazia, and L. E. Medeiros (2006), Intermittency and the Exchange of Scalars in the Nocturnal Surface Layer, *Bound. Lay. Meteorol.*, *119*(1), 41–55, doi:10.1007/s10546-005-9019-3.

Acevedo, O. C., L. Mahrt, F. S. Puhales, F. D. Costa, L. E. Medeiros, and G. A. Degrazia (2016), Contrasting structures between the decoupled and coupled states of the stable boundary layer, *Q. J. R. Meteor. Soc.*, *142*(695), 693–702, doi:10.1002/qj.2693.

Andreae, M. O., O. C. Acevedo, A. Araùjo, P. Artaxo, C. G. G. Barbosa, H. M. J. Barbosa, J. Brito, S. Carbone, X. Chi, B. B. L. Cintra, N. F. da Silva, N. L. Dias, C. Q. Dias-Júnior, F. Ditas, R. Ditz, A. F. L. Godoi, R. H. M. Godoi, M. Heimann, T. Hoffmann, J. Kesselmeier, T. Könemann, M. L. Krüger, J. V. Lavric, A. O. Manzi,

A. P. Lopes, D. L. Martins, E. F. Mikhailov, D. Moran-Zuloaga, B. W. Nelson, A. C. Nölscher, D. Santos Nogueira, M. T. F. Piedade, C. Pöhlker, U. Pöschl, C. A. Quesada, L. V. Rizzo, C.-U. Ro, N. Ruckteschler, L. D. A. Sá, M. de Oliveira Sá, C. B. Sales, R. M. N. dos Santos, J. Saturno, J. Schöngart, M. Sörgel, C. M. de Souza, R. A. F. de Souza, H. Su, N. Targhetta, J. Tóta, I. Trebs, S. Trumbore, A. van Eijck, D. Walter, Z. Wang, B. Weber, J. Williams, J. Winderlich, F. Wittmann, S. Wolff, and A. M. Yáñez Serrano (2015), The Amazon Tall Tower Observatory (ATTO): overview of pilot measurements on ecosystem ecology, meteorology, trace gases, and aerosols, *Atmos. Chem. Phys.*, *15*(18), 10,723–10,776, doi:10.5194/acp-15-10723-2015.

Ansorge, C., and J. P. Mellado (2014), Global Intermittency and Collapsing Turbulence in the Stratified Planetary Boundary Layer, *Bound. Lay. Meteorol.*, *153*(1), 89–116, doi:10.1007/s10546-014-9941-3.

Baas, P., F. C. Bosveld, H. K. Baltink, and A. A. M. Holtslag (2009), A Climatology of Nocturnal Low-Level Jets at Cabauw, *J. Appl. Meteor. Climatol.*, *48*(8), 1627–1642, doi:10.1175/2009JAMC1965.1.

Baklanov, A. A., B. Grisogono, R. Bornstein, L. Mahrt, S. S. Zilitinkevich, P. Taylor, S. E. Larsen, M. W. Rotach, and H. J. S. Fernando (2011), The Nature, Theory, and Modeling of Atmospheric Planetary Boundary Layers, *Bull. Amer. Meteor. Soc.*, *92*, 123–128, doi:10.1175/2010BAMS2797.1.

Banta, R. M., L. Mahrt, D. Vickers, J. Sun, B. B. Balsley, Y. L. Pichugina, and E. J. Williams (2007), The Very Stable Boundary Layer on Nights with Weak Low-Level Jets, *J. Atmos. Sci.*, *64*, 3068–3090, doi:10.1175/JAS4002.1.

Barthlott, C., N. Kalthoff, and F. Fiedler (2003), Influence of high-frequency radiation on turbulence measurements on a 200 m tower, *Meteorol. Z*, *12*(21), 67–71(5), doi:10.1127/0941-2948/2003/0012-0067.

Basu, S., F. Porté-agel, E. Foufoula-Georgiou, J.-F. Vinuesa, and M. Pahlow (2006), Revisiting the Local Scaling Hypothesis in Stably Stratified Atmospheric Boundary-Layer Turbulence: an Integration of Field and Laboratory Measurements with Large-Eddy Simulations, *Bound. Lay. Meteorol.*, *119*(3), 473–500, doi:10.1007/s10546-005-9036-2.

Bechtold, P., M. Köhler, T. Jung, F. Doblas-Reyes, M. Leutbecher, M. J. Rodwell, F. Vitart, and G. Balsamo (2008), Advances in simulating atmospheric variability with the ECMWF model: From synoptic to decadal time-scales, *Quarterly Journal of the Royal Meteorological Society*, *134*(634), 1337–1351, doi:10.1002/qj.289.

Beeken, A., T. Neumann, and A. Westerhellweg (2008), Five Years of Operation of the First Offshore Wind Research Platform in the German Bight – FINO1, *Tech. rep.*, German Wind Energy Institute (DEWI GmbH), DEWEK, DEWI GmbH, Ebertstraße 96, D-26382 Wilhelmshaven, article available at: http://www.dewi.de/dewi/fileadmin/pdf/publications/Publikations/5_Beeken.pdf.

Berner, J., U. Achatz, L. Batté, L. Bengtsson, A. de la Cámara, H. M. Christensen, M. Colangeli, D. R. B. Coleman, D. Crommelin, S. I. Dolaptchiev, C. L. E. Franzke, P. Friederichs, P. Imkeller, H. Järvinen, S. Juricke, V. Kitsios, F. Lott, V. Lucarini, S. Mahajan, T. N. Palmer, C. Penland, M. Sakradzija, J.-S. von Storch, A. Weisheimer, M. Weniger, P. D. Williams, and J.-I. Yano (2017), Stochastic Parameterization: Toward a New View of Weather and Climate Models, *Bull. Amer. Meteor. Soc.*, pp. 565–587, doi:10.1175/BAMS-D-15-00268.1.

Blay-Carreras, E., D. Pino, J. V.-G. de Arellano, A. van de Boer, O. D. Coster, C. Darbieu, O. Hartogensis, F. Lohou, M. Lothon, and H. Pietersen (2014), Role of the residual layer and large-scale subsidence on the development and evolution of the convective boundary layer, *Atmos. Chem. Phys.*, *14*, 4515–4530, doi:10.5194/acp-14-4515-2014.

Blumen, W. (1984), An observational study of instability and turbulence in nighttime drainage winds, *Bound. Lay. Meteorol.*, *28*(3-4), 245–269, doi:10.1007/BF00121307.

Blumen, W., R. Banta, S. P. Burns, D. C. Fritts, R. Newsom, G. S. Poulos, and J. Sun (2001), Turbulence statistics of a Kelvin–Helmholtz billow event observed in the nighttime boundary layer during the Cooperative Atmosphere–Surface Exchange Study field program, *Dyn. Atmos. Oceans*, *34*(2-4), 189–204, doi:10.1016/S0377-0265(01)00067-7.

Bosveld, F. C., P. Baas, G.-J. Steeneveld, A. A. M. Holtslag, W. M. Angevine, E. Bazile, E. I. F. de Bruijn, D. Deacu, J. M. Edwards, M. Ek, V. E. Larson, J. E. Pleim, M. Raschendorfer, and G. Svensson (2014), The Third GABLS Intercomparison Case for Evaluation Studies of Boundary-Layer Models. Part B: Results and Process Understanding, *Bound. Lay. Meteorol.*, *152*(2), 157–187, doi:10.1007/s10546-014-9919-1.

Bowen, B. M., J. A. Baars, and G. L. Stone (2000), Nocturnal Wind Direction Shear and Its Potential Impact on Pollutant Transport, *J. Appl. Meteor. Climatol.*, *39*(3), 437–445, doi:10.1175/1520-0450(2000)039<0437:NWDSAI>2.0.CO;2.

Brümmer, B., I. Lange, and H. Konow (2012), Atmospheric boundary layer measurements at the 280 m high Hamburg weather mast 1995-2011: mean annual and diurnal cycles, *Meteorol. Z.*, *21*(4), 319–335, doi:10.1127/0941-2948/2012/0338.

Coulter, R. L., and J. C. Doran (2002), Spatial and Temporal Occurrences of Intermittent Turbulence During CASES-99, *Bound. Lay. Meteorol.*, *105*(2), 329–349, doi:10.1023/A:1019993703820.

Davy, R., and I. Esau (2016), Differences in the efficacy of climate forcings explained by variations in atmospheric boundary layer depth, *Nature Communications*, *7*, 11,690, doi:10.1038/ncomms11690.

de Bruin, H. A. R. (1994), Analytic solutions of the equations governing the temperature fluctuation method, *Boundary-Layer Meteorology*, *68*(4), 427–432, doi:10.1007/BF00706800.

Dempster, A. P., N. M. Laird, and D. B. Rubin (1979), Maximum Likelihood from Incomplete Data via the EM Algorithm, *J. Roy. Stat. Soc.*, *39B*, 1–38.

Dethloff, K., C. Abegg, A. Rinke, I. Hebestadt, and V. F. Romanov (2001), Sensitivity of arctic climate simulations to different boundary-layer parameterizations in a regional climate model, *Tellus A*, *53*(1), 1–26, doi:10.1034/j.1600-0870.2001.01073.x.

Donda, J. M. M., I. G. S. van Hooijdonk, A. F. Moene, H. J. J. Jonker, G. J. F. van Heijst, H. J. H. Clercx, and B. J. H. van de Wiel (2015), Collapse of turbulence in stably stratified channel flow: a transient phenomenon, *Quarterly Journal of the Royal Meteorological Society*, *141*(691), 2137–2147, doi:10.1002/qj.2511.

Doran, J. C. (2004), Characteristics of Intermittent Turbulent Temperature Fluxes in Stable Conditions, *Bound. Lay. Meteorol.*, *112*(2), 241–255, doi:10.1023/B:BOUN.0000027907.06649.d0.

Dörenkämper, M., B. Witha, G. Steinfeld, D. Heinemann, and M. Kühn (2015), The impact of stable atmospheric boundary layers on wind-turbine wakes within offshore wind farms, *Journal of Wind Engineering and Industrial Aerodynamics*, *144*, 146–153, doi:10.1016/j.jweia.2014.12.011.

Durst, C. S. (1933), The breakdown of steep wind gradients in inversions, *Q. J. R. Meteor. Soc.*, *59*(249), 131–136, doi:10.1002/qj.49705924906.

Edwards, J. M. (2009), Radiative processes in the stable boundary layer: Part ii. the development of the nocturnal boundary layer, *Boundary-Layer Meteorology*, *131*(2), 127–146, doi:10.1007/s10546-009-9363-9.

Edwards, J. M., J. R. McGregor, M. R. Bush, and F. J. A. Bornemann (2011), Assessment of numerical weather forecasts against observations from Cardington: seasonal diurnal

cycles of screen-level and surface temperatures and surface fluxes, *Q. J. R. Meteorol. Soc.*, *137*, 656–672, doi:10.1002/qj.742.

Fischer, J.-G., C. Senet, O. Outzen, A. Schneehorst, and K. Herklotz (2012), Regional oceanographic distincions in the South-Eastern part of the North Sea: Results of two years of monitoring at the research platforms FINO1 and FINO3, in *German Wind Energy Conference DEWEK 2012*, J.-G. Fischer, Ed., Bremen, Germany, 2012.

Floors, R., A. Peña, and S.-E. Gryning (2014), The effect of baroclinicity on the wind in the planetary boundary layer, *Q. J. R. Meteor. Soc.*, *141*(687), 619–630, doi:10.1002/qj.2386.

Flores, O., and J. J. Riley (2011), Analysis of turbulence collapse in the stably stratified surface layer using direct numerical simulation, *Boundary-Layer Meteorology*, *139*(2), 241–259, doi:10.1007/s10546-011-9588-2.

Fu, G., S. P. Charles, and S. Kirshner (2013), Daily rainfall projections from general circulation models with a downscaling nonhomogeneous hidden markov model (nhmm) for south-eastern australia, *Hydrological Processes*, *27*(25), 3663–3673, doi:10.1002/hyp.9483.

Genthon, C., M. S. Town, D. Six, V. Favier, S. Argentini, and A. Pellegrini (2010), Meteorological atmospheric boundary layer measurements and ECMWF analyses during summer at Dome C, Antarctica, *J. Geophys. Res. Atmos.*, *115*(D5), doi:10.1029/2009JD012741.

Genthon, C., D. Six, H. Gallée, P. Grigioni, and A. Pellegrini (2013), Two years of atmospheric boundary layer observations on a 45-m tower at Dome C on the Antarctic plateau, *J. Geophys. Res. Atmos.*, *118*(8), 3218–3232, doi:10.1002/jgrd.50128.

Gerbig, C., S. Körner, and J. C. Lin (2008), Vertical mixing in atmospheric tracer transport models: error characterization and propagation, *Atmos. Chem. Phys.*, *8*, 591–602, doi:10.5194/acp-8-591-2008.

Gifford, F. (1952), The breakdown of a low-level inversion studied by means of detailed soundings with modified radiosonde, *Bull. Amer. Meteor. Soc.*, *33*, 373–379.

Grachev, A. A., E. L. Andreas, C. W. Fairall, P. S. Guest, and P. O. G. Persson (2013), The Critical Richardson Number and Limits of Applicability of Local Similarity Theory in the Stable Boundary Layer, *Bound. Lay. Meteorol.*, *147*(1), 51–82, doi:10.1007/s10546-012-9771-0.

Gryning, S.-E., R. Floors, A. Peña, E. Batchvarova, and B. Brümmer (2016), Weibull Wind-Speed Distribution Parameters Derived from a Combination of Wind-Lidar and Tall-Mast Measurements Over Land, Coastal and Marine Sites, *Bound. Lay. Meteorol.*, *159*(2), 329–348, doi:10.1007/s10546-015-0113-x.

He, Y., A. H. Monahan, C. G. Jones, A. Dai, S. Biner, D. Caya, and K. Winger (2010), Probability distributions of land surface wind speeds over North America, *Journal of Geophysical Research: Atmospheres*, *115*(D4), D04,103, doi:10.1029/2008JD010708.

He, Y., N. A. McFarlane, and A. H. Monahan (2012), The Influence of Boundary Layer Processes on the Diurnal Variation of the Climatological Near-Surface Wind Speed Probability Distribution over Land, *J. Climate*, *115*, D04,103, doi:10.1175/JCLI-D-11-00321.1.

He, Y., A. H. Monahan, and N. A. McFarlane (2013), Diurnal variations of land surface wind speed probability distributions under clear-sky and low-cloud conditions, *Geophys. Res. Lett.*, *40*(12), 3308–3314, doi:10.1002/grl.50575.

Holdsworth, A. M., T. Rees, and A. H. Monahan (2016), Parameterization Sensitivity and Instability Characteristics of the Maximum Sustainable Heat Flux Framework for Predicting Turbulent Collapse, *J. Atmos. Sci.*, *73*, 3527–3540, doi:10.1175/JAS-D-16-0057.1.

Holtslag, A. A. M., G. Svensson, P. Baas, S. Basu, B. Beare, A. C. M. Beljaars, F. C. Bosveld, J. Cuxart, J. Lindvall, G. J. Steeneveld, M. Tjernström, and B. J. H. V. D. Wiel (2013), Stable Atmospheric Boundary Layers and Diurnal Cycles: Challenges for Weather and Climate Models, *Bull. Amer. Meteor. Soc.*, *94*, 1691–1706, doi:10.1175/BAMS-D-11-00187.1.

Hughes, J. P., P. Guttorp, and S. P. Charles (1999), A non-homogeneous hidden markov model for precipitation occurrence, *Journal of the Royal Statistical Society: Series C (Applied Statistics)*, *48*(1), 15–30, doi:10.1111/1467-9876.00136.

Kaimal, J. C., and J. E. Gaynor (1983), The Boulder Atmospheric Observatory, *J. Appl. Meteor. Climatol.*, *22*, 863–880, doi:10.1175/1520-0450(1983)022<0863:TBAO>2.0.CO;2.

Kalthoff, N., and B. Vogel (1992), Counter-current and channelling effect under stable stratification in the area of Karlsruhe, *Theor. Appl. Climatol.*, *45*(2), 113–126, doi:10.1007/BF00866400.

Kohler, M., J. Metzger, and N. Kalthoff (2017), Trends in temperature and wind speed from 40 years of observations at a 200-m high meteorological tower in Southwest Germany, *Int. J. Climatol.*, *38*(1), 23–34, doi:10.1002/joc.5157.

Kondo, J., O. Kanechika, and N. Yasuda (1978), Heat and Momentum Transfers under Strong Stability in the Atmospheric Surface Layer, *J. Atmos. Sci.*, *35*, 1012–1021, doi:10.1175/1520-0469(1978)035<1012:HAMTUS>2.0.CO;2.

Kyselý, J., and E. Plavcová (2012), Biases in the diurnal temperature range in Central Europe in an ensemble of regional climate models and their possible causes, *Clim. Dyn.*, *39*, 1275–1286, doi:10.1007/s00382-011-1200-4.

Lang, F., D. Belušić, and S. Siems (2018), Observations of Wind-Direction Variability in the Nocturnal Boundary Layer, *Bound. Lay. Meteorol.*, *166*(1), 51–68, doi:10.1007/s10546-017-0296-4.

Mahrt, L. (1998a), Stratified atmospheric boundary layers and breakdown of models, *Theor. Comput. Fluid Phys.*, *11*, 263–279, doi:10.1007/s001620050093.

Mahrt, L. (1998b), Nocturnal Boundary-Layer Regimes, *Bound. Lay. Meteorol.*, *88*(2), 255–278, doi:10.1023/A:1001171313493.

Mahrt, L. (2007), Weak-wind mesoscale meandering in the nocturnal boundary layer, *Environmental Fluid Mechanics*, *7*(4), 331–347, doi:10.1007/s10652-007-9024-9.

Mahrt, L. (2008), Mesoscale wind direction shifts in the stable boundary-layer, *Tellus A*, *60*(4), 700–705, doi:10.1111/j.1600-0870.2008.00324.x.

Mahrt, L. (2010), Common microfronts and other solitary events in the nocturnal boundary layer, *Q. J. R. Meteor. Soc.*, *136*(652), 1712–1722, doi:10.1002/qj.694.

Mahrt, L. (2014), Stably Stratified Atmospheric Boundary Layers, *Annu. Rev. Fluid Mech.*, *46*, 23–45, doi:10.1146/annurev-fluid-010313-141354.

Mahrt, L., S. Richardson, N. Seaman, and D. Stauffer (2012), Turbulence in the nocturnal boundary layer with light and variable winds, *Q. J. R. Meteor. Soc.*, *138*(667), 1430–1439, doi:10.1002/qj.1884.

Malhi, Y. S. (1995), The significance of the dual solutions for heat fluxes measured by the temperature fluctuation method in stable conditions, *Boundary-Layer Meteorology*, *74*(4), 389–396, doi:10.1007/BF00712379.

Mauritsen, T., and G. Svensson (2007), Observations of Stably Stratified Shear-Driven Atmospheric Turbulence at Low and High Richardson Numbers, *J. Atmos. Sci.*, *64*, 645–655, doi:10.1175/JAS3856.1.

McCabe, A., and A. R. Brown (2007), The role of surface heterogeneity in modelling the stable boundary layer, *Bound. Lay. Meteorol.*, *122*(3), 517–534, doi:10.1007/s10546-006-9119-8.

McNider, R. T., G. J. Steeneveld, A. A. M. Holtslag, R. A. Pielke, S. Mackaro, A. Pour-Biazar, J. Walters, U. Nair, and J. Christy (2012), Response and sensitivity of the nocturnal boundary layer over land to added longwave radiative forcing, *Journal of Geophysical Research: Atmospheres*, *117*(D14), doi:10.1029/2012JD017578.

Medeiros, B., C. Deser, R. A. Tomas, , and J. E. Kay (2011), Arctic inversion strength in climate models, *J. Climate*, *24*, 4733–4740, doi:10.1175/2011JCLI3968.1.

Medeiros, L. E., and D. R. Fitzjarrald (2014), Stable Boundary Layer in Complex Terrain. Part I: Linking Fluxes and Intermittency to an Average Stability Index, *J. Appl. Meteor. Climatol.*, *53*, 2196–2215, doi:10.1175/JAMC-D-13-0345.1.

Medeiros, L. E., and D. R. Fitzjarrald (2015), Stable Boundary Layer in Complex Terrain. Part II: Geometrical and Sheltering Effects on Mixing, *J. Appl. Meteor. Climatol.*, *54*(1), 170–188, doi:10.1175/JAMC-D-13-0346.1.

Monahan, A. H. (2006), The Probability Distribution of Sea Surface Wind Speeds. Part I: Theory and SeaWinds Observations, *J. Climate*, *19*(4), 497–520, doi:10.1175/JCLI3640.1.

Monahan, A. H. (2007), Empirical Models of the Probability Distribution of Sea Surface Wind Speeds, *J. Climate*, *20*, 5798–5814, doi:10.1175/2007JCLI1609.1.

Monahan, A. H. (2018), Idealized models of the joint probability distribution of wind speeds, *Nonlinear Proc. Geoph.*, *25*(2), 335–353, doi:10.5194/npg-25-335-2018.

Monahan, A. H., Y. He, N. McFarlane, and A. Dai (2011), The Probability Distribution of Land Surface Wind Speeds, *J. Climate*, *24*, 3892–3909, doi:10.1175/2011JCLI4106.1.

Monahan, A. H., T. Rees, Y. He, and N. McFarlane (2015), Multiple Regimes of Wind, Stratification, and Turbulence in the Stable Boundary Layer, *J. Atmos. Sci.*, *72*, 3178–3198, doi:10.1175/JAS-D-14-0311.1.

Nappo, C., J. Sun, L. Mahrt, and D. B. ić (2014), Determining Wave–Turbulence Interactions in the Stable Boundary Layer, *Bull. Amer. Meteor. Soc.*, *95*, ES11–ES13, doi:10.1175/BAMS-D-12-00235.1.

Nappo, C. J. (1991), Sporadic breakdowns of stability in the PBL over simple and complex terrain, *Bound. Lay. Meteorol.*, *54*(1), 69–87, doi:10.1007/BF00119413.

Newsom, R. K., and R. M. Banta (2003), Shear-Flow Instability in the Stable Nocturnal Boundary Layer as Observed by Doppler Lidar during CASES-99, *J. Atmos. Sci.*, *60*, 16–33, doi:10.1175/1520-0469(2003)060<0016:SFIITS>2.0.CO;2.

Nieuwstadt, F. T. M. (1984), The Turbulent Structure of the Stable, Nocturnal Boundary Layer, *J. Atmos. Sci.*, *41*(14), 2202–2216, doi:10.1175/1520-0469(1984)041<2202:TTSOTS>2.0.CO;2.

O'Brien, T. A., W. D.Collins, S. A.Rauscher, and T. D.Ringler (2014), Reducing the computational cost of the ECF using a nuFFT: A fast and objective probability density estimation method, *Comput. Stat. Data Anal.*, *79*, 222–234, doi:10.1016/j.csda.2014.06.002.

O'Brien, T. A., K. Kashinath, N. R. Cavanaugh, W. D.Collins, and J. P. O'Brien (2016), A fast and objective multidimensional kernel density estimation method: fastKDE, *Comput. Stat. Data Anal.*, *101*, 148–160, doi:10.1016/j.csda.2016.02.014.

Ohya, Y., R. Nakamura, and T. Uchida (2008), Intermittent Bursting of Turbulence in a Stable Boundary Layer with Low-level Jet, *Bound. Lay. Meteorol.*, *126*(3), 349–363, doi:10.1007/s10546-007-9245-y.

Optis, M., and A. Monahan (2017), A comparison of equilibrium and time-evolving approaches to modeling the wind profile under stable stratification, *Journal of Applied Meteorology and Climatology*, *56*(5), 1365–1382, doi:10.1175/JAMC-D-16-0324.1.

Optis, M., A. Monahan, and F. C. Bosveld (2014), Moving Beyond Monin–Obukhov Similarity Theory in Modelling Wind-Speed Profiles in the Lower Atmospheric Boundary Layer under Stable Stratification, *Bound. Lay. Meteorol.*, *153*(3), 497–514, doi:10.1007/s10546-014-9953-z.

Poulos, G. S., W. Blumen, D. C. Fritts, J. K. Lundquist, J. Sun, S. P. Burns, C. Nappo, R. Banta, R. Newsom, J. Cuxart, E. Terradellas, B. Balsley, and M. Jensen (2002), CASES-99: A Comprehensive Investigation of the Stable Nocturnal Boundary Layer, *Bull. Amer. Meteor. Soc.*, *83*(4), 555–582, doi:10.1175/1520-0477(2002)083<0555:CACIOT>2.3.CO;2.

Prabha, T., G. Hoogenboom, and T. Smirnova (2011), Role of land surface parameterizations on modeling cold-pooling events and low-level jets, *Atmos. Res.*, *99*(1), 147–161, doi:10.1016/j.atmosres.2010.09.017.

Rabiner, L. R. (1989), A tutorial on hidden Markov models and selected applications in speech recognition, *Proc. IEEEE*, *77*, 257–286, doi:10.1109/5.18626.

Rees, J. M., and S. D. Mobbs (1988), Studies of internal gravity waves at Halley Base, Antarctica, using wind observations, *Q. J. R. Meteor. Soc.*, *114*(482), 939–966, doi:10.1002/qj.49711448206.

Reina, N., and L. Mahrt (2005), A study of intermittent turbulence with cases-99 tower measurments, *Bound. Lay. Meteorol.*, *114*(2), 367–387, doi:10.1007/s10546-004-0857-1.

Rishel, J., S. Johnson, and D. Holt (2003), Meteorological monitoring at Los Alamos. Los Alamos National Progress Report LA-UR-03-9097, *Tech. rep.*, Los Alamos National Laboratory, available at: http://environweb.lanl.gov/downloads/LA-UR-03-8097_webcopy.pdf.

Salmond, J. A., and I. G. McKendry (2005), A review of turbulence in the very stable nocturnal boundary layer and its implications for air quality, *Progress in Physical Geography*, *29*(2), 171–188, doi:10.1191/0309133305pp442ra.

Samelson, R. M., E. D. Skyllingstad, D. B. Chelton, S. K. Esbensen, L. W. O'Neill, and N. Thum (2006), On the Coupling of Wind Stress and Sea Surface Temperature, *Journal of Climate*, *19*(8), 1557–1566, doi:10.1175/JCLI3682.1.

Sorbjan, Z. (1986), On similarity in the atmospheric boundary layer, *Bound. Lay. Meteorol.*, *34*(4), 377–397, doi:10.1007/BF00120989.

Sterk, H. A. M., G. J. Steeneveld, and A. A. M. Holtslag (2013), The role of snow-surface coupling, radiation, and turbulent mixing in modeling a stable boundary layer over Arctic sea ice, *J. Geophys. Res. Atmos.*, *118*, 1199–1217, doi:10.1002/jgrd.50158.

Sterk, H. A. M., G. J. Steeneveld, T. Vihma, P. S. Anderson, F. C. Bosveld, and A. A. M. Holtslag (2015), Clear-sky stable boundary layers with low winds over snow-covered surfaces. part 1: Wrf model evaluation, *Quarterly Journal of the Royal Meteorological Society*, *141*(691), 2165–2184, doi:10.1002/qj.2513.

Storm, B., and S. Basu (2010), The WRF Model Forecast-Derived Low-Level Wind Shear Climatology over the United States Great Plains, *Energies*, *3*(2), 258–276, doi:10.3390/en3020258.

Sun, J., S. P. Burns, D. H. Lenschow, R. Banta, R. Newsom, R. Coulter, S. Frasier, T. Ince, C. Nappo, J. Cuxart, W. Blumen, X. Lee, and X.-Z. Hu (2002), Intermittent Turbulence Associated with a Density Current Passage in the Stable Boundary Layer, *Bound. Lay. Meteorol.*, *105*(2), 199–219, doi:10.1023/A:1019969131774.

Sun, J., D. H. Lenschow, S. P. Burns, R. M. Banta, R. K. Newsom, R. Coulter, S. Frasier, T. Ince, C. Nappo, B. B. Balsley, M. Jensen, L. Mahrt, D. Miller, and B. Skelly (2004), Atmospheric Disturbances that Generate Intermittent Turbulence in Nocturnal Boundary Layers, *Bound. Lay. Meteorol.*, *110*(2), 255–279, doi:10.1023/A:1026097926169.

Sun, J., L. Mahrt, R. M. Banta, and Y. L. Pichugina (2012), Turbulence Regimes and Turbulence Intermittency in the Stable Boundary Layer during CASES-99, *J. Atmos. Sci.*, *69*, 338–351, doi:10.1175/JAS-D-11-082.1.

Sun, J., L. Mahrt, C. Nappo, and D. H. Lenschow (2015), Wind and Temperature Oscillations Generated by Wave–Turbulence Interactions in the Stably Stratified Boundary Layer, *J. Atmos. Sci.*, *72*, 1484–1503, doi:10.1175/JAS-D-14-0129.1.

Svensson, G., and A. A. M. Holtslag (2009), Analysis of model results for the turning of the wind and related momentum fluxes in the stable boundary layer, *Bound. Lay. Meteorol.*, *132*, 261–277, doi:10.1007/s10546-009-9395-1.

Svensson, G., A. A. M. Holtslag, V. Kumar, T. Mauritsen, G. J. Steeneveld, W. M. Angevine, E. Bazile, A. Beljaars, E. I. F. de Bruijn, A. Cheng, L. Conangla, J. Cuxart, M. Ek, M. J. Falk, F. Freedman, H. Kitagawa, V. E. Larson, A. Lock, J. Mailhot, V. Masson, S. Park, J. Pleim, S. Söderberg, W. Weng, and M. Zampieri (2011), Evaluation of the diurnal cycle in the atmospheric boundary layer over land as represented by a variety of single-column models: The second gabls experiment, *Boundary-Layer Meteorology*, *140*(2), 177–206, doi:10.1007/s10546-011-9611-7.

Tastula, E.-M., T. Vihma, and E. L. Andreas (2012), Evaluation of Polar WRF from modeling the atmospheric boundary layer over antarctic sea ice in autumn and winter, *Mon. Wea. Rev.*, *140*, 3919–3935, doi:10.1175/MWR-D-12-00016.1.

Tomas, J. M., M. J. B. M. Pourquie, and H. J. J. Jonker (2016), Stable Stratification Effects on Flow and Pollutant Dispersion in Boundary Layers Entering a Generic Urban Environment, *Boundary-Layer Meteorology*, pp. 159–221, doi:10.1007/s10546-015-0124-7.

Ulden, A. P. V., and J. Wieringa (1996), Atmospheric boundary layer research at Cabauw, *Bound. Lay. Meteorol.*, *78*(1), 39–69, doi:10.1007/BF00122486.

van de Wiel, B. J. H., R. J. Ronda, A. F. Moene, H. A. R. D. Bruin, and A. A. M. Holtslag (2002a), Intermittent Turbulence and Oscillations in the Stable Boundary Layer over Land. Part I: A Bulk Model, *J. Atmos. Sci.*, *59*, 942–958, doi:10.1175/1520-0469(2002)059<0942:ITAOIT>2.0.CO;2.

van de Wiel, B. J. H., A. F. Moene, R. J. Ronda, H. A. R. D. Bruin, and A. A. M. Holtslag (2002b), Intermittent Turbulence and Oscillations in the Stable Boundary Layer over Land. Part II: A System Dynamics Approach, *J. Atmos. Sci.*, *59*, 2567–2581, doi:10.1175/1520-0469(2002)059<2567:ITAOIT>2.0.CO;2.

van de Wiel, B. J. H., A. F. Moene, O. K. Hartogensis, H. A. R. D. Bruin, and A. A. M. Holtslag (2003), Intermittent Turbulence in the Stable Boundary Layer over Land. Part III: A Classification for Observations during CASES-99, *J. Atmos. Sci.*, *60*, 2509–2522, doi:10.1175/1520-0469(2003)060<2509:ITITSB>2.0.CO;2.

van de Wiel, B. J. H., A. F. Moene, G. J. Steeneveld, O. K. Hartogensis, and A. A. M. Holtslag (2007), Predicting the Collapse of Turbulence in Stably Stratified Boundary Layers, *Flow, Turbulence and Combustion*, *79*(3), 251–274, doi:10.1007/s10494-007-9094-2.

van de Wiel, B. J. H., A. F. Moene, and H. J. J. Jonker (2012a), The Cessation of Continuous Turbulence as Precursor of the Very Stable Nocturnal Boundary Layer, *J. Atmos. Sci.*, *69*, 3097–3127, doi:10.1175/JAS-D-12-064.1.

van de Wiel, B. J. H., A. F. Moene, H. J. J. Jonker, P. Baas, S. Basu, J. M. M. Donda, J. Sun, and A. A. M. Holtslag (2012b), The Minimum Wind Speed for Sustainable Turbulence in the Nocturnal Boundary Layer, *J. Atmos. Sci.*, *69*, 3116–3127, doi:10.1175/JAS-D-12-0107.1.

van de Wiel, B. J. H., E. Vignon, P. Baas, I. G. S. van Hooijdonk, S. J. A. van der Linden, J. A. van Hooft, F. C. Bosveld, S. R. de Roode, A. F. Moene, and C. Genthonc (2017), Regime Transitions in Near-Surface Temperature Inversions: A Conceptual Model, *J. Atmos. Sci.*, *74*, 1057–1073, doi:10.1175/JAS-D-16-0180.1.

van der Linden, S. J. A., P. Baas, J. A. van Hooft, I. G. S. van Hooijdonk, F. C. Bosveld, and B. J. H. van de Wiel (2017), Local characteristics of the nocturnal boundary layer in response to external pressure forcing, *Journal of Applied Meteorology and Climatology*, *56*(11), 3035–3047, doi:10.1175/JAMC-D-17-0011.1.

van Hooijdonk, I., A. Moene, M. Scheffer, H. Clercx, and B. van de Wiel (2017a), Early Warning Signals for Regime Transition in the Stable Boundary Layer : A Model Study, *Bound. Lay. Meteorol.*, *162*(2), 283–306, doi:10.1007/s10546-016-0199-9.

van Hooijdonk, I. G. S., J. M. M. Donda, H. J. H. C. F. C. Bosveld, and B. J. H. van de Wiel (2015), Shear Capacity as Prognostic for Nocturnal Boundary Layer Regimes, *J. Atmos. Sci.*, *72*, 1518–1532, doi:10.1175/JAS-D-14-0140.1.

van Hooijdonk, I. G. S., H. J. H. Clercx, C. Abraham, A. M. Holdsworth, A. H. Monahan, E. Vignon, A. F. Moene, P. Baas, and B. J. H. van de Wiel (2017b), Near-Surface Temperature Inversion Growth Rate during the Onset of the Stable Boundary Layer, *J. Atmos. Sci.*, *74*(10), 3433–3449, doi:10.1175/JAS-D-17-0084.1.

Vercauteren, N., and R. Klein (2015), A Clustering Method to Characterize Intermittent Bursts of Turbulence and Interaction with Submesomotions in the Stable Boundary Layer, *J. Atmos. Sci.*, *72*, 1504–1517, doi:10.1175/JAS-D-14-0115.1.

Vignon, E., B. J. H. van de Wiel, I. G. S. van Hooijdonk, C. Genthon, S. J. A. van der Linden, J. A. van Hooft, P. Baas, W. Maurel, O. Traullé, and G. Casasanta (2017a), Stable boundary-layer regimes at Dome C, Antarctica: observation and analysis, *Q. J. R. Meteor. Soc.*, *143*(704), 1241–1253, doi:10.1002/qj.2998.

Vignon, E., C. Genthon, H. Barral, C. Amory, G. Picard, H. Gallée, G. Casasanta, and S. Argentini (2017b), Momentum- and Heat-Flux Parametrization at Dome C, Antarctica: A Sensitivity Study, *Bound. Lay. Meteorol.*, *162*(2), 341–367, doi:10.1007/s10546-016-0192-3.

Vose, R. S., D. R. Easterling, and B. Gleason (2005), Maximum and minimum temperature trends for the globe: An update through 2004, *Geophysical Research Letters*, *32*(23), doi:10.1029/2005GL024379.

Walsh, J. E., W. L. Chapman, V. Romanovsky, J. H. Christensen, and M. Stendel (2008), Global Climate Model Performance over Alaska and Greenland, *J. Climate*, *21*, 6156–6174, doi:10.1175/2008JCLI2163.1.

Walters, J. T., R. T. McNider, X. Shi, W. B. Norris, and J. R. Christy (2007), Positive surface temperature feedback in the stable nocturnal boundary layer, *Geophysical Research Letters*, *34*(12), L12,709, doi:10.1029/2007GL029505.

Wenzel, A., N. Kalthoff, and V. Horlacher (1997), On the profiles of wind velocity in the roughness sublayer above a coniferous forest, *Bound. Lay. Meteorol.*, *84*(2), 219–230, doi:10.1023/A:1000444911103.

Westerhellweg, A., and T. Neumann (2012), FINO1 Mast Correction, *DEWI Magazin*, *40*, 60–66.

White, L. D. (2009), Sudden Nocturnal Warming Events in Mississippi, *J. Appl. Meteor. Climatol.*, *48*, 758–755, doi:10.1175/2008JAMC1971.1.

Williams, A. G., S. Chambers, and A. Griffiths (2013), Bulk Mixing and Decoupling of the Nocturnal Stable Boundary Layer Characterized Using a Ubiquitous Natural Tracer, *Bound. Lay. Meteorol.*, *149*(3), 381–402, doi:10.1007/s10546-013-9849-3.

Zhou, B., and F. K. Chow (2012), Turbulence Modeling for the Stable Atmospheric Boundary Layer and Implications for Wind Energy, *Flow, Turbulence and Combustion*, *88*(1), 255–277, doi:10.1007/s10494-011-9359-7.

Zilitinkevich, S. S., T. Elperin, N. Kleeorin, I. Rogachevskii, I. Esau, T. Mauritsen, and M. W. Miles (2008), Turbulence energetics in stably stratified geophysical flows: Strong and weak mixing regimes, *Q. J. R. Meteor. Soc.*, *134*(633), 793–799, doi:10.1002/qj.264.